R-10-30

Conceptual and numerical modelling of radionuclide transport in near-surface systems at Forsmark

SR-Site Biosphere

Àngels Piqué, Fidel Grandia, Clara Sena, David Arcos,
Jorge Molinero, Lara Duro, Jordi Bruno,
Amphos[21] Consulting S.L.

November 2010

Svensk Kärnbränslehantering AB
Swedish Nuclear Fuel
and Waste Management Co

Box 250, SE-101 24 Stockholm
Phone +46 8 459 84 00

ISSN 1402-3091
SKB R-10-30

Conceptual and numerical modelling of radionuclide transport in near-surface systems at Forsmark

SR-Site Biosphere

Àngels Piqué, Fidel Grandia, Clara Sena, David Arcos,
Jorge Molinero, Lara Duro, Jordi Bruno,
Amphos[21] Consulting S.L.

November 2010

Keywords: SKBdoc 1265028.

Abstract

In the framework of the SR-Site safety assessment, a conceptual and numerical modelling of radionuclide reactive transport in near-surface systems (including till and clay systems) at Forsmark has been carried out. The objective was to evaluate the retention capacity of the near-surface systems, composed of Quaternary deposits, which would be the last natural barrier for an eventual radionuclide release from the deep repository prior to reaching the biosphere. The studied radionuclides are ^{14}C, ^{129}I, ^{36}Cl, ^{94}Nb, ^{59}Ni, ^{93}Mo, ^{79}Se, ^{99}Tc, ^{230}Th, ^{90}Sr, ^{226}Ra, ^{135}Cs and U.

Conceptual description and numerical simulations of radionuclide reactive transport show that cation exchange and surface complexation on illite are active processes for the retention of several radionuclides (U, Th, Ni, Cs, Sr, Ra). Surface complexation on iron hydroxide is an active process in the till system, able to effectively retain U and Ni. Another retention process of importance is the incorporation of the radionuclides into mineral phases, either by the precipitation of pure phases or solid solutions. Quantitative modelling has been useful to illustrate the incorporation of C and Sr in the carbonate solid solution in the considered model domains (till and clay), as well as the precipitation of uraninite in the clay sediments and the precipitation of native selenium and radiobarite in the till.

Other mineral phases that could, a priori, retain U, Se, Nb and Tc do not precipitate in the simulations, either due to the pH-Eh conditions and/or because the dissolved concentration of the element is not high enough under the considered simulation conditions. It is important to keep in mind that changes in these parameters and in the boundary conditions could modify the predicted behaviour of these elements.

The radionuclides that are most significantly retarded are Th, Ni and Cs, mainly through sorption onto illite. Therefore, if the amount of illite (or available sorption sites) decreases, the retardation of these elements will also decrease accordingly, as illustrated by the sensitivity analyses performed. The high retardation predicted for these elements is in good agreement with reported Kd values for Forsmark till and lake sediments. According to the models, Cs, Th and Ni are highly retained, while C, U, Sr and Ra are more mobile. The simulations also show that Nb and Tc behave conservatively in both domains, as expected due to their anionic character under these conditions, and Se only in the clay domain. The reported Kd in Forsmark soils and sediments, although not directly comparable to the calculated effective Kds, show a similar general trend (i.e. the most strongly retained elements are Th, Cs and Ni, followed by U and Sr).

The computed behaviour of Se and Nb are the two exceptions that do not agree with reported Kd values. It needs to be recalled also that not all the possible retention processes considered in the conceptual model were included in the simulation, due to either the lack of reliable knowledge and/or the scarcity of thermodynamic data.

Besides the retention mechanisms, other processes that produce attenuation of the radionuclides are dilution of the radionuclide-bearing deep groundwater, which applies to all elements, and decay, as we are dealing with radionuclides. The radionuclides that will be more significantly reduced by decay are ^{226}Ra and ^{90}Sr, although ^{226}Ra is a permanent product of the decay of ^{238}U. In this sense, if one considers the possibility that carbonate will be dissolved in a future evolution of the simulated domains, the release into water of the previously retained Sr will not be of significance. Conversely, ^{14}C has a longer half-life and could still be present in the system and contribute to increased radioactive doses.

Contents

1 Introduction

1.1 Motivation and context

In 2009 the Swedish Nuclear Fuel and Waste Management Company (SKB) selected the Forsmark site to locate a deep geological repository for the final disposal of high level nuclear waste (HLNW). SKB's intention is to assemble all the information that is required to submit a license application to build the deep geological repository. In this context, SKB is submitting a further analysis of the long-term safety of the final repository – SR-Site – to support the application. This safety assessment is based on the collected data available at the completion of the site investigations and the planning of the repository.

One important component of the system considered in SR-Site is the so-called near-surface system, which is mainly composed of Quaternary deposits. The near-surface system is actually the transitional zone between the bedrock and the surface biosphere. The near-surface system would be the last natural barrier for an eventual radionuclide release from the deep repository before it enters the surface biosphere. Therefore, the evaluation of the retention capacity of the near-surface system is an important part of the SR-Site analysis.

The retention capacity of the near-surface system at Forsmark was evaluated in /Grandia et al. 2007/ and /Sena et al. 2008/ for the radionuclides Cs, Sr, U and Ra. Numerical models of reactive transport were applied to two case studies of sub-systems of the near-surface system consisting of different types of Quaternary deposits: a till and a glacial clay deposit. The results attained in those numerical models show that the near-surface system at Forsmark constitutes a geochemical reactive barrier able to retain radionuclides by several key processes.

1.2 Objectives

This work has two main objectives:

1) To conceptually evaluate the behaviour of the radionuclides ^{14}C, ^{129}I, ^{36}Cl, ^{94}Nb, ^{59}Ni, ^{93}Mo, ^{79}Se, ^{99}Tc and ^{230}Th in the near-surface Quaternary deposits (including till, and lake and wetland sediments) of the Forsmark site; the geochemical behaviour of ^{129}I and ^{79}Se were already introduced in /Grandia et al. 2007/ and they are refined and updated in the present work.
2) To develop reactive-transport models of the till and glacial clay deposits in order to quantitatively evaluate the retention capacity of the Forsmark near-surface systems. Besides the abovementioned radionuclides, the modelling will also include Sr, Ra, U and Cs, which were previously implemented by /Grandia et al. 2007, Sena et al. 2008/.

1.3 Selection of radionuclides

In the performance and safety assessment of deep repositories of HLNW, only radionuclides with long half-lives are expected to reach the surface and, therefore, need to be taken into consideration in such studies. Among these long-lived radionuclides, the ones selected for this work include elements with different geochemical behaviour and also different levels of scientific knowledge about their properties.

Due to their different chemical nature, these elements are expected to be selectively retained by distinct mechanisms. From the available data and by comparing with other examples in similar environments, the most favourable retention mechanisms will be evaluated. This evaluation will be made considering that radionuclides would migrate from the deep bedrock to the surface so that the near-surface deposits will eventually interact with these radionuclides.

1.4 Report organisation

The report starts with a review of the available data for surface and shallow waters as well as for Quaternary deposits in the Forsmark area: geology, hydrogeology and major geochemistry are reviewed in Chapter 2. Investigations of the geochemistry of selected radionuclides based on previous information and site data on water chemistry and sediment geochemistry for these radionuclides are dealt with in Chapter 3, where also information from other similar sites is considered. The geochemical behaviour of Cs, U and Sr previously reported in /Grandia et al. 2007/ and of Ra in /Grandia et al. 2008/ have also been included in this chapter.

All this information is used to evaluate the most likely retardation mechanisms for the studied radionuclides in the near-surface environment. The geochemical conceptual model for the selection of the mechanisms to be implemented in the numerical models is given in Chapter 4. Chapter 5 is devoted to the numerical modelling set-up. The results of the numerical modelling of the till system are presented in Chapter 6 and those of the clay system in Chapter 7. Chapter 8 is devoted to the discussion of the results and a chapter of conclusions, Chapter 9, is also included at the end.

2 Summary of surface and near-surface geology, hydrogeology and hydrogeochemistry data from the Forsmark site

The Forsmark area consists of crystalline bedrock affected by both ductile and brittle deformation. The ductile deformation has resulted in large-scale ductile high-strain zones and the brittle deformation has given rise to large-scale fracture zones. Tectonic lenses, in which the bedrock is much less affected by ductile deformation, are enclosed between the ductile high-strain zones. The candidate area is located in the north-westernmost part of one of these tectonic lenses /Lindborg 2008/.

The study area is characterised by small-scale topographic variations and is almost entirely located below 20 m.a.s.l. (metres above sea level). Till is the dominant Quaternary deposit, whereas granite is the dominant bedrock type. The surface water and shallow groundwater at Forsmark are characterised by high pH values and high concentrations of certain major constituents, especially calcium and bicarbonate.

The main lakes are Lake Fiskarfjärden (0.752 km^2), Lake Bolundsfjärden (0.609 km^2), Lake Eckarfjärden (0.282 km^2) and Lake Gällsboträsket (0.185 km^2). The lakes are shallow with mean depths and maximum depths ranging from approximately 0.1 to 1 m and 0.4 to 2 m, respectively. Seawater flows into the most low-lying lakes during events of very high sea water levels /Lindborg 2008/.

Below a brief summary of the site data that provide the site-specific background information to the present work is given. In addition to the data presented in the reports referred to in the text, SKB made a special delivery of chemical data on Quaternary deposits (including soils and sediments) and waters (surface waters and groundwater) to be used within the project (stored as "Forsmark Chemistry water deposits biota 090313.xls", rev. 1428, at http://svn.skb.se/trac, also part of the dataset in SKBdoc 1263189). This data delivery constitutes the main input to the descriptions of the site chemistry in (especially) Chapters 2 and 3.

2.1 Typology and stratigraphy of the Quaternary deposits

All regolith in the Forsmark area was formed during the Quaternary period and will be therefore referred to as QD (Quaternary deposits). The QD are divided into two main categories according to the environment in which they were formed: *glacial* and *postglacial deposits*, which are briefly summarised below (all the information given in this section is from /Hedenström and Sohlenius 2008/ unless otherwise stated).

The glacial deposits include till, glaciofluvial sediments, clay and silt. They contain little (or no) organic matter (OM). Till is generally characterised by poor sorting, with particles ranging from clay size to large boulders. In contrast, glaciofluvial deposits are formed by well-sorted sediments and are often deposited directly on the bedrock or on top of the till. Glacial clay and silt are restricted to local depressions, such as the bottom of lakes and small ponds.

A characteristic property of the till in Forsmark is the high content of calcium carbonate ($CaCO_3$) generally found in the fine and coarse fractions. Based on the surface layer, the till in the terrestrial part of Forsmark is divided into three areas: Till Areas I, II and III (see distribution in /Hedenström and Sohlenius 2008, figure 5-13/). Till Area I, which constitutes the major part of the Forsmark area, consists of sandy and silty till with a medium frequency of boulders. Till Area II consists of clayey till and boulder clay with a low frequency of boulders, whereas Till Area III is dominated by till with a high frequency of large boulders in the surface layer.

The postglacial deposits often contain OM and re-deposited, wave-washed clay, sand and gravel. In general, they overlie till and glacial clay or rest directly on crystalline bedrock. Postglacial clay containing organic material is referred to as gyttja clay (2–6% OM), clay gyttja (6–20% OM) or gyttja (> 20% OM). Gyttja sediments containing > 20% OM were formed in lakes and consist mainly of plant remnants. In areas with calcareous soils, such as Forsmark, calcareous gyttja will form when calcium carbonate precipitates in the lake.

Organic deposits occur frequently in the surface parts of the wetlands. Wetlands have a peat thickness greater than 0.5 m at altitudes from the 5 m isoline and upwards (approximately). In the youngest parts of the regional model area, postglacial clays, including gyttja clay, clay gyttja and gyttja, occur frequently as the superficial QD and covers many small (less than 50×50 m) areas.

In general, the distribution of QD is related to the bedrock morphology. The most elevated areas are characterised by bedrock outcrops, till and peatlands. The lower parts of the model area are characterised by fine-grained sediments. In the Forsmark regional model area, bedrock exposures occupy c 13% of the land area, QD cover c 84% and artificial fill 3%. QD is dominated by till (65% of the land area), followed by peat (8%), glacial clay (4%), postglacial clay including gyttja (4%), postglacial sand and gravel (2%) and glaciofluvial sediment (1%). Table 2-1 presents a summary of grain size distributions, sorting coefficients (D60/D10) and calcium carbonate contents of the different deposits in the terrestrial area.

Compared to the QD distribution in the terrestrial area, the sea floor is mainly covered by clay rather than till. The QD in the marine area are dominated by glacial and postglacial clays, together covering c 58% of the sea floor, while till covers only 30%. In the shallow coastal area, gyttja and gyttja clay cover 15% and postglacial sand and gravel 29% of the area. The clay deposits are predominantly overlain by a thin layer of silt, sand or gravel, i.e. similar to the distribution in the terrestrial area. The thickness of the QD in the marine area varies between 0 m and 42 m.

A geometric model for the regolith depth was constructed based on the surface distribution and stratigraphy of the QD. The model is based on evaluation of drillings and corings, excavations and geophysical investigations, and describes the total regolith depth, subdivided into seven layers and three lake sediment lenses (see Figure 4-2 in /Hedenström and Sohlenius 2008/). The modelled regolith depth varies between 0.1 m and 42 m. Generally, the regolith is thicker in the marine area, where the average regolith depth is c 8 m, whereas the average total depth in the terrestrial area is approximately 4 m. Within the terrestrial area, Till Area II (clayey till) generally has a thicker regolith than the rest.

Based on information from drillings, it was suggested that the till below the lakes and mires has similar properties (e.g. texture and thickness) to those in the terrestrial areas, with the exception of an absence of soil forming processes and wave washing. Of the three larger lakes at Forsmark, Lake Eckarfjärden and Lake Fiskarfjärden have a more or less continuous layer of glacial clay on top of the till, whereas Lake Bolundsfjärden has postglacial sediments that partially lay directly on the till. In a majority of the lakes investigated, the total thickness of the sediments (not including glacial till) was less than 2 m /Hedenström 2004/. Table 2-2 shows the distribution of QD in lakes and ponds in the Forsmark region.

Table 2-1. Summary of some physical parameters of the most common deposits in the terrestrial area at Forsmark (from /Hedenström and Sohlenius 2008/).

Deposit	Gravel (%)	Sand (%)	Silt (%)	Clay (%)	D60/D10	$CaCO_3$ (%)
Sandy and sandy silty till (Till area I) n=66	22.1 (±7.8)	50.8 (±10.1)	23.5 (±8.9)	3.6 (±1.1)	46.4 (±29.5)	19.1 (±5.7)
Clayey till and boulder clay (Till area II) n=103	15.8 (±8.1)	41.2 (±6.8)	32.3 (±7.2)	10.8 (±4.4)	104.0 (±155.4)	23.4 (±6.6)
Gravely till n=15	44.8 (±8.8)	40.7 (±10.7)	12.7 (±5.4)	2.4 (±1.1)	132.6 (±105.7)	17.5 (±5.3)
Gravel n=5	53.1 (±6.7)	44.2 (±6.1)	1.5 (±1.2)	1.2 (±1.1)	16.8 (±4.1)	
Sand n=15	16.9 (±16.2)	68.0 (±14.1)	13.0 (±15.4)	2.7 (±2.2)	10.6 (±8.1)	
Silt n=4	0.2 (±0.5)	15.9 (±13.7)	68.9 (12.6)	15.0 (±6.8)	9.9	
Clay n=30	0.6 (±1.8)	3.0 (±7.2)	41.6 (±16.1)	54.8 (±13.8)		18.0 (±13.3)

Table 2-2. Generalised stratigraphical distribution of QD in lakes and mires (from /Hedenström and Sohlenius 2008/).

Environment/facies	Lithology	Relative age
Bog	Bog peat	Youngest
Fen	Fen peat	
Freshwater lake	Microphytobenthos/Gyttja/ Calcareous gyttja	↑
Freshwater lake and shallow coastal basin	Algal gyttja	
Postglacial Baltic basin	Clay gyttja-gyttja clay	↑
Coast and off-shore	Post-glacial sand and gravel	
Postglacial Baltic basin	Postglacial clay	↑
Late glacial Baltic basin	Glacial clay	
Late glacial	Glaciofluvial sediment	
Glacial	Till	Oldest

2.2 Mineralogy and geochemistry of the Quaternary deposits

/Hedenström and Sohlenius 2008/ report a detailed listing of references on chemical data of QD from the Forsmark area. Unfortunately, a detailed mineral characterisation, accounting for minor and accessory minerals that can be highly relevant for the present study, has not yet been conducted. At present there is only information on the content of $CaCO_3$, quartz, organic matter and clay minerals. In this section only data on the chemical properties that are relevant in the perspective of the work developed in this project are reported.

2.2.1 Till deposits

As stated earlier, an outstanding geochemical feature of the till deposits at Forsmark is the high content of $CaCO_3$. A comparison between the different till types shows that till with a clay content higher than 5% (Till Area II) has a slightly higher content of calcite (average content 23%, n=106) in the fine fraction (grain sizes < 63μm), compared to the sandy till (average content 19% n=66). Interestingly, according to /Tröjbom and Söderbäck 2006/ there is no clear correlation between calcium carbonate content and depth.

Qualitative XRD analyses of bulk soil material /Sohlenius and Rudmark 2003/ show that the till samples contain almost 40% of quartz, and two samples from west of Lake Bolundsfjärden have a relatively high content of hornblende. The qualitative XRD analyses of clay mineralogy show that illite is the most common clay mineral in the analysed till samples and the illite/chlorite ratio is higher in the clayey till compared to the silty-sandy till.

The analyses of the elemental content of the till available in the dataset used in this work reveal a close relationship between Fe and Al (Figure 2-1A), which is consistent with the mineralogy previously reported. A relatively strong correlation exists also between Fe and Mn (Figure 2-1B). Based on this correlation, /Grandia et al. 2007/ suggested that Fe and Mn could be present as oxy-hydroxide mixtures. Nevertheless, their association with aluminosilicates can not be disregarded based on the positive correlation between Fe and Al (Figure 2-1A) and between Mn and Al (Figure 2-1C). Ca is not correlated with Al, in consistence with the fact that Ca is mainly found in carbonate minerals.

2.2.2 Lake and wetland sediments

In many lakes, glacial clays underlying the gyttja sediments have an average $CaCO_3$ content of 26%. In some lakes, the $CaCO_3$ content is higher in the youngest sediments, formed during the present lake stage. The highest $CaCO_3$ content of over 60% was recorded in the calcareous gyttja from Lake Stocksjön /Hedenström 2004/.

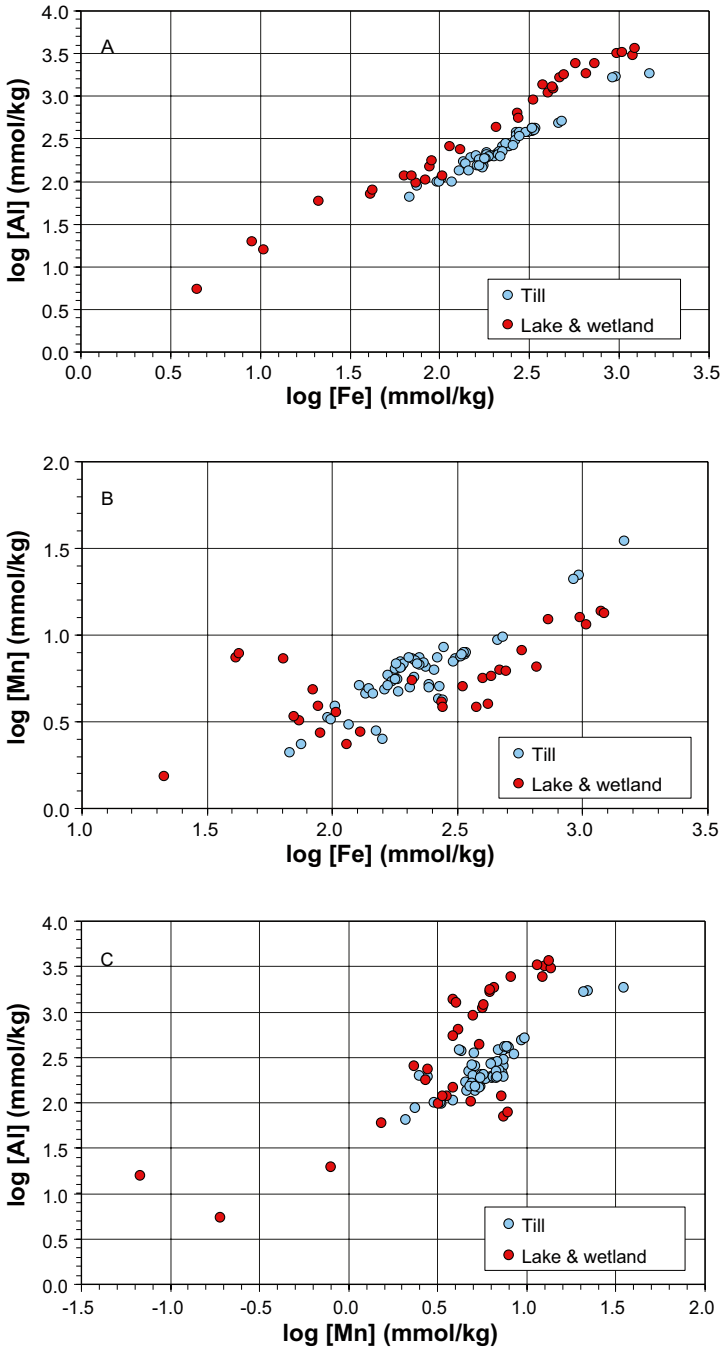

Figure 2-1. *Plots of (A) Al vs. Fe; (B) Mn vs. Fe; and (C) Al vs. Mn concentrations in till, lake and wetland sediments.*

/Hedenström 2004/ analysed sediment cores from three lakes, and in all investigated lake sediments the concentrations of C, N and S show an increasing trend from the oldest to the youngest ones (Table 2-3). The S contents are close to or higher than 1% in all sediments overlying the glacial clay. The highest values, up to 3%, were recorded in the organic rich gyttja sediments. Sulphur in the sediments may be partly associated to organic material, but according to /Hedenström and Sohlenius 2008/ it is likely that the postglacial gyttja sediments and clays in the Forsmark area contain significant amounts of iron sulphides, something that needs to be confirmed through a detailed mineral characterisation.

The qualitative XRD analyses of three clay samples collected at Lake Fiskarfjärden and a small pond close to the Börstilåsen Esker showed an almost identical clay mineral content /Hedenström 2004/. The results showed similar distributions of clay minerals in glacial and postglacial clays, with illite as the dominating clay mineral, followed by chlorite and small amounts of kaolinite.

Table 2-3. General stratigraphical distribution and average contents of carbon (C), nitrogen (N), sulphur (S) and phosphorous (P), as recorded in marine and lacustrine sediments and peat at Forsmark (from /Hedenström and Sohlenius 2008/).

Environment	Lithology	Relative age	C %	N %	S %	P %	Water content %	Porosity %	Bulk density g/cm³
Bog/Fen	Peat	Youngest	55	0.68	0.7	0.02	90	89.6	1.004
Freshwater lake	Gyttja	↑	18	1.4	1.9		93	90.1	1.031
Shallow Baltic basin	Clay gyttja	↑	6.2	0.6	1.6	0.09	86	79.2	1.085
Coast	Postglacial sand and gravel						8.5	32	1.600–2.000
Postglacial Baltic basin	Postglacial clay	↑	1.8						
Late glacial Baltic basin	Glacial clay	Oldest	1.00	0.11	0.76		53	37.8	1.400

With regard to the elemental composition of the lake and wetland sediments (including peat), the analyses available in the dataset used in this work reveal a close relationship between Fe and Al (Figure 2-1A), like in the case of the till sediments, as well as a certain degree of correlation between Fe and Mn (Figure 2-1B), and between Mn and Al (Figure 2-1C).

2.3 Hydrology and hydrogeology of the Quaternary deposits

The conceptual modelling and the quantitative flow modelling associated with the hydrology and near-surface hydrogeology of Forsmark are described in detail in /Bosson et al. 2008, Johansson 2008, Johansson and Öhman 2008/. All the information summarised below in this section is from /Johansson 2008/.

Best estimates of hydraulic parameters of QD in Forsmark are presented in Table 2-4. Due to the influence of soil forming processes on the uppermost part of the soil profile, a differentiation of the hydraulic properties was made between the upper 0.6 m and the deeper part of the profile for some of the Quaternary deposits. The conductivities given in Table 2-4 are horizontal conductivities (K_h). The only vertical conductivity (K_v) values in till are from laboratory permeameter tests. The geometric mean of these tests for samples below one metre was approximately $4.4 \cdot 10^{-8}$ m/s while the geometric mean of K_h in till from the slug tests is $1.3 \cdot 10^{-6}$ m/s.

Table 2-4. Best estimates of hydraulic parameters of Quaternary deposits in Forsmark based on site specific data and supported by generic data when site specific data are scarce. The K-values given are for the horizontal direction (K_h) (from /Johansson 2008/).

Deposit	K_h (m/s)	Total porosity (–)	Specific yield (–)
Peat	Depth < 0.6 m: $1.0 \cdot 10^{-5}$ Depth > 0.6 m: $3.0 \cdot 10^{-7}$	Depth < 0.6 m: 0.60 Depth > 0.6 m: 0.40	Depth < 0.6 m: 0.20 Depth > 0.6 m: 0.05
Gyttja, Clay-gyttja, Gytttja-clay	$3.0 \cdot 10^{-7}$	0.50	0.03
Glaciofluvial and postglacial sand	$1.5 \cdot 10^{-4}$	0.35	0.20
Clay (glacial and post-glacial)	Depth < 0.6 m: $1.0 \cdot 10^{-5}$ Depth > 0.6 m: $1.5 \cdot 10^{-8}$	Depth < 0.6 m: 0.55 Depth > 0.6 m: 0.45	Depth < 0.6 m: 0.05 Depth > 0.6 m: 0.03
Till	Till (fine and coarse), Depth < 0.60: $1.5 \cdot 10^{-5}$ Depth > 0.6 m: Fine-grained: $1.0 \cdot 10^{-7}$ Coarse: $1.5 \cdot 10^{-6}$	Depth < 0.60 m: 0.35 Depth > 0.60 m: 0.25	Depth < 0.6 m: 0.15 Depth > 0.6 m: Fine-grained: 0.03 Coarse: 0.05
Till/bedrock interface	$1.5 \cdot 10^{-5}$	0.25	0.05

This corresponds to a K_h/K_v ratio of about 30; however, this result should be used with caution since the tests were done at different scales. The vertical K-values for gyttja and peat/gyttja/clay obtained from leakage coefficients from the pumping tests were approximately $1 \cdot 10^{-8}$ m/s. Also for these tests the vertical K-values are about 30 times lower than the K_h-values given for these deposits in Table 2-4.

Based on generic and site specific data, the saturated hydraulic conductivity in the uppermost part of the till can be estimated to 10^{-5}–10^{-4} m/s and the specific yield to between 10 and 20%, with the higher values close to the surface. The total porosity can be typically estimated to 30–40%, mainly depending on depth. Below the depth interval strongly influenced by the soil forming processes, the hydraulic conductivity and the porosity of the till are considerably lower. The results from the slug tests indicate a higher hydraulic conductivity at the Quaternary deposits/bedrock interface than in the till itself.

Direct recharge from precipitation is the dominant source of groundwater recharge. However, groundwater level measurements in the vicinity of Lake Bolundsfjärden and Lake Eckarfjärden show that the lakes may act as recharge sources to the till aquifers in the immediate vicinity of the lakes during summer, rather than acting as discharge areas. Groundwater levels in the QD are very shallow (mean depths within less than a metre below ground in most of the area) and are highly correlated with the topography of the ground surface. The decreasing hydraulic conductivity with depth and the anisotropy ($K_h > K_v$) of the tills prevailing in the area mean that a most of the groundwater will move along very shallow flow paths.

The upper bedrock is characterised by horizontal and sub-horizontal fracture zones, giving rise to a relatively strong anisotropy ($K_h > K_v$), which means that long, shallow flowpaths dominate. These highly transmissive horizontal and sub-horizontal fracture zones also collect groundwater flow from below and probably to a great extent prevent deep groundwater to discharge within the central part of the site investigation area. Instead, the deep groundwater discharges into the Baltic Sea. However, the existence of discharge areas within the investigated site cannot be completely excluded. Data indicate prevailing downward vertical flow gradients from the Quaternary deposits to the bedrock within the area of the planned repository, but evapotranspiration induced flow may change these directions during dry conditions in some areas.

Finally, the flow systems around and below the lakes seem quite complex. The chemistry of the water below the lakes indicates a very limited flow, since relict water of marine origin is found. The wetlands can either be in direct contact with the groundwater zone and constitute typical discharge areas or be separate hydrological systems with low-permeable bottom materials and with little or no hydraulic contact with the underlying aquifer.

2.4 Hydrogeochemistry of major elements

The chemistry of groundwater is of special interest since it may give an insight into the radionuclide retention capacity of the Quaternary deposits. The main features are briefly summarised here, and for detailed descriptions of the water chemistry the reader is referred to /Tröjbom and Söderbäck 2006/, /Tröjbom et al. 2007/ and /Laaksoharju et al. 2008/, of which the first and the second are focused on the surface system and the third on the deep rock.

In an initial characterisation, waters in the Forsmark area were subdivided into surface waters (lakes and streams) and shallow groundwaters. The latter type basically refers to waters flowing through the Quaternary till, since they have been collected at shallow depths (< 10 m).

Marine remnants in the regolith, as well as modern seawater intrusions, strongly influence the hydrochemistry, especially in areas at low altitude close to the coast. Accordingly, the shallow groundwaters and some lake waters in the Forsmark area are characterised by different degrees of mixing with seawater (Figure 2-2). Other characteristics of the waters in the area are high pH values and particularly high concentrations of calcium and bicarbonate (Figure 2-3). In the Piper diagram (Figure 2-4) it can be observed that most shallow groundwaters are calcium-bicarbonate type, while surface waters range from calcium-bicarbonate to sodium-chlorine type.

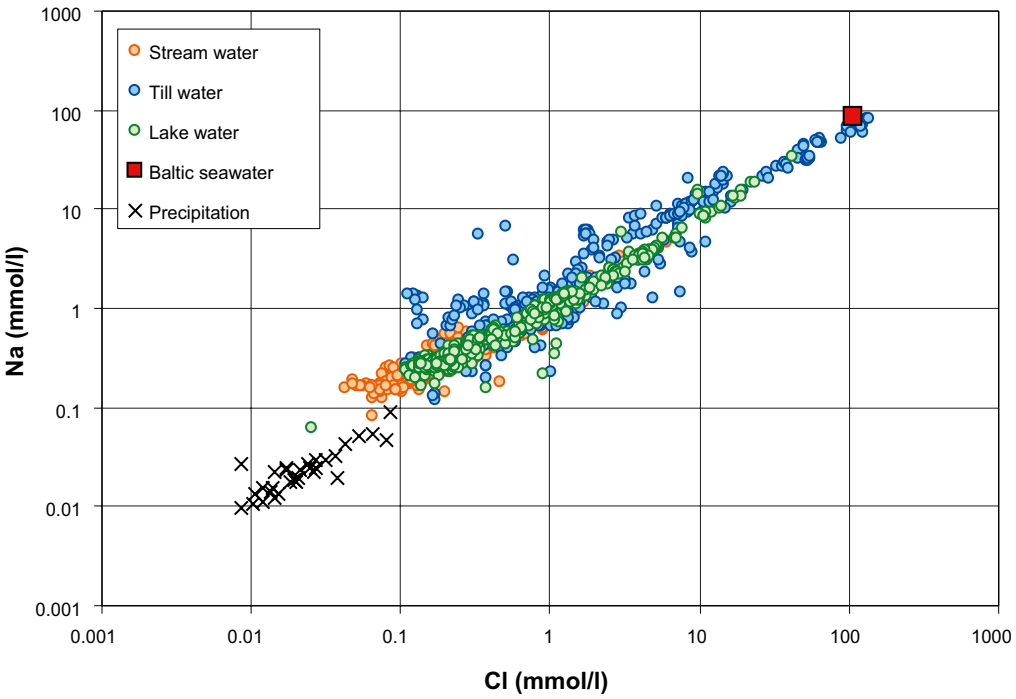

Figure 2-2. *Na vs. Cl plot of surface waters and shallow groundwaters in the Forsmark area.*

Some surface waters show large seasonal changes in many ions, such as Cl, Br, Na, K and Mg (see Figure 2-3 in /Grandia et al. 2007/). These changes were interpreted as saline inflows from relict or present-day seawater (e.g. in Lake Bolundsfjärden). Similar large variations are not as evident in individual shallow groundwater sampling points /Grandia et al. 2007/.

Lake waters also show a very large seasonal variability in both Ca^{2+} and HCO_3^-, which is caused by organic activity: the loss of dissolved CO_2 due to photosynthetic activity in summertime leads to a decrease of bicarbonate, favouring calcite dissolution, and thus increasing pH. In periods of low organic productivity, putrefaction releases CO_2 and pH decreases /Grandia et al. 2007/. The inverse correlation between pH and bicarbonate and the positive correlation between calcium and bicarbonate in Forsmark lake waters can be observed in Figure 2-3. The same positive correlation between calcium and bicarbonate can be observed for stream waters, although the effect on pH is not as clear as for lake waters.

According to the HCO_3^- versus Ca relationship, the shallow groundwaters can be subdivided into two groups: GROUP-1 waters show a trend equivalent to that of stream waters, whereas GROUP-2 waters follow a trend of increasing calcium but decreasing bicarbonate concentration (Figure 2-3B). Interestingly, most GROUP-1 waters are diluted (with chloride and sodium concentrations close to that from surface waters) and GROUP-2 waters follow a mixing trend between surface waters and present/ancient seawater (Figure 2-2).

According to the evolutions depicted in Figure 2-3, one of the most significant geochemical processes affecting surface waters during their infiltration to the sub-surface system can be identified. The increase of calcium and carbonate in GROUP-1 and the more or less constant pH (7–7.5) can be interpreted as a result of organic matter degradation as the main process controlling the evolution of these waters.

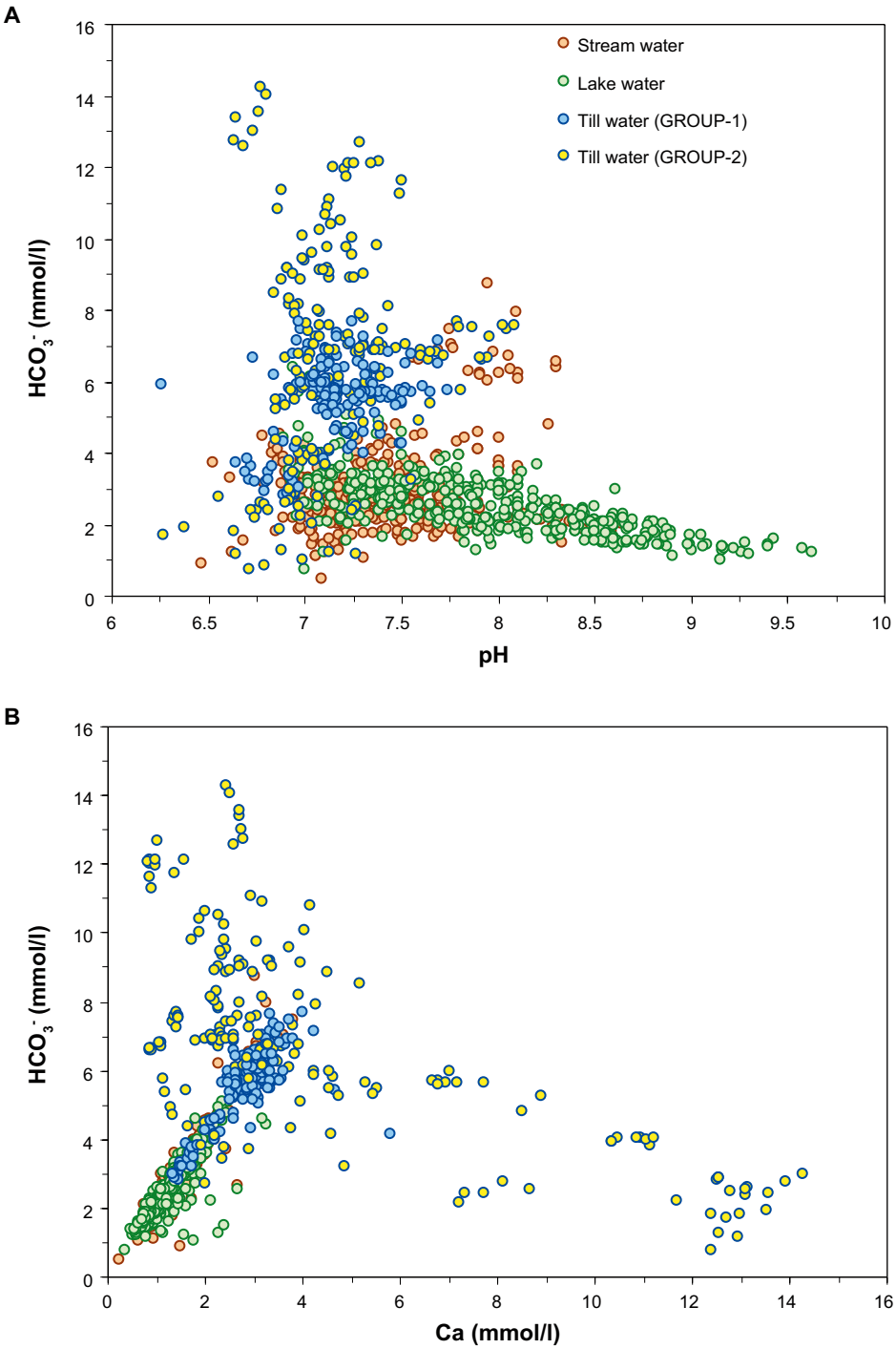

Figure 2-3. *(A) HCO_3^- vs. pH and (B) HCO_3^- vs. Ca plots of surface waters and shallow groundwater in the Forsmark area.*

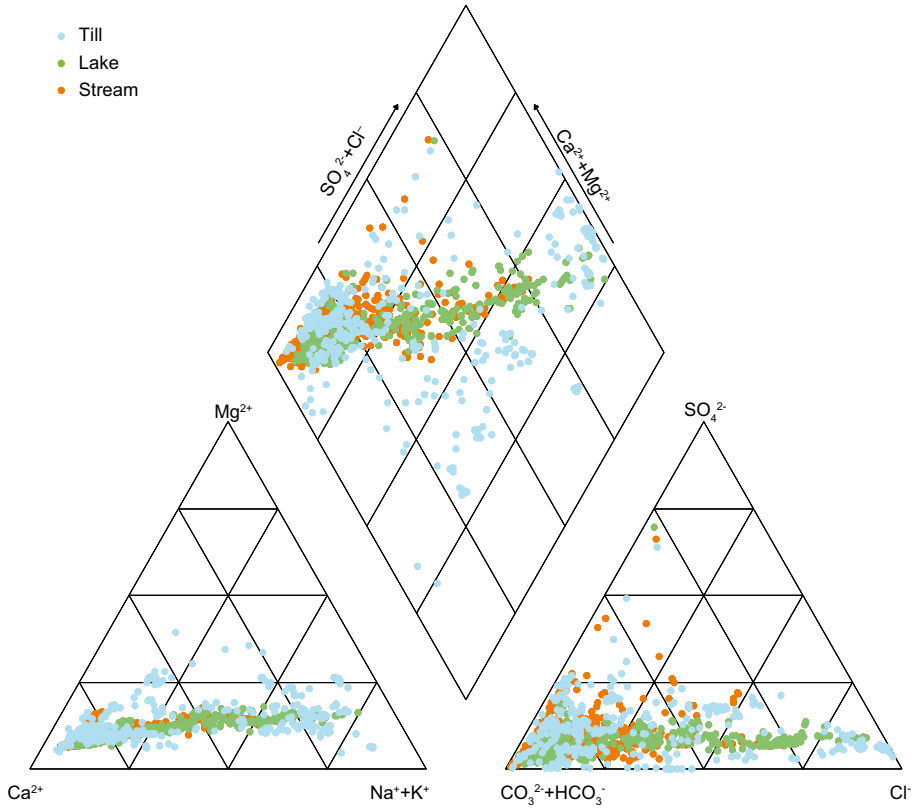

Figure 2-4. *Piper diagram representing the surface waters and shallow groundwater major composition in the Forsmark area.*

Organic matter degradation increases inorganic carbon in solution and produces protons, which triggers calcite dissolution, thus buffering pH and increasing calcium concentration. A mass balance calculation was performed in order to see if other additional processes occur in the system. For each mol of calcium increasing in water there is an increase of two moles of carbonate (Figure 2-3B). This is consistent with the degradation of organic matter and dissolution of calcite:

$$CH_2O + CaCO_3 + O_2 \rightarrow 2HCO_3^- + Ca^{2+}$$ Equation 2-1

However, other reactions, such as cation exchange in the clay fraction and dissolution of other minor phases, cannot be disregarded.

The evolution of GROUP-2 waters is clearly the result of the mixing with seawater, leading to in an increase of calcium, which results in the oversaturation of calcite. The precipitation of calcite results in a decrease in the carbonate concentration and the pH. It can be expected that cation exchange also affects the evolution of GROUP-2 waters, although the mixing with high salinity water can mask the effect of this process.

Concerning the dynamic redox conditions of the near-surface system, data for lakes in the Forsmark area indicate that the whole water column is under oxidising conditions during periods of high organic production (spring-summer). In winter times low Eh values (down to –270 mV) have been registered in the Forsmark lakes. These reducing conditions, probably resulting from the anaerobic breakdown of organic matter, are favourable to the formation of iron sulphides. On the other hand, shallow groundwaters in the till deposits could have relatively high dissolved oxygen contents (from 9×10^{-6} to 3×10^{-4} mmol/L), although no data are available for most wells.

Fe and Mn concentrations in the studied waters are also of interest, since they can give information on the redox conditions in the studied waters and on the possibility of oxy-hydroxide precipitation. In Figure 2-5 it can be observed how the surface waters have low concentrations of both Fe and Mn, while the till groundwaters have similar low values in some points, but higher values in most cases,

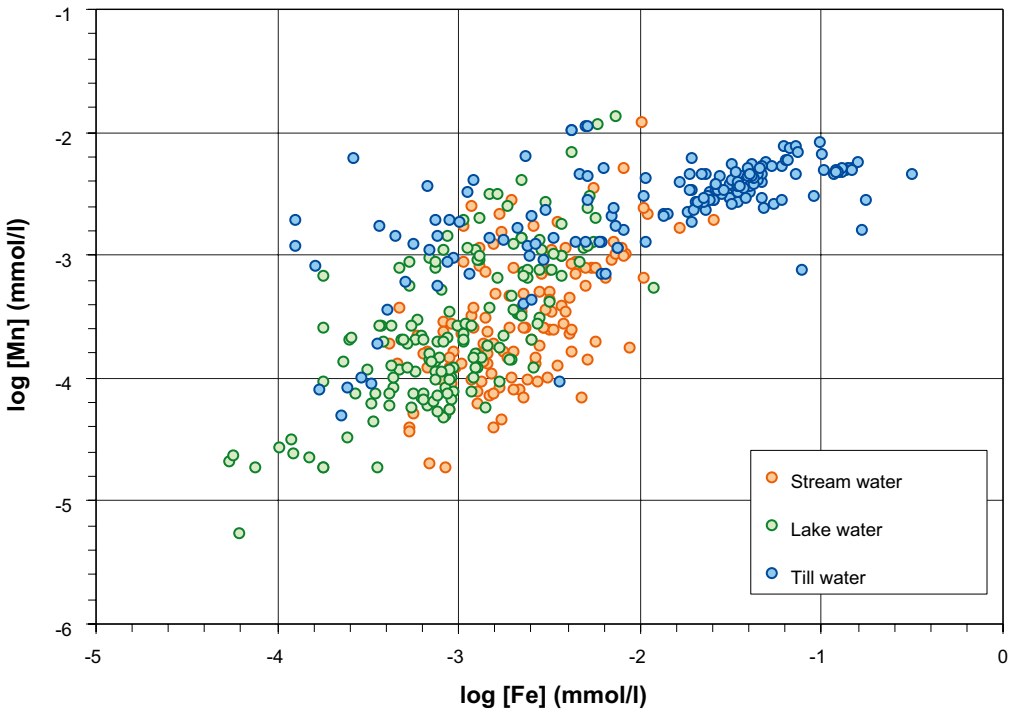

Figure 2-5. *Fe vs. Mn concentrations in the surface waters and shallow groundwaters in the Forsmark area.*

defining a positive correlation. This correlation could be an effect of dilution of deep groundwater with shallow water, however, no clear correlation exists between the concentrations of these elements and the conductivity in the till groundwaters, therefore elucidating the existence of different processes controlling their solubility.

Finally, it is interesting to note the elevated content of dissolved organic matter (DOC) in the surface waters (mean of 1.4 mmol/L), but also in the shallow groundwaters (mean of 1.2 mmol/L). Organic matter may have the ability to transport and/or retain radionuclides and therefore its presence in the studied waters is important.

3 Geochemical behaviour of selected elements

In the Forsmark area, data from lakes indicate that the whole water column is under oxidising conditions during periods of high organic production (spring-summer). These conditions are favourable to the mobilisation of radionuclides but also to the formation of mineral phases able to retain them (mainly Fe-Mn oxy-hydroxides). Instead, in winter times, reducing conditions are favourable to the formation of iron sulphides. On the other hand, shallow groundwater in the till deposits could have relatively oxidising conditions.

The presence of calcium carbonate is thought to buffer the proton concentrations in lakes, wetlands and groundwaters flowing through the till, so that acidic waters are not present in the Forsmark area. In fact, the pH in shallow groundwaters and stream waters in the Forsmark area is mostly between 6.6 and 8.0, while it in the lakes is between 6.9 and 9.6. It is important to keep in mind that the Quaternary deposits could be the last natural barrier for radionuclides and, therefore, a thorough evaluation of the potential retention mechanisms in this zone is relevant.

In order to establish the main chemical constraints of the near-surface system, Pourbaix (Eh, pH) diagrams of the selected radionuclides under the possible chemical conditions of the system are plotted. The diagrams have been obtained with the MEDUSA code /Puigdomènech 2009/, using the SKB thermodynamic database (SKB-TDB). This database is that developed by /Hummel et al. 2002/ with modifications reported in /Duro et al. 2006a/ and some additional updates; the SR-Site version of the database is stored in SKB's document handling system (SKBdoc id 1261302). For some of the radionuclides a revised set of thermodynamic data is used. In such cases, it is indicated in the corresponding section. The major ion composition of water selected to construct the diagrams is from the SFM0032 groundwater monitoring well (sample taken in January 2007).

3.1 Carbon

Carbon is a major constituent of the studied sediments, since both calcite and organic matter are present in the Quaternary deposits, as shown before. As explained in the previous section, surface and near-surface waters show a very large seasonal variability in both bicarbonate and calcium concentrations, caused by organic activity and by calcite dissolution/precipitation processes.

With its half-life of 5730 years and high mobility in the environment, ^{14}C can be a radionuclide of major concern after mixing with stable carbon isotopes followed by the incorporation into biota. Carbon can exist in various oxidation states, from the +IV state (as CO_2, including the carbonic acid species) to the -IV state (as methane). CO_2 is the most stable species under acidic standard ambient conditions, while the fully dissociated carbonate is most stable under alkaline conditions. Under strongly reducing conditions, methane is thermodynamically stable for the full pH range (Figure 3-1), although the reduction of carbonate to methane does not occur in the absence of bacteria under low temperature regimes.

The ^{14}C concentration in groundwater may be influenced by calcite precipitation/dissolution, since C is a major constituent of the calcite mineral structure. Obviously, it can also be incorporated in dolomite and other carbonate minerals. Other geochemical factors that can be taken into consideration are sorption and isotope exchange with the more abundant, stable ^{12}C, see e.g. /Yim and Caron 2006/.

Also, ^{14}C-contaminated methane and CO_2 can be generated through microbial degradation of ^{14}C-bearing organic materials. Under aerobic conditions organic substrates decompose and consume oxygen to produce CO_2; under anaerobic conditions, methanogenic bacteria use hydrogen and carbon to produce methane and CO_2. Gas phase ^{14}C may be available for release at greater rates than would normally be observed through the groundwater pathway /Yim and Caron 2006/. At the same time, if significant amounts of gaseous ^{14}C are released through the air pathway, this will deplete the inventory of ^{14}C available for release through the groundwater pathway.

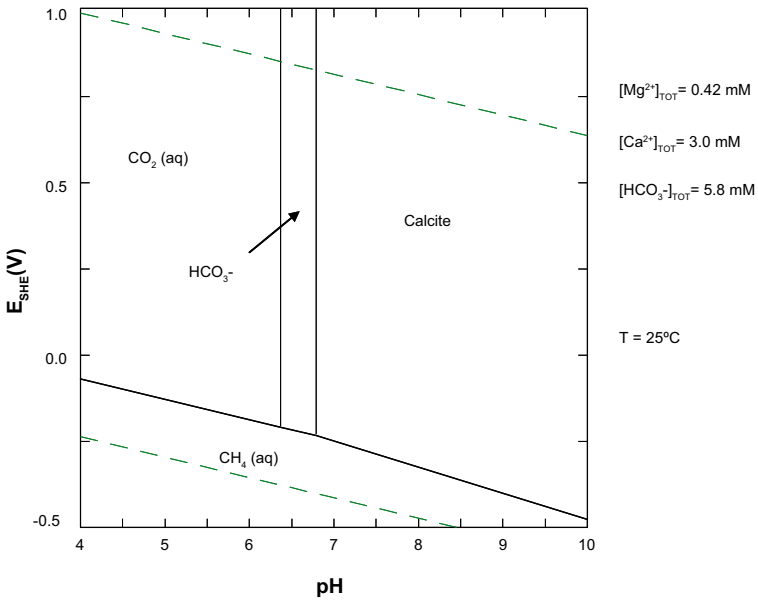

Figure 3-1. *Eh-pH diagram for carbonate in the range of environmental conditions expected in the near-surface system at Forsmark.*

/Killey et al. 1998/ studied a wetland where a plume containing both dissolved inorganic and organic C was discharging, and concluded that most of the radiocarbon found in vegetation had passed through an atmospheric pathway. Results of that study also suggest that plant litter may be the major source of radiocarbon found in the wetland soil, rather than direct sorption of compounds containing ^{14}C dissolved in the groundwater.

3.2 Iodine

The iodine concentrations in lake sediments and wetlands are up to 1.4×10^{-3} mol/kg. Insufficient data are available to establish any clear correlation with chlorine, or with TOC. No data on iodine contents in till from the Forsmark Quaternary system are available in the dataset considered in this work.

Iodine concentrations are up to 6×10^{-7} mol/L in Forsmark surface waters, while in shallow groundwaters they can reach 2.3×10^{-6} mol/L. According to /Grandia et al. 2007/, iodine concentration in shallow groundwaters, like chlorine, is mainly controlled by the contribution of saline fluids of deep or marine origin. However, there is not a clear correlation between iodine and chlorine contents (Figure 3-2), which suggests that in addition to the mixing with saline waters, there are other processes that control the iodine concentration in the near-surface waters at Forsmark.

Iodine is a biophilic and redox-sensitive element and occurs in nature mainly as iodide (I^-) and, under highly oxidising conditions, as the oxyanion iodate (IO_3^-). The stability field of iodide extends almost over the entire pH and Eh range for the thermodynamic stability of water (Figure 3-3), so that iodine is present as iodide in most aqueous environments. Only in marine and highly oxidising environments such as surface waters and some highly oxygenated shallow groundwaters, iodine may be present as iodate. For the calculation of the Eh-pH diagram of Figure 3-3, the SKB-TDB has been used, together with the aqueous species listed in Table 3-1. The species I_2, present in the SKB-TDB, has not been selected.

Organically bound iodine can be a significant fraction of total iodine in aqueous systems and in the atmosphere. For example, methyl iodide is an important gaseous form of iodine in the marine atmosphere and in releases from nuclear fuel reprocessing facilities, while large fractions of iodine were found to be associated with organic matter in fresh, estuarine and surface marine water (/Santschi and Schwehr 2004/ and references therein). In addition, the transformation of inorganic iodide into humic substance/iodine species is thought to be enhanced by microorganisms (/Radlinger and Heuman 2000/ and references therein).

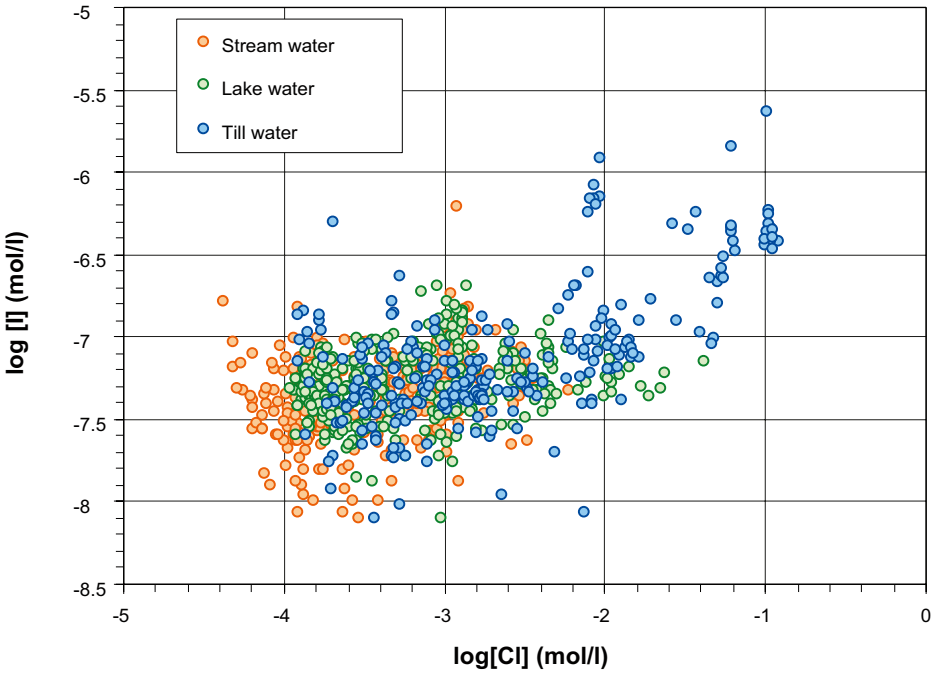

Figure 3-2. *Plot of iodine versus chlorine in Forsmark surface waters and shallow groundwaters.*

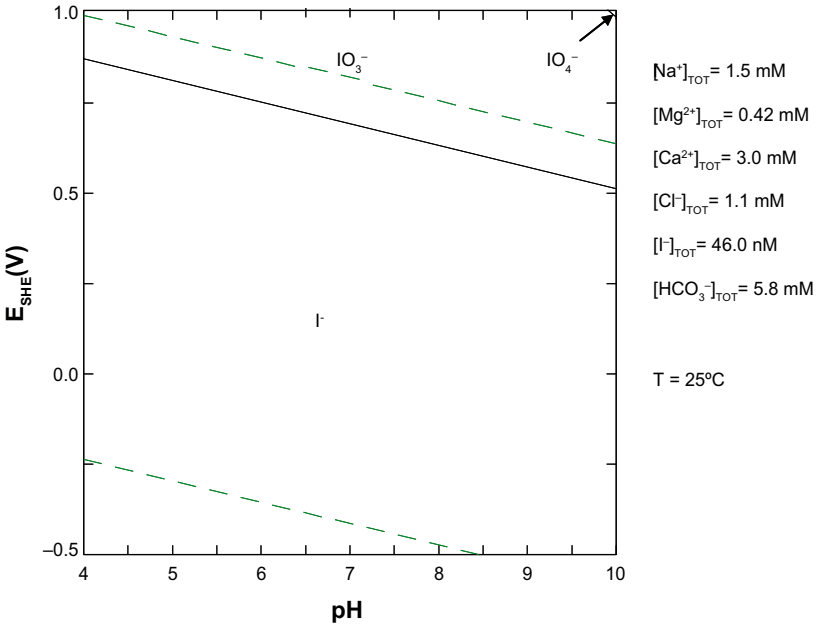

Figure 3-3. *Eh-pH diagram for iodine in the range of environmental conditions expected in the near-surface system at Forsmark.*

Table 3-1. Thermodynamic data of iodine species added to SKB-TDB.

Species	Reaction	log K	Reference	Notes
I_3^-	$3I^- - 2\ e^- = I_3^-$	–18.17	(1)	Replaces that in SKB-TDB
ICl_2^-	$I^- - 2\ e^- + 2\ Cl^- = ICl_2^-$	–26.8	(2)	Added
IO^-	$I^- - 2\ e^- - 2\ H^+ + H_2O = IO^-$	–44	(2)	Added
IO_3^-	$I^- - 6\ e^- - 6\ H^+ + 3\ H_2O = IO_3^-$	–111.56	(3)	Added
IO_4^-	$I^- - 8\ e^- - 8\ H^+ + 4\ H_2O = IO_4^-$	–164.98	(4)	Added

(1) /Johnson et al. 1992/; (2) /Falk et al. 1996/; (3) /Grenthe et al. 1992/; (4) /Cross and Ewart 1991/.

Due to the inherent negative charge of most mineral surfaces at near neutral and basic pH conditions, dissolved iodide and iodate are electrostatically repelled and show relatively weak adsorption behaviour. In general, calcite, silicates and aluminosilicates have low capacities for sorption of I^- or IO_3^-, while reduced metal oxides and sulphides have more potential, although still limited, to sorb iodine /Muramatsu et al. 1990, Fuhrmann et al. 1998, Kaplan et al. 2000/. Conversely, positively charged adsorption sites may exist on the edges of 2:1 clays (such as smectite and illite), on 1:1 clays (such as kaolinite) and on Al and Fe-oxide surfaces /Hu et al. 2005/. Indeed, /Kaplan et al. 2000/ have shown that an appreciable amount of iodine is sorbed onto illite even under alkaline conditions. However, the same authors also evidenced that large amounts of iodide could easily be desorbed from illite with halide salts, which suggests that most iodide was weakly adsorbed. Therefore, if the concentration of competing ions or pH level increases, iodide could easily desorb from illite and presumably from natural sediments.

Interactions between water and soil play a key role in the terrestrial iodine cycle. Especially the chemical forms of iodine in soils and soil water are poorly known, but have great bearing on retention vs. mobility of iodine. All studies show that most of the iodine retained in soil and sediment is sorbed onto organic matter, mainly humic substances, and part of it is also adsorbed on oxides and hydroxides /Schmidtz and Aumann 1995, Hou et al. 2003/. /Whitehead 1974/ carried out iodide sorption experiments in which substantial amounts of iodide were sorbed onto freshly precipitated hydrated ferric oxide from solutions of pH < 5.5, but the amount decreased to zero as the pH approached 7.

/Ashworth et al. 2003/ pointed out that the association of iodine with organic matter may be only temporary, since organic matter degradation over time may alter its ability to retain iodine. Because other soil components appear to have a much lesser affinity for iodine, this could result in iodine re-mobilisation and further upward migration.

Iodide is thought to be less well sorbed than iodate /Muramatsu et al. 1990, Fukui et al. 1996, Yoshida et al. 1998, Hu et al. 2005, Kodama et al. 2006/. Consequently, iodine is thought to have a higher migration potential and bioavailability under anoxic reductive conditions, e.g. /Ashworth and Shaw 2006a/. An accumulation of ^{129}I at the boundary between anoxic and oxic soil regions should also be taken into account in risk assessments, since this could become a significant biosphere reservoir over prolonged time periods, especially in those soils where the water table is, if only periodically, close to the soil surface /Ashworth and Shaw 2006b/.

Sulphate and Fe(III)-reducing bacteria are capable of mediating both direct, enzymatic, as well as abiotic reduction of iodate to iodide in natural anaerobic environments /Councell et al. 1997/. Also illite, montmorillonite and kaolinite show an appreciable capability for iodate reduction, probably mediated by structural iron /Hu et al. 2005/. Other studies have shown the existence of microorganisms capable of oxidising iodide to elemental iodine, which can then bind to metal oxide surfaces as well as to aquatic humic material, see /Councell et al. 1997/ for references.

3.3 Chlorine

In the Forsmark surface waters chlorine concentration ranges from 2.5×10^{-5} to 4.2×10^{-2} mol/L and in shallow groundwaters from 1.1×10^{-4} to 0.14 mol/L. In both cases it is well correlated with Na (Figure 2-2), since both elements mainly derive from seawater. Chlorine is thought to behave mainly conservatively in water, although part of it could be associated to organic matter and retained in soils and sediments (e.g. /Ashworth and Shaw 2006b/). The narrow range of DOC values (mostly between 1 and 2 mmol/L) precludes any correlation with chlorine to be recognised in the Forsmark shallow and surface waters. Chlorine contents in lake and wetland sediments are up to 0.11 mol/kg. No data on chlorine contents in till sediments from the Forsmark Quaternary systems are available in the dataset considered in this work.

Chlorine is assumed to be present in the geosphere as the monovalent anion chloride (Cl^-). Chloride has often been used as a conservative or non-sorbing groundwater tracer, although there is some evidence that it might travel slightly faster than tritiated water as a result of ion exclusion /Ogard et al. 1988/. This high affinity for the water phase results in the solid-solution partition coefficient of chloride

generally being assumed to be zero in soils. Therefore, ^{36}Cl is expected to be one of the most mobile and biologically available important radionuclides in the context of radioactive waste disposal.

Chloride generally occurs as an exchangeable ion in the water adhering to soil particles and free ion following the water movement through soil. However, organic matter may play a role in the formation of organo-chlorine species in soils /Oberg 1998/. A large number of microorganisms can form chlorinated compounds, such as chloromethane, which is highly volatile. Another process that can take place in soil is the microbially induced formation of reactive chlorine, which then chlorinates the organic matter (see /Oberg 1998/ for references). /Lee et al. 2001/ identified associations of ^{36}Cl with low molecular weight fractions of the soil humic substances. However, they also pointed out that even if a substantial fraction of the total ^{36}Cl in the soil is associated with humic substances there is still a proportion that is highly mobile within the soil.

Recently, /Ashworth and Shaw 2006b/ also reported soil adsorption of the ^{36}Cl, and the soil extraction data indicated that the accumulation of ^{36}Cl at the soil surface was accelerated by the fluctuating water table. Since chlorine associated with soil organic matter is likely to exist primarily in the soil solid phase, such conditions would result in a Kd value of chlorine greater than zero.

3.4 Thorium

The thorium concentrations in surface water reach up to 2.4×10^{-10} mol/L, while in shallow Forsmark groundwaters concentrations up to 3.5×10^{-9} mol/L have been measured. Thorium can be complexed with many dissolved species, such as carbonate ions, and can also be strongly associated with organic complexes /Langmuir and Herman 1980/. In the Forsmark shallow groundwaters Th is reasonably well correlated with DOC and iron (Figure 3-4).

Thorium concentration in the Quaternary sediments of Forsmark is between 10^{-5} and 8.6×10^{-5} mol/kg and shows an apparent correlation only with Fe (Figure 3-5), and to a minor extent with aluminium and manganese. Thorium is apparently not correlated with TOC. The SKB-TDB has been used for the thermodynamic calculations, after an update with the recently published thermodynamic review of thorium data by the NEA /Rand et al. 2009/.

Thorium is a non redox-sensitive radioelement. At near-neutral to basic pH and under oxidising conditions, Th can be found as hydroxo-carbonate complexes (Figure 3-6) and under more reducing conditions as hydrolysed complexes. If enough Th is available in the system, precipitation of amorphous ThO_2 can take place under reducing and near-neutral to basic conditions. Under more acidic pH and in the presence of phosphates, a thorium phosphate can form (Figure 3-6).

Th(IV) can be sorbed onto inorganic surfaces, such as silica, clays and Fe oxides, but also onto organic matter. The association of Th with humic acids (HA) is strong and can influence the properties governing sorption on mineral surfaces /Reiller et al. 2002, Reiller et al. 2003/. The strong association of Th(IV) with humic substances has been observed and quantified (see /Chen and Wang 2007/ for references). According to /Langmuir and Herman 1980/ the mobility of Th is enhanced when organic complexes are formed.

Experiments carried out by /Reiller et al. 2002, Reiller et al. 2003/ show that, in the natural pH range, sorption of Th(IV) onto hematite and silica is hindered in the presence of an excess concentration of HA, which likely is due to the complexation of Th(IV) in solution by HA. However, /Reiller et al. 2005/ reported that when HA was added after a 24-hour equilibration of the hematite-Th(IV) system, Th(IV) was barely desorbed from the iron oxide surface. In the case of natural systems, the sorption of tetravalent elements onto hematite could be hindered when the mineral and humic substances are pre-equilibrated before the intrusion of radionuclides in the system.

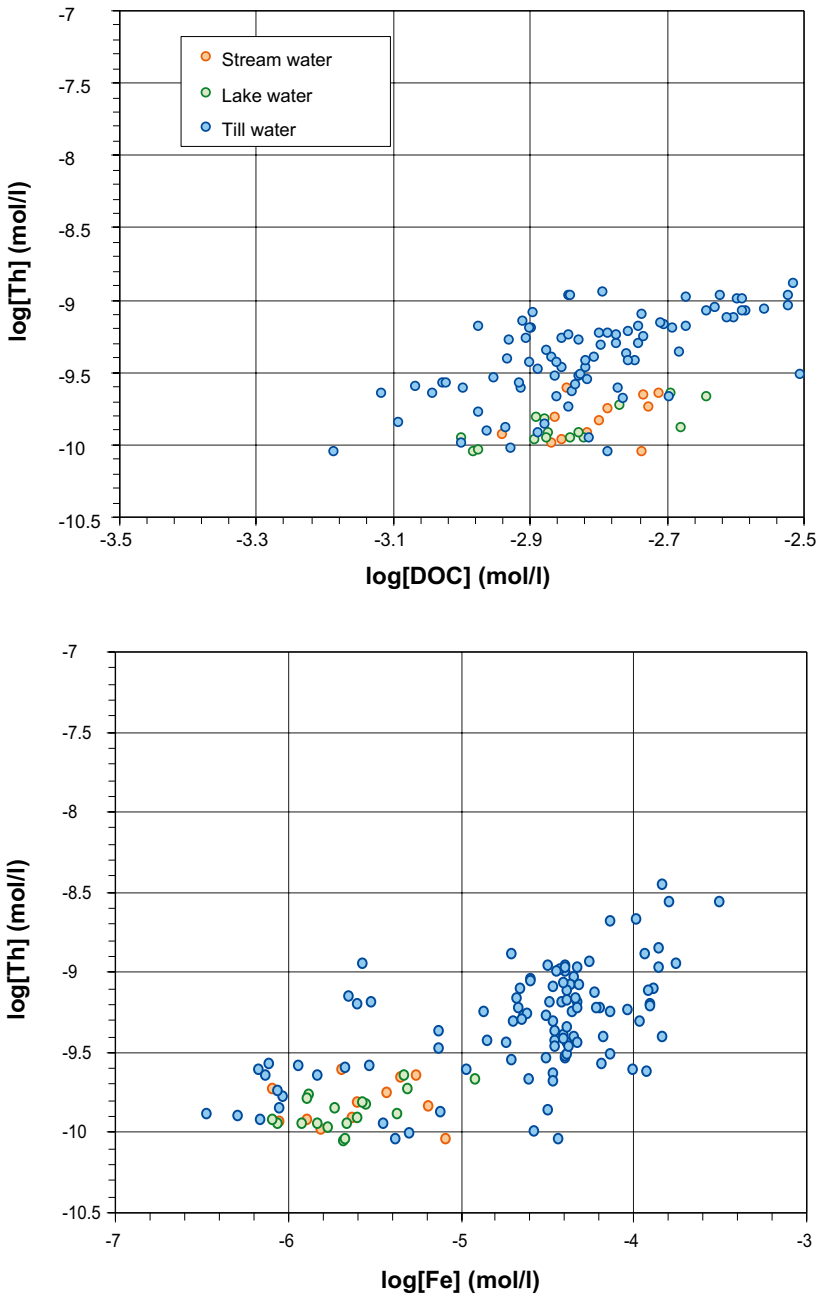

Figure 3-4. *Plot of thorium concentration versus DOC in Forsmark surface waters and shallow groundwater.*

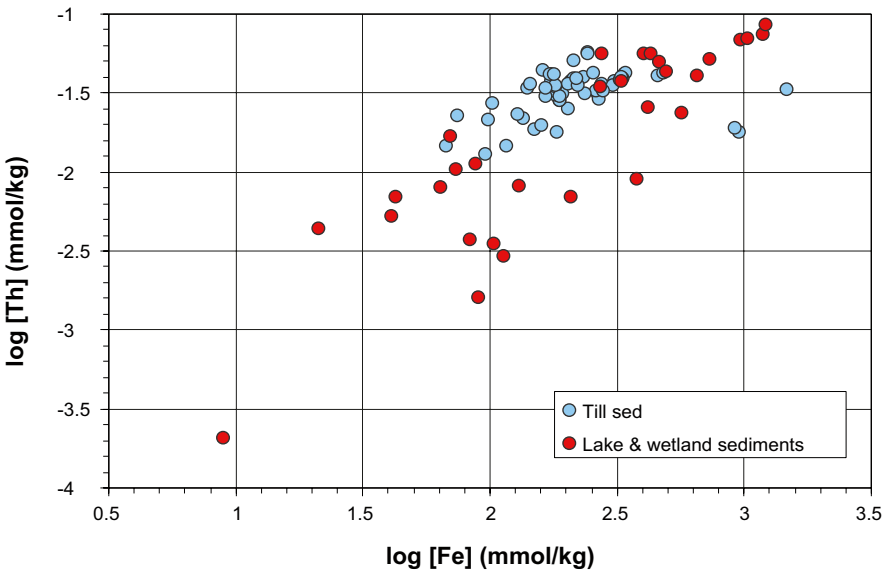

Figure 3-5. *Plot of Th content versus Fe in till, lake and wetland sediments from Forsmark.*

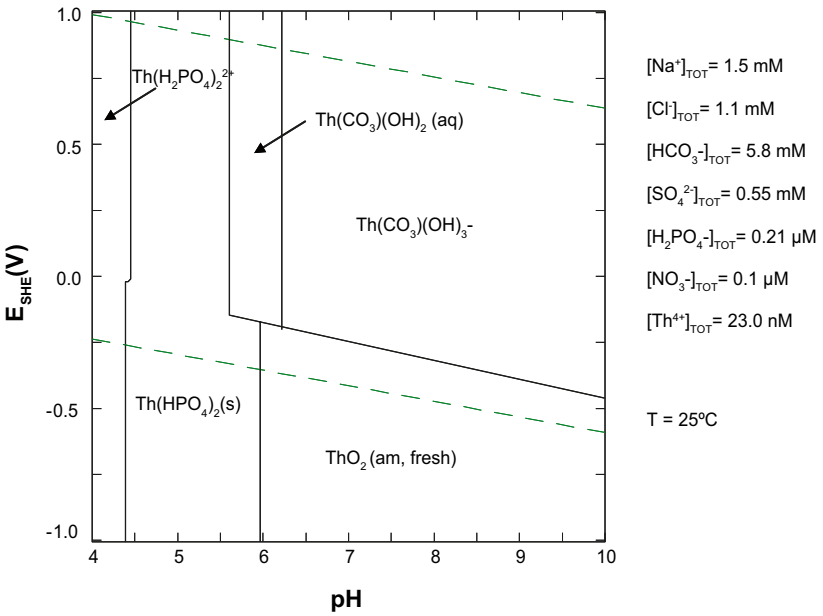

Figure 3-6. *Eh-pH diagram for thorium in the range of environmental conditions expected in the near-surface system at Forsmark.*

3.5 Nickel

In Forsmark surface waters the nickel concentration is up to 5×10^{-8} mol/L, while in shallow groundwaters the levels can be slightly higher, up to 4×10^{-7} mol/L. Ni can be strongly sorbed onto humic substances and it can also be bound to Fe-Mn oxy-hydroxides. However, no clear correlation exists between Ni and DOC or between Ni and Mn in the studied waters. Instead, a positive correlation trend is observed between Ni and Fe in the surface waters, while shallow groundwaters show more scattered data (Figure 3-7). Nickel can be also sorbed on clay mineral surfaces.

The Ni content in the till ranges from 4×10^{-5} to 5.4×10^{-4} mol/kg, and it shows a weak correlation with Al and Fe (Figure 3-8). In the lake sediments and wetlands the Ni content is up to 9×10^{-4} mol/kg, and it also displays some correlation with Fe and Al (Figure 3-8).

For the thermodynamic calculations, the SKB-TDB has been complemented with the selection of Ni species made by the NEA /Gamsjäger et al. 2005/. Nickel is a transition metal mainly found in the +2 oxidation state in aqueous and solid phases. The aqueous nickel speciation is dominated by free Ni^{2+}, while at higher pH it is dominated by $Ni(OH)_2$ (Figure 3-9). In the presence of aqueous sulphide, the solubility of Ni under reducing conditions can be controlled by sulphides (Figure 3-9).

Humic substances play an important role in the binding and transport of metal ions in the aqueous environment and, unlike the adsorption of metal ions onto clay minerals or hydrous ferric oxides, the binding of metal ions with humic substances could take place even at low pH values /Zhou et al. 2005/. According to /Doig and Liber 2007/, Ni^{2+} is more easily complexed with humic acid (HA) than with fulvic acid (FA). /Zhou et al. 2005/ investigated the affinity of three ions with a HA isolated from a soil, which can be expressed as Ni > Ca > Al.

Ni^{2+} is also known to strongly sorb on Al and Fe oxy-hydroxides, e.g. /Ticknor 1994, Scheidegger et al. 1997, Green-Pedersen and Pind 2000/. /Green-Pedersen and Pind 2000/ reported that the sorption of Ni on Fe-oxy-hydroxides increased with both pH and solution concentration. It has been suggested that the sorption mechanism may involve a combination of ion exchange and surface complexation processes.

/Bradbury and Baeyens 2009a, b/ determined the sorption properties of nickel on illite. They quantitatively described the uptake characteristics of Ni, together with Co, Eu, Sn, Am, Th, Pa and U, on Na-illite, with the help of titration experiments and a non electrostatic surface complexation and cation exchange sorption model.

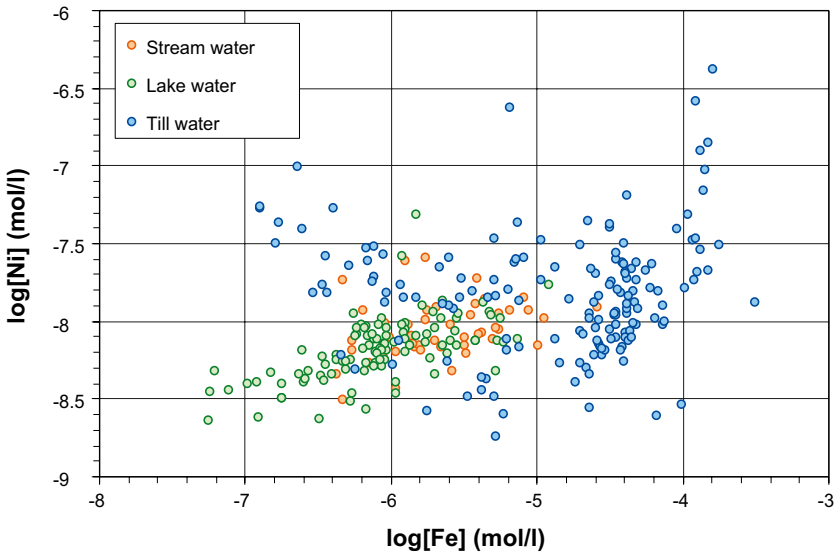

Figure 3-7. *Plot of nickel concentrations versus Fe concentrations in Forsmark surface and shallow groundwaters.*

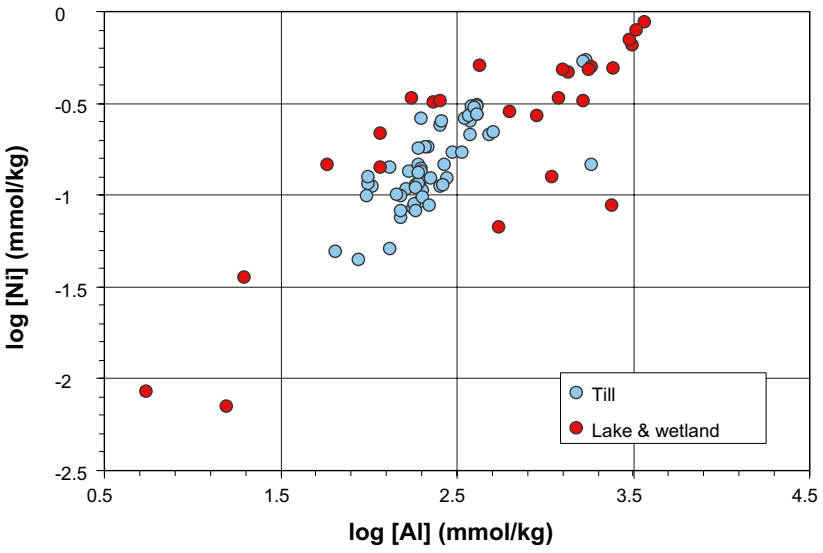

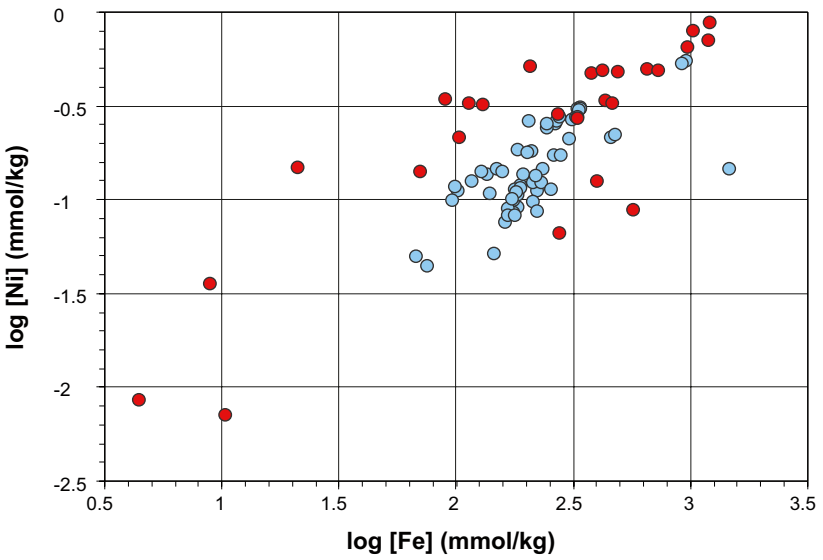

Figure 3-8. *Plots of Ni versus Al and Ni versus Fe in till, lake and wetland sediments in Forsmark.*

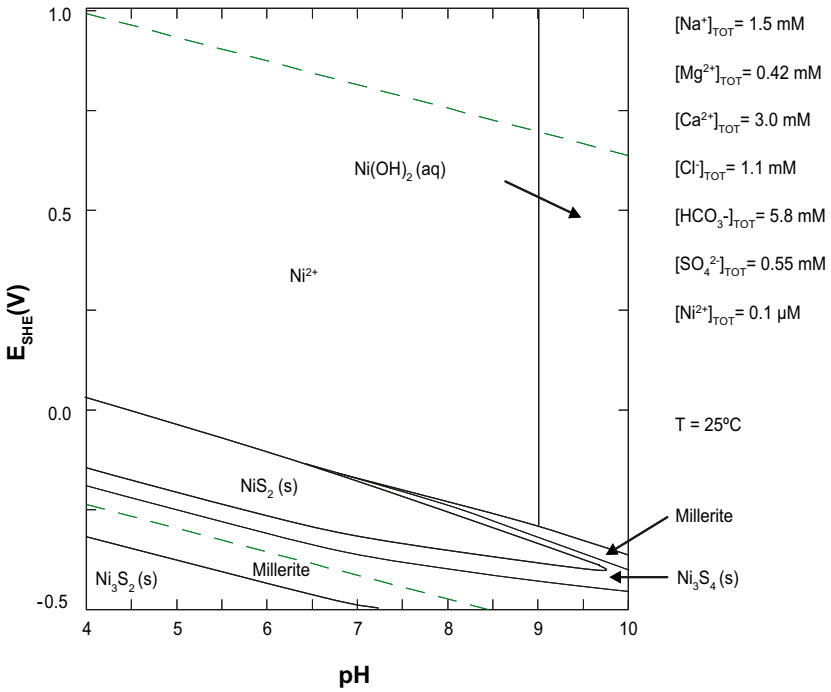

Figure 3-9. *Eh-pH diagram for nickel in the range of environmental conditions expected in the near-surface system at Forsmark.*

In anoxic environments such as wetlands, Ni could be removed from solution in the presence of H_2S and be incorporated as a trace metal in iron sulphides. Also Ni co-precipitation with calcite is likely to be an effective mechanism for reducing Ni mobility in natural groundwater systems (e.g. /Lakshtanov and Stipp 2007/).

3.6 Molybdenum

The molybdenum concentration is up to 2×10^{-8} mol/L in surface water and up to 3×10^{-7} mol/L in shallow groundwater at Forsmark. There is no clear correlation between molybdenum and other major elements in waters from the Forsmark site. Mo concentration in the till and lake sediments is up to 1.4×10^{-5} mol/kg and in wetland sediments it reaches 8×10^{-4} mol/kg. Not in this case either, a clear relationship between molybdenum and other major elements in the Quaternary sediments is observed.

Molybdenum is a transition metal with several oxidation states, i.e. +2, +3, +4, +5 and +6. Dissolved Mo in oxygenated waters mainly occurs in the +6 oxidation state, as the molybdate anion (MoO_4^{2-}). Under reducing conditions the solubility of Mo is mainly controlled by molybdenite (Figure 3-10). Since Mo is not included in the SKB-TDB, thermodynamic data for Mo aqueous and solid species used in the construction of the Pourbaix diagram are summarised in Table 3-2, together with their references.

Molybdenum behaves conservatively in sea water and this is thought to be due to the non-reactivity of the molybdate ion /e.g. Calvert and Pedersen 1993/. In oxygenated marine waters, molybdate displays little affinity for surfaces of clay minerals, $CaCO_3$ and Fe oxy-hydroxides /Goldberg et al. 1998/. However, several mechanisms can play a role in the removal of Mo from the water column, such as fixation in reducing sediments, scavenging by oxides and complexation with humic substances /Dellwig et al. 2007/. In soils, Mo can be sorbed onto Al and Fe oxides and organic matter /Bibak and Borggaard 1994/. Experiments reported by /Bibak and Borggaard 1994/ show that Mo adsorption onto Al and Fe oxides is maximum at pH 4–5, while the Mo absorption capacity of humic acid is high at pH of 3.5, but decreases almost exponentially at increasing pH until pH 7.

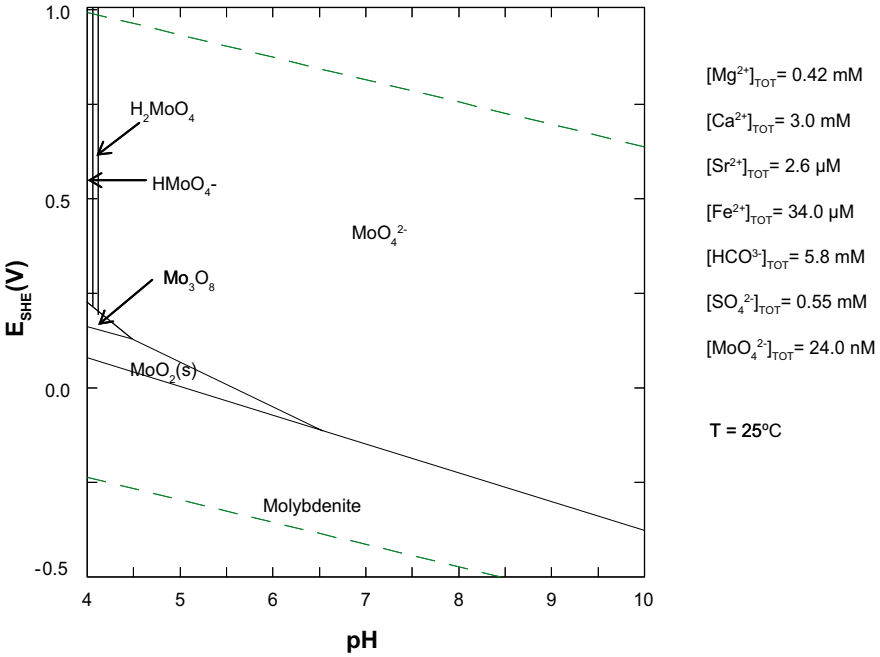

Figure 3-10. *Eh-pH diagram for molybdenum in the range of environmental conditions expected in the near-surface system at Forsmark.*

Table 3-2. Thermodynamic data of Mo species used in the speciation calculations.

Species	Reaction	log K	Reference	Notes
Mo^{3+}	MoO_4^{2-} +8 H^+ +3 e^- -4 H_2O = Mo^{3+}	21.76	(1)	
$Mo_7O_{24}^{6-}$	7 MoO_4^{2-} +8 H^+ -4 H_2O = $Mo_7O_{24}^{6-}$	50.35	(1)	I = 3M
$Mo_7O_{23}(OH)^{5-}$	7 MoO_4^{2-} +9 H^+ -4 H_2O = $Mo_7O_{23}(OH)^{5-}$	57.21	(1)	I = 3M
$Mo_7O_{22}(OH)_2^{4-}$	7 MoO_4^{2-} +10 H^+ -4 H_2O = $Mo_7O_{22}(OH)_2^{4-}$	62.71	(1)	I = 3M
$Mo_7O_{21}(OH)_3^{3-}$	7 MoO_4^{2-} +11 H^+ -4 H_2O = $Mo_7O_{21}(OH)_3^{3-}$	66.48	(1)	I = 3M
$Mo_{19}O_{59}^{4-}$	19 MoO_4^{2-} +34 H^+ -17 H_2O = $Mo_{19}O_{59}^{4-}$	196.3	(1)	I = 3M
$Mo_2O_5(OH)^+$	2 MoO_4^{2-} +5 H^+ -2 H_2O = $Mo_2O_5(OH)^+$	19	(1)	I = 3M
$HMoO_4^-$	MoO_4^{2-} + H^+ = $HMoO_4^-$	4.11	(1)	I = 3M
H_2MoO_4 (aq)	MoO_4^{2-} +2 H^+ = H_2MoO_4	8.15	(1)	I = 3M
H_2MoO_4 (s)	MoO_4^{2-} +2 H^+ = H_2MoO_4	13.17	(2)	
Mo (s)	MoO_4^{2-} +8 H^+ +6 e^- -4 H_2O = Mo	19.58	(3)	
Molybdenite	MoO_4^{2-} +6 H^+ +2 e^- +2 HS- -4 H_2O = MoS_2	69.91	(4)	
MoS_3 (s)	MoO_4^{2-} +5 H^+ +3 HS- -4 H_2O = MoS_3	68.07	(2)	
Molybdite	MoO_4^{2-} +2 H^+ - H_2O = MoO_3	11.98	(5)	
MoO_2 (s)	MoO_4^{2-} +4 H^+ +2 e^- -2 H_2O = MoO_2	29.88	(5)	
Mo_3O_8 (s)	3 MoO_4^{2-} +8 H^+ +2 e^- -4 H_2O = Mo_3O_8	63.56	(6)	
$MgMoO_4$ (s)	MoO_4^{2-} + Mg^{2+} = $MgMoO_4$	0.64	(7)	
$CaMoO_4$ (s)	MoO_4^{2-} + Ca^{2+} = $CaMoO_4$	7.9	(4)	
$FeMoO_4$ (s)	MoO_4^{2-} + Fe^{2+} = $FeMoO_4$	8.35	(3)	

(1) /Cruywagen et al. 1976/; (2) /Bard et al. 1985/; (3) /Wagman et al. 1982/; (4) /Robie and Hemingway 1995/; (5) /Robie et al. 1979/; (6) /Kaback and Runnells 1980/; (7) /Naumov et al. 1974/.

In a laboratory study of various scavenging processes under anoxic "marine" conditions, /Bertine 1972/ found that the most effective short-term Mo scavenging mechanism involved its co-precipitation with iron sulphide. However, over longer timescales, reduction to Mo(V) followed by adsorption on various substrates, including peat, was viewed by the same author as possibly a more important mechanism. /Szilagyi 1967/ showed that humic acids from peat have the ability to reduce molybdate to a cationic form (presumably MoO_2^+) and hence to sorb the species on the time scale of hours without the presence of sulphate-reducing bacteria. This effect is strongly pH dependent, as was confirmed by /Bertine 1972/.

/Helz et al. 1996/ introduced the concept of a geochemical switch, in which HS^- transforms the marine behaviour of Mo from a conservative element to a particle reactive element. In anoxic environments, molybdate in the presence of sufficient amounts of H_2S is readily converted to thiomolybdate, which is scavenged by forming bonds with metal-rich (notably Fe) particles, sulphur-rich organic molecules /Helz et al. 1996/ and iron sulphide /Vorlicek et al. 2004/. The transformation reactions are catalysed by proton donors or by active-surface minerals such as kaolinite /Erickson and Helz 2000, Vorlicek and Helz 2002/. /Tribovillard et al. 2004/ confirmed the enhanced trapping of Mo in the presence of sulphidised OM in ancient marine deposits.

3.7 Niobium

The few niobium concentration measurements available in Forsmark surface waters are below 10^{-10} mol/L (n=9), while in shallow groundwaters they are below 2.5×10^{-9} mol/L (n=6). Dissolved Nb could be bound to humic substances or be associated with colloidal Fe oxy-hydroxides /Åström et al. 2008/. The same authors related the abundance of Nb in the Forsmark waters to its association with Fe. Despite the few Nb data available for Forsmark, a very good correlation is observed between Nb and Fe (Figure 3-11), for both surface waters and shallow groundwaters, while no association between Nb and DOC can be ascertained.

Nb in lake and wetland sediments is up to 2.3×10^{-4} mol/kg and it is well correlated with Fe and Al (Figure 3-12), and to some degree with Mn. No data on niobium contents in till from the Forsmark Quaternary system are available in the dataset considered in this work. For the thermodynamic calculations, the SKB-TDB was complemented with the thermodynamic data on Nb(V) oxides from /Peiffert et al. 1997/. The species NbO_3^- and $NbO_2(s)$ were not selected.

Although niobium exists in all the oxidation states from +5 down to –1, it is mostly found in the pentavalent oxidation state in natural waters. Under near-neutral pH, niobium speciation is governed by the negatively charged $Nb(OH)_6^-$ species and under more basic pH as the $Nb(OH)_7^{2-}$ species (Figure 3-13). If enough Nb is present in solution, the solid species Nb_2O_5 will precipitate at acidic pH, and at higher concentration of Nb, this solid will be also stable at neutral pH.

/Charles and Prime 1983/ carried out a series of desorption tests on silt contaminated with radioactive waste from Sellafield. They concluded that niobium was sorbed chemically or physically in the form of complex hydrous oxides. Niobium desorption with citric acid pointed to Nb existing as a compound precipitated on the surface of the sediment particles (e.g. niobic acid, niobate, or polymeric hydrous oxide), rather than being sorbed onto silt on ion-exchange positions.

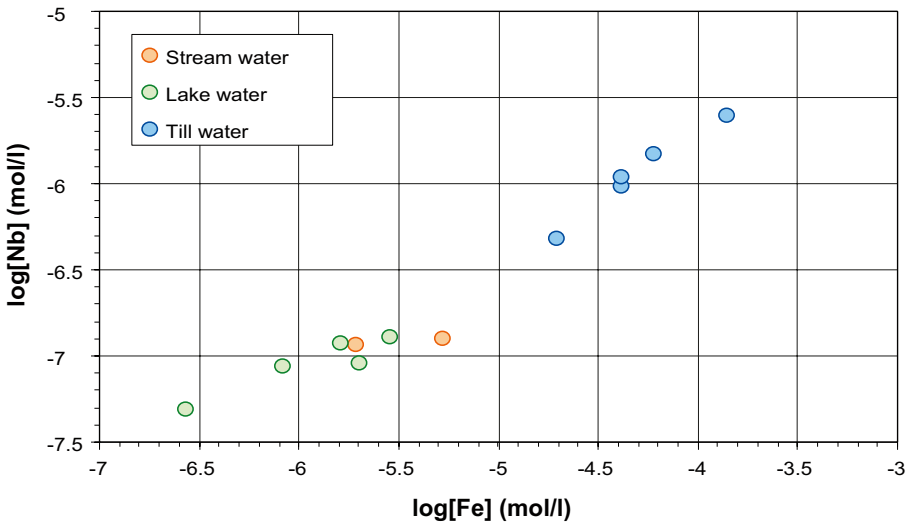

Figure 3-11. *Plot of niobium versus iron concentrations in Forsmark surface waters and shallow groundwater.*

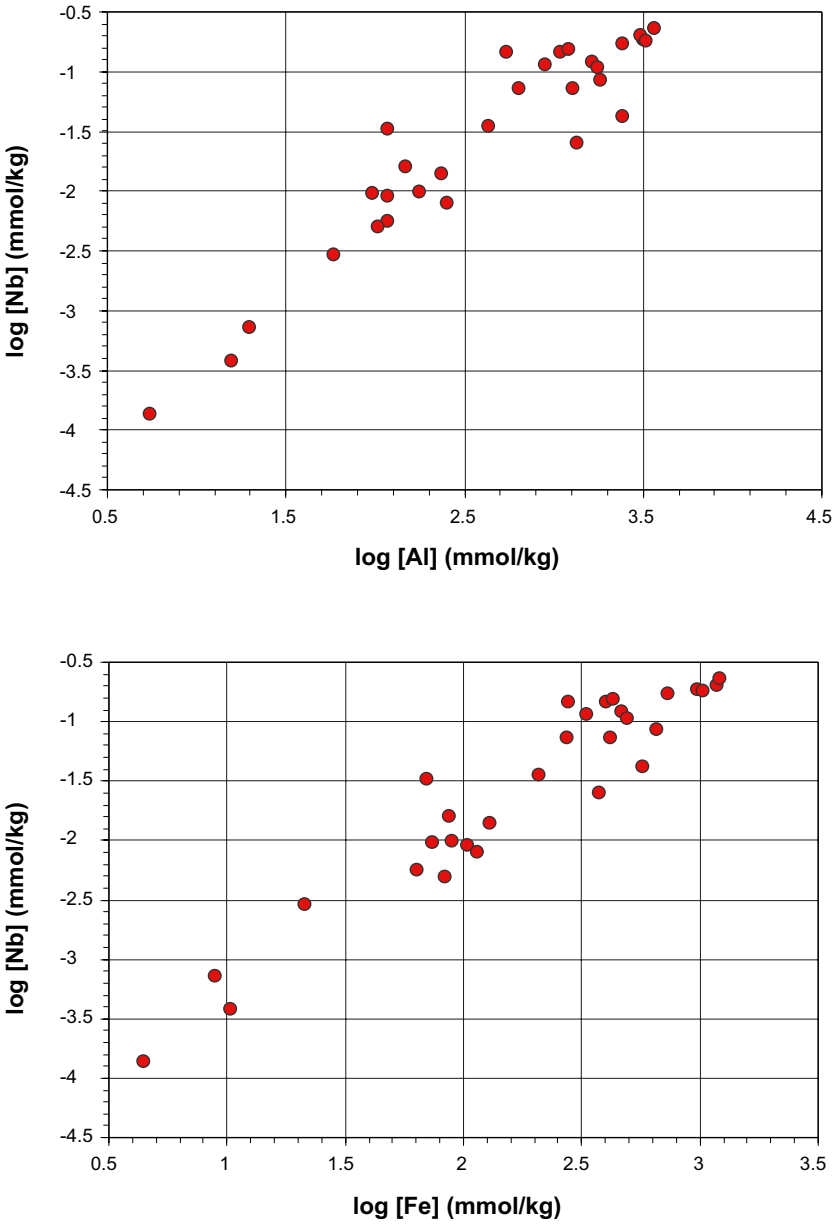

Figure 3-12. *Plots of Nb versus Al and Nb versus Fe in lake and wetland sediments in Forsmark.*

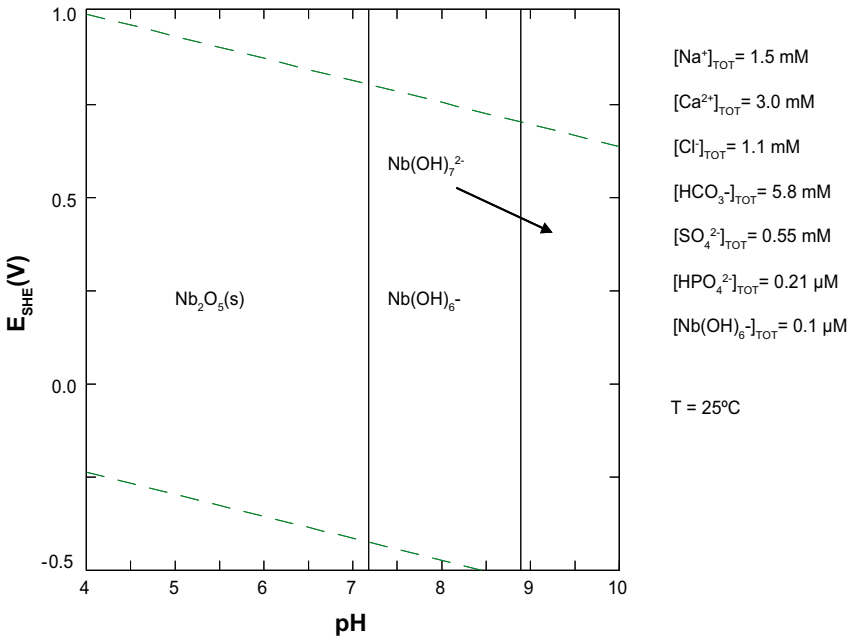

Figure 3-13. *Eh-pH diagram for niobium in the range of environmental conditions expected in the near-surface system at Forsmark.*

/Åström et al. 2008/ analysed stream waters in the boreal zone of Europe and found that dissolved Nb (0.45 µm-filtered) was correlated with DOC and dissolved Fe. According to the same authors, dissolved Nb may thus be bound to humic substances, which have a negative charge in the pH range of the studied waters (4.5–6.2), or be associated with colloidal Fe oxy-hydroxides mixed with the organic compounds. Dissolved Nb concentrations in groundwater in glacial till overlying Proterozoic granitoids are about one order of magnitude higher than in stream waters and are strongly correlated with dissolved Fe. Although Nb can be considered relatively immobile, /Åström et al. 2008/ show that under certain conditions its abundance in the aquatic environment increases; this includes streams rich in dissolved humic substances and Fe-rich groundwaters in glacial till overlying Proterozoic granitoids.

3.8 Selenium

In the area of study, there are reported concentrations of selenium in porewaters from lake sediments. Six data points are available, with values ranging from 7×10^{-10} to 1×10^{-9} mol/L. In general, concentrations of Se in natural waters are lower than 10^{-7} mol/L /MacNeal and Balistrieri 1989/.

Se content in the till is up to 6.3×10^{-6} mol/kg and, like Mo, it does not display any correlation with major elements. Se content in lake and wetland sediments is up to 3.6×10^{-5} mol/kg and the few data available display some correlation with Al, Fe and S (Figure 3-14).

The NEA thermodynamic review on selenium /Olin et al. 2005/ is the main source of thermodynamic data for Se in this study. Selenium is a redox-sensitive element and in aqueous solution it may occur in three oxidation states (–II, +IV, +VI). In surface waters and groundwater dissolved selenium is mainly found as Se(IV) (selenite) and Se(VI) (selenate). Selenate predominates under oxidising and alkaline conditions. Se(–II) is thermodynamically stable in solution under reducing or acidic conditions. At circumneutral pH values, selenium speciation is highly dependent on the redox state of the water (Figure 3-15).

The determination of the selenium speciation is crucial to evaluate the retention potential of near-surface systems. If selenium migrating from the bedrock meets an anoxic near-surface system, it can be reduced and precipitated as native Se or $FeSe_x$ solid phases (where x=1 or 2). The reducing capacity of NOM (natural organic matter) has been observed for Se(IV), which is probably reduced to Se(0) /Bruggeman 2008/.

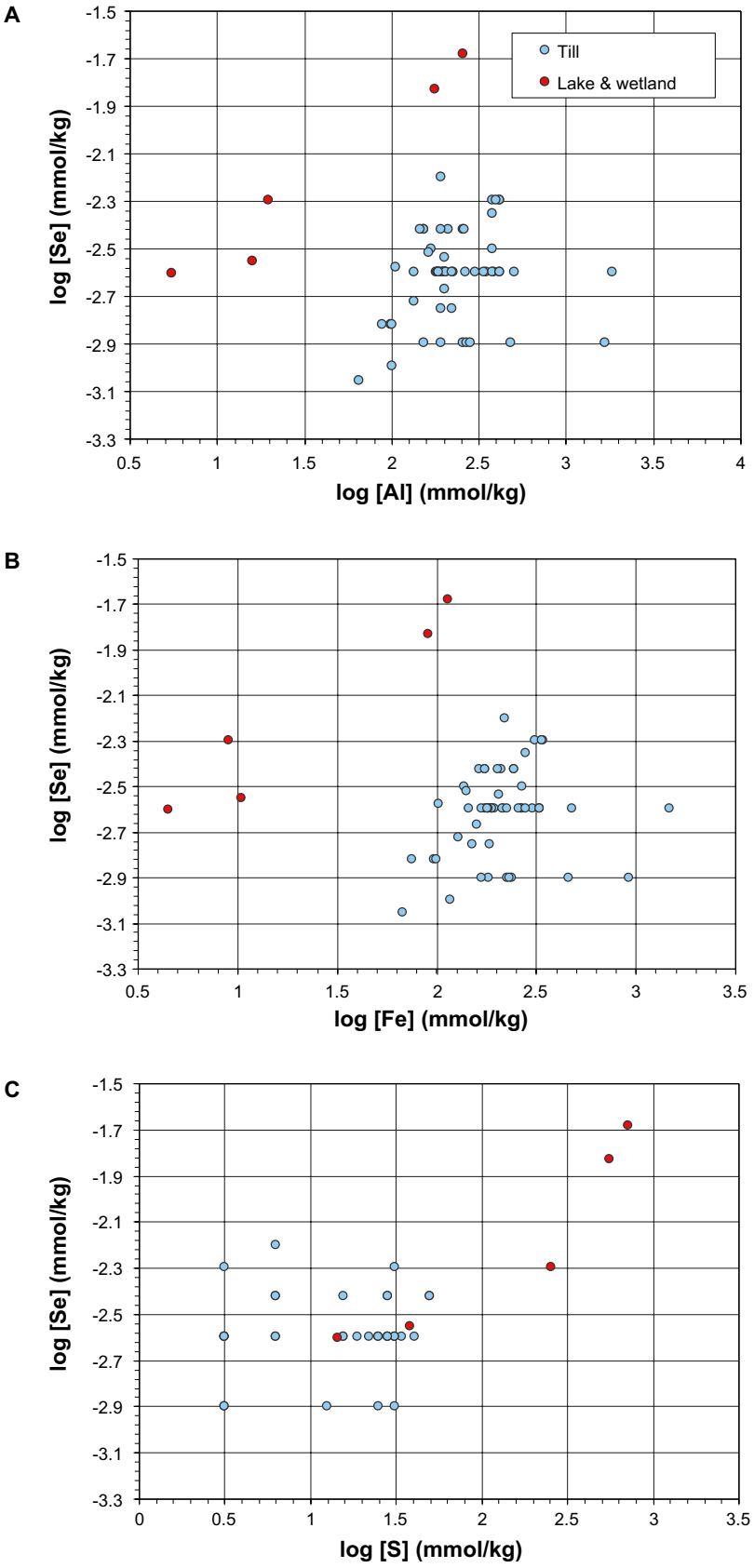

Figure 3-14. *Plot of (A) Se versus Al, (B) Se versus Fe, and (C) Se versus S in till, lake and wetland sediments in Forsmark.*

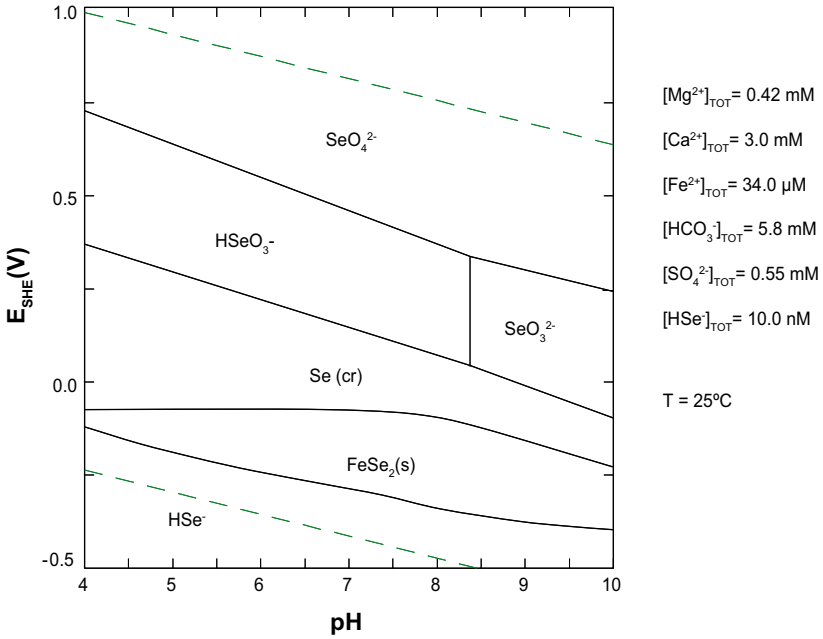

Figure 3-15. *Eh-pH diagram for selenium in the range of environmental conditions expected in the near-surface system at Forsmark.*

Fe(II)-containing minerals also have the capacity to reduce Se(IV), leading to the precipitation of Se(0) and Se(–II) solid phases (e.g. /Scheinost et al. 2008/ and references therein). The microbial reduction of Se(IV) and Se(VI) to Se(0) has been confirmed by several laboratory studies. On the other hand, abiotic reduction of Se(VI) to Se(0) has been reported for green rust only (/Charlet et al. 2007/ and references therein). /Charlet et al. 2007/ studied the reduction of Se(IV) in Fe(II)-montmorillonite systems and observed a significant Se reduction at pH below 7, and the formation of stable and insoluble Se(0) on clay edges.

The solubility-limiting phase of Se in slightly reducing environments may be Se(0) or ferroselite ($FeSe_2$) (Figure 3-15), while in more reducing conditions it would be the $Fe_{1.04}Se$ solid species (Figure 3-16). The precipitation of one or another is not only conditioned by the Eh and pH of the water, but also the concentrations of dissolved Fe(II) and Se will determine the thermodynamically stable Se phase for a specific Eh and pH. This is important in the solubility assessment of selenium and is evident from field examples; in the "Mina Fe" uranium deposit (Spain) native Se is found in the transition zone between the reduced native ore and the oxidised front /Pérez del Villar et al. 2002/.

Sampled groundwaters in this transition zone plot in the stability field of pyrite. Unfortunately, no Se concentration in groundwater was reported. On the other hand, /Howard 1977/ reported the occurrence of ferroselite in roll front-type uranium deposits in sandstones. Ferroselite was found at the interface between oxidised sandstone (containing goethite, limonite and hematite) and reduced pyritic uranium ore. This implies that selenium and Fe(II) in aqueous solution produced by the oxidation of seleniferous pyrite combined to form ferroselite. Therefore, in this case, ferroselite was stable under conditions more oxidising than those required for pyrite.

Recently, /Breynaert et al. 2008/ studied the solid phase Se speciation after short contact (3 weeks) of selenite with pyrite and troilite. They found that the nature of the sulphide mineral dictated the final speciation, since Se(0) and $FeSe_x$ were formed with pyrite and troilite, respectively. Although the authors do not report experimental Eh data, it is interesting to note that the lower part of the stability field of Se(0) overlaps that of pyrite (Figure 3-16a).

The formation of a $FeSe_x$ phase in the experiments with troilite is consistent with the stability of troilite in a more reducing environment. /Bruggeman et al. 2005/ carried out similar experiments with pyrite, and observed the reduction of selenite to Se(0). Experimental Eh were always above 60 mV and the pH was of 8.2. The authors, however, did not believe the measured Eh and considered the theoretical

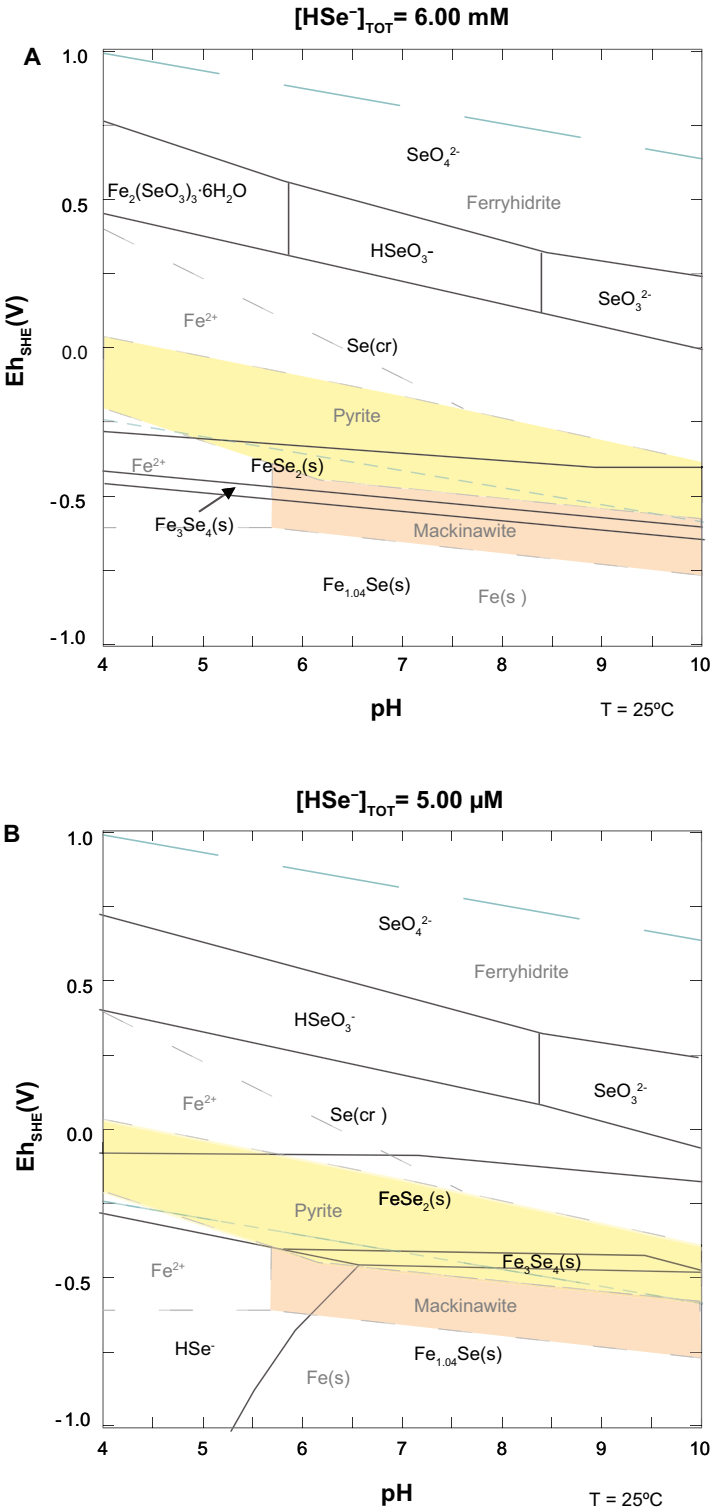

Figure 3-16. *Eh-pH diagrams for selenium and iron, constructed with a concentration of total Fe and total S in solution of 34 µmol and 0.55 mmol, respectively. Concentrations of Se in solution are those reported at the beginning of the experiments of /Breynaert et al. 2008/ (plot A) and /Bruggeman et al. 2005/ (plot B). Stability fields of Se species are limited by black solid lines, and those of iron with grey dashed lines.*

Eh of –290 mV in equilibrium with pyrite. In these theoretical Eh conditions, the expected selenium phase to precipitate would be ferroselite (Figure 3-16b); instead, Se(0) is observed, which is consistent with the measured Eh and pH. This could easily be explained by considering the measured Eh to be true and the possibility that pyrite was in thermodynamic disequilibrium.

Because of the similarity of ionic radius between sulphide (S^{2-} = 1.8 Å) and selenide (Se^{2-} = 1.91 Å), substitution of selenium for sulphur can occur. Mineralogical studies on sulphides reported the incorporation of selenium in the crystalline lattice of sulphides to a maximum of 300 ppm in pyrite and 100 ppm in pyrrhotite /Vaughan and Craig 1978/.

If selenium as selenite reaches oxidised soils and sediments, it can be scavenged by Fe-Al-Mn oxy-hydroxides, e.g. /Duc et al. 2003, Templeton et al. 2003, Peak 2006/, via adsorption as inner-sphere complexes. In contrast, if selenium has been oxidised to selenate, it is not well sorbed onto these phases. Hematite has a strong sorption ability for selenite over a large pH range, from acid solutions to pH 9. The sorption proceeds via a surface complexation process, followed by the precipitation of ferric selenite /Duc et al. 2006/. Selenate and selenite are better adsorbed onto goethite under acidic to near-neutral conditions /Zhang and Sparks 1990, Rovira et al. 2008/.

In calcite-rich till, selenium could be co-precipitated with calcite, although few studies have been focused on quantifying the extent of solid carbonate-selenium interactions. /Lamble et al. 1995/ and /Wang and Liu 2005/ performed with significant success adsorption (co-precipitation) experiments of selenium in calcite, showing the ability of a calcium carbonate lattice to accommodate this element.

The sorption of selenium on organic compounds has long been considered as one of the more significant retention mechanisms, and laboratory and field studies have been developed /Zhang and Moore 1997, Belzile et al. 2000/. Recently, /Chabroullet et al. 2006/ carried out experiments in selenite-doped soils, and determined that most selenium was sorbed in organic particulate. However, they also found a clear correlation with iron and they suggest that adsorption of iron oxides within the particulate could be the real retention mechanism.

It is worth mentioning that some bacteria strains, both aerobic and anaerobic, are able to reduce selenite and selenate and incorporate the reduced Se into cell structures /Garbisu et al. 1996, Lloyd et al. 2001, Siddique et al. 2006/. Methylation reactions are also of importance in the selenium cycle as a mobilisation process. It has been demonstrated that the microbial methylation of Se, by both aerobic and anaerobic bacteria and fungi, can result in the generation of volatile methyl selenide species /Oremland et al. 1989, Masscheleyn et al. 1991, Losi and Frankenberger 1998, Martens and Suarez 1999/. These species can subsequently be oxidised (e.g. by MnO_2), and selenium then be adsorbed back onto the soil.

The studies of selenium retention in wetlands developed by /Zhang and Moore 1996, 1997/ are of particular interest when assessing the conditions in the Forsmark area. They found that the governing processes of selenium retention in wetland sediments were the adsorption onto organic compounds and the bacterial reduction to elemental Se(0). In contrast, adsorption onto oxy-hydroxide surfaces was minor.

3.9 Technetium

Waters and sediments from the Forsmark Quaternary system are considered free of technetium. Technetium is a transition metal of group 7 and the most stable redox states are IV and VII. The solid phase that controls Tc concentration in reduced groundwater is $Tc(IV)O_2(cr)$, while under oxidising conditions the aqueous Tc(VII) complexes are highly stable, mainly in the form of pertechnetate (TcO_4^-) (Figure 3-17). For the thermodynamic calculations, the SKB-TDB has been used, complemented with data on technetium species from the NEA selection /Rard et al. 1999/.

Due to its weak interactions with mineral surfaces, TcO_4^- is considered as one of the most mobile radionuclides in the environment; it is poorly sorbed onto soils and sediments due to their predominantly negatively charged surfaces. In contrast, Tc solubility can be drastically decreased by the reduction of Tc(VII) to Tc(IV).

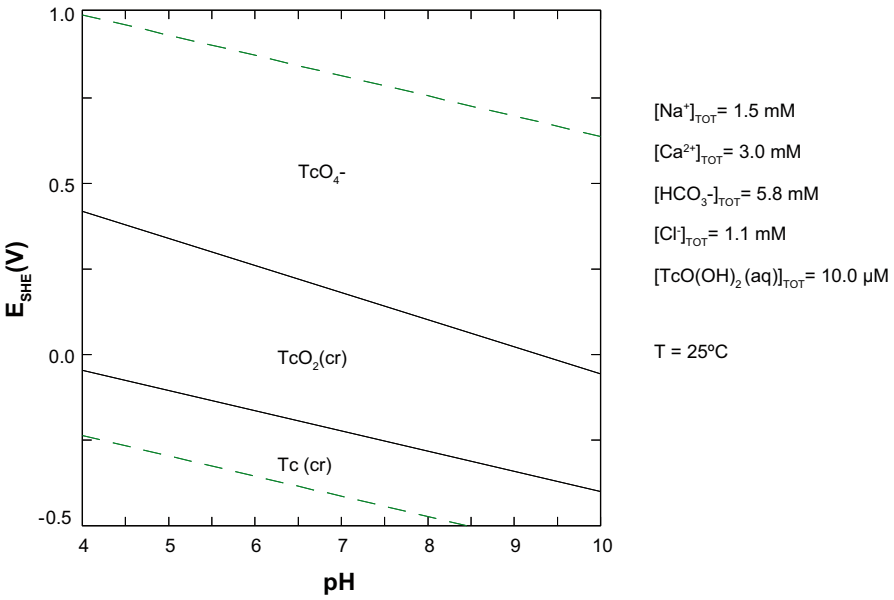

Figure 3-17. *Eh-pH diagram for Tc in the range of environmental conditions expected in the near-surface system at Forsmark.*

Tc(VII) can be abiotically reduced using zerovalent iron or Fe(II)-containing minerals under anoxic conditions (/Farrell et al. 1999/ and references therein) but Tc reduction by aqueous Fe(II) species is highly unlikely /Cui and Eriksen 1996a/. Magnetite has been shown to be a particularly efficient reductant for Tc(VII), with rates of reduction higher than those recorded for the Fe(II)-containing minerals hornblende and chlorite /Cui and Eriksen 1996b/. Green rusts concentrate Tc from aqueous solution, apparently by reduction and formation of strong Tc(IV) surface complexes /Pepper et al. 2003/.

Microbial metabolism may affect Tc speciation by indirect (chemically mediated by either sulphide or Fe(II)) and direct (enzymatic) mechanisms and various bacteria have been reported to possess the ability to reduce TcO_4^- and precipitate Tc(IV) species (e.g. $TcO_2 \cdot nH_2O$) at neutral pH, such as sulphate- and metal-reducing bacteria /Henrot 1989, Lloyd et al. 1999, 2000, 2001, Abdelouas et al. 2005, Burke et al. 2005/. Interestingly, /Wildung et al. 2000/ identified soluble Tc(IV) carbonates as a reaction product in pure culture experiments with *Shewanella putrefaciens*.

Experiments by /Sheppard et al. 1990/ show that under aerobic conditions Tc was not retained by mineral soils and was only retained slightly by organic soil. In contrast, under anaerobic conditions K_d values increased up to 500 fold. Bound Tc(IV) has not been found to reoxidise to mobile TcO_4^- when contaminated soils/sediments /Tagami and Uchida 1999/ and environmentally relevant reduced phases /Cui and Eriksen 1996b, Wharton et al. 2000/ are exposed to oxygen. However, the solubility of Tc(IV) can be enhanced due to the complexation with mobile humic substances /Geraedts and Maes 2008/.

3.10 Strontium

Strontium concentrations in Forsmark surface waters range from 1.3×10^{-4} to 6.9×10^{-3} mmol/L, while in near-surface groundwater they range from 4×10^{-4} to 0.1 mmol/L. The Forsmark near-surface system contains large amounts of calcium carbonate, mainly in till and glacial clay sediments. Consequently, calcite could be considered a highly relevant sink for strontium. Taking into account the interaction between water and the till, a correlation between strontium and calcium is expected. Indeed, when Ca and Sr are plotted together, a clear positive correlation is observed in the stream waters, which is followed by most of the lake waters and roughly by the near-surface groundwaters (Figure 3-18). This relationship is consistent with Sr-bearing calcite from till, confirming the role of carbonate rocks in the strontium transport. Some lake waters and near-surface groundwaters have a higher Sr/Ca ratio, following a mixing trend with more saline groundwaters (Figure 3-18).

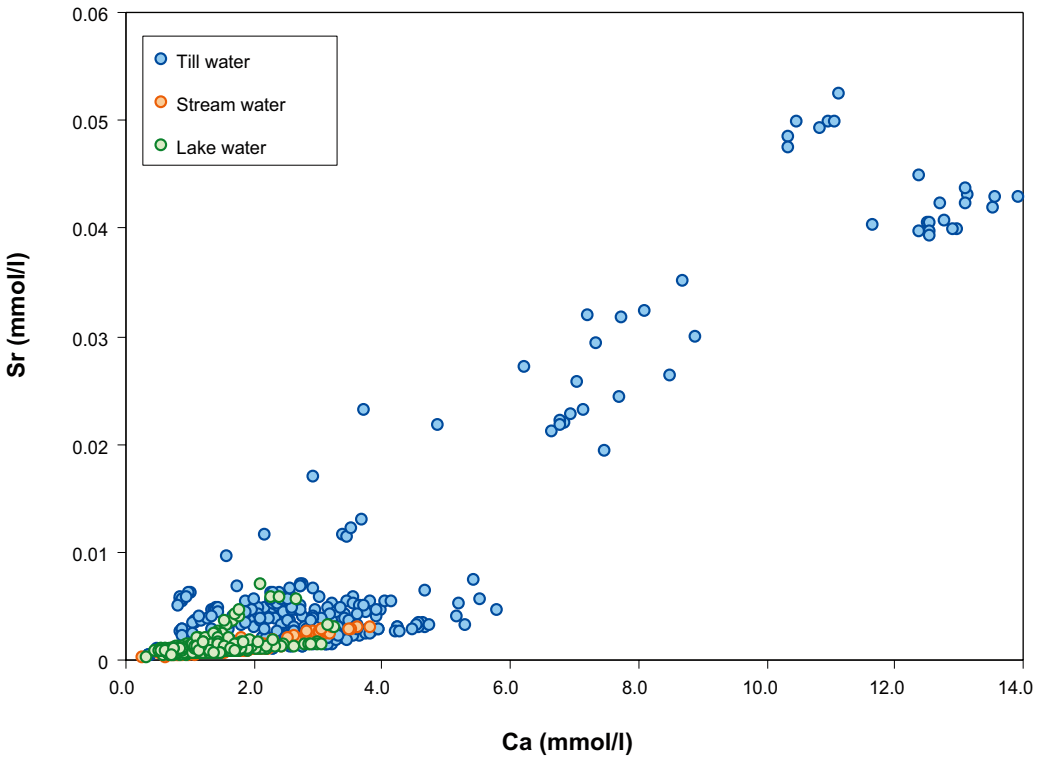

Figure 3-18. *Plot of calcium versus strontium concentrations in Forsmark surface waters and shallow groundwaters.*

The strontium content in the till samples from the Forsmark area is highly variable, between 0.36 and 2.6 mmol/kg but indistinctly linked to calcium. In Figure 3-19 a clear positive correlation is observed between strontium and calcium. This correlation suggests a unique host mineral with a fixed Sr/Ca ratio of 4×10^{-4}. This clear correlation is not seen when comparing strontium with other exchangeable cations in charged mineral surfaces (Na, K and Mg). Moreover, the lack of correlation with K also rules K-feldspar out. Calcite is a reasonable candidate as a solubility-limiting phase for strontium rather than strontium minerals such as celestite or strontianite.

The strontium speciation in most natural waters is dominated by the cation Sr^{2+}. Except in special geological and anthropogenic environments, saturation of pure strontium-bearing phases such as celestite ($SrSO_4$) or strontianite ($SrCO_3$) is rarely attained. Instead, carbonates (especially calcite) are considered the common solubility limiting phases /Lorens 1981, Tesoriero and Pankow 1996, Bruno et al. 1998/. The similar geochemical behaviour of Sr and Ca allows the formation of a set of (Ca,Sr) CO_3 solid solutions. Consequently, calcite-bearing rocks and soils will be favourable host aquifers for radiostrontium retention if saturation of these solid solutions is reached.

Recent studies have shown that strontium can be retained in carbonate minerals that result from biogenic reduction of iron and manganese oxides, following the reaction:

$$CH_2O + 2MnO_2 + 3CO_2 + H_2O \rightarrow 2Mn^{2+} + 4HCO_3^- \qquad \text{Equation 3-1}$$

The bicarbonate production from the reduction may lead to siderite or calcite precipitation, with strontium co-precipitation /Roden et al. 2002/.

The oxides can also adsorb strontium; such adsorption can take place in two steps /Trivedi and Axe 1999, van Beinum et al. 2005/: (1) a rapid and reversible adsorption reaction to the external surface including the macropores, and (2) a slow surface diffusion along the micropore walls of the oxides. In addition to calcite, strontium is known to readily exchange within surface-charged, layered silicates (e.g., montmorillonite, kaolinite and illite, see /Chen and Hayes 1999, Lu and Mason 2001/).

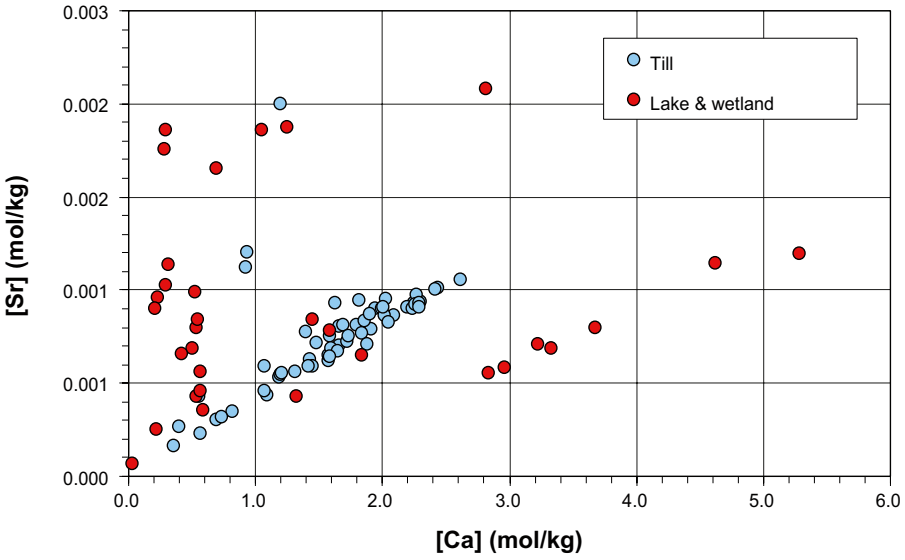

Figure 3-19. *Plot of Sr versus Ca in till, lake and wetland sediments in Forsmark.*

3.11 Uranium

Uranium in shallow groundwaters from the Forsmark area is found in concentrations ranging from 7×10^{-5} to 0.4 µmol/L. This wide range indicates variable redox conditions. Lakes and stream waters have similar uranium concentrations (0.001 to 0.12 µmol/L). Some clues on uranium mobility may come to light by plotting the uranium concentration against ions concentration such as bicarbonate, phosphate, iron and DOC. Uranium is commonly transported forming complexes with these ions; however, none of them shows any clear correlation with the uranium concentration.

The uranium content in the Forsmark till ranges from 0.002 to 0.04 mmol/kg, and in the lake sediments and wetlands it is between 4.2×10^{-5} and 0.4 mmol/kg. Rough correlations are observed between uranium and Fe, Mn and P in till sediments (Figure 3-20), indicating that uranium could be incorporated in Fe-Mn oxy-hydroxides or phosphates. However, the uranium content in the till increases as the sampling depth increases. Considering that no significant differences in mineral paragenesis exist along the till column, this could indicate that uranium is not fixed in oxy-hydroxides but is progressively incorporated into sediments via reduction /Grandia et al. 2007/.

/Grandia et al. 2007/ also found a relatively strong correlation between uranium and sodium in till sediments. One candidate mineral group was proposed to be clays, which could sorb uranium on their surface edges. Some of the wetland and lake sediments follow the trend, while some others, those with the highest Na contents, show an inverse relationship (Figure 3-20).

The uranium distribution in fine-grained sediments shows a marked increase down to depths of 40–50 cm, and a decrease down to 55 cm. These variations could be attributed to changes in the redox conditions, which may cause significant changes in the speciation of uranium

Uranium occurs in nature in two different oxidation states: U(IV) and U(VI). The former is found in reducing environments and the latter under oxidising conditions. U(IV) is rather immobile so that waters with low Eh are not able to transport much uranium ($<10^{-8}$M /Langmuir 1997/). U(IV) solid phases are mainly oxides, especially uraninite (or amorphous analogues, Figure 3-21). Coffinite ($USiO_4{\cdot}n(H_2O)$) is a very common U(IV) phase in many uranium ores but its formation has long been debated.

Direct precipitation from U(IV)-bearing solutions is believed to be kinetically limited, since laboratory experiments failed to synthesise it /Robit-Pointeau et al. 2006/. It is likely that a previous U(VI) reduction step is required before coffinite precipitates /Goldhaber et al. 1987/. The reduction would be favoured by uranyl adsorption onto mineral surfaces and organic matter. Both uraninite and coffinite can be expected to form if uranium from the geosphere, transported as U(VI), interacts with potentially reducing environments.

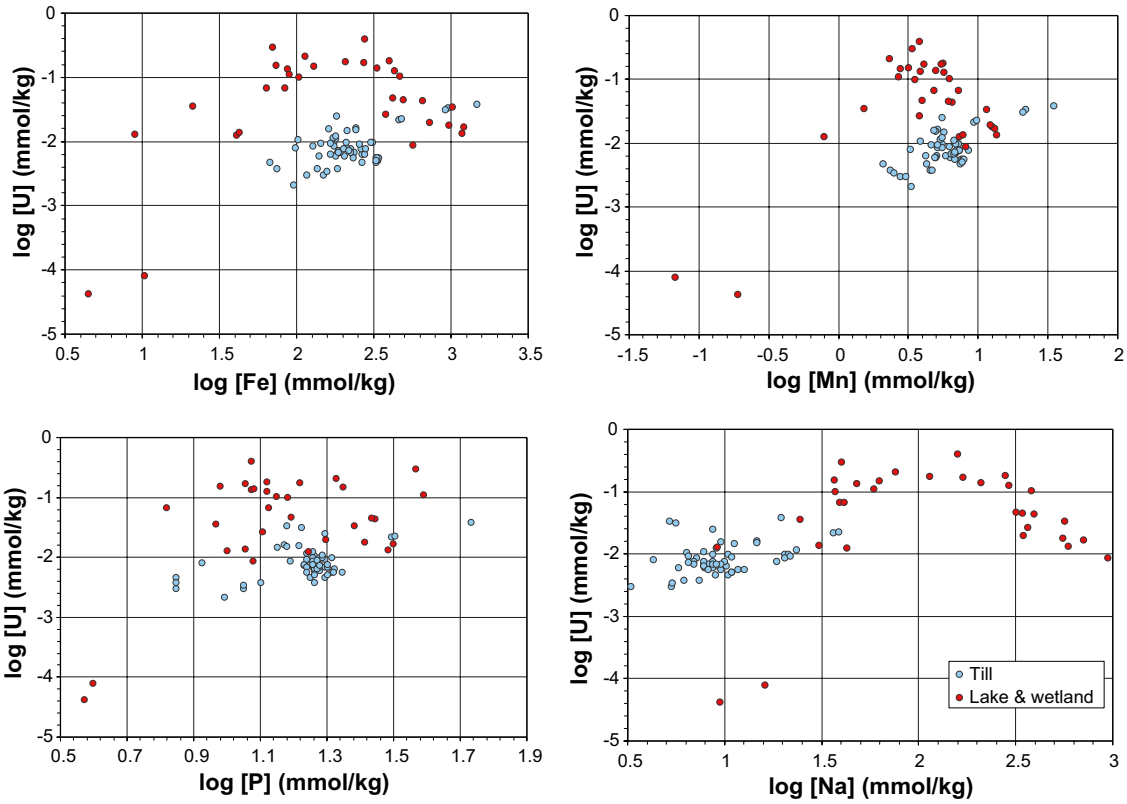

Figure 3-20. *Plots of U versus Fe, Mn, P and Na in Forsmark till, lake and wetland sediments.*

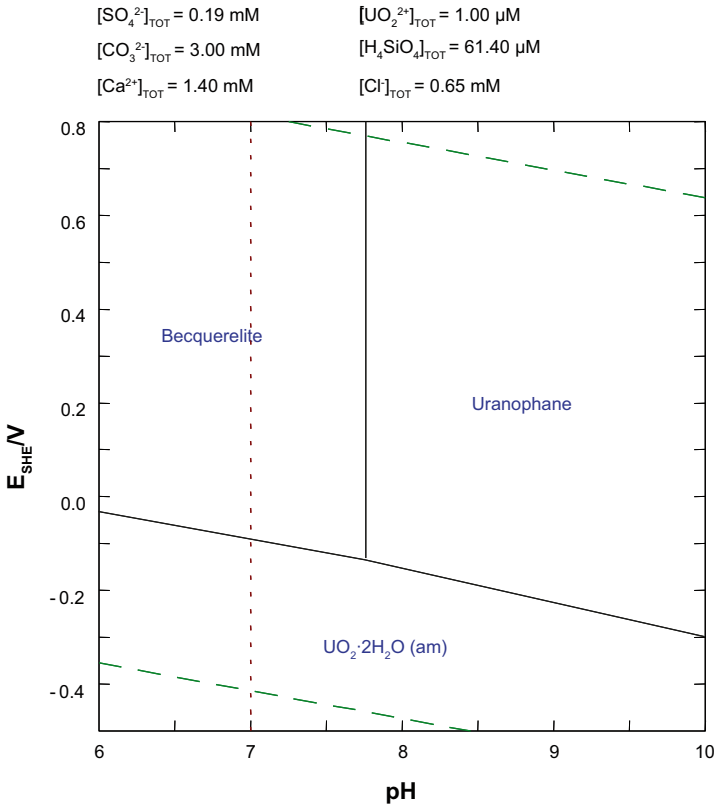

Figure 3-21. *Eh-pH diagram for uranium in the range of environmental conditions expected in the near-surface system at Forsmark. Water composition used for diagram construction is taken from data in Lake Bolundsfjärden (January 2004; /Tröjbom and Söderbäck 2006/). Uranium concentration is 1×10^{-6} M, which is higher than present-day concentrations in surface waters at Forsmark.*

If uranium from repository eventually reaches shallower, oxidising conditions, its mobility is enhanced. Under these conditions, uranium is found as U(VI), forming soluble hydroxide and carbonate complexes at pH>5 (Figure 3-22). At high pCO_2 conditions, U(VI) is mainly transported as carbonate complexes. The presence of CO_2 is, therefore, highly relevant to retention processes at circumneutral pH.

Another important element that commonly forms complexes with uranium is phosphorous. At very high phosphorous concentrations with respect to carbonate ($[PO_4^{3-}]/[CO_3^{2-}]>10^{-1}$), uranium-phosphate complexes predominate over uranium-carbonate complexes /Sandino and Bruno 1992/.

Under aerobic conditions, uranium is commonly precipitated as uranophane ($Ca(UO_2)(SiO_3OH)_2(H_2O)_5$) in silica and calcium-rich waters at neutral to alkaline pH /Finch and Murakami 1999/. At low Si concentrations, becquerelite ($Ca(UO_2)_6O_4(OH)_6{\cdot}8H_2O$) precipitation is favoured /Duro et al. 2006b/ (Figure 3-21). Uranophane can be replaced by soddyite ($(UO_2)_2SiO_4(H_2O)_2$) if pCO_2 is low enough /Finch 1994, Casas et al. 1994/. In many oxidised halos around uranium ores, the occurrence of vanadium in groundwaters forces a quick precipitation of uranium as vanadates (carnotite, $K_2(UO_2)_2(V_2O_8)(H_2O)_3$, tyuyamunite, $Ca(UO_2)_2(V_2O_8)(H_2O)_8$), due to the low solubility of these phases. Phosphates, such as saléeite ($Mg[(UO_2)(PO_4)]_2(H_2O)_{10}$), can be a sink for uranium even if groundwater is, apparently, undersaturated in these phases. /Murakami et al. 1997/ suggested that local release of P adsorbed onto ferrihydrite when this mineral is replaced by other Fe (III) phases (hematite and goethite) could cause uranyl phosphate precipitation.

The co-precipitation of uranium with iron oxides is proven to be a very effective process that controls the uranium concentration in natural waters. Results from projects dealing with natural analogues /Bruno et al. 1998, 2002/ show that uranium concentration in groundwaters flowing through uranium-rich rocks are best explained if mixed Fe(III)-U(VI) oxides are considered as the solubility limiting phases.

U(VI) may be involved in many sorption reactions, especially onto clays /Turner et al. 1996/, aluminium /Pabalan et al. 1998/ and iron oxides /Hsi and Langmuir 1985, Payne et al. 1996, Duff et al. 2002/, hydroxyapatite /Seaman et al. 2001, Fuller et al. 2002, Krestou et al. 2004/ and organic compounds

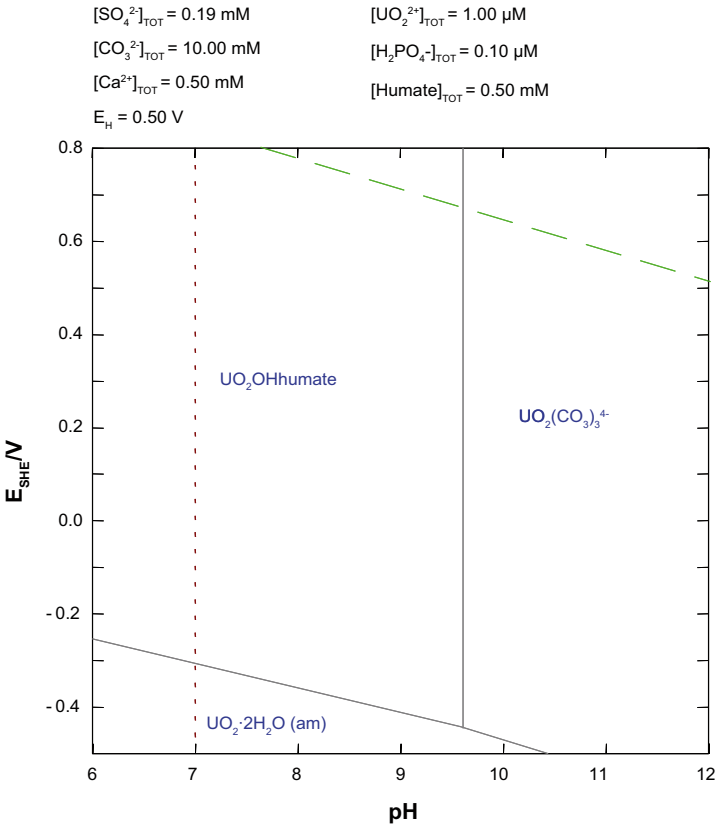

Figure 3-22. *Eh-pH diagram for uranium in water at high P_{CO2} conditions. Total concentration of humic acids is 1×10^{-4} M. Thermodynamic data are based on /Grenthe et al. 1992/ and /Guillaumont et al. 2003/ for the inorganic compounds and on /Lenhart et al. 2000/ for the organic complexes.*

/Lenhart et al. 2000, Reiller 2005/. Recently, /Bradbury and Baeyens 2009b/ reported thermodynamic data for sorption of uranium onto illite, which is the most abundant clay in the near-surface Forsmark environment.

The interaction between uranium and organic substances (Natural Organic Matter, NOM) is still not fully understood. /Reiller 2005/ has recently evaluated the retention of uranium in organic compounds (mainly humic substances) from soils and sediments. In principle, uranium could be strongly complexed by these acids. However, in many surface waters, major cations, especially calcium, are expected to compete with uranium and other trace metals for these binding sites, limiting the organic complexation of these elements.

Speciation of uranium considering humic substances reveals that U(VI) is mainly present as dissolved humates (Figure 3-22). The total concentration of humic acids used in these speciation calculations is 10^{-4} M. This concentration is reasonable, provided the presence of soils with very high contents of organic matter. On the other hand, the complexation of U(IV) with humic acids has not been considered in this plot, since thermodynamic data is much less known than for U(VI).

At more alkaline conditions, mobile carbonate complexes are predominant at relatively high pCO_2, which are expected in lakes due to the organic production. Adsorption of U(VI) onto humic substances seems to play a very significant role in the availability of uranium to metal-reducing microbes, which subsequently may reduce and immobilise it /Gu and Chen 2003/. /Ohnuki et al. 2005/ performed experiments with bacteria and kaolinite to test their affinity for uranium. The results indicate that bacteria mainly retained uranium, which may suggest that in organic-rich environments the organic activity has much more significance than adsorption in common clays.

3.12 Caesium

Data of caesium concentrations are scarce in shallow groundwaters in the Forsmark area, ranging from 5×10^{-11} to 10^{-9} M. Based on the available data, no clear correlations with other ions have been observed. The few concentrations from surface waters that are available are even lower. No data on caesium concentrations in Forsmark till are available. With regard to lake sediments, the concentration of caesium ranges from 0.00075 to 0.076 mmol/kg.

The relevance of caesium for near-surface system studies is mainly based on: (1) the ready incorporation to organisms due to its similarity to K and ammonium, (2) the very high solubility in natural waters, and (3) the concern about the presence in soils of two radioactive isotopes related to nuclear waste and operations (long-lived ^{135}Cs and short-lived ^{137}Cs) /Avery 1996/.

The retention capacity of caesium in soils and sediments is commonly related to some silicates; particularly, the adsorption on zeolites and clays has been long known (e.g. /Sawhney 1972/). Two different mechanisms of retention in clays are known: (1) cation exchange with hydrated cations on planar sites on expansive layer silicates (e.g., smectites), and (2) sorption on wedge or frayed edge sites (FES) in non-expansive phyllosilicates (e.g., mica, illite, kaolinite /Bradbury and Baeyens 2000/.

The most important minerals are 2:1 clays, especially illite and vermicullite, which have large layer charge. /Poinssot et al. 1999/ performed a detailed study of Cs sorption on illite over a range of pH, [Cs] and salinity, and their results showed quick sorption kinetics of these minerals, though Cs^+ competes with K^+ and NH_4^+ for sorption sites /Comans et al. 1989, Shaw and Bell 1991, Poinssot et al. 1999/. /Shenber and Eriksson 1993/ show that ammonium can be more effective than K^+ in competing with caesium for binding sites.

Many studies reveal that the Cs sorption on clays may be strongly reduced by the influence of NOM (see review by /Staunton et al. 2002/). /Hird et al. 1995/ noted that some illite-bearing soils were not able to immobilise much caesium and they suspected that interaction with organic compounds could be responsible for such anomalous behaviour. These suspicions were subsequently confirmed by a number of experimental investigations (see references in /Staunton et al. 2002/). As an example, /Dumat and Staunton 1999/ observed a significant decrease of Cs sorption on illite due to the presence of humic acids. The results from all these studies are in disagreement with recent data from /Loft et al. 2002/. These authors found that illite is able to retain much more caesium than organic substances even at very high concentrations of humic acids.

The adsorption of caesium in other solid soil constituents, such as quartz, carbonates and Fe-Mn-Al oxy-hydroxides is very limited compared with that associated with clays. Consequently, they are usually not considered as relevant sorption phases for caesium in studies of sorption in soil systems.

3.13 Radium

Very few data are available for radium contents in till groundwaters and lake waters. In the former, concentrations of ^{226}Ra up to 0.9 Bq/L have been reported, while in lake waters the ^{226}Ra content is up to 0.5 Bq/L. No data are available for radium concentrations in Forsmark sediments in the dataset considered in this work.

The abundant information from early radiochemical research, natural system studies and anthropogenic systems would indicate that Ra(II) is mainly associated to $BaSO_4(s)$ precipitation. The affinity of radium to barium sulphate was first reported by Marie Curie in her radium discovery work /Curie et al. 1898/. The formation of $(Ba,Ra)SO_4$ solid solutions was thoroughly studied by /Doerner and Hoskins 1925/.

The affinity of the radium ion to the barite crystal lattice comes from the similarity of barium and radium ionic radii (1.36 Å and 1.43 Å, respectively), which means that they are expected to be similarly incorporated in this structure. In addition, the fact that the polarisability of both ions is almost identical indicates a clear preference for Ra^{2+} to substitute for Ba^{2+} in the ionic crystal lattice of Ba(II) sulphate /Goldschmidt 1938/.

Consequently, radium will preferentially be incorporated into barite, lowering the aqueous radium concentrations in equilibrium. The formation of $(Ba,Ra)SO_4$ solid solutions in natural environments has long been known, specially in geothermal areas, where barite was early recognised to be radioactive /Knett 1904/. For a thorough and comprehensive review of the radiochemical and geochemical information concerning the Ra(II) and Ba(II) sulphate solid solution-aqueous system, the reader is referred to the report of /Grandia et al. 2008/.

Besides precipitation as a solid solution with Ba^{2+}, cation-exchange processes on clays could also be an efficient retention mechanism for Ra^{2+}. As in the case of Sr^{2+} and other alkaline earth elements, Ra^{2+} could be readily exchanged on the surfaces of illite, chlorite and kaolinite, among other sheet silicates, e.g. /Shahwan and Erten 2004/, this process being potentially more effective than solid solution with barite.

3.14 Partition coefficients of selected elements

The solid/liquid partition coefficient (Kd) is defined as the concentration of a given element in the solid phase over its concentration in the contacting or pore water, which for solid phase and pore water concentrations in units of mg/kg dry soil and mg/L, respectively, gives a Kd in units of L/kg.

/Sheppard et al. 2009/ reported Kds from three Forsmark soils and sediments, two classified as clayey till, with different proportion of calcite, and the third as peat. The sampling depth was 30 cm. Kd were measured in indigenous elements, and besides, spiking was done to measure Kd for I and Cl (Table 3-3). They made a correction of all Kd values for the soil moisture: $Kd_{(corrected)} = Kd_{(uncorrected)} – MC$, where MC is the soil moisture content (L/kg dry soil) of the soil when dried for analysis.

According to the Kd values of /Sheppard et al. 2009/, Nb, Ni, Th, Cs, and to somewhat lesser extent Mo and U, are strongly retained in the Forsmark soils, while Cl, I and Se are much more mobile. /Sheppard et al. 2009/ also made a comparison with other soils and concluded that the Kd values for these soils fall in the range of other soil Kd values except for Cl, I and Se. Retention of Cl and I seems to be higher in Forsmark than in other soils, while that for Se is lower.

In the present study, Kd values between water and till sediments have been calculated for Ni, Mo, Th, U and Sr. For the Kd calculation, concentrations of the studied element in the solid and the liquid phases are needed. Only in two cases data were available for water and sediments at the same sampling point and depth (or very close to): these are the till samples from SFM0005 and SFM0008. Since several water analyses were available for each point (5 for SFM0005 and 6 for SFM0008), the mean value was used in the Kd calculation. Results are presented in Table 3-4. The calculated Kds are of

Table 3-3. Kd (L/kg) for the elements of interest in this study and other properties of soils from Forsmark (from /Sheppard et al. 2009/, see their work for sampling site locations).

	site A clayey till, fen	site G clayey till, arable	site B peat
pH	6.5	5.5	3.5
Organic C (%)	0.29	1.8	56
Cl native	4.4	12	37
Cl spike	0.017	0.24	3.5
I native	>90	>210	>140
I spike	0.0041	0.069	2.9
Mo	70	240	1200
Nb		36000	
Ni	3800	3000	
Se	10	14	11
Th	31000	250000	34000
Cs	28000	120000	
U	610	3300	1500

the same order to those obtained by /Sheppard et al. 2009/ in Forsmark clayey till soils (Table 3-3). However, some differences exist: the Kds of Ni and Mo are higher in the deeper till sediments, while uranium, according to these results, is less retained in the deeper till sediments than in the soils.

/Engdahl et al. 2008/ reported analyses of water, suspended material, sediments and porewater from lakes in the Forsmark area, in order to provide Kd. At each sampling point, sediment samples from two different layers were collected; one surface layer (0–5 cm) and one layer below the redox-front (at approximately 20–30 cm of sediment depth). In the report the sediments are described as algal mats, with TOC contents between 12 and 36%. Kd values are reported in Table 3-5. These Kd values were also summarised and evaluated by /Sheppard et al. 2009/.

According to the Kds from Forsmark lake sediments (Table 3-5), Nb, Th, Ni and Se are more retained, Mo, U, Cs and I are also retained but to a lesser extent, while Sr and especially Cl are much more mobile. Se is much more retained in these sediments than in the soils analysed by /Sheppard et al. 2009/ and also Ni, Nb and Th have higher Kd values in the lake sediments than in the reported soils and the till samples from SFM0005 and SFM0008.

Table 3-4. Kd (L/kg) in Forsmark till sediments for Ni, Mo, Th, U and Sr.

	Till (SFM0005) 1.5-2 m	Till (SFM0008) 5.5 m
Mo	838	443
Ni	6231	5211
Th	161551	>325000
U	313	154
Sr	723	374

Table 3-5. Kd (L/kg) of the elements of interest in this study in Forsmark lake sediments (data from /Engdahl et al. 2008/).

	PFM000074	PFM000107	PFM000117	PFM000074	PFM000107	PFM000117
Sampling depth	0-5 cm	0-5 cm	0-5 cm	25-30 cm	25-30 cm	25-30 cm
TOC (%) in sed.	36	17	35	30	12	36
Cl	28	7	60	34	11	93
I	384	302	1,133	1,812	1,140	2,471
Mo	3,000	824	478	2,438	2,308	887
Nb	91,667	272,414	72,222	133,333	226,923	81,000
Ni	22,892	9,375	15,789	30,645	31,081	17,647
Se	100,000	9,726	14,815	16,129	9,545	16,140
Th	250,000	185,714	288,889	160,000	218,182	133,333
U	3,265	2,683	1,435	5,200	2,818	2,561
Sr	389	214	282	269	245	355
Cs	9,412	113,333	16,250	13,793	6,857	13,333

4 Conceptual model for radionuclide retention at the Forsmark site

4.1 Overview of processes

From the information summarised in the previous sections it can be concluded that the near-surface system of the Forsmark area consists of three hydraulically and chemically distinct environments:

1) the till,
2) the fine-grained glacial sediments (such as glacial clay),
3) the fine-grained organic matter-rich post-glacial sediments (such as clay gyttja and gyttja clay).

In terms of hydraulic conductivity, the till is much more conductive than the fine-grained sediments. With respect to their chemical composition, the till and fine-grained glacial sediments are rich in calcium carbonate, and the fine-grained sediments are much richer in clay minerals than the till. The post-glacial sediments are especially rich in organic matter.

The capacity of the near-surface system to retain radionuclides via sorption or precipitation strongly depends on the pH and redox state of porewater. Both parameters, together with the water composition, control the speciation of the radionuclides and the stability of the organic and mineral surfaces where they can be sorbed. In organic matter-rich sediments, biological fixation of some radionuclides (e.g. thorium) may be even more relevant than inorganic retention.

The main generic processes producing retention of the studied radionuclides in the environments of interest are summarised as follows.

- Sorption processes.
  - Sorption on organic matter.
  - Sorption on mineral surfaces. The main surfaces that are able to sorb radionuclides and are present in the Forsmark area are those of the clays and the Mn and Fe oxy-hydroxides.
- Precipitation processes.
  - Precipitation of pure solid phases. Despite the very low concentrations at which the radionuclides of interest are expected to occur in the studied environment, precipitation of very insoluble pure phases cannot be ruled out.
  - Precipitation of mixed solid phases, that is, association with major solids and co-precipitation. Main minerals able to host minor components present in the Forsmark area are sulphides, sulphates and carbonates.

Not being a retention process, in some cases dilution will be the main process producing a decrease in the aqueous concentrations of radionuclides in the studied systems.

Finally, decay should not be forgotten, since we are dealing with radionuclides. Due to the very slow decay of most of the studied radioisotopes, their concentrations will not diminish significantly by this process during the 3000 years time period of the numerical simulations (Table 4-1). In the cases of ^{14}C and ^{93}Mo, which have relatively short half-lives, the decrease in their concentrations due to radioactive decay will be 30 and 40%, respectively. For ^{226}Ra and ^{90}Sr, the loss of mass due to decay will be more significant, i.e. 77% and 100%, respectively, in the time span of 3000 years.

Although the half-life of ^{226}Ra is only 1599 years, this radionuclide is a permanent product of the 4N+2 decay chain (^{238}U). This means that the spreading of ^{226}Ra in the near-surface system will not be determined only by the retention processes affecting this particular radionuclide, but also by processes affecting uranium and thorium (i.e. Ra will be produced in the places were U and Th are retained, and depending on its affinity for the surfaces it may be released to the groundwater or not). However, radioactive decay and decay chains have not been implemented in the numerical simulations at the present-day state of development. In this sense, the results of the numerical modeling regarding to ^{90}Sr, will be accurate only at the beginning of the simulation.

Table 4-1. Half-lives (in years) of selected radionuclides and amount remaining after 3000 years of simulation time.

Radionuclide	Half-life (years)	% left*	Source of half-life
Carbon-14	5730	69.56	/Ekström and Firestone 1999/
Caesium-135	2.3E+06	99.91	/Ekström and Firestone 1999/
Chlorine-36	3.01E+05	99.31	/Ekström and Firestone 1999/
Iodine-129	1.57E+07	99.99	/Ekström and Firestone 1999/
Molibdenum-93	4.0E+03	59.46	/Ekström and Firestone 1999/
Nickel-59	7.6E+04	97.30	/Ekström and Firestone 1999/
Niobium-94	2.03E+04	90.26	/Ekström and Firestone 1999/
Radium-226	1599	23.24	/Wieser 2006/
Selenium-79	range of 10^5–10^6	>98	/He et al. 2002, Zhou and Wu 2006/
Strontium-90	28.79	0	/Ekström and Firestone 1999/
Technetium-99	2.1E+05	99.02	/Wieser 2006/
Thorium-230	7.54E+04	97.28	/Ekström and Firestone 1999/
Uranium-235	7.04E+08	99.9997	/Wieser 2006/
Uranium-238	4.468E+09	99.99995	/Wieser 2006/

* % of radionuclide mass remaining after 3000 years.

Obviously, the relevance of one or another retention mechanism will depend on the radionuclide under study. We have seen in the previous chapter that radionuclides present in anionic form in groundwater, such as iodine or selenium, will have low affinity for mineral surfaces, given the expected negative charge of those surfaces in the pH range of Forsmark groundwaters. On the hand, radionuclides of a metallic character, such as thorium, will tend either to sorb or to precipitate. The association of radionuclides to one or another surface is also element dependent. For example, ion exchange processes will be favoured for those radionuclides able to substitute clay interlayer cations, while oxide or hydroxide surfaces will preferably act as sorbents for radionuclides with a stronger tendency towards hydrolysis.

Although a conceptual model of how each radionuclide will interact with the media can be constructed by considering the properties of the geological media and the geochemistry of the radionuclide, our main aim is not only to conceptually indicate the main processes responsible for the retention of radionuclides, but also to quantitatively assess their retention capacities. This quantification needs a parameterisation and, in many cases, the required parameters are not available. Sorption is normally parameterised in terms of the distribution coefficient, Kd. Precipitation needs a value of the solubility constant to be computed, besides the speciation scheme of the solution. Sorption of radionuclides onto inorganic surfaces is easier to study than when organic substances are present. This has to do with the variety and dynamic nature of organic species and of microorganisms, which normally are important in this type of processes.

The information reported and analysed in the previous chapters allows us to briefly present the main processes responsible for the retention of the radionuclides of interest and to indicate which of them have sufficiently good data available to be implemented in the numerical model, and which can be only conceptualised but not numerically simulated. This type of analysis, on an element-by-element basis, is presented below.

4.2 Carbon

In the Forsmark near-surface environment, the concentration of (non-radioactive) carbonate is mainly controlled by carbonate mineral equilibrium, while in surface waters it is driven by organic activity. In the near-surface groundwaters the main processes responsible for the decrease of the concentration of the radionuclide ^{14}C would be dilution, carbonate precipitation and loss due to decay during the simulation period.

4.3 Iodine

The expected major species of iodine in the Forsmark near-surface groundwaters is iodide (I^-). Iodide has less affinity for solid surfaces than iodate, although it can interact with humic substances, especially in the presence of microorganisms. Sorption of iodide onto oxy-hydroxides is not expected at the pH range of Forsmark groundwaters, since most active oxy-hydroxides have near neutral or negative surface charge at the pH of interest.

The degree of iodine retention in soils and sediments is usually reported as a Kd. Kd can be affected by numerous physico-chemical parameters, including sediment type, composition, concentration and surface area, pH, Eh, salinity, biological activity, dissolved organic compounds, and the chemical composition of the solution (e.g. /Bird and Schwartz 1996/ and references therein). Several studies have been carried out on soils in order to determine the effects of these parameters on iodine Kd; to our knowledge, only a few studies of sediments are available.

The available data of Kd for iodine in the area of study are plotted in Figure 4-1. For comparative purposes, literature data on Kd of iodide are also plotted in Figure 4-1. Most of the plotted soils from the literature have a low content of organic matter, in contrast to the Forsmark soils. No clear correlation is observed between the amount of organic carbon and the Kd of iodine. Nevertheless, the samples from Forsmark lake sediments with high content of organic matter have high Kd, reflecting the affinity to organic matter reported for iodide. With regard to pH, no clear relationship is observed between this parameter and the Kd of I (not shown).

Despite the fact that iodine can be sorbed onto organic matter in the Forsmark near-surface sediments, iodine will be considered to behave conservatively in the numerical modelling. Complexation onto organic matter will not be included in the numerical modelling, because no thermodynamic data are available and there are also too many unknowns in the parameters related to the surfaces of the organic matter.

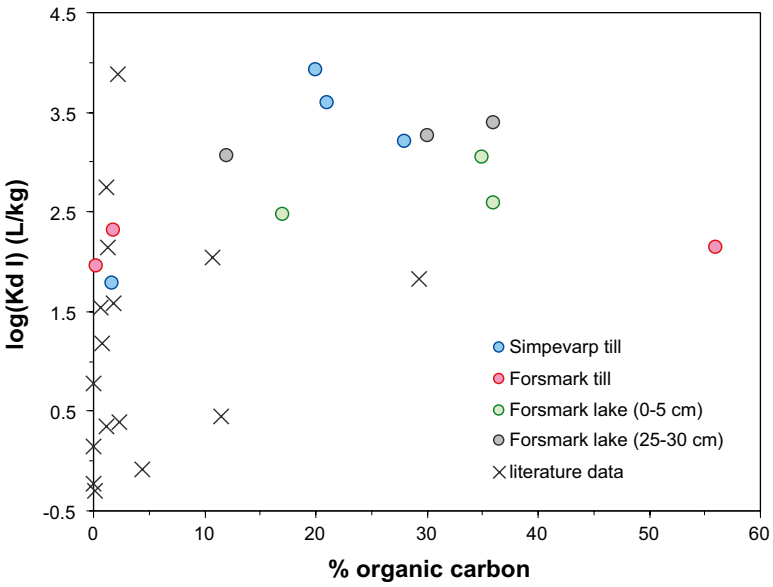

Figure 4-1. *Log (Kd I) versus % of organic C in the sediment for Forsmark and Simpevarp soils and Forsmark lake sediments (see Section 3.14 for references). Also literature data for soils are represented (data from /Muramatsu et al. 1990, Bird and Shwartz 1996, Fukui et al. 1996, Kaplan 2003, Sheppard 2003, Ashworth and Shaw 2006/).*

4.4 Chlorine

Chlorine, in the form of Cl^-, would mainly behave conservatively in the Forsmark near-surface groundwater. Only in wetlands and organic-rich sediments, microbially induced formation of organo-chlorine species could take place and chloride could be partially retained. Chlorine, as iodine, will be considered to behave conservatively in the numerical modelling.

Native Kd in seven Forsmark and Simpevarp soils range from 0.036 to 41 L/kg for Cl, while spike Kd are between 0.017 and 3.5 L/kg /Sheppard et al. 2009/. The highest native Kds correspond to peat soils, in consistence with the fact that only organic matter has an appreciable effect on chloride retention. The desorption (native) Kd values were all higher than the corresponding sorption (spike) Kd values, consistent with the concept that less soluble forms may become more prominent with time. Biological incorporation of Cl by soil microbes or by the plants into recalcitrant organic compounds, which then persist in the soil, could also contribute to this difference in Kd /Bastviken et al. 2007/ and related papers.

The desorption Kd of Cl from Forsmark soils define a positive correlation with organic matter content (Figure 4-2) and an inverse relationship with pH (not shown). In the case of Forsmark lake sediments, the samples with the highest Kd are also those with the highest contents of organic carbon (Figure 4-2).

4.5 Thorium

In the near-surface waters of Forsmark, Th would likely be associated with organic matter. Th can also sorb onto clay minerals and oxy-hydroxides in the oxygenated waters. Due to the low solubility of ThO_2, this phase can also form.

From the available Kd of Th in sediments from the area of study, it can be suspected that Th is at least in part retained by organic matter (Figure 4-3). Nevertheless, for some samples from Forsmark (e.g. till soils), other processes are needed to explain the high retention of Th in the solid fraction. One possibility is the sorption of Th onto illite. In order to test this possibility, Kd calculations were done after equilibrating the till reference porewater used in previous numerical models (see e.g. /Sena et al. 2008/) with a till sediment with 10% of illite, and using the thermodynamic data for Th sorption on illite from /Bradbury and Baeyens 2009a, b/.

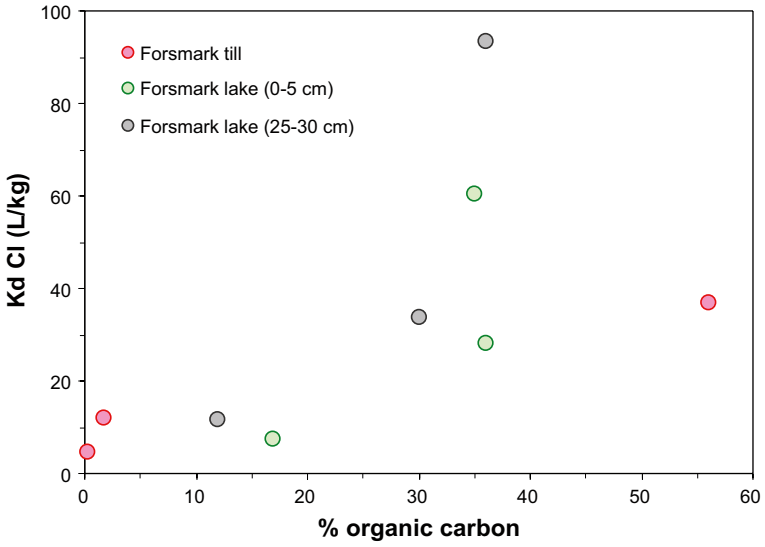

Figure 4-2. *Kd of Cl versus % of organic C in the sediment for Forsmark soils and lake sediments (see Section 3.14 for references).*

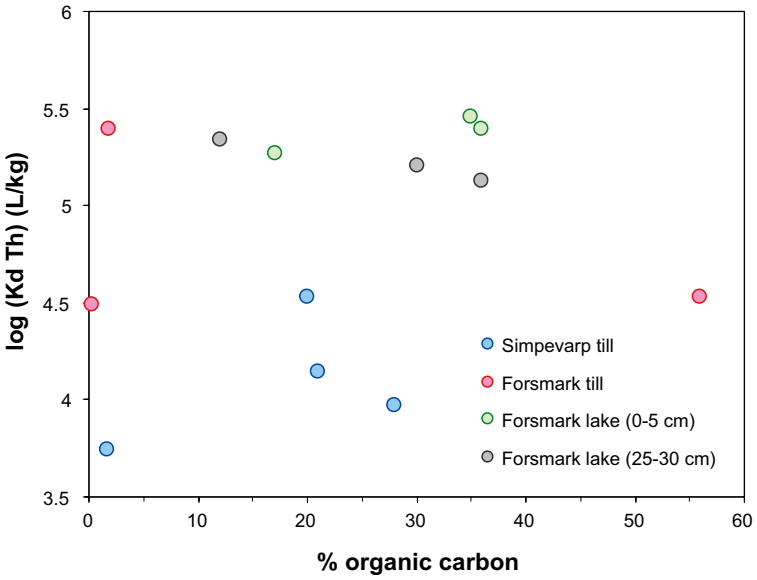

Figure 4-3. *Log (Kd Th) versus % of organic C in the sediment for Forsmark and Simpevarp soils and Forsmark lake sediments (see Section 3.14 for references).*

The amount of Th in solution was 6.09×10^{-10} mol/L, and the resulting Kd was 1,318 L/kg. This Kd is significantly lower than those reported for the till soils, even those with low organic matter content (see Table 3-3). The same calculation was applied to determine the Kd in the clay sediments, considering a 50% of illite and the clay porewater used in previous numerical modelling, with a Th concentration of 9.76×10^{-8} mol/L in solution. The resulting Kd is 17,458 L/kg, which is again significantly lower than those reported for clay sediments. This could indicate that organic matter plays a role in the retention of Th in the Forsmark soils.

The retention of Th will be numerically implemented by allowing the precipitation of ThO_2 in case of reaching its solubility. Sorption of thorium onto clay minerals and solid humic acids, which most likely occurs in the organic matter-rich lake sediments, can be implemented through existing values of sorption equilibrium constants and distribution coefficients in the literature. Complexation of thorium with humic acid will be considered in the simulation of the clay system.

4.6 Nickel

In the slightly oxidising conditions of the Forsmark near-surface groundwaters, Ni could bind to organic matter, oxy-hydroxides and clay minerals. Under more reducing conditions, such as those of wetlands and lake sediments, Ni can form sulphides and/or be incorporated to newly formed iron sulphides. This element can also be found in several places associated with calcite, substituting Ca from the crystalline cell of the solid.

Thermodynamic data are available for elemental Ni, Ni sulphides and also for Ni sorption on hydrous ferric oxides and clays. Therefore, all the main identified processes can be implemented in the numerical model in this case.

4.7 Molybdenum

In the oxidising conditions of the Forsmark near-surface groundwaters, molybdenum could be partially retained by oxy-hydroxides and organic matter. Experiments carried out in soils showed that Mo absorption onto humic acid was high at acidic pH, but decreased almost exponentially until a pH of 7 /Bibak and Borggaard 1994/. According to /Szilagyi 1967/ and /Bertine 1972/, the sorption of Mo onto peat seems to be related to the reduction of molybdate to a cationic form, and it is strongly pH

dependent, in consistence with the experiments of /Bibak and Borggaard 1994/. Therefore, at the circumneutral pH of the Forsmark waters, the retention of Mo by organic matter is not expected to be significant.

Available Kd from Forsmark and Simpevarp till sediments elucidate some degree of Mo retention in the studied soils /Sheppard et al. 2009/. In both cases it seems to exist a positive relationship between the amount of organic C and the Kd of Mo (Figure 4-4). pH defines an inverse correlation with the Kd of Mo in the Forsmark till soils (not shown). These results seem consistent with the abovementioned experimental data.

The retention of Mo by oxy-hydroxides should also be considered, since according to /Bibak and Borggaard 1994/ experiments in soils, the adsorption of Mo onto Al and Fe oxides is at its maximum at pH 4–5. Under more reducing conditions, such as those found in the wetland and lake sediments, molybdate could be reduced or converted to thiomolybdate and be retained by solid organic matter or other substrates, and could also be incorporated in iron sulphides. The available Kd data from Forsmark lake sediments also reveal some degree of Mo retention (Figure 4-4).

Unfortunately there are no available thermodynamic data of Mo sorption onto organic matter or oxy-hydroxides. Available Kd data should not be used to calculate log K for these sorption processes, since the Kd are presumably the result of more than one retention process.

The concentration of ^{93}Mo to be used in the modelling of radionuclide migration is not available, neither from calculations of solubility limits nor from deterministic calculations of radiation dose in the near-field. Due to the number of unknowns related to Mo, we do not recommend to implement it in the numerical modelling.

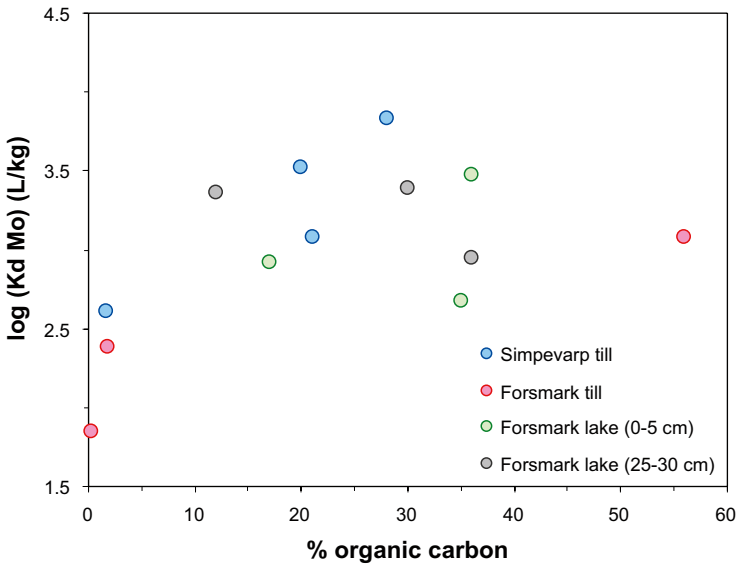

Figure 4-4. *Log (Kd Mo) versus % of organic C in the sediment for Forsmark and Simpevarp soils and Forsmark lake sediments (see Section 3.14 for references).*

4.8 Niobium

According to available data, niobium could be sorbed onto oxy-hydroxides and/or bound to organic compounds in the near-surface system of Forsmark. However, few studies are available on the behaviour of Nb in sediments and the building of a conceptual model for Nb retention is not straightforward. Kd data of Nb in soils, although scarce in the literature /Sheppard et al. 2009/, reveal a high affinity of Nb for the solid phase.

At the Eh and pH conditions of Forsmark groundwaters, Nb is found as an oxyanion; therefore, its sorption onto oxy-hydroxides is pH-dependent, the higher the pH the lower the Nb sorption. The binding of Nb on organic matter seems plausible according to the observed relationship between Kd of Nb and organic matter content in the Simpevarp soils, while the only available Kd value of Nb from Forsmark is out of the trend (Figure 4-5). For the lake sediments from Forsmark, there is not a clear correlation between Kd and amount of organic matter (Figure 4-5).

The Kd of Nb in the Forsmark till soil is significantly higher than that in the Simpevarp soils, but the content of organic matter is low. This fact could indicate that processes other than sorption on organic matter take place, and the same reasoning would apply to the lake sediment with highest Kd. One possibility could be the precipitation of Nb solid phases; in fact, at the pH-Eh conditions of the Forsmark groundwater the Nb_2O_5 solid species is stable (see Figure 3-13). /Charles and Prime 1983/ reported the precipitation of Nb compounds like niobic acid, niobate, or polymeric hydrous oxide on silt particles from an area contaminated with radioactive waste.

Given the scarcity of available data, the conceptual model of Nb retention is difficult to construct. It seems that Nb has a high affinity for soils, but the retention processes cannot be ascertained. Nevertheless, since the stability field of Nb_2O_5 solid species falls in the range of pH-Eh values expected to be found in Forsmark near-surface groundwaters (Figure 3-13), this phase will be allowed to precipitate in the numerical modelling if saturation is reached.

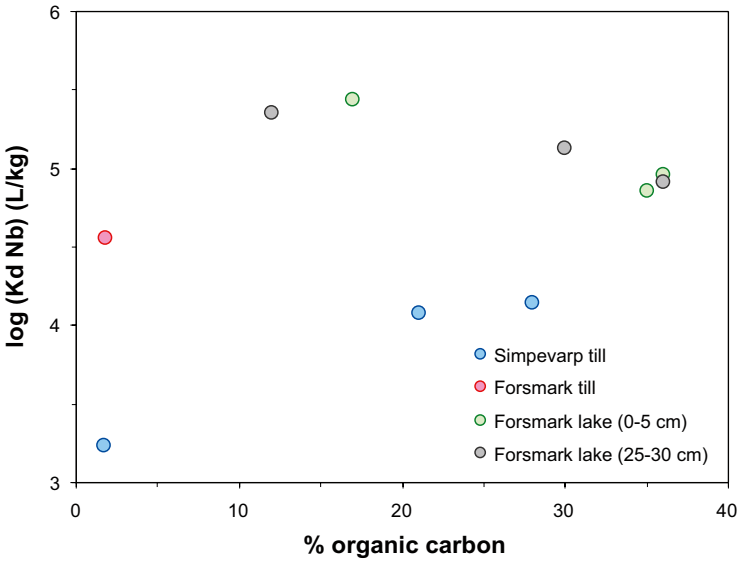

Figure 4-5. *Log (Kd Nb) versus % of organic C in the sediment for Forsmark and Simpevarp soils and Forsmark lake sediments (see Section 3.14 for references).*

4.9 Selenium

As discussed before, if selenium migrating from the bedrock meets an anoxic near-surface system, it can be reduced and precipitated as native Se(0) or $FeSe_x$ solid phases, depending on the Eh-pH conditions and the concentration of dissolved species. This reduction is favored by the presence of bacteria, organic matter and Fe(II)-containing minerals.

Under more oxidising conditions, oxy-hydroxides can retain selenite via sorption. Also the sorption of selenium on organic compounds has long been considered as one of the more significant retention mechanisms of selenium. At the range of Eh-pH expected in the Forsmark near-surface groundwater, the native selenium solid phase is stable (Figure 3-15). Therefore, selenite sorption onto organic matter or oxy-hydroxide phases will not be very important. The same reasoning applies to the co-precipitation of Se with calcite.

Therefore, in the case of selenium, taking into account the availability of thermodynamic data for the numerical implementation, the precipitation of Se(0), $FeSe_2$ and $Fe_{1.04}Se$ will be allowed to occur in the reactive transport simulations if oversaturation of these minerals is attained.

4.10 Technetium

Tc will not be affected by any important retention process in the oxidising Forsmark groundwaters unless it is reduced to Tc(IV) through surface or microbial processes. Microbially induced Tc reduction and precipitation as TcO_2 could take place in wetlands and lake sediments. Reduced Tc(IV) could be complexed with organic matter and can also associate with iron sulphides.

Given that the most effective retention mechanism for Tc in this environment will be its reduction to Tc(IV), in terms of numerical implementation of the retention of Tc, we will allow the precipitation of the reduced form of Tc as the hydrated solid phase $TcO_2 \cdot 1.6\ H_2O(s)$ if the solubility limit is reached.

4.11 Strontium

In the Forsmark near-surface environment, strontium could be effectively retained via co-precipitation with calcite, which is a major mineral in the till and glacial clays, and via ion exchange in clays, although strontium can be easily desorbed in the latter case. The retention processes implemented in the numerical modelling will be the sorption onto illite and the co-precipitation with calcite if saturation is reached.

4.12 Uranium

The most efficient mechanisms for uranium retention in the Forsmark near-surface asystem would be found in those places where anaerobic conditions are met. There, uranium is reduced to U(IV) by microbial activity and subsequently immobilised as uraninite or coffinite.

In shallower environments, U(VI) can be adsorbed onto NOM and deposited and buried in the lake bottom. These sediments contain high concentrations of humic acids, which are products of decomposition of organisms. The adsorption of uranium onto humic acids is a favourable mechanism at slightly acidic pH, whereas at alkaline conditions carbonate complexes will predominate, even in periods of low organic activity. In this case, the main retention process will be the adsorption onto inorganic phases such as iron oxy-hydroxides and clays.

U(VI) is not expected to be transported as uranium-phosphate complexes since the ratio between carbonate and phosphate is too high (according to /Sandino and Bruno 1992/). However, some lake bottoms and wetlands may retain enough phosphate to reach apatite saturation; if so, apatite can be a sink for uranium via adsorption. In soils originating from granite alteration, apatite can be a common phase, leading to the retention of uranium by phosphate phases.

In the reactive transport simulations, a set of minerals have been selected as possible solubility-limiting phases of aqueous uranium. For U(IV), a hydrated amorphous phase ($UO_2 \cdot 2H_2O$) has been preferred instead of a crystalline phase (e.g. uraninite). Moreover, coffinite formation is not allowed since it is considered that its precipitation is not kinetically favoured /Grandia et al. 2007/. For U(VI) schoepite, soddyite, uranophane and becquerelite are allowed to precipitate if the solution becomes oversaturated with any of these phases.

There is no evidence of apatite in the till, but deep groundwater intrusion could lead to precipitation of this phase, becoming a potential uranium sorbent, therefore apatite precipitation is allowed in the model if oversaturation is reached. Also the sorption of uranium onto both oxy-hydroxides and illite will be implemented in the numerical modelling. Complexation of uranium with humic acid will be considered in the simulation of the clay system.

4.13 Caesium

Sediments in wetlands and lakes contain glacial and post-glacial clays with significant amounts of illite. As mentioned above, this mineral is a strong sink for caesium. Also in the case of the till, clay minerals such as illite should be the main sink for caesium. Therefore, the sorption of caesium onto illite will be the only retention process considered in the numerical modelling of this radionuclide.

4.14 Radium

The very low concentrations of aqueous radium measured (from 10^{-14} to 10^{-11} M) in both natural and anthropogenic environments indicate that the solubility of radium is not controlled by pure phases ($RaSO_4$ would be the main candidate). Instead, the formation of solid solutions of Ba-Ca-Sr sulphates and carbonates is considered to be the solubility-limiting process. In many aqueous systems radium is strongly co-precipitated with barite due to the chemical similarity between radium and barium. (Ba,Ra)SO_4 solid solutions are commonly found in scales in facilities of oil extraction, in geothermal systems and in uranium mining areas.

This solid solution series can be considered as ideal; nevertheless, only very small fractions of $RaSO_4$ are typically measured due to the low radium concentration in water compared with barium. Initially, till groundwater in the Forsmark area is very close to barite saturation, and the precipitation of this mineral (and radium co-precipitation) is allowed in the model if oversaturation is reached.

Also the sorption of radium onto clay minerals is considered a retention process, which can be significant in the modelled domains, especially if precipitation of radiobarite does not take place. Unfortunately, thermodynamic data is not available for cation exchange of radium on illite. Data for barium could be used instead, assuming that the behaviour of the two elements is similar. According to this, an attempt will be made to simulate the sorption of radium onto illite in the numerical modelling.

4.15 Summary of retention processes

A summary of the most relevant retention processes possibly influencing the transport of the radionuclides of interest in the near-surface system at Forsmark is given in Table 4-2. For each radionuclide, the mechanisms that can actively retard its migration in the Quaternary soils and sediments at Forsmark are indicated by white cells. Retention processes that could be active but that due to the characteristics of the Forsmark media are not very likely to occur in this environment, are grey-shadowed. Those processes that are not relevant and/or unlikely are indicated by black cells in the table.

This classification is based on the information obtained from previous sections and the conceptual model developed for each of the selected radionuclides. As discussed in the previous sections, the availability of numerical parameters for the implementation of each of the processes of interest in the models for the considered media is highly relevant for the construction of the numerical model. Therefore we have indicated data availability with a tick in Table 4-2.

Table 4-2. Retention processes that may be relevant under the conditions of the Forsmark near-surface system.

Retention process	^{14}C	^{129}I	^{36}Cl	^{94}Nb	^{59}Ni	^{93}Mo	^{79}Se	^{99}Tc	^{230}Th	^{235}U	^{135}Cs	^{90}Sr	^{226}Ra
Sorption onto organic matter													
Sorption onto Fe-Mn-Al oxyhydroxides					✓		✓			✓			
Sorption onto phyllosilicates					✓				✓	✓	✓	✓	
Precipitation as pure phases	✓			✓	✓	✓	✓	✓	✓	✓			
Association with sulfides													
Association with carbonates												✓	
Incorporation into bacteria													
Association with phosphates													
Association with sulfates													✓

Processes likely to be active in the QD of Forsmark

Processes not likely to be active in the QD of Forsmark

Retention processes not relevant for the indicated element

✓ Available thermodynamic data

5 Numerical modelling setup

5.1 Description of model domains

In our previous modelling studies /Grandia et al. 2007, Sena et al. 2008/, the retention capacity of the near-surface Quaternary deposits in Forsmark was evaluated for Ra, U, Sr and Cs by means of reactive solute transport simulations, considering two distinct domains.

(1) The first reference case simulates a Quaternary till deposit overlying the granite bedrock. In this model, deep groundwater containing dissolved radionuclides is assumed to migrate upwards through a fracture in the granite rock and eventually transfer these radionuclides to the Quaternary deposits (through the bottom boundary of the modelled domain). The Quaternary deposits are assumed to be hydraulically connected to a surface discharge zone. Figure 5-1 shows the conceptual sketch of this case.

(2) The second reference case simulates a glacial clay that is present at the bottom of a discharge zone (such as a lake or the Baltic Sea), and is overlying the till deposit. In order to evaluate the retention capacity of the glacial clay, it is assumed that deep groundwater can flow through a preferential path in the till, which contacts directly with the bottom of the clay layer. Figure 5-2 shows the conceptual sketch of this second reference case. Note that the sketch shows the left half of a symmetric 2D domain. This "half-domain" is considered also in the numerical model discussed below; the symmetry implies that a no-flow boundary can be set through the centre of the lake (i.e. the right-hand model boundary in Figure 5-2).

In the present study the same two domains will be considered for modelling. The reactive transport simulations will include the radionuclides already implemented in the simulations made by /Grandia et al. 2007/ and /Sena et al. 2008/, namely Sr, U, Ra and Cs, and will also include the radionuclides Ni, Nb, Se, Tc, C and Th.

The results of numerical simulations by /Grandia et al. 2007/ revealed that the deep groundwater discharge into Quaternary deposits caused relatively long transient states of reactive transport. Deep groundwaters, which would be the carrier of radionuclides from the repository, have been discharging into Quaternary deposits for long periods of time. In order to simulate more realistic conditions and reproduce the initial geochemical conditions prior to the release of radionuclides from repository, /Sena et al. 2008/ simulated the reference cases during 2,700 years (which is approximately the time needed to reach stable hydrogeochemical conditions in the numerical simulations) before the release of radionuclides. The same procedure has been followed in the new models developed here.

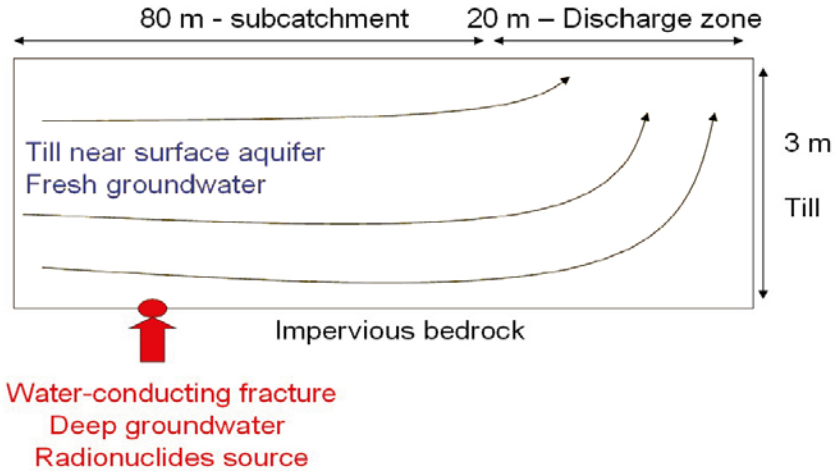

Figure 5-1. *Sketch of reference case #1, the till system.*

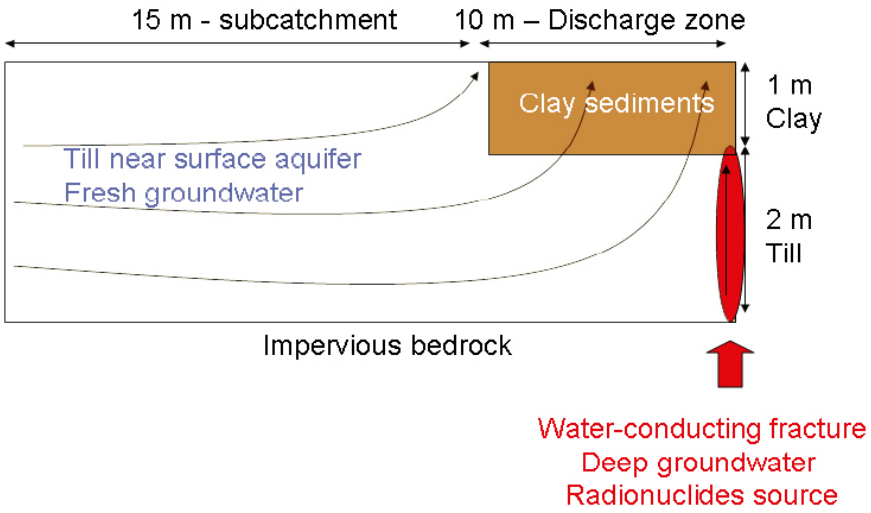

Figure 5-2. *Sketch of reference case #2, the glacial clay system.*

5.2 Groundwater selection for modelling

Three different groundwaters are considered in the numerical models: (a) till shallow groundwater, (b) glacial clay porewater, and (c) deep groundwater.

(a) Till shallow groundwater: overall, the chemistry of shallow groundwater flowing through the till is fairly constant in space and time, with a predominance of Ca^{2+} and HCO_3^- that reflects the equilibrium with the host rock. The average composition of water sampled in well SFM0002 /Tröjbom and Söderbäck 2006/ was selected by /Grandia et al. 2007/ as the till reference water for numerical calculations. This selection was made according to the following considerations: (1) this soil pipe has been repeatedly sampled; (2) it shows small seasonal changes; (3) it is saturated with calcite (i.e., equilibrium with the till); (4) analytical data on redox sensitive elements (Fe, Mn, U) are available; and (5) data on other elements of interest in the present work are available. Points 2 and 3 provide evidence that the residence time of this groundwater in the till is relatively long. The availability of data on redox sensitive elements is especially relevant to determine the redox state of the water since little information on the redox potential is provided. The reference water for the till shallow groundwater, used for the numerical simulations, was calculated by averaging the concentration of the data available from the water samples collected in the well SFM0002 /Sena et al. 2008/. The complete chemical composition of the water sample taken from SFM0002 soil pipe is listed in Table 5-1.

(b) Glacial clay porewater: the chemical composition of this porewater is expected to be similar to bottom lake waters, perhaps with some modification due to biologic activity and water-sediment interaction. /Grandia et al. 2007/ selected water samples collected at the bottom of Lake Eckarfjärden (sampling point PFM117; /Andersson et al. 2003/) to set up the initial conditions of the glacial clay sediments (Table 5-1). These waters are relatively diluted (ionic strength ~6.0×10^{-3} mol/L) and of Ca-HCO_3–type. Characteristically, they have large amounts of organic compounds either dissolved or as suspended particulate ([DOC]~1.50×10^{-3} mol/L). This water is more representative of post-glacial clay (organic-rich); for this reason, in order to approach the composition of an eventual glacial clay porewater at Forsmark, the water sample collected at the sampling point PFM117 was equilibrated with the reactive minerals considered for the simulation of the glacial clay (see Section 5.8.2 for further details).

(c) Deep groundwater: it is difficult to select a single sample for the bottom boundary condition since several chemically different waters occur underground in the Forsmark area. For the calculations, we have used a groundwater chosen to be representative of a deep saline signature (shield brines) by the ChemNet group, which differs from the one previously used in the numerical modelling of /Grandia et al. 2007/ and /Sena et al. 2008/. The selected groundwater for the present work was sampled in the KFM01D borehole. This borehole is located within the tectonic lens and the deep signature reaches shallower levels of approximately 200–400 meters of vertical depth. Several analyses were available for this borehole in the ChemNet database of Forsmark, version 2.3 /Laaksoharju el al. 2008/,

corresponding to sampling depth between 194.5 to 571.6 m. For the selection of the groundwater to be used in the calculations, only those from the highest-ranked category in the database were taken into consideration. From six selected groundwater samples, the one chosen was that with reported concentrations of iron and other elements of interest for the reactive transport simulations. The selected groundwater was sampled at a depth of 316 m and the water chemistry is reported in Table 5-1. This groundwater is of Na-Cl type with a moderate salinity (ionic strength of 0.13 mol/L).

5.3 Numerical tool

The reactive transport simulations have been performed using the code PHAST, version 1.5.1 /Parkhurst et al. 2004/. This code is the result of coupling the transport code HST3D /Kipp 1997/ and the geochemical code PHREEQC /Parkhurst and Appelo 1999/. PHAST is able to simulate multi-component, reactive solute transport in three-dimensional saturated groundwater flow systems. A number of flow boundary conditions are available (specified-head, flux and leakage conditions), and chemical reactions include homogeneous equilibrium using an ion-association thermodynamic model, heterogeneous equilibrium between the aqueous solution and minerals, gases, surface complexation sites, ion exchange sites, solid solutions, and kinetic reactions.

The reaction and transport equations are solved by sequential iteration approach in which solute transport and chemical reactions are decoupled into separate calculations for each time step. First, the primary species are transported, and then the outcome of the geochemical reactions occurring in the cell is calculated. The transport and geochemical calculations are evaluated by an iterative approach until prescribed convergence criteria are fulfilled.

Table 5-1. Chemistry of the selected waters for numerical calculations. Concentrations in mol/L. Data taken from: (1) /Tröjbom and Söderbäck 2006/, (2) /Andersson et al. 2003/ and (3) ChemNet database of Forsmark, version 2.3 /Laaksoharju et al. 2008/.

	SFM0002[(1)]	PFM117 bottom[(2)]	KFM01D[(3)]
pH	7.2	8.0	7.6
$[Na]_{total}$	1.22×10^{-3}	2.65×10^{-4}	6.13×10^{-2}
$[K]_{total}$	1.22×10^{-4}	5.20×10^{-5}	7.98×10^{-4}
$[Ca]_{total}$	2.89×10^{-3}	1.19×10^{-3}	1.82×10^{-2}
$[Mg]_{total}$	3.53×10^{-4}	1.17×10^{-4}	4.73×10^{-3}
$[Sr]_{total}$	2.09×10^{-6}	6.23×10^{-7}	6.94×10^{-5}
$[Ba]_{total}$	7.28×10^{-7}	1.44×10^{-7}	2.14×10^{-6}
$[C]_{total}$	5.66×10^{-3}	2.51×10^{-3}	4.72×10^{-3}
$[Cl]_{total}$	1.90×10^{-3}	1.53×10^{-4}	1.04×10^{-1}
$[S]_{total}$	2.41×10^{-4}	6.39×10^{-5}	2.21×10^{-3}
$[Si]_{total}$	9.74×10^{-5}	4.63×10^{-5}	5.63×10^{-4}
$[Fe]_{total}$	3.46×10^{-5}	8.34×10^{-7}	5.78×10^{-5}
$[Mn]_{total}$	3.86×10^{-6}	–	1.74×10^{-5}
$[NH_4^+]$	6.61×10^{-6}	1.82×10^{-5}	7.28×10^{-5}
$[PO_4^{3-}]$	1.39×10^{-7}	4.80×10^{-8}	6.46×10^{-8}
$[O_2]$	4.27×10^{-5}	–	–
DOC	1.22×10^{-3}	1.49×10^{-3}	6.66×10^{-4}
$[U]_{total}$	2.27×10^{-8}	5.02×10^{-9}	2.00×10^{-8}
$[Cs]_{total}$	6.47×10^{-11}	4.51×10^{-11} (**)	3.65×10^{-9}
$[I]_{total}$	6.40×10^{-8}	5.28×10^{-5}	3.36×10^{-7}
$[Th]_{total}$	6.09×10^{-10}	1.51×10^{-10}	1.19×10^{-9}
$[Ni]_{total}$	4.42×10^{-8}	4.89×10^{-9}	7.17×10^{-9}
$[Nb]_{total}$	1.14×10^{-9} (*)	8.72×10^{-11}	–

(*) Average [Nb] reported for till groundwater in Forsmark.

(**) Maximum [Cs] in water sample from KFM01A.

5.4 Hydrodynamic processes and parameters

This subsection has been extracted from /Sena et al. 2008/. For numerical modelling purposes groundwater flow through porous media is assumed to be governed by Darcy's Law. The code used for the numerical simulations solves the groundwater flow equation that combines Darcy's law and the mass balance equation of water. In addition, the solute transport processes considered in the model are: (1) advection, (2) molecular diffusion and (3) hydrodynamic dispersion. The equation governing solute transport through porous media is derived from the principle of mass conservation accounting for the mass fluxes due to the three abovementioned processes.

In the models it is assumed that the till deposits host a near-surface aquifer with an average recharge of 66 mm/year. On the other hand, from the fracture in the underlying granitic bedrock, 2 mm/year of deep groundwater are transferred into the till phreatic aquifer. All these values were obtained from water balance calculations in the Forsmark area MIKE SHE models in /Johansson et al. 2005/. According to available characterisation data of the Quaternary deposits, a thickness of 3 m was assumed in the model for the till /Johansson et al. 2005/. The modelled till domain was divided along the vertical axis into three layers. The top 0.8 m layer and the bottom 0.8 m layer are more conductive than the intermediate layer (1.4 m) of lower permeability (Figure 5-3). However, in the final site description a two layer model was proposed /Johansson 2008/.

The whole till domain is assumed anisotropic with a vertical hydraulic conductivity 10 times lower than the horizontal hydraulic conductivity. The effective porosity is also stratified with higher porosity values in the surface layer, reflecting a higher level of weathering and physical degradation closer to the surface /Johansson et al. 2005/. Table 5-2 shows all the hydrodynamic parameters used in the numerical simulations. Hydraulic conductivity and porosity values have been taken from /Johansson et al. 2005/. The values of transverse and longitudinal dispersivities used in the numerical simulations have been attributed according to realistic values for the dimension of the modelled domain that do not lead to a significant numerical dispersion. The diffusion coefficient has been set according to characteristic values of clayey sediments, while for the till system it is considered negligible.

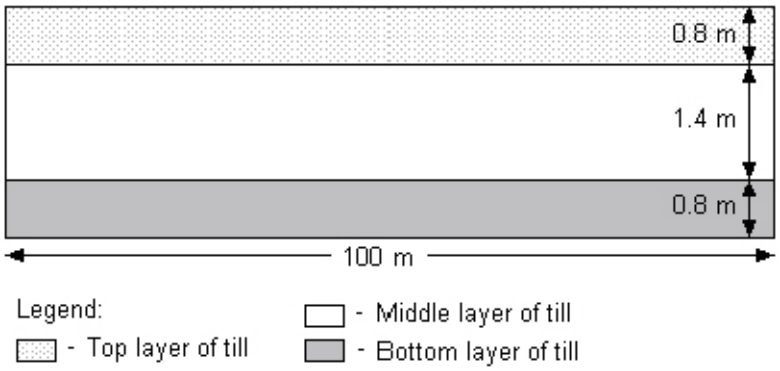

Figure 5-3. *Layering of the till domain, from /Johansson et al. 2005/. The till is composed of three layers that show distinct hydraulic properties (Y axis magnified 15 times).*

Table 5-2. Values of the hydrodynamic parameters used in the numerical models. Data taken from: (1) /Johansson et al. 2005/, (2) attributed values.

Material		$K_{horizontal}$[(1)] (m/s)	$K_{vertical}$[(1)] (m/s)	$\alpha_{longitudinal}$[(2)] (m)	$\alpha_{transverse}$[(2)] (m)	Porosity[(1)] (–)	Diffusion coefficient [(2)] (m^2/s)
Till	Top	1.5×10^{-5}	1.5×10^{-6}	0.5	0.2	0.15	negligible
	Middle	1.5×10^{-6}	1.5×10^{-7}	0.5	0.2	0.05	negligible
	Bottom	1.5×10^{-5}	1.5×10^{-6}	0.5	0.2	0.05	negligible
Clay		1.0×10^{-8}	1.0×10^{-9}	0.5	0.2	0.2	5×10^{-10}

5.5 Geochemical processes and parameters

5.5.1 Aqueous speciation

Solute speciation in groundwater is calculated by considering the chemical composition of each water type at the different conditions (i.e. Eh and pH) for each domain considered. The thermodynamic database used in the calculations is described in the beginning of Chapter 3. Since the studied groundwaters are rich in aqueous carbonate, Fe(III) carbonate complexes were added to the thermodynamic database. These species are $Fe(CO_3)_3^{3-}$ and $FeOHCO_3$. The complexation reactions together with the corresponding equilibrium constants are shown in Table 5-3. Constants were taken from /Grivé 2005/.

Activity coefficients for charged species are calculated by using the Davies equation:

$$\log \gamma_i = -Az_i^2\left(\frac{I^{1/2}}{1+I^{1/2}} - 0.3 \cdot I\right) \qquad \text{Equation 5-1}$$

where I is the ionic strength of the solution, z_i is the electric charge of the species in solution and A is a constant that depends on temperature.

For uncharged species, the Setchenow equation is used, which is a reduction of the WATEQ Debye-Hückel equation (see /Parkhurst and Appelo 1999/):

$$\log\gamma_i = b_i I \qquad \text{Equation 5-2}$$

where b_i is a ion-specific parameter fitted from mean-salt activity-coefficient data. Unless otherwise specified, b_i is assumed to be 0.1 for all uncharged species.

The aqueous species selected and the thermodynamic database are the same for the reference case #1 and #2. Moreover, in reference case #2 (the clay system) organic species were included as humic acids to simulate the metal complexation in waters with high concentration of organic compounds. The metals considered for complexation with humic acids are calcium, uranium and thorium. Eight different organic species have been considered: $Humate^-$, $CaHumate^+$, $UHumate^{3+}$, $U(Humate)_2^{2+}$, $UO_2Humate^+$, $UO_2(Humate)_2$, $Th(Humate)_2^{2+}$ and $ThHumate^{3+}$. The first two complexes of uranium are for U(IV), and the last two are for U(VI). The reactions and thermodynamic constants for these species are listed in Table 5-4.

Table 5-3. Complexation reaction of aqueous Fe(III) carbonates and corresponding thermodynamic constants from /Grivé 2005/.

Reaction	Log K (25ºC)
$Fe^{3+} + CO_3^{2-} + H_2O \leftrightarrow FeOHCO_3 + H^+$	10.76
$Fe^{3+} + 3CO_3^{2-} \leftrightarrow Fe(CO_3)_3^{3-}$	24.24

Table 5-4. Complexation reactions of organic compounds and their corresponding thermodynamic constants.

Reaction	Log K (25ºC)	Reference
$Ca^{2+} + Humate^- \leftrightarrow CaHumate^+$	4.7	(1)
$U^{4+} + Humate^- \leftrightarrow UHumate^{3+}$	7.0	(2)
$U^{4+} + 2Humate^- \leftrightarrow U(Humate)_2^{2+}$	11.5	(2)
$UO_2^{2+} + Humate^- \leftrightarrow UO_2Humate^+$	7.64	(3)
$UO_2^{2+} + 2Humate^- \leftrightarrow UO_2(Humate)_2$	11.54	(3)
$Th^{4+} + Humate^- \leftrightarrow ThHumate^{3+}$	17.0	(4)
$Th^{4+} + 2Humate^- \leftrightarrow Th(Humate)_2^{2+}$	18.4	(4)

(1) /Choppin and Shanbhag 1981/; (2) /Li et al. 1980/; (3) /Shanbhag and Choppin 1981/; (4) /Nash and Choppin 1980/.

5.5.2 Equilibrium with pure mineral phases

The mineralogical composition of the till shows the existence of calcite, quartz and illite as major minerals (>5 wt%) /Lindborg 2005/. According to /Hedenström 2004/, the glacial clays present in the lake sediments of Forsmark and the Baltic Sea show considerable amounts of illite, quartz and calcite. Therefore, for both reference cases, the major minerals are the same, but differ in their relative proportions.

In the reactive transport calculations, calcite is considered to contain trace amounts of Sr, forming a solid solution /Grandia et al. 2007, Section 3.2.1/. The set of the initial amount of Sr-bearing calcite and respective strontium molar fraction in the modelled domains is shown in Section 5.8.

Illite dissolution kinetics are very slow under the environmental conditions modelled in this study. /Köhler et al. 2003/ found very slow dissolution rates at circumneutral pH, from 10^{-14} to 10^{-15} mol·m^{-2}·s^{-1}. Consequently, dissolution of illite is not considered in the numerical simulations, and only participates as a charged surface for cation exchange.

As discussed in /Grandia et al. 2007, Section 2.5/, it is very likely that other phases exist at minor and trace concentrations, some of which can play a very important role in the control of the redox conditions and radionuclide retention. Among these, Fe(III)-hydroxide (ferrihydrite) is thought to be the controlling phase for the redox of the till porewater and to be the main uranium sorbent. In the reactive transport modelling of the till domain, it has been arbitrarily (due to the lack of field data), but reasonably, considered an initial concentration of 0.1 wt% of ferrihydrite in the till. The log K of the reaction involving this mineral has been long discussed and a wide range of values has been reported in the literature. The disparity in the log K values is mainly caused by the variable crystallinity of the samples used in the laboratory experiments. For the numerical simulations, we have used the equilibrium constant previously selected by /Sena et al. 2008/, which corresponds to microcrystalline ferrihydrite (log K (25ºC) = 3).

Another mineral that is not cited in the mineralogical inspections of the till samples is siderite ($FeCO_3$). This mineral can precipitate in the till domain after the deep inflow. Therefore, in the reactive transport model it is allowed to precipitate if oversaturation is reached. It is worth mentioning that this mineral rarely precipitates as a pure $FeCO_3$, but it forms solid solutions with calcium carbonate [ankerite, $(Ca,Fe)CO_3$]. The thermodynamics of this solid solution series is still not well known, and therefore the pure phase is selected for the current model calculations.

For the clay domain, again it is very likely that other phases exist at minor and trace concentrations, some of which can play important roles in the control of the redox conditions and radionuclide retention. Among these, pyrite is considered to significantly affect the redox of the glacial clay porewater. Since no data on pyrite content in glacial clay sediments is available for Forsmark, an initial concentration of 1 mol/L of pyrite (which corresponds to approximately 1.5 wt% of pyrite, considering a clay bulk density of 2 kg/L and a total porosity of 20%) has been considered in the model in order to ensure the relatively reducing conditions in the glacial clays.

A set of minerals has been selected as possible solubility-limiting phases of aqueous uranium in both reference cases. For U(IV), a hydrated, amorphous phase ($UO_2{\cdot}2H_2O$) has been preferred instead of a crystalline phase (e.g. uraninite, UO_2). Moreover, coffinite ($USiO_4{\cdot}nH_2O$) formation is not allowed since it is considered that its precipitation is not kinetically favoured /Grandia et al. 2007, Section 3.1/. For U(VI) schoepite [$UO_2(OH)_2$], soddyite [$(UO_2)_2SiO_4(H_2O)_2$], uranophane [$Ca(UO_2)(SiO_3OH)_2(H_2O)_5$] and becquerelite [$Ca(UO_2)_6O_4(OH)_6{\cdot}8H_2O$] are allowed to precipitate if the solution becomes oversaturated in any of these phases. For the case of becquerelite and soddyite, two log K are available in the SKB-TDB. The log K of "becquerelite (nat)" and of "soddyite (2)" have been selected in the present simulations.

According to /Seaman et al. 2001/, /Fuller et al. 2002/ and /Krestou et al. 2004/, apatite [$Ca_5(OH)(PO_4)_3$] is a good sorbent for uranium, so it is interesting to include it in the reactive transport calculations. There is no evidence of apatite neither in the till nor the clay system, but deep groundwater intrusion could lead to precipitation of this phase, becoming a potential uranium sorbent. For this reason, the predicted evolution of the saturation index of this mineral has been monitored in the numerical simulations. Since this mineral phase is not in the SKB-TDB, the reaction and log K from /Johnson et al. 2000/ have been added (Table 5-5).

Table 5-5. Thermodynamic equilibrium constants of selected dissolution reactions.

Reaction	Log K (25ºC)	Reference
$Ca_5(OH)(PO_4)_3 \leftrightarrow H_2O + 3HPO_4^{2-} + 5Ca^{2+} - 4H^+$	–3.07	(1)
$Se(cr) \leftrightarrow HSe^- - H^+ - 2\ e^-$	–7.62	(2)
$Nb_2O_5 \leftrightarrow 2\ Nb(OH)_6^- + 2\ H^+ - 7\ H_2O$	–28.38	(3)
$BaSO_4 \leftrightarrow Ba^{2+} + SO_4^{2-}$	–9.97	(4)

(1) /Johnson et al. 2000/; (2) /Olin et al. 2005/; (3) /Peiffert et al. 1997/; (4) /Blount 1977/.

The selected possible solubility-limiting phases for selenium are ferroselite ($FeSe_2$), $Fe_{1.04}Se$ and native selenium. For niobium the selected solubility-limiting phase is Nb_2O_5 and for technetium it is $TcO_2 \cdot 1.6H_2O$. For two of these solid phases (Se(cr) and Nb_2O_5) the log K used in the calculations is slightly different from that available in the SKB-TDB. The equilibrium constants used in the present numerical modellings are reported in Table 5-5.

5.5.3 Equilibrium with solid solutions

Pure mineral phases are rarely found in natural environments. Instead, many solid phases are "mixtures" of two or more end-members at variable proportions forming solid solutions. A well-known example of solid solution is the uptake of strontium in calcite, forming $Ca_{1-\chi}Sr_\chi CO_3$, where x is the molar fraction of strontium. At Forsmark, the strontium concentration in shallow groundwaters is influenced by the equilibrium with the host rock. The till is made of carbonate particles derived from the erosion of Cambro-Ordovician marine carbonate rocks, and contains significant amounts of strontium (see Section 3.10).

The incorporation of strontium in the calcium carbonate lattice has been widely studied, since it was suggested that $(Ca,Sr)CO_3$ solid solutions could control the strontium concentrations in seawater /Stumm and Morgan 1996/. This solid solution series is highly non-ideal, i.e., the activity coefficients of the end-members are not equal to 1 (for more details see /Grandia et al. 2007, Section 5.3.1/). Following /Sena et al. 2008/, the present models are set with a strontium molar fraction in the solid solution that is in equilibrium with the selected reference groundwaters of the till and glacial clay domains.

The very low concentration of aqueous radium measured (from 10^{-14} to 10^{-11} M) in both natural and anthropogenic environments indicates that the solubility of radium is not controlled by pure phases (such as $RaSO_4$). Instead, the formation of solid solutions of Ba-Ca-Sr sulphates and carbonates is considered to be the solubility-limiting process. The Ba-Ca sulphate solid solution series can be considered as ideal; nevertheless, only very small fractions of $RaSO_4$ are typically measured due to the low radium concentration in water compared with barium. Initially, till groundwater in the Forsmark area is very close to barite saturation, and the precipitation of this mineral (and radium co-precipitation) is allowed if oversaturation is reached. The equilibrium constant of the barite end-member used in the numerical simulations is reported in Table 5-5, since it is not included in the SKB-TDB.

5.5.4 Sorption onto mineral phases

For some of the selected radionuclides (Sr, U, Ni, Th, Ra and Cs), the sorption onto mineral surfaces is considered a retention mechanism, and for some of them this sorption could be the main retention process (e.g. for Cs). In the considered till domain, sorption is assumed to take place onto illite and iron oxy-hydroxides. In the glacial clay domain, only sorption onto illite is considered.

Like other clay minerals, illite balances its electric charge deficit through sorption of cations on its surfaces. The composition of these surfaces is conditioned on the equilibrium with the porewater and the selectivity coefficients of each cation involved. According to available studies dealing with the sorption of caesium on illite, it is known that sorption in this mineral takes place on different surface sites (/Poinssot et al. 1999/ and references therein).

/Bradbury and Baeyens 2000/ proposed a model of cation exchange in illite considering three types of sites (Table 5-6). The most abundant sites (~80% of the total CEC) are the so-called "Planar sites", which can adsorb either divalent cations such as Ca^{2+}, Mg^{2+}, Sr^{2+}, Ni^{2+} and UO_2^{2+} or monovalent cations (Na^+, K^+ and Cs^+); these sites are considered of "low affinity", and are usually associated with the fixed negative charge on the surface of illite arising from isomorphous substitution (e.g. Al^{3+} for Si^{4+} in tetrahedral sites /Poinssot et al. 1999/). Due to steric reasons, divalent cations are only involved in this type of sites (Poinssot et al. 1999). The second and the third types of sites, called "Type II" and "Frayed Edge Sites" (FES), respectively, are considered of "high affinity" and involve monovalent species such as Na^+, K^+, Cs^+ and NH_4^+. The site density is much lower (20% "Type II" and 0.25% "FES" of the total sites), but the uptake of some cations such as Cs^+ on these sites (especially on FES) is particularly efficient and dominant. Interestingly, these sites are not generally associated to other sheet silicates, such as smectite, chlorite or kaolinite /Bradbury and Baeyens 2000/.

In two recently published papers, /Bradbury and Baeyens 2009a, b/ quantitatively describe the sorption of uranium, nickel and thorium (among other elements) in Na-illite, by means of a two site protolysis non electrostatic surface complexation and cation exchange model. Three types of surface complexation sites are considered in their modelling, one strong site and two amphoteric edge sites, with different site capacities and surface protolysis constants (see Table 9 in /Bradbury and Baeyens 2009a/). Cation exchange capacity for Na-illite is 225 meq/kg /Baeyens and Bradbury 2004/. Since sorption edges were measured at trace concentrations, metal uptake was modelled as occurring on strong-type sites ($\equiv S^SOH$) only. Accordingly, for the case of uranium, thorium and nickel uptake, the model proposed by /Bradbury and Baeyens 2009a/ has been implemented in the numerical simulations. Thermodynamic data for the surface complexation modelling have been taken from /Bradbury and Baeyens 2009a, b/.

The configuration of the illite interlayer applied to the till and clay systems is the same, except for the percentage of illite in the modelled domain, as will be shown in Section 5.8. The Gaines-Thomas cation exchange selectivity coefficients implemented in the numerical modelling are reported in Table 5-6. Compared to the numerical models previously developed by /Sena et al. 2008/ there are slight differences in the selectivity coefficients used for Ca^{2+}, Mg^{2+} and Sr^{2+}. The sorption of radium, uranium and nickel on illite was not implemented in their models. The addition of these elements will not affect the sorption behaviour of the major cations, including strontium, due to the relatively low concentrations of (natural + repository derived) Ra, U and Ni in solution.

Table 5-6. Cation exchange reactions and Gaines-Thomas selectivity coefficients in the illite interlayer.

Reaction	Log K (25ºC)	Reference
Planar sites		
$X^- + Na^+ \leftrightarrow NaX$	0.0	(1)
$X^- + K^+ \leftrightarrow KX$	1.1	(1)
$X^- + Cs^+ \leftrightarrow CsX$	1.6	(1)
$2X^- + Sr^{2+} \leftrightarrow SrX_2$	1.13	(2)
$2X^- + Ca^{2+} \leftrightarrow CaX_2$	1.13	(2)
$2X^- + Mg^{2+} \leftrightarrow MgX_2$	1.13 [(a)]	
$2X^- + Ba^{2+} \leftrightarrow BaX_2$	1.13	(2)
$2X^- + Ra^{2+} \leftrightarrow RaX_2$	1.13 [(b)]	
$2X^- + Ni^{2+} \leftrightarrow NiX_2$	1.1	(3)
$2X^- + UO_2^{2+} \leftrightarrow UO_2X_2$	0.65	(4)
Type II sites		
$X^{II-} + Na^+ \leftrightarrow NaX^{II}$	0.0	(1)
$X^{II-} + K^+ \leftrightarrow KX^{II}$	2.1	(1)
$X^{II-} + Cs^+ \leftrightarrow CsX^{II}$	3.6	(1)
FES		
$X^{FES-} + Na^+ \leftrightarrow NaX^{FES}$	0.0	(1)
$X^{FES-} + K^+ \leftrightarrow KX^{FES}$	2.4	(1)
$X^{FES-} + Cs^+ \leftrightarrow CsX^{FES}$	7	(1)
$X^{FES-} + NH_4^+ \leftrightarrow NH_4X^{FES}$	3.5	(1)

(1) /Bradbury and Baeyens 2000/, (2) /Brouwer et al. 1983/, (3) /Bradbury and Baeyens (2009a/, (4) /Bradbury and Baeyens 2009b/.

(a) Value assumed, considering equal sorption behaviour for Mg^{2+}, Ca^{2+} and Sr^{2+}, (b) Value assumed, considering an equal behaviour for Ba^{2+} and Ra^{2+}.

Under oxidising conditions, uranium (as U(VI)) can also be adsorbed onto iron oxy-hydroxides. In the reactive transport simulations of the till domain, uranium, together with Ni^{2+}, are assumed to be adsorbed onto ferrihydrite. The surface complexation model implemented is that of /Waite et al. 1994/. This model considers two types of adsorption sites (of strong and weak binding, respectively). The total concentration of sites is 0.875 mol/mol Fe /Waite et al. 1994/. Most of these sites are of low affinity (weak binding) and only 0.0018 mol/mol Fe corresponds to high-affinity (strong binding) sites. Adsorbing carbonate species have also been included in the simulations, because the amount of aqueous carbonate is expected to be high due to the equilibrium with the $(Ca,Sr)CO_3$ solid solution present in the till, and, under these conditions, carbonate adsorption on ferrihydrite surface can be significant /Bruno et al. 1992, van Geen et. 1994/. The sorption constants for Ni^{2+} are those reported in /Dzombak and Morel 1990/.

Unlike illite surfaces, ferrihydrite is a reactive mineral very sensitive to changes in the redox state of the system. Intrusion of deep groundwaters into the till domain may lead to dissolution or precipitation of ferrihydrite. For this reason, the total amount of sites available for adsorption in the reactive transport simulations depends on the remaining moles of ferrihydrite in each time step.

It is important to note that although it is known that some of the radionuclides considered have a certain capacity to sorb onto organic matter, the lack of data for most of them makes the evaluation of these processes difficult. This introduces a certain degree of uncertainty on the quatitative estimation of the retention processes.

5.5.5 Repository derived radionuclides

As explained in /Sena et al. 2008/, repository derived radionuclides were labelled with RD (e.g., ^{RD}Sr), in order to trace radionuclides released from repository and distinguish them from naturally occurring isotopes. Ra, Se and Tc were not labelled since, before repository release, they are considered to be below detection limits in the porewater of the studied Quaternary deposits.

The labelling of repository-derived radionuclides involved the addition of the labelled species as primary species to the thermodynamic database used in the numerical reactive transport simulations. Also the secondary aqueous species and the reactions involving solid phases were added for the labelled radionuclides by duplicating the reactions of the non-labelled isotopes and replacing the isotope with the labelled radionuclide, as in the following example:

The following speciation reaction for non-labelled uranium,

$$4CO_3^{2-} + U^{4+} \leftrightarrow U(CO_3)^{4-} \qquad \log K = 35.12 \qquad \text{Equation 5-3}$$

was duplicated for the labelled uranium as follows

$$4CO_3^{2-} + {}^{RD}U^{4+} \leftrightarrow {}^{RD}U(CO_3)^{4-} \qquad \log K = 35.12 \qquad \text{Equation 5-4}$$

In the numerical simulations and after repository release, the total concentration of a selected element at any given time and any given node of the modelled domain, can be calculated by simply adding repository derived species to natural occurring species of the element.

In order to involve repository-derived radionuclides and the naturally occurring isotopes in the same solid phase without causing isotopic fractionation, new solid solutions that involve both species have been added to the thermodynamic database. In the next paragraphs, the modifications applied for the case of U and amorphous uraninite, and Sr and the calcite-strontianite solid solution, are shown.

The dissolution reaction of amorphous uraninite applied in the present simulations is defined as:

$$UO_2{\cdot}2H_2O_{(am)} + 4H^+ \leftrightarrow U^{4+} + 4H_2O \qquad \log K = 1.50 \qquad \text{Equation 5-5}$$

In order to trace the incorporation of ^{RD}U and natural U in amorphous uraninite, the following ideal solid solution was introduced in the reactive transport simulations, replacing the pre-existing Equation 5-5:

$$(U_{1-\chi}\,{}^{RD}U_{\chi})\,O_2{\cdot}2H_2O\,(am) + 4H^+ \leftrightarrow (1-\chi)\,U^{4+} + \chi\,{}^{RD}U^{4+} + 4H_2O \qquad \log K = 1.50 \qquad \text{Equation 5-6}$$

where χ is the molar fraction of ^{RD}U in amorphous uraninite.

As already mentioned, Sr forms a non-ideal solid solution with calcite. In order to trace the incorporation of RDSr and natural Sr in this solid solution, a new solid solution with three end-members (Sr, RDSr, and Ca) was defined in the numerical simulations.

The binary non-ideal solid solution between strontianite and calcite is defined by the solubility constant of each end-member, as follows:

$CaCO_{3(calcite)} + H^+ \leftrightarrow Ca^{2+} + HCO_3^-$ log K = 1.85 Equation 5-7

$SrCO_{3(strontianite)} + H^+ \leftrightarrow Sr^{2+} + HCO_3^-$ log K = 1.05 Equation 5-8

/Sena et al. 2008/ implemented a new solid solution that involves the three end-members Sr, RDSr, and Ca, by defining a conditional solubility constant for the strontianite end-members. This approach is necessary since ternary non-ideal solid solutions cannot be considered in PHAST. Only ideal multicomponent solid solutions and binary non-ideal solid solutions can be treated. The non-ideality behaviour implies that the activity of the solid phase end-members depends not only on its molar fraction in the solid solution, but also on an activity coefficient.

In order to take this non-ideality into account, conditional solubility constants were considered for the strontianite end-members. Therefore, by taking this approach the solid solution can be treated as ideal. This approach is valid only when the molar fractions of the trace end-members do not change much through time and if they are always within the natural miscibility range. The values for the conditional solubility constants were calculated as follows:

$K^*_{SrCO3} = K_{SrCO3} \times \chi_{SrCO3} \times \lambda_1$ Equation 5-9

$K^*_{RDSrCO3} = K_{RDSrCO3} \times \chi_{RDSrCO3} \times \lambda_2$ Equation 5-10

$K^*_{CaCO3} = K_{CaCO3} \times \chi_{CaCO3} \times \lambda_3$ Equation 5-11

where K* is the conditional solubility constant, K is the solubility constant, χ is the molar fraction and λ is the activity coefficient that is proportional to the interaction parameter (nondimensional Guggenheim parameter) a_0. In the case of the non-ideal $(Ca_{(1-\chi)}Sr_\chi)CO_3$ solid solution a_0 = 5.7 /Tesoriero and Pankow 1996/. According to the aqueous concentration of Sr and RDSr, it can be assumed that both $SrCO_3$ and $^{RD}SrCO_3$ will have a molar fraction close to 1×10^{-4} during the simulation time. This value is below the miscibility gap defined for the $(Ca_{(1-\chi)}Sr_\chi)CO_3$ /Tesoriero and Pankow1996/. Also, the consideration of these trace molar fractions for Sr and RDSr implies that $\chi_{CaCO3} \approx 1$, and then, $K^*_{CaCO3} \approx K_{CaCO3}$.

Between natural and repository-derived strontium end-members ($SrCO_3$ and $^{RD}SrCO_3$) the solid solution is considered ideal, and therefore $\lambda_1 = \lambda_2$. Consequently, the conditional solubility constants of $SrCO_3$ and $^{RD}SrCO_3$ are the same. The calculated conditional solubility constants for both $SrCO_3$ and $^{RD}SrCO_3$ are:

$^{RD}SrCO_3 + H^+ \leftrightarrow {}^{RD}Sr^{2+} + HCO_3^-$ log K* = 3.53 Equation 5-12

$SrCO_3 + H^+ \leftrightarrow Sr^{2+} + HCO_3^-$ log K* = 3.53 Equation 5-13

5.5.6 Isotopic fractionation

Among the modelled radionuclides, ^{14}C is a light isotope and therefore can be subject to isotopic fractionation processes. Isotopic fractionation is a result of variations in thermodynamic properties of molecules that are dependent on mass. Details of the thermodynamic basis for understanding isotope fractionation have been presented by /Urey 1947/, /Bigeleisen and Mayer 1947/ and /Bigeleisen 1952/.

Since stable carbon (^{12}C and ^{13}C) is a major component initially present in Forsmark groundwater, it has been considered necessary to implement temperature-dependant isotopic fractionation in the numerical modelling to simulate the incorporation of ^{12}C + ^{13}C and ^{14}C into the $(Ca,Sr)CO_3$ solid solution. Isotopic fractionation should be considered between all the dissolved carbonate species and between the dissolved species and the solid phase.

The implementation of the isotopic fractionation to the reactive-transport models has been done according to /Thorstenson and Parkhurst 2002/. These authors calculate the equilibrium constants for isotope exchange reactions from the fractionation factors. The individual isotope equilibrium constant for the molecular species composed of the most abundant isotope of each element can be calculated from, or assumed to equal, the standard thermochemical equilibrium constant. This provides a basis for calculating the individual isotope equilibrium constants for each isotopic species. The temperature dependence of the individual isotope equilibrium constants can be calculated from the temperature dependence of the fractionation factors and the temperature dependence of the standard thermochemical equilibrium constants.

5.6 Spatial and temporal discretisations

The model discretisations in space and time are the same as described in /Grandia et al. 2007/. A summary of the spatial and temporal discretisations is presented here, taken from /Sena et al. 2008/. For further details, the reader is referred to /Grandia et al. 2007, Section 5.4/.

5.6.1 Reference case #1: The till system

The modelled domain of reference case #1 is a 2D vertical cross-section of the till deposit. Following /Johansson et al. 2005/, the thickness is 3 m, and, based on the dimensions of the subcatchments in the Forsmark area, the horizontal length is 100 m. The modelled till deposit was divided into three layers following the simplified till profile proposed by /Johansson et al. 2005/ (Figure 5-3). These three layers have different hydraulic properties (Table 5-2).

Since the till deposit hosts phreatic aquifers that may be locally confined, and that may discharge to distinct surface water bodies /Johansson et al. 2005/, it was decided to simulate a confined aquifer that discharges into a surface water body located at the top-right corner of the modelled domain.

The spatial discretisation of the modelled domain was adapted according to the main features of the boundary conditions, which will influence the groundwater flow directions and the groundwater chemistry of the modelled domain, namely the position of the deep groundwater inflow and the position of the discharge area (outflow boundary).

In the reference case #1, the spatial discretisation along the X-axis is refined in the till directly overlying the area where the deep groundwater enters the till domain. Similarly, the discretisation is also refined under the discharge area. The spatial discretisation along the Y axis is also finer in the discharge area due to the large upward vertical component of the shallow groundwater flow (Figure 5-4).

There are two important time stages regarding the chemical conditions of the system: the first stage occurs at the beginning of the simulation period, when the deep groundwater flows into the modelled domain and triggers major geochemical changes, and the second stage occurs when the increased concentration of radionuclides in the deep groundwater disturbs the previous geochemical state. Therefore, time discretisation was refined at the beginning of the simulation period, then set progressively coarser until approximately 2,700 years, and then refined again when the increment of radionuclides takes place. Finally, the time discretisation becomes coarser again, until the end of the simulation period. According to these criteria, the time discretisation for both modelled domains (till and clay systems) was set as shown in Figure 5-5.

5.6.2 Reference case #2: The clay system

The modelled domain considered for the reference case #2 is a 2D symmetric vertical cross section of a glacial clay layer that can be present at the bottom of discharge areas of Forsmark. Based on the characterisation of the lake sediments reported in /Johansson et al. 2005/, the thickness of the clay layer in the model was set to 1 m, and taking into account the present-day aerial extent of the lakes at Forsmark, the length of the X-axis was set to 10 m. The hydrodynamic parameters of the clay deposit to be used in the numerical simulations were set according to /Johansson et al. 2005/, and are shown in Table 5-7.

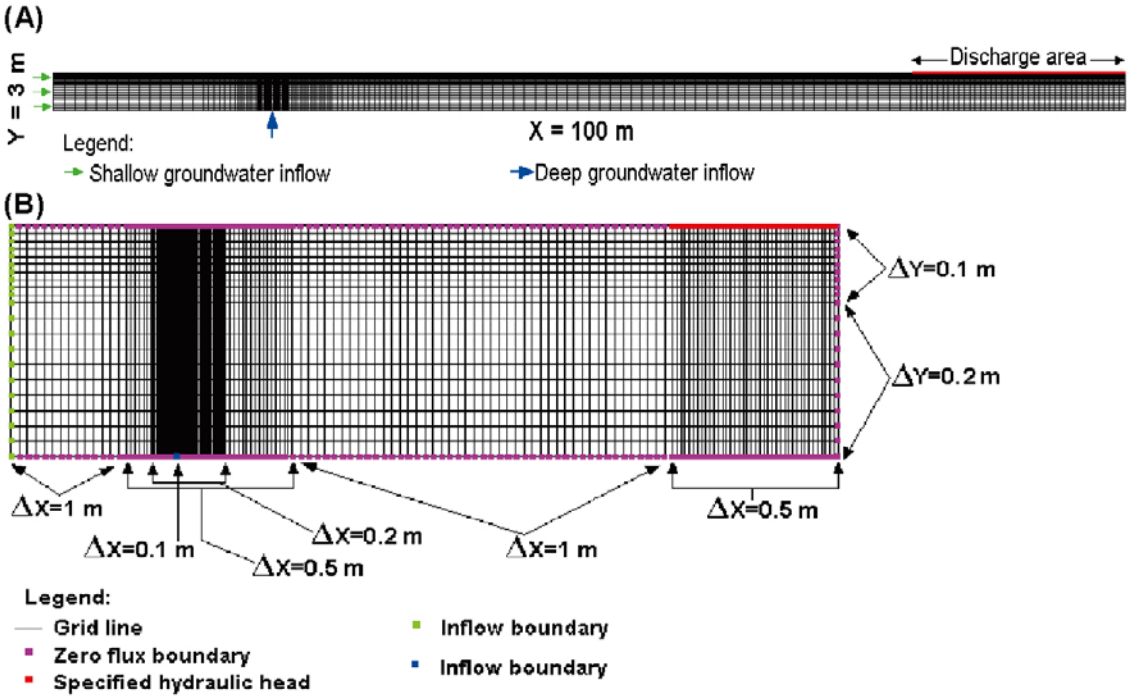

Figure 5-4. *Numerical grid showing the distinct spatial discretisations along the X- and Y-axes, and the boundary conditions assigned to the till system (reference case #1). Grid A shows the lengths in each direction, whereas grid B explains where the finer discretisations occur and the boundary conditions (Y-axis is magnified 10 times).*

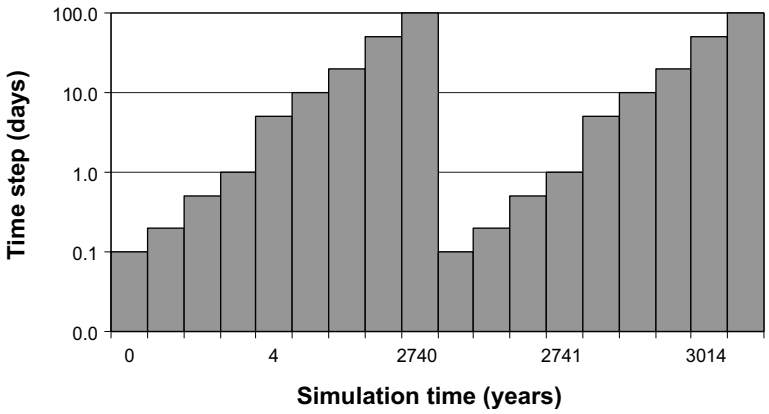

Figure 5-5. *Time discretisation for reference case #1 and reference case #2.*

In this case, the shallow groundwater flowing in the underlying till aquifer enters in the clay domain through the left and bottom boundaries. The deep groundwater inflow for the reference case #2 will occur at the bottom right corner of the domain that represents a higher permeability area of the underlying till deposit. The water flowing in this domain will flow out through the whole top boundary. Since the modelled domain in the reference case #2 is relatively small (1×10 m), it was set a fine spatial discretisation of 0.1 m along both axes for the whole domain (Figure 5-6).

The time discretisation is the same as in reference case #1 (Figure 5-5), since it is expected that major chemical changes will occur at the same time, i.e. at the beginning of the simulation time and after the input of radionuclides derived from the repository. To ensure stability in the numerical calculations, the Péclet criterion (Pe≤2) is met for the maximum ΔX (maximum ΔX = 1 m, and longitudinal dispersivity = 0.5 m) in both numerical models.

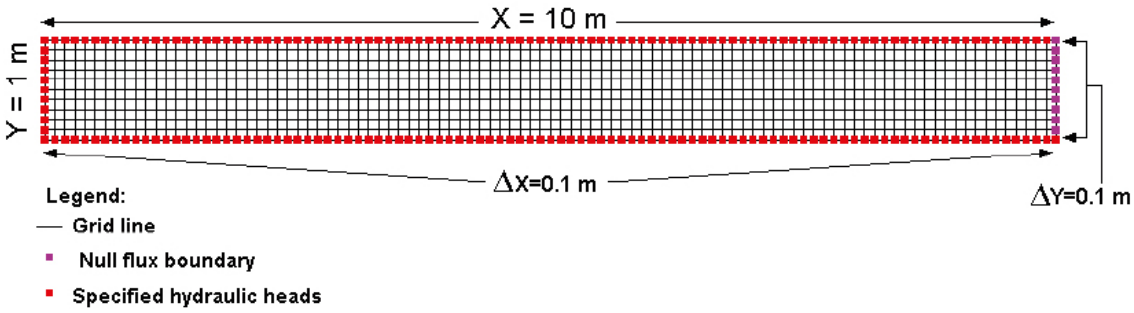

Figure 5-6. *Numerical grid showing the spatial discretisation of the modelled domain and the boundary conditions assigned to the clay system (reference case #2).*

5.7 Hydrogeological initial and boundary conditions

5.7.1 Reference case #1: The till system

According to the water balance calculations developed with the MIKE SHE model for the Forsmark site /Johansson et al. 2005/, the shallow aquifers hosted by till deposits discharge 66 mm/year to the surface water bodies. Therefore, for the present numerical model, a flow of 66 mm/year has been prescribed in the top boundary of the modelled domain.

Of the total length of the top boundary, only 80 m correspond to the recharge area, and the remaining 20 m correspond to the discharge area. The numerical code PHAST uses a three dimensional coordinate system, therefore, a third transversal dimension of 0.5 m in length has been introduced in the simulated till domain. Considering a surface of 80×0.5 m, the net recharge flow entering the system would be:

$$\frac{6.6\times10^{-2}\,m^3}{m^2\cdot year}\times 80\,m\times 0.5\,m = 2.64\,m^3/year = 7.25\,L/day$$

The net recharge flow of 7.25 L/day is applied to the left boundary to simulate a locally confined aquifer with a predominantly horizontal flow direction, before reaching the discharge area (Figure 5-7). The discharge area of the modelled domain is located in the last 20 m of the top right boundary, where a constant head of 3 m is set.

At the bottom boundary of the modelled domain, between X = 20 m and X = 20.2 m, the deep groundwater flows into the domain. The remaining bottom boundary (from X = 0 m to X = 19.9 m, and from X = 20.3 to X = 100 m) is considered impervious. The flux of deep groundwater entering through the 0.2 m of the bottom boundary was calculated from the 2 mm/year of inflow across bottom boundary, obtained in the water balance from the MIKE SHE model applied to the Forsmark area /Johansson et al. 2005/.

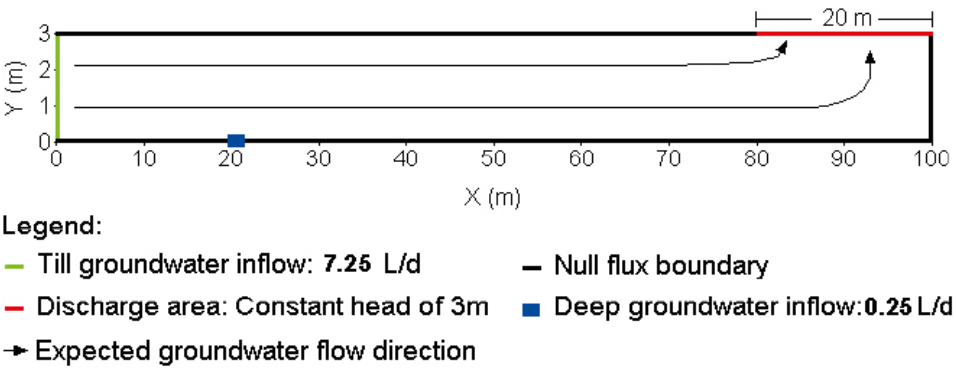

Figure 5-7. *Boundary conditions for the numerical model applied to reference case #1.*

The 2 mm/year were multiplied by the total bottom area of 100×0.5 m, and applied to the discrete deep inflow boundary of 0.2 m. Therefore, the total deep inflow passing through the 0.2 m is:

$$\frac{2\times10^{-3}\,m^3}{m^2\cdot year}\times100\,m\times0.5\,m=0.1\,m^3/year=0.25\,L/day$$

It is assumed that the simulated catchment has a deep groundwater inflow concentrated at a single point, which would correspond to a hypothetical fracture zone (Figure 5-7).

5.7.2 Reference case #2: The clay system

As already mentioned, the reference case #2 simulates the water flow and geochemical processes that occur in a glacial clay layer located immediately underneath a surface water body that constitutes a discharge area of the till aquifer. The flow conditions prescribed for the clay system depend on the flow conditions of the surrounding till aquifer. After analysing the flow conditions in a complex model with a layer of clay in the top right corner of a till aquifer, the prescribed boundary conditions were set as shown in Figure 5-8 (for more details see /Grandia et al. 2007, Section 5.5.2/).

5.8 Hydrogeochemical initial and boundary conditions

The geochemical initial and boundary conditions of the numerical models developed in the present project are the same as implemented in the models of /Sena et al. 2008/ with some modifications, as explained below.

From available geochemical data of Forsmark it is seen that calcium carbonate is present in both till and glacial clays. In the reactive transport simulations, the initial till and clay systems are assumed to contain calcium carbonate with trace amounts of strontium, forming a $(Ca,Sr)CO_3$ non-ideal solid solution that is supposed to be in equilibrium with the reference waters. This solid solution may re-precipitate in a new phase with higher strontium content as a response to the inflow of a strontium-enriched deep groundwater. Consequently strontium may be retained in the solid phase, or it may be released by dissolution of the $(Ca,Sr)CO_3$ solid solution as a response to changes in the pH conditions and/or carbonate equilibrium.

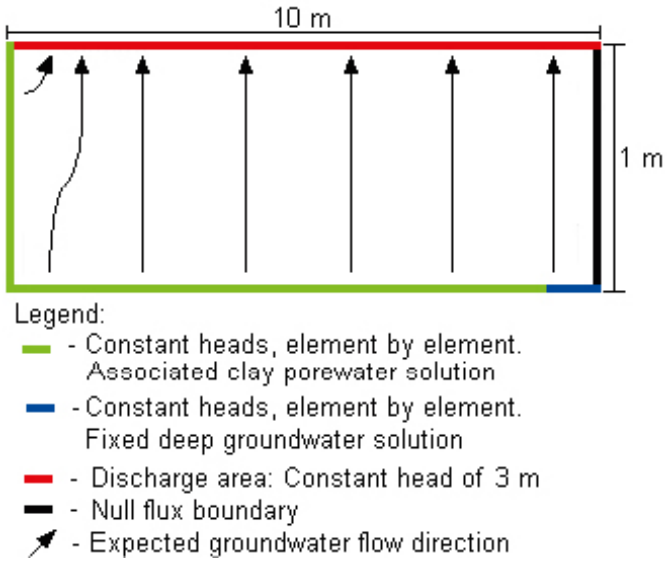

Figure 5-8. *Boundary conditions for reference case #2.*

The dissolution of the carbonate mineral has additional implications in the clay system, since the release of Ca^{2+} into solution will increase the competition for the complexation with humic acids. Consequently, the concentration of free aqueous uranium increases, favouring the precipitation of uranium pure phases. However, the dissolution of carbonate minerals also releases CO_3^{2-} into solution that may form aqueous uranium carbonate complexes that prevent the precipitation of uranium pure phases.

For these reasons it is important to have a good estimation of the reactive carbonate mineral pool in both numerical models. /Sena et al. 2008/ estimated the carbonate content of the till and clay systems and calculated the amount of reactive carbonate to be used in the numerical simulations, considering that only an external layer of 0.05 mm is reactive for each calcite grain present in the system. For both reference cases they set the amount of reactive calcite to 1 mol/L.

The cation exchange capacity (CEC) is a parameter with a significant influence in the geochemistry of groundwaters that flow through clay-rich sediments. The CEC of a sediment does not only depend on the clay content but also on the mineralogy of the clay fraction. /Sena et al. 2008/ used a CEC value of 200 meq/kg for the reference case. This was the value reported for illite in /Bradbury and Baeyens 2000/, which is very similar to maximum CEC value reported for till in Laxemar /Sohlenius et al. 2006/. In the present study a CEC value of 225 meq/kg is used, which is the one selected as reference value for illite in /Baeyens and Bradbury 2004/.

According to the adopted CEC value, the concentration of available cation exchange sites (CES) for the reference case of the till deposit is set using the following input data:

- CEC = 225 meq/kg = 0.225 eq/kg = 0.225 mol/kg (exchange species is a monovalent X^-).
- Total porosity in the till = 25% /Johansson et al. 2005/.
- Illite content in the till: 10 wt% (estimated value, not reported in the literature).
- Till bulk density: 1.95 kg/L ((1-Total porosity)×2.6 kg/L, estimated value, not reported in the literature).

Considering a CEC of 225 meq/kg, the concentration of CES in the till deposit is:

$$[CES] = \frac{0.225 mol}{1 kg} \times \frac{10 kg Illite}{100 kg Till} \times \frac{1.95 kg Till}{1 L} \times \frac{1}{0.25} = 0.1755 mol/L \qquad \text{Equation 5-14}$$

The same procedure is followed to calculate the CES in the clay system, considering the following input data:

- CEC = 200 meq/kg = 0.200 eq/kg = 0.200 mol/kg (exchange species is a monovalent X^-).
- Total porosity = 20% /Johansson et al. 2005/.
- Illite content: 50 wt% (estimated value, not reported in the literature).
- Clay bulk density: 2 kg/L ((1-Total porosity)×2.5 kg/L, estimated value, not reported in the literature).

The concentration of CES is calculated as

$$[CES] = \frac{0.225 mol}{1 kg} \times \frac{50 kg Illite}{100 kg Clay} \times \frac{2 kg Clay}{1 L} \times \frac{1}{0.20} = 1.125 mol/L \qquad \text{Equation 5-15}$$

The number of surface complexation sites on illite is calculated following the same procedure as for CES, but replacing the CEC by the moles of sorption sites per kilogram of illite in the previous equations (i.e. for the till and the clay system). /Bradbury and Baeyens 2009a/ report 2×10^{-3} mol of strong sites per kg illite and 4×10^{-2} mol of each of the two edge sites per kg illite, which are the values used to calculate the number of sites in our system.

5.8.1 Reference case #1: The till system

Initial groundwater composition in the till

The chemistry of the groundwater in equilibrium with the till deposit has been obtained after equilibration of the sample taken in soil pipe SFM0002 with $(Ca,Sr)CO_3$ solid solution, siderite and ferrihydrite (Table 5-8). As this groundwater is close to the equilibrium with these minerals, the resulting composition does not differ much from the sampled water. The iron concentration is slightly modified by the equilibrium with ferrihydrite, and strontium by the equilibrium with the solid solution. The redox state of the solution is controlled by the Fe^{2+}/ferrihydrite pair, and the pH is slightly lower than the original pH (shown in Table 5-1) due to equilibrium with the $(Ca,Sr)CO_3$ solid solution and siderite.

Initially, uranium is found as U(VI) and the dominant aqueous species are carbonate complexes, mainly $UO_2(CO_3)_3^{4-}$. All uranium solid phases are far from saturation. Thorium, like U(VI), is mainly found as carbonate complexes in solution, predominantly $Th(OH)_3CO_3^-$ and $Th(OH)_2(CO_3)_2^{2-}$. All Th solid phases are far from saturation.

Strontium is found almost completely as Sr^{2+} cation. The most abundant Sr solid phases in nature, celestite ($SrSO_4$) and strontianite ($SrCO_3$) are undersaturated, with saturation indexes (SI) of –3.16 and –2.29, respectively. The composition of the $(Ca,Sr)CO_3$ solid solution in equilibrium with the till groundwater is $Ca_{0.999983}Sr_{0.000017}CO_3$.

Carbon (IV) is mainly found as the bicarbonate ion at the pH of the till groundwater. As already mentioned, the water is in equilibrium with a $(Ca,Sr)CO_3$ solid solution. Chlorine and iodine are mainly found in solution as chloride and iodide species. The relatively low chloride content in the till groundwater prevents a significant complexation of Cs, and, therefore, the free species Cs^+ is dominant in the till groundwater.

Niobium is found in solution mainly as $Nb(OH)_6^-$, and the concentration is low enough to prevent the precipitation of Nb_2O_5 solid species (SI of –3.87). Finally, nickel in solution is found as Ni^{2+} and in much lesser amounts as carbonate complexes. All the solid species containing nickel are undersaturated in the till groundwater.

Deep groundwater before repository release

The composition of the reference water that represents the deep groundwater prior to repository release results from the equilibrium of the water sampled in the borehole KFM01D (see Section 5.2) with pyrite and calcite, which are the pure phases expected to control the pe and pH, respectively. This equilibration produces a slight change in the pH of the water. At the calculated pe and pH values, groundwater is oversaturated with barite and $UO_2{\cdot}2H_2O$. Since both phases can play a role in the retention of the selected radionuclides, it was considered necessary to diminish the concentrations of Ba and U in solution (see Table 5-7) until reaching a saturation index of 0 for these solids.

As already mentioned in Section 5.2, the selected deep groundwater is not the same that was previously used in the numerical modelling by /Grandia et al. 2007/ and /Sena et al. 2008/. Both groundwaters have very similar pH and Eh values, and also have very similar concentrations of Na, Ca, Sr and Cl. Concentrations of Mg and SO_4 are slightly different in both groundwaters. Those of Ba and C (inorganic) show a two-fold increase, and those of ammonium and K show a two-fold decrease in the deep groundwater selected in the present study. The concentration of Fe in the new deep groundwater is one order of magnitude lower and that of uranium is 24 times higher than in the previously selected one.

Deep groundwater after repository release

The increment of radionuclide concentration in the deep groundwater, due to repository release, is set according to a very pessimistic assumption. In this case, the geosphere does not have any retention capacity for radionuclides, and the advective travel time between the repository and the near-surface systems is assumed to be instantaneous. In this context, radionuclide concentrations calculated for the near-field (i.e. the canister containing the spent fuel and the engineered barrier system surrounding it) in case of dissolution of the spent nuclear fuel, are applied as the input concentrations in the simulations.

Table 5-7. Initial composition of till groundwater and deep groundwater in reference case #1. Concentrations in mol/L.

	Till GW	Deep GW (before repository release)	Deep GW (after repository release)
pH	7.12	6.86	6.86
pe	0.053	–2.58	–2.58
Na	1.22×10^{-3}	6.13×10^{-2}	6.13×10^{-2}
K	1.22×10^{-4}	8.00×10^{-4}	8.00×10^{-4}
Ca	2.79×10^{-3}	1.82×10^{-2}	1.82×10^{-2}
Mg	3.54×10^{-4}	4.73×10^{-3}	4.73×10^{-3}
Sr	2.10×10^{-6}	5.24×10^{-5}	5.24×10^{-5}
Ba	7.28×10^{-7}	4.38×10^{-7}	4.38×10^{-7}
C(IV)	5.58×10^{-3}	4.72×10^{-3}	4.72×10^{-3}
Cl	1.90×10^{-3}	1.04×10^{-1}	1.04×10^{-1}
SO_4^{2-}	2.41×10^{-4}	2.21×10^{-3}	2.21×10^{-3}
Si	9.74×10^{-5}	5.63×10^{-4}	5.63×10^{-4}
Fe_{total}	1.75×10^{-5}	5.80×10^{-5}	5.80×10^{-5}
NH_4^+	6.62×10^{-6}	7.28×10^{-5}	7.28×10^{-5}
PO_4^{3-}	1.29×10^{-6}	6.00×10^{-8}	6.00×10^{-8}
U	2.23×10^{-8}	1.13×10^{-8}	5.66×10^{-9}
Cs	6.48×10^{-11}	3.65×10^{-9}	3.65×10^{-9}
I	6.40×10^{-8}	3.36×10^{-7}	3.36×10^{-7}
Nb	1.14×10^{-9}	–	–
Ni	4.42×10^{-8}	7.17×10^{-9}	7.17×10^{-9}
Th	6.09×10^{-10}	1.19×10^{-9}	1.19×10^{-9}
^{RD}Cs	–	–	3.48×10^{-7}
^{RD}U	–	–	5.66×10^{-9}
^{RD}Sr	–	–	1.56×10^{-3}
^{RD}I	–	–	1.58×10^{-5}
^{RD}Nb	–	–	5.25×10^{-8}
^{RD}Ni	–	–	4.96×10^{-7}
^{RD}Th	–	–	1.75×10^{-7}
^{RD}Cl	–	–	5.05×10^{-7}
^{RD}C	–	–	2.89×10^{-7}
Ra	–	–	9.15×10^{-11}
Se	–	–	3.77×10^{-11}
Tc	–	–	5.27×10^{-9}

The groundwater composition in this case is the same as before repository release, except for the repository-derived radionuclide concentrations (Table 5-7). Remember that repository-derived radionuclides are labelled RD in order to distinguish them from natural isotospes. Ra, Se and Tc are not labelled because they are considered to be below the detection limit in the porewater before repository release. The repository-derived radionuclide concentrations have been calculated to be in equilibrium with their respective solubility limiting phases in the near field, according to the methodology described in /Duro et al. 2006b/.

The concentrations of ^{RD}Sr, ^{RD}U, ^{RD}Th, Tc and ^{RD}Nb in the deep groundwater after repository release are calculated by assuming the equilibrium of the reference deep groundwater with their solubility limiting phases in the near field (only the concentration of the radionuclide is modified), which correspond to $SrSO_4$ (celestite), $UO_2{\cdot}2H_2O$(am), $ThO_2{\cdot}2H_2O$, $TcO_2{\cdot}1.6H_2O$ and Nb_2O_5, respectively /Duro et al. 2006b/.

In the case of uranium, the selected deep groundwater is already saturated with $UO_2{\cdot}2H_2O$(am) before repository release, therefore, to maintain thermodynamic equilibrium no more uranium should be carried in solution. For this reason it has been decided to label half of the uranium concentration already present in deep groundwater as repository-derived (^{RD}U) and the other half as natural uranium (Table 5-7).

The solubility limiting phases selected to calculate the maximum concentrations of Ni and Se in solution differ from those used in /Duro et al. 2006b/. In the case of nickel, the solubility-liming phase selected by /Duro et al. 2006b/ was $NiCO_3$; however, this is a high temperature phase (not expected to form below 220ºC). On the other hand, the low temperature $Ni(CO_3)\cdot 5.5H_2O$ phase is highly soluble, leading to concentrations of Ni in solution in the order of 10^{-2} mol/L. For this reason it was decided to select millerite (NiS) as the solubility-limiting phase for RDNi. For the case of Se, /Duro et al. 2006b/ selected FeSe, while in the present work ferroselite has been selected as the solubility-limiting phase (see discussion in Section 3.8).

Since the solubility limiting phases for Ra and RDCs in the near-field were difficult to define, /Sena et al. 2008/ calculated the corresponding concentrations from the radioactive release doses estimated at the near-field /SKB 2006/. The same procedure has been followed to calculate the concentrations of the radionuclides RDC, RDCl and RDI in solution, as briefly summarised below for Ra (extracted from /Sena et al. 2008/). Doing this, it is implicitely assumed that there is no natural presence of these radionuclides in the system.

The concentration of radionuclides in the deep groundwater depends on the type of repository release considered (growing pinhole failure, advection/corrosion failure, or the shear movement failure /SKB 2006/) and on the migration path of the radionuclides in the geosphere (fracture intersecting the deposition hole (Q1), the excavation damaged zone (Q2), fracture intersecting the deposition tunnel (Q3)) /SKB 2006/. The Q1 case (growing pinhole failure combined with the fracture intersecting the deposition hole) was selected for the calculation of the radionuclide concentrations, since it is considered the worst case. This is because Q1 leads to higher groundwater flow velocities from the spent nuclear fuel to the geosphere and, consequently, larger radionuclide releases.

In /SKB 2006, Figure 10-14/, the radioactive dose in the near-field at the time of repository release is 450 Bq/yr for ^{135}Cs, 170 Bq/yr for ^{226}Ra, 150,000 Bq/yr for ^{14}C, 5,000 Bq/yr for ^{36}Cl and 3,000 Bq/yr for ^{129}I. By dividing the radioactive doses expressed in Bq/yr by the Q1 flow (2.25×10^{-4} m^3/yr /SKB 2006, Table 10-5/) we obtain the radionuclide concentration expressed in Bq/L, which is converted to mol/L for the numerical simulations developed in the present work:

$$[^{226}Ra] = \frac{170 Bq/yr}{2.25\times10^{-4} m^3/yr} \times \frac{1 m^3}{1000 dm^3} = 7.55\times10^{2} Bq/dm^3 = 7.55\times10^{2} Bq/L$$

Knowing that the radioactive decay constant (λ) of ^{226}Ra is 1.37×10^{-11} s^{-1} and using the Avogadro constant, we obtain the following concentration in mol/L:

$$[^{226}Ra] = \frac{7.55\times10^{2} Bq/L}{1.37\times10^{-11} s^{-1}} \times \frac{1 atoms/L}{6.023\times10^{23} atoms/mol} = 9.15\times10^{-11} mol/L$$

The radionuclide concentrations are very high (Table 5-7), taking into consideration that the engineered barriers and geosphere would be able to retain much of these radionuclides, preventing them from accessing the near-surface systems. Nevertheless, since the objective of the simulations is to evaluate the retention capacity of the Quaternary sediments, an extreme case has been considered in this work.

Initial composition of the exchanger

The clay content in the till is usually more than 5 wt%, with illite being the most abundant clay mineral. For modelling purposes the content of illite was set 10 wt%, which represents a site density of 0.1755 mol/L. The total concentration of sites in illite is kept constant during the reactive transport simulations since it is assumed that this mineral does not dissolve (or precipitate) under the environmental conditions considered in the model.

The composition of the exchangeable sites in illite from the till at Forsmark is unknown. For this reason, the initial exchanger composition has been considered to be in equilibrium with the reference groundwater. This calculation has been conducted using the PHREEQC code /Parkhurst and Appelo 1999/ and the Gaines-Thomas selectivity coefficients presented in Table 5-6. The resulting initial composition is shown in Table 5-8. From this calculation, the interlayer of illite in equilibrium with the reference water is rich in calcium, which is the dominant cation in the illite exchanger, occupying approximately 35% of the total number of exchangeable sites.

Considering only the planar sites, calcium covers approximately 88% of this type of sites. Magnesium is the second most important cation on these sites (occupying approximately 12% of the planar sites, one order of magnitude lower than calcium). The concentrations of sodium and potassium are almost two orders of magnitude lower than the concentration of calcium (Table 5-8). Caesium is weakly retained on this type of sites, in contrast, in the FES and Type II sites it is strongly retained, despite the relatively low site density (Table 5-8). Strontium and nickel are not much retained in the planar sites, and the sorption of uranium is almost nonexistent. In Type II and FES, potassium is the most abundant cation. Interestingly, ammonium is also abundant in FES (Table 5-8).

Initial composition of the illite surface

In the model of /Bradbury and Baeyens 2009a, b/ the sorption of Ni, U and Th onto illite was described by means of a two site protolysis non-electrostatic surface complexation and cation exchange model. Accordingly, for the case of the three above-mentioned elements, surface complexation has been incorporated in the numerical simulations.

Three different types of sites are considered in the surface complexation model, one strong site and two amphoteric edge sites, with different site capacities and surface protolysis constants (see Table 9 in /Bradbury and Baeyens 2009a/). The surface complexation equilibrium constants for the modelling have been taken from /Bradbury and Baeyens 2009a, b/.

The initial composition of the illite surface in equilibrium with the selected groundwater has been calculated with the PHREEQC code and is reported in Table 5-9. According to the surface complexation reactions, Th, Ni and U are sorbed onto strong sites, and of the three, Ni^{2+} has more affinity for this type of sites, while the amount of Th sorbed, in the form of the complex $\equiv S^sOTh(OH)_4^-$, is two orders of magnitude lower, and that of uranium is three orders of magnitude lower.

Table 5-8. Calculated initial composition of the illite interlayer in reference case #1.

Site	mol·L_{water}^{-1}
Planar sites	
CaX_2	6.13×10^{-2}
MgX_2	7.82×10^{-3}
KX	1.17×10^{-3}
NaX	9.32×10^{-4}
SrX_2	4.58×10^{-5}
BaX_2	1.56×10^{-5}
NiX_2	8.32×10^{-7}
CsX	1.97×10^{-9}
UO_2X_2	1.73×10^{-13}
Type II sites	
KX^{II}	3.25×10^{-2}
NaX^{II}	2.59×10^{-3}
CsX^{II}	5.46×10^{-7}
Frayed edge sites (FES)	
KX^{FES}	2.51×10^{-4}
NH_4X^{FES}	1.72×10^{-4}
NaX^{FES}	1.00×10^{-5}
CsX^{FES}	5.32×10^{-6}

Table 5-9. Initial concentration of the species adsorbed on illite surface sites in reference case #1.

Site	mol·L_{water}^{-1}
Strong sites	
$\equiv S^sO^-$	1.22×10^{-3}
$\equiv S^sONi^+$	1.98×10^{-4}
$\equiv S^sOH$	1.29×10^{-4}
$\equiv S^sOTh(OH)_4^-$	5.02×10^{-6}
$\equiv S^sONiOH$	3.74×10^{-6}
$\equiv S^sOTh(OH)_3$	1.06×10^{-6}
$\equiv S^sOTh(OH)_2^+$	1.78×10^{-7}
$\equiv S^sOUO_2(OH)_2^-$	1.30×10^{-7}
$\equiv S^sOUO_2OH$	1.09×10^{-7}
$\equiv S^sOH_2^+$	8.63×10^{-8}
$\equiv S^sONi(OH)_2^-$	4.45×10^{-8}
$\equiv S^sOUO_2(OH)_3^{2-}$	7.76×10^{-9}
$\equiv S^sOUO_2^+$	2.31×10^{-9}
$\equiv S^sOThOH^{2+}$	5.95×10^{-10}
$\equiv S^sOTh^{3+}$	5.00×10^{-12}
Amphoteric edge site 1	
$\equiv S^{wI}O^-$	2.81×10^{-2}
$\equiv S^{wI}OH$	2.99×10^{-3}
$\equiv S^{wI}OH_2^+$	1.99×10^{-6}
Amphoteric edge site 2	
$\equiv S^{wII}OH_2^+$	2.98×10^{-2}
$\equiv S^{wII}OH$	1.41×10^{-3}
$\equiv S^{wII}O^-$	6.69×10^{-7}

Initial composition of the ferrihydrite surface

The initial composition of the ferrihydrite surface in equilibrium with the till system is shown in Table 5-10. The most abundant surface complex is the neutral $\equiv HFO^wOH$, although the concentration of surface carbonate complexes is also significant. Nickel is sorbed both on the strong and weak sites, as the $\equiv HFO^sONi^+$ and $\equiv HFO^wONi^+$ species respectively. Uranium is mainly sorbed as the carbonate complex $\equiv(HFO^sO)_2UO_2CO_3^{2-}$ in the high-affinity sites. According to these results and the illite cation exchange and surface equilibrium values (Table 5-8 and Table 5-9), Ni is preferentially sorbed onto illite, while U has more affinity for the ferrihydrite surface.

The initial concentration of total uranium sorbed in ferrihydrite is 8.31×10^{-6} mol/L_{water}, corresponding to a uranium concentration in the till of 1.07×10^{-6} mol·kg^{-1}_{till} (considering a total porosity of 25% and a bulk density of 1.95 kg/L) if all immobilised uranium in the system is considered to sorb onto ferrihydrite. The U/Fe molar ratios in the till range from 1.5×10^{-5} to 1.5×10^{-4} /Grandia et al. 2007, Figure 2-15/. In the numerical model, an initial ferrihydrite concentration of 0.1 wt% has been considered in the till, which corresponds to 1.1×10^{-2} mol Fe/kg till. Assuming that most Fe and U are linked to iron oxy-hydroxides, which is a realistic approach, the resulting U/Fe molar ratio in the numerical model is 9.68×10^{-5}, which is within the range of U/Fe actually measured in the till.

Initial partition coefficients of selected elements

The calculated surfaces in equilibrium with the till groundwater can be used to obtain Kd values of the sorbed elements. Since the concentrations of species in the surface and cation exchange sites are reported as mole per liter of water, they have to be converted to mole per kilogram of rock in order to determine Kds. For this calculation we need the porosity and the density of the bulk rock (Equation 5-16). The total porosity of the till is 0.25 /Johansson et al. 2005/ and a density of 1.95 kg/L has been taken for the calculations /Sena et al. 2008/.

$$Kd = \frac{[sorbate]\,mol/L}{[solute]\,mol/L} \times \frac{0.25}{1.95\,kg/L} \qquad \text{Equation 5-16}$$

Table 5-10. Initial concentration of the species adsorbed on ferrihydrite surfaces in reference case #1.

Site	mol·L_{water}^{-1}
Strong sites	
≡$HFO^{s}OH$	7.83×10^{-5}
≡$HFO^{s}CO_3H$	3.67×10^{-5}
≡$HFO^{s}ONi^{+}$	3.52×10^{-5}
≡$HFO^{s}OH_2^{+}$	1.06×10^{-5}
≡$HFO^{s}CO_3^{-}$	8.98×10^{-6}
≡$(HFO^{s}O)_2UO_2CO_3^{2-}$	8.31×10^{-6}
≡$HFO^{s}O^{-}$	1.39×10^{-6}
≡$(HFO^{s}O)_2UO_2$	5.64×10^{-7}
Weak sites	
≡$HFO^{w}OH$	5.03×10^{-2}
≡$HFO^{w}CO_3H$	2.36×10^{-2}
≡$HFO^{w}OH_2^{+}$	6.80×10^{-3}
≡$HFO^{w}CO_3^{-}$	5.77×10^{-3}
≡$HFO^{w}O^{-}$	8.91×10^{-4}
≡$HFO^{w}ONi^{+}$	3.05×10^{-5}
≡$(HFO^{w}O)_2UO_2CO_3^{2-}$	4.34×10^{-7}
≡$(HFO^{w}O)_2UO_2$	7.06×10^{-8}

The calculated Kd for nickel is 778 L/kg, which is significantly lower than those reported in Table 3-3 and Table 3-4. In the case of uranium, the calculated Kd is 55 L/kg, which again is lower than those Kd reported for till soils and sediments (see Table 3-3 and Table 3-4). Finally, the calculated Kd of Th is 1,318 L/kg, which is much lower than those reported in the tables cited above. The systematically lower Kd values obtained in the modelling results, as compared to those obtained from the real sediments, could be explained by the fact that in the till sediments other processes besides those considered in the numerical modelling retain these elements in the solid phase, either by sorbing or by forming part of the solid species.

5.8.2 Reference case #2: The clay system

Initial groundwater composition in the clay

The redox state of glacial clay porewaters is expected to be controlled by microbial activity. In some lakes similar to those at Forsmark, reducing conditions are evidenced by the presence of biogenic pyrite /Percival et al. 2001, Outridge et al. 2005/. Given that a relatively reducing environment in the lake bottom sediments is expected, and that these sediments are relatively rich in calcite /Hedenström 2004/, the porewater in the glacial clay layer simulated has been considered to be in equilibrium with pyrite, siderite and calcite.

Consequently, the composition of the initial porewater in the reference case #2 results from the equilibration of the water sample collected at the bottom of sampling point PFM117 with these minerals (Table 5-11). This water was also equilibrated with amorphous uraninite since this phase represents the solubility-limiting phase in this system, and the precipitation of this uranium phase is expected to be the only process able to retain uranium in the clay system. The composition of the deep groundwater before and after repository release is the same as in reference case #1 (see Table 5-7).

For the glacial clay porewater, also the presence of organic acids has been considered, in order to assess the role of dissolved organic matter in the inhibition of radionuclide retention (mainly of uranium and thorium). The presence of organic acids dissolved in the porewater is represented by 1.0×10^{-4} mol/L of humic acid. This value corresponds to 10% of the total DOC in the bottom lake porewater. The main dissolved humate is the complex formed with calcium ($CaHumate^{+}$), which represents the 97.6% of dissolved humics.

Table 5-11. Initial composition of glacial clay porewater. Concentrations are in mol/L.

	Clay porewater
pH	7.75
pe	–3.94
Na	2.64×10^{-4}
K	5.19×10^{-5}
Ca	1.18×10^{-3}
Mg	1.17×10^{-4}
Sr	6.23×10^{-7}
Ba	1.37×10^{-7}
C(IV)	2.50×10^{-3}
Cl	1.53×10^{-4}
SO_4^{2-}	6.39×10^{-5}
Si	4.63×10^{-5}
Fe_{total}	8.35×10^{-7}
NH_4^+	1.82×10^{-5}
PO_4^{3-}	4.14×10^{-8}
U	1.12×10^{-9}
Cs	4.51×10^{-11}
I	5.28×10^{-5}
Nb	8.72×10^{-11}
Ni	4.89×10^{-9}
Th	1.51×10^{-10}
Humic acid	1.00×10^{-4}

Under the pH and redox conditions of the clay porewater, approximately 65% of the dissolved U is found as U(IV) and the other 35% as U(VI). The U(IV) dominant species is $U(OH)_4$, whereas the U(VI) dominant species are uranium carbonate complexes, namely $UO_2(CO_3)_3^{4-}$ and $UO_2(CO_3)_2^{2-}$. Similar to U(VI), thorium is mainly found as carbonate complexes in solution, predominantly as $Th(OH)_3CO_3^-$ and $Th(OH)_2(CO_3)_2^{2-}$. All Th solid phases are far from saturation.

Strontium is found almost completely as Sr^{2+} cation. The most abundant solid phases in nature, celestite ($SrSO_4$) and strontianite ($SrCO_3$) are undersaturated, with saturation indices (SI) of –4.09 and –2.40, respectively. The composition of the $(Ca,Sr)CO_3$ solid solution in equilibrium with the clay porewater is $Ca_{0.999987}Sr_{0.000013}CO_3$.

Carbon (IV) is mainly found as the bicarbonate ion at the pH of the clay groundwater. As already mentioned, the water is in equilibrium with a $(Ca,Sr)CO_3$ solid solution. Chlorine and iodine are mainly found in solution as chloride and iodide species. The relatively low chloride content in the clay porewater prevents a significant complexation of Cs, and, therefore, the free species Cs^+ is dominant.

Niobium is found in solution mainly as $Nb(OH)_6^-$, and the concentration is low enough to prevent the precipitation of Nb_2O_5 solid species (SI of –7.37). Finally, nickel in solution is found as the Ni^{2+} ion, and in much smaller amounts as carbonate complexes.

Initial composition of the exchanger

The modelled domain of the clay system is composed of glacial clays that are rich in illite /Hedenström 2004/. An illite content of 50 wt% has been considered in the model, which leads to an exchange site density of 1.125 mol/L, as shown in the beginning of Section 5.8. As in reference case #1, the total concentration of sites in illite is kept constant during the reactive transport simulations, and the implemented exchange constants follow the Gaines-Thomas convention (Table 5-6).

The initial composition of the exchangeable sites in the illite present in the glacial clays has been calculated by equilibrating these exchangeable sites with the glacial clay porewater, using the PHREEQC code /Parkhurst and Appelo 1999/. The resulting initial exchanger composition is shown in Table 5-12.

Table 5-12. Initial composition of the illite interlayer in reference case #2.

Site	mol·L_{water}^{-1}
Planar sites	
CaX_2	4.03×10^{-1}
MgX_2	4.36×10^{-2}
KX	4.98×10^{-3}
NaX	2.02×10^{-3}
SrX_2	2.32×10^{-4}
BaX_2	5.06×10^{-5}
NiX_2	1.53×10^{-6}
CsX	1.37×10^{-8}
UO_2X_2	8.53×10^{-15}
Type II sites	
KX^{II}	2.16×10^{-1}
NaX^{II}	8.75×10^{-3}
CsX^{II}	5.93×10^{-6}
Frayed edge sites (FES)	
KX^{FES}	5.15×10^{-4}
NH_4X^{FES}	2.27×10^{-3}
NaX^{FES}	1.05×10^{-5}
CsX^{FES}	1.77×10^{-5}

The illite exchanger composition after the equilibration of the illite exchangeable sites with the glacial clay porewater may be summarised as follows: (1) the most abundant cation in the illite interlayer is calcium, which occupies 88% of the planar sites, with a concentration of 4.03×10^{-1} mol·L_{water}^{-1}. Magnesium is the second most abundant cation in the planar sites, with a concentration one order of magnitude lower than that of calcium; (2) in the planar sites, UO_2^{2+} is the less abundant species, followed by Cs^+ and Ni^{2+}, while potassium, sodium and strontium show intermediate concentrations in this type of sites; (3) potassium is the most abundant cation in the type II sites, while in the FES ammonium is the most abundant cation (Table 5-12). As shown in Table 5-12, caesium is most effectively retained in the FES, followed by the type II sites, as expected by the exchange constants given in Table 5-6.

Initial composition of the illite surface

According to the model of /Bradbury and Baeyens 2009a, b/ the sorption of Ni, U and Th onto illite was described by means of a two site protolysis non-electrostatic surface complexation and cation exchange model. The calculated surface complexation site density in the modelled domain is 0.01 mol/L for strong sites and 0.2 mol/L for edge sites. The initial composition of the illite surface in equilibrium with the selected groundwater has been calculated with the PHREEQC code and is reported in Table 5-13.

In the model, Ni, Th and U are considered to sorb onto strong sites only. Of the three, nickel has more affinity for these sites, and is sorbed mainly as Ni^{2+}. Th is sorbed mainly as the complex $\equiv S^sOTh(OH)_4^-$, but the number of sites occupied by Th is almost two orders of magnitude below that of Ni. Uranium has much less affinity for the illite surface, compared to Ni and Th (Table 5-13).

Initial partition coefficients of selected elements

The calculated surfaces in equilibrium with the clay porewater can be used to obtain Kd values of the sorbed elements. As explained for case #1, since the concentration of species in the surface and cation exchange sites are reported as mole per liter of water, they have to be converted to mole per kilogram of rock in order to determine Kds (Equation 5-17). The total porosity of the clay is 0.2 /Johansson et al. 2005/ and a density of 2 kg/L has been taken for the calculations /Sena et al. 2008/.

$$Kd = \frac{[sorbate]\,mol/L}{[solute]\,mol/L} \times \frac{0.2}{2\,kg/L} \qquad \text{Equation 5-17}$$

Table 5-13. Initial concentrations of the species adsorbed on illite surface sites in reference case #2.

Site	mol·L_{water}^{-1}
Strong sites	
$\equiv S^sO^-$	8.55×10^{-3}
$\equiv S^sONi^+$	9.04×10^{-4}
$\equiv S^sOH$	4.89×10^{-4}
$\equiv S^sONiOH$	3.15×10^{-5}
$\equiv S^sOTh(OH)_4^-$	2.09×10^{-5}
$\equiv S^sOTh(OH)_3$	2.39×10^{-6}
$\equiv S^sONi(OH)_2^-$	6.94×10^{-7}
$\equiv S^sOTh(OH)_2^+$	2.17×10^{-7}
$\equiv S^sOH_2^+$	1.77×10^{-7}
$\equiv S^sOUO_2(OH)_2^-$	5.46×10^{-8}
$\equiv S^sOUO_2OH$	2.48×10^{-8}
$\equiv S^sOUO_2(OH)_3^{2-}$	6.03×10^{-9}
$\equiv S^sOThOH^{2+}$	3.92×10^{-10}
$\equiv S^sOUO_2^+$	2.83×10^{-10}
$\equiv S^sOTh^{3+}$	1.78×10^{-12}
Amphoteric edge site 1	
$\equiv S^{WI}O^-$	1.89×10^{-1}
$\equiv S^{WI}OH$	1.08×10^{-2}
$\equiv S^{WI}OH_2^+$	3.90×10^{-6}
Amphoteric edge site 2	
$\equiv S^{WII}OH_2^+$	1.84×10^{-1}
$\equiv S^{WII}OH$	1.61×10^{-2}
$\equiv S^{WII}O^-$	1.41×10^{-5}

The calculated Ni Kd is 19,176 L/kg, which fits within the range of the Kd values reported by /Engdahl et al. 2008/ for Forsmark lake sediments (Table 3-5). The calculated Kd of Th is 15,568 L/kg, which is one order of magnitude lower than those reported by /Engdahl et al. 2008/. Finally, the calculated Kd of uranium is 7.7 L/kg, which is much lower (more than two orders of magnitude) than the Kd reported by /Engdahl et al. 2008/ (Table 3-5). In the case of uranium, the large difference could in part be due to the fact that in the calculation of the Kd from the modelling results, the contribution of uranium solid phases has not been considered, although the clay porewater is initially saturated with amorphous uraninite.

5.9 Set-up of the sensitivity analysis

Due to the natural geochemical variability of the modelled Quaternary deposits, a sensitivity analysis of key geochemical parameters that affect radionuclide mobility has been carried out, following /Sena et al. 2008/. The sensitivity analysis is developed in order to estimate the impact of considering distinct values of the most important geochemical parameters on model results. In order to have a realistic approach to the natural geochemical variability at Forsmark and its impact on model results, the ranges of the parameters selected for sensitivity analysis are set according to site specific features of the till and the clay deposits.

5.9.1 Reference case #1: The till system

The sensitivity analysis developed for the till system focuses on three main geochemical features: the $(Ca,Sr)CO_3$ solid solution, the cation exchange capacity and number of complexation sites in illite. As mentioned above, the calcium carbonate present in the till and clay deposits is considered to have trace amounts of strontium and, therefore, the $CaCO_3$ contents calculated for each system actually correspond to the contents of a $(Ca,Sr)CO_3$ solid solution.

The sensitivity analysis for $(Ca,Sr)CO_3$ solid solution is based on three cases. The first case, being the reference case #1, is set with 1 mol/L of Sr-bearing calcium carbonate that forms a non-ideal solid solution between both end-members ($CaCO_3$ and $SrCO_3$) and the equilibrium with siderite. The second case is as the reference case #1, but without considering the equilibrium with siderite. The third case is set without solid solution nor calcite, in order to evaluate the role of the $(Ca,Sr)CO_3$ solid solution in strontium mobility, and the relative importance of cation exchange and $(Ca,Sr)CO_3$ solid solution for the retention of Sr.

In reference case #1, the strontium molar fraction of the solid solution initially present in the modelled domain was set by adjusting the strontium molar fraction in the solid solution to a value that is in equilibrium with the natural aqueous strontium concentration. The resulting strontium molar fraction is 1.73×10^{-5}.

In order to study the impact of variable CEC values in the till deposit, which lead to distinct concentrations of available cation exchange sites, two cases will be evaluated. One case corresponds to the reference case with a CEC of 225 meq/L (1.755×10^{-1} mol/L of cation exchange sites), and an alternative case with a CEC of 20 meq/L, which corresponds to 1.6×10^{-2} mol/L of cation exchange sites in the till deposit. The change in CEC is expected to influence the retention of Cs, U, Sr, Ra and Ni.

In the simulation with a CEC of 20 meq/L, a decrease in the number of complexation sites on illite has been included. In this case, the number of strong sites was 2×10^{-4} mol/kg illite and the number of each of the edge sites 4×10^{-3} mol/kg illite. This decrease can influence the retention of U, Th and Ni. Table 5-14 shows the summary of the sensitivity analysis set for the till system.

Table 5-14. Summary of the sensitivity analysis set for the till system. RC refers to reference case #1.

Radionuclide	Initial geochemical conditions	
Sr	With $(Ca,Sr)CO_3$ solid solution (Sr molar fraction = 1.73×10^{-5})	With siderite (RC)
		Without siderite
	Without $(Ca,Sr)CO_3$ solid solution	
Sr, Cs, U, Ni, Th, Ra	Illite CEC = 225 meq/L (RC)	
	Illite CEC = 20 meq/L	

5.9.2 Reference case #2: The clay system

In the clay system, the sensitivity analysis developed focuses on four main features: the $(Ca,Sr)CO_3$ solid solution, the isotopic fractionation of carbon, the cation exchange capacity (CEC) and complexation sites on illite and the humic acids.

In a similar way as in the till system, the sensitivity analysis for Sr deals with the variation of the concentration of $(Ca,Sr)CO_3$ solid solution and the CEC. The reference case #2 is set with 1 mol/L of $(Ca,Sr)CO_3$, with a strontium molar fraction of 1.4×10^{-5}, which is in equilibrium with the reference water selected for the clay system. As in the till system, the effect of not considering siderite will be evaluated. An alternative case will be simulated without $(Ca,Sr)CO_3$ solid solution.

The temperature-dependent isotopic fractionation is modelled for carbon, and it is considered that fractionation occurs between dissolved carbon species and between dissolved species and the solid solution $(Ca,Sr)CO_3$. The reference case # 2 is modelled at 15ºC, and in order to determine the effect of fractionation at different reaction temperatures and to see if there are significant differences in the ^{14}C retention related to the isotopic fractionation, two other simulations will be run, one at 5ºC and the other at 25ºC.

The reference case #2 considers a CEC of 225 meq/L, which corresponds to 1.125 mol/L of exchange sites. As an alternative case, a CEC of 20 meq/L, which corresponds to 0.1 mol/L of cation exchange sites, has been simulated. The change in CEC is expected to influence the retention of Cs, U, Sr, I, Ra and Ni. Also in the same simulation a decrease in the number of complexation sites on illite has been included. In this case, the number of strong sites was 2×10^{-4} mol/kg illite and the number of each of the edge sites 4×10^{-3} mol/kg illite. This decrease can influence the retention of U, Th and Ni.

The sensitivity analysis for the concentration of humic acids is based on the changes in the uranium and thorium speciation caused by the increment of the concentration of these organic acids in the clay porewater (Figure 5-9). In reference case #2, the clay porewater has 1×10^{-4} M of humic acids (which corresponds approximately to 10% of the DOC in the reference water collected in sampling point PFM117. Under these conditions the complexation of uranium and thorium with humic acids is not very important; the concentration of these aqueous complexes is extremely low, with $U(OH)_4$ and $Th(OH)_3CO_3^-$ being the dominant aqueous species (Figure 5-9).

When the concentration of humic acids increases, the aqueous complex $UO_2(humate)_2$ becomes progressively more abundant (Figure 5-9), which may prevent the precipitation of amorphous uraninite. Since the precipitation of this uranium solid phase is one of the processes able to retain uranium in the clay system, /Sena et al. 2008/ decided to evaluate three alternative cases: humic acid concentrations of (1) 3×10^{-3} M, (2) 0.1 M, and (3) a case without humic acids. In the present study the sensitivity analysis with a 0.1 M of humic acid has not been considered. To maintain equilibrium with the calcite initially present in the clay sediments, a clay porewater with 0.1 M of HA should have a pH of 10.4, which is significantly different from the measured pH of 8.0. In order to avoid this pH increase, humic acid should be modelled as a product of degradation of organic matter. Table 5-15 shows the summary of the sensitivity analysis performed for the clay system.

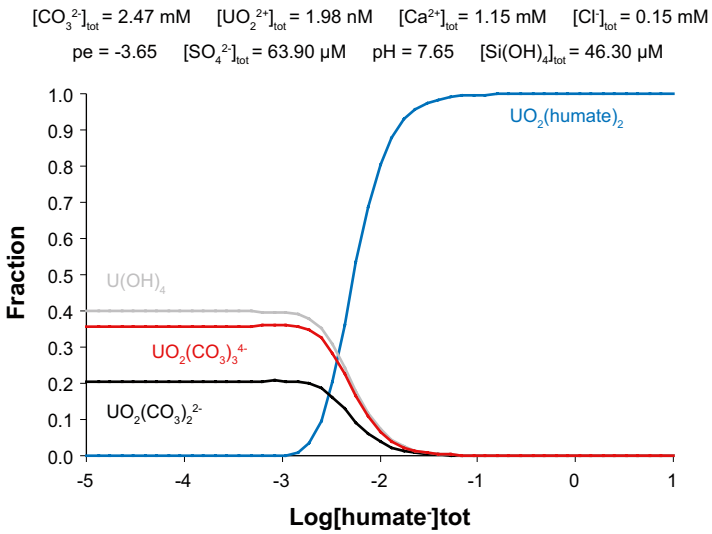

Figure 5-9. *Evolution of the uranium speciation in a solution with a variable humic acid concentration, under the hydrochemical conditions of the clay porewater.*

Table 5-15. Summary of the sensitivity analysis set for the clay system. RC refers to reference case #2.

Radionuclide	Initial geochemical conditions	
Sr	With $(Ca,Sr)CO_3$ solid solution (Sr molar fraction = 1.4×10^{-5})	With siderite (RC)
		Without siderite
	With $CaCO_3$ solid solution	
C	Isotopic fractionation at 15ºC (RC)	
	Isotopic fractionation at 5ºC	
	Isotopic fractionation at 25ºC	
Sr, Cs, U, Ni, Th, Ra	Illite CEC = 225 meq/L (RC)	
	Illite CEC = 20 meq/L	
U, Th	With humic acids	1×10^{-4} mol/L (RC)
		3×10^{-3} mol/L
	Without humic acids	
	Without siderite	

6 Till system numerical modelling results

6.1 Conservative transport

The transport of solutes is affected by geochemical processes and by the hydraulic gradient and groundwater flow generated from the prescribed boundary conditions. Figure 6-1 shows the groundwater flow directions and hydraulic gradient calculated by the numerical tool. In this figure it is possible to see that the groundwater entering through the left boundary, moves horizontally along most of the domain, and flows out through the last 20 m of the top boundary, where an upward flow is generated.

It is interesting to note that the flux is not homogeneous through the 20 m of the discharge surface, instead, the maximum flux (900 L/yr) is registered at the first point of discharge (X = 80 m, Y = 3 m), and then it decreases exponentially, being 9 times lower at X = 82 m and 40 times lower at X = 90 m (Figure 6-2). This huge heterogeneity in the flux will have implications for the predicted transport of radionuclides to the surface.

The conservative transport in the reference case #1 has been studied using a tracer. The initial concentration of the tracer in the deep groundwater is 0.1 mol/L and in the till groundwater is 0 mol/L. In Figure 6-3 the migration of the conservative tracer in the till domain is tracked at different simulation time steps. In the first days of groundwater input, the distribution of the tracer is constrained to the bottom layers of the till, which is due to the horizontal flow direction (see Figure 6-1) and the fact that the intermediate till layer has lower vertical and horizontal hydraulic conductivities than the bottom layer. However, some dispersion occurs and the tracer reaches the upper layer of the till (see cross-sections at 1,000 and 5,000 days in Figure 6-3).

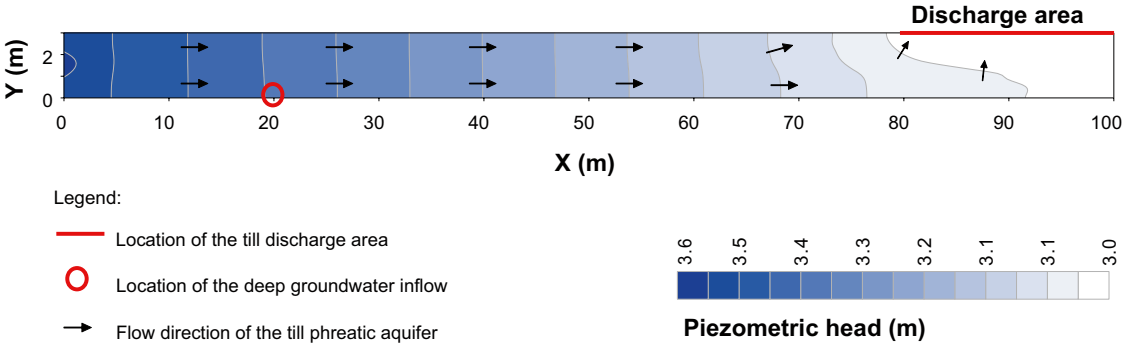

Figure 6-1. *Groundwater flow directions and hydraulic gradients obtained from the numerical transport simulation after setting the prescribed boundary conditions.*

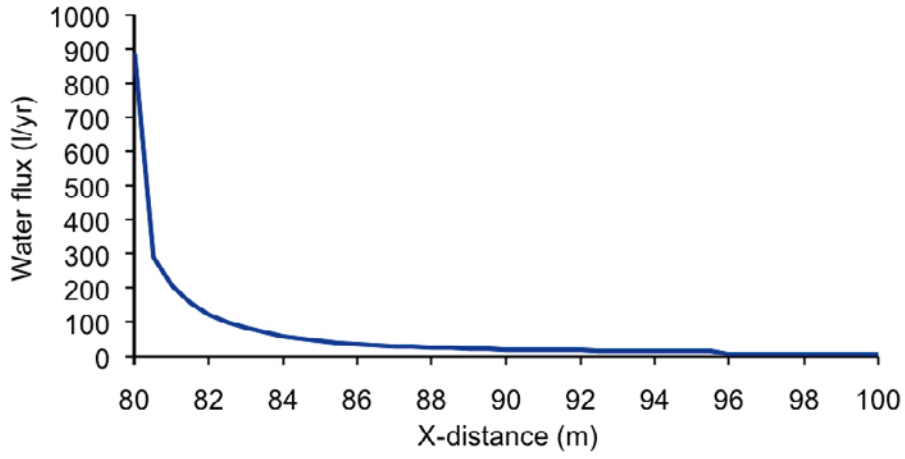

Figure 6-2. *Water flux at the discharge surface (X = 80–100 m, Y = 3 m) obtained in the numerical simulation of the till domain. It can be seen that most of the water flows out in the left corner of the discharge zone.*

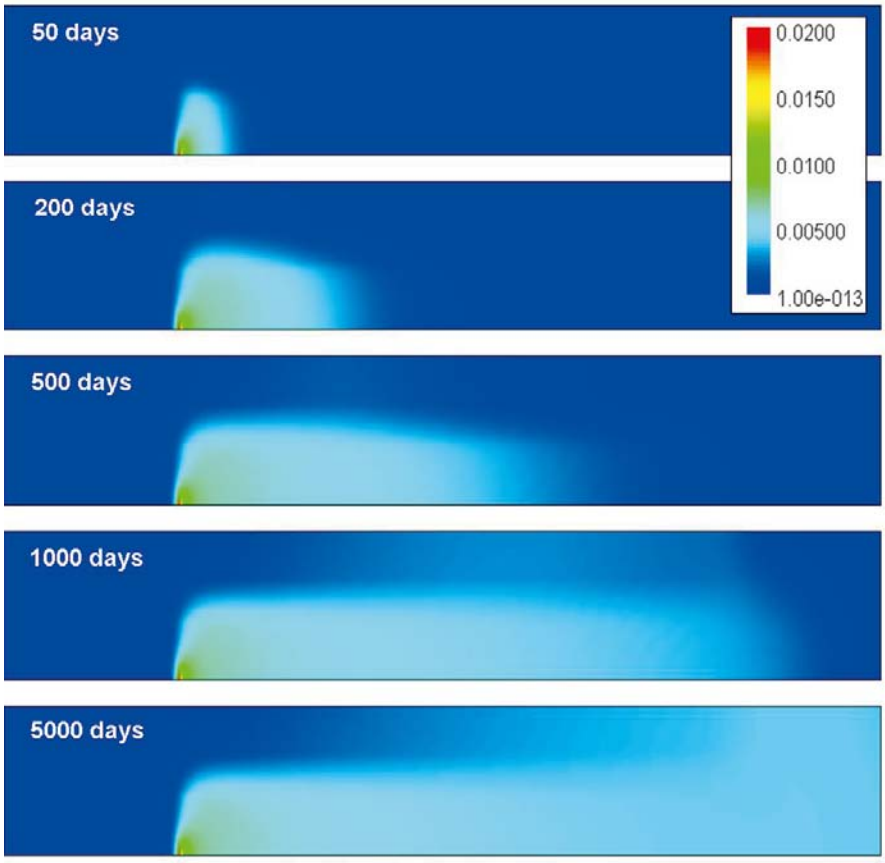

Figure 6-3. *Migration of the conservative tracer in the till domain at 50, 200, 500, 1,000 and 5,000 days of simulation of deep groundwater input. The scale bar shows concentration in mol/L.*

The tracer reaches the discharge area (X = 80–100 m, Y = 3 m) approximately between 5 and 20 years after the intrusion of the deep groundwater (Figure 6-4). This means that after this time, a steady state is reached for the conservative transport. In Figure 6-4 it is also observed that at the point X = 80 m, Y = 3 m the concentration of the tracer is slightly lower than that at the point X = 100 m, Y = 3 m. This can be explained by the fact that at the first point of discharge, the contribution of the till groundwater flowing from the left of the domain is larger than that from the rest of the discharge area. Computed results show that if there was no dispersion the nuclides coming with the deep groundwater would have longer residence times than if they could move by transverse dispersion to faster "streamlines" (like they do in the present model).

The dilution of the deep groundwater in the till domain has been assessed with the conservative tracer. A dilution factor of 96% has been calculated for the discharge area of the till system (between nodes X= 80 m, Y = 3 m and X = 100 m, Y = 3 m). The following formula has been used in the calculation:

$$dilution\ \ factor = 100 \times \left(1 - \frac{[tracer]_{obspnt}}{[tracer]_{dgw}} \right) \qquad \text{Equation 6-1}$$

where $[tracer]_{obspnt}$ is the concentration of the tracer at the point of interest in the till domain and $[tracer]_{dgw}$ is the concentration of the tracer in the deep groundwater. Due to the small difference in the tracer concentration across the discharge area (Figure 6-5), the variation in the dilution factor is not significant (the dilution factor is 96.5% at the node X = 80 m, Y = 3 m, and 96% at X = 100 m, Y = 3 m).

Figure 6-5 shows the concentration of the tracer at the discharge area at steady state. All average concentrations of dissolved species that represent the whole discharge area of the till domain (X = 80–100, Y = 3 m) are flux-weighted concentrations. This is the case for the results presented in Figure 6-4 and in the other figures showing results from the model of the till system in the following subsections.

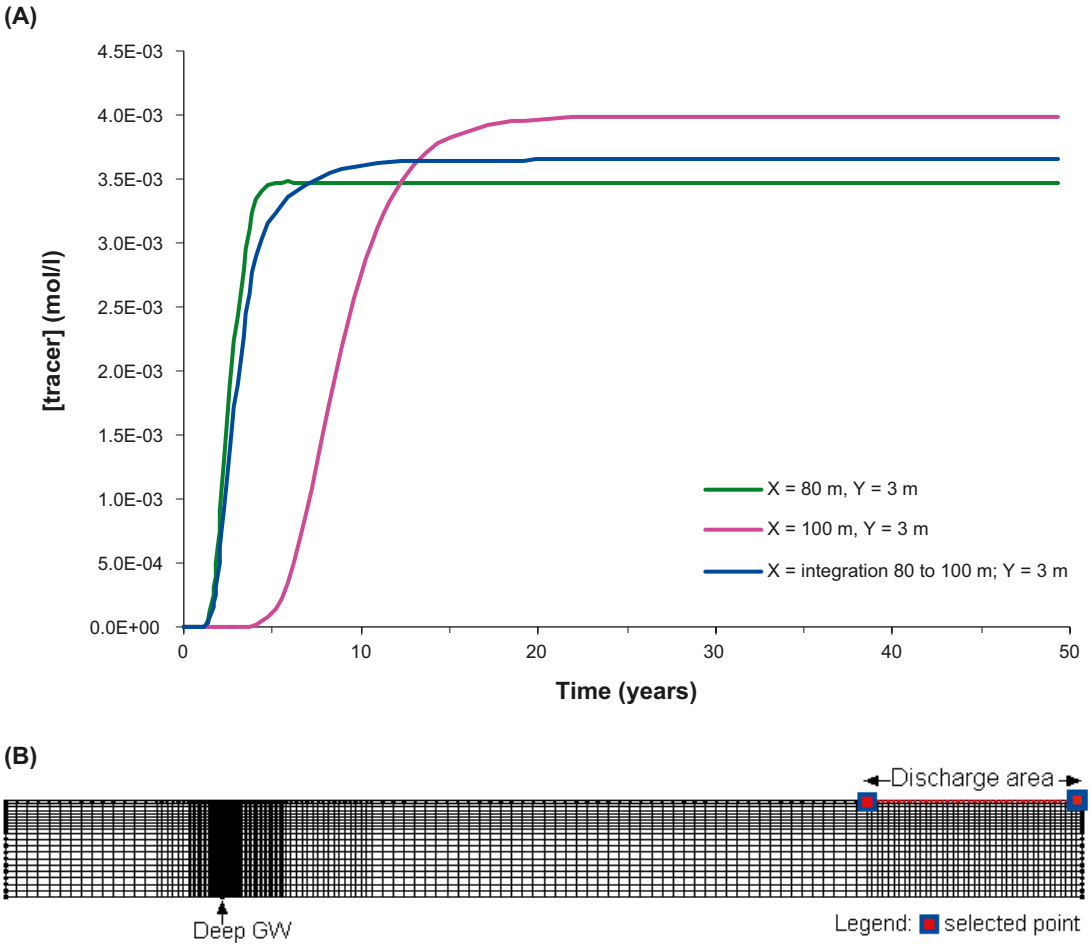

Figure 6-4. *(A) Breakthrough curve of A in the nodes X = 80 m, Y = 3 m and X = 100 m, Y = 3 m. The time needed to reach the stationary state of solute transport is approximately between 5 and 20 years. (B) Location of selected points for the study of the evolution of the outflowing solution.*

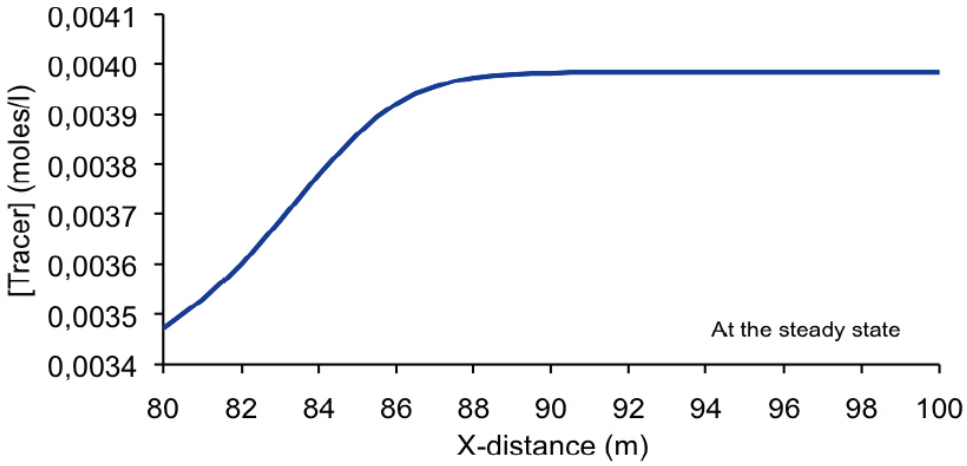

Figure 6-5. *Concentration of the tracer at the discharge area (X = 80–100 m, Y = 3 m), once the steady state is reached in the numerical simulation of the till domain.*

6.2 Reactive transport

The reactive behaviour of the elements Sr, U, Cs, C, Nb, Th and Ni has been simulated during 2,700 years, prior to the radionuclide release from the repository. Also Cl and I are included in the simulation, although they are considered to behave conservatively. After this period, the release of radionuclides has been included in the simulation and the leakage from the repository has been simulated for another 2,700 years. During the initial 100 years of reactive transport simulation, small oscillations of the pe occur at the monitoring point (X = 80 m, Y = 3 m; Figure 6-6). After repository release (2,700 years), also a small oscillation of the pe is predicted. The pH is almost stable at 7.1 during the whole simulation period.

The results obtained for each radionuclide of interest will be reported in the following sub-sections, including a quantitative assessment of the retention efficiency and a sensitivity analysis when applicable. For the radionuclides that are affected by retention, the reactive transport results are compared with the corresponding results for conservative transport. This means that for comparative purposes the reactive radionuclides are modelled also without including the retention processes in the model.

6.2.1 Carbon

Carbon is a major element in the Forsmark groundwaters, and the concentration of dissolved carbon prior to repository release is very similar in the two water types considered in the model, deep groundwater and till porewater. The contribution of ^{RD}C to the total carbon concentration in deep groundwater due to repository release is very small, 2.9×10^{-7} mol/L, which is four orders of magnitude lower than the concentration of natural carbon in solution.

The concentration of ^{RD}C increases gradually with time at the discharge area, until reaching a steady state (Figure 6-7). Repository-derived carbon is partially retained in the modelled domain by incorporation in calcite solid solution [$Ca(^{RD}C,C)O_3$] (Figure 6-8). The numerical modelling predicts that the till system is not efficient in retaining ^{RD}C in the solid phase, since after 1,000 years of repository release ^{RD}C shows the same concentration as in the corresponding conservative transport case (Figure 6-7). Nevertheless, the amount of ^{RD}C flowing out of the till deposit is almost six orders of magnitude lower than the natural carbon (Figure 6-7).

Quantitative assessment of carbon retention efficiency

The efficiency of the near-surface Quaternary system for radionuclide retention can be quantitatively evaluated by comparison of the conservative versus reactive transport computed results. This evaluation is done by integrating the results from the whole discharge surface (X = 80–100 m; Y = 3 m). The radionuclide retention efficiency (E) of the system at a given time (τ) can be quantitatively evaluated according to:

$$E^{\tau} = 100 \times \left(1 - \frac{R^{\tau}}{C^{\tau}}\right) \qquad \text{Equation 6-2}$$

where R^{τ} stands for the concentration of a solute at a given time (τ) when reactive transport is considered, and C^{τ} stands for the concentration of a solute at a given time (τ) when conservative transport is considered.

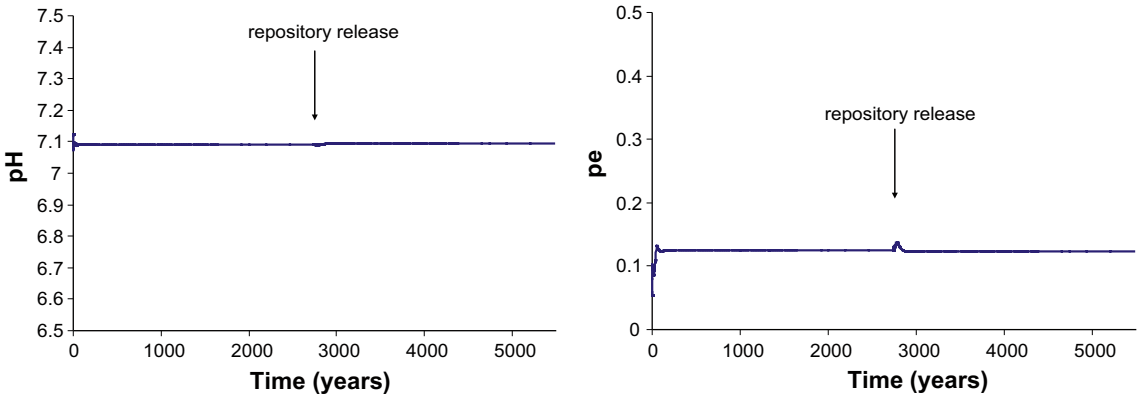

Figure 6-6. *Evolution of pH and pe during 5,400 years of reactive transport simulation (monitoring point located at X = 80 m, Y = 3 m).*

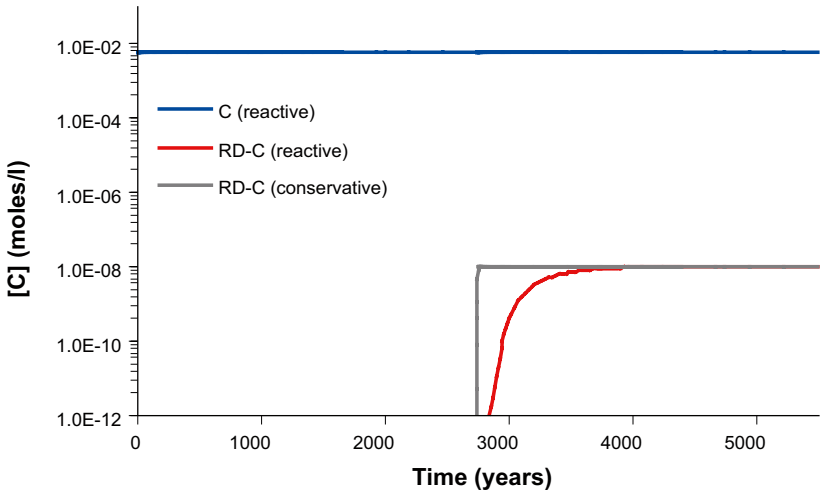

Figure 6-7. *Predicted evolution of natural carbon and of repository-derived carbon at the discharge area (integration of the monitoring points X = 80 to 100 m, Y = 3 m). Also the corresponding conservative breakthrough curve of ^{RD}C is represented (no retention processes, but otherwise the same simulation).*

Figure 6-8. *Concentration of ^{RD}C retained in calcite solid solution at the end of the simulation period (2,700 years after repository release).*

According to this expression, a zero reactive concentration (R) at a given time (τ) means that no mass of radionuclide is leaving the system at that time, resulting in a retention efficiency of 100%. A reactive concentration (R) equal to the conservative concentration means that no retention is occurring, so that the corresponding retention efficiency would be 0%. Negative efficiency means that in the reactive transport the solid phase is releasing a radionuclide into solution, and therefore the reactive concentration is higher than the conservative concentration.

In Figure 6-9 it is observed how the efficiency of retention for repository-derived carbon reached a maximum at the beginning of the simulation of repository release, while after 2,700 years the retention efficiency has dropped to less than 1%.

6.2.2 Iodine

The concentration of iodine in solution prior to repository release is higher in the deep groundwater (3.4×10^{-7} mol/L) than in the till porewater (6.4×10^{-8} mol/L). The initial concentration of ^{RD}I in deep groundwater due to repository release is 1.6×10^{-5} mol/L, which is approximately 2 orders of magnitude higher than the concentration of natural iodine in the deep groundwater.

In the numerical modelling, iodine has been considered to behave conservatively; therefore, dilution will be the only process that will diminish the concentration of ^{RD}I from the source to the discharge area. In Figure 6-10 it is observed how, after repository relase, the concentration of ^{RD}I is one order of magnitude higher than natural iodine. Therefore, during the simulation of repository release, nearly 90% of iodine flowing out of the till deposit corresponds to ^{RD}I. However, the concentration of ^{RD}I at the discharge area is less than 4% of the ^{RD}I concentration in deep groundwater after repository release, indicating a strong dilution effect.

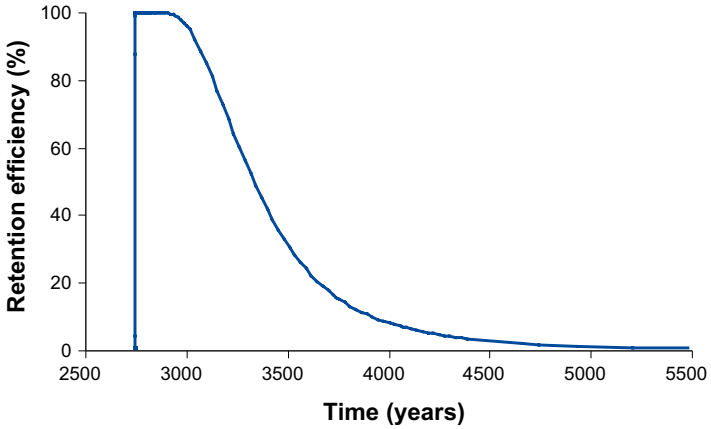

Figure 6-9. *Retention efficiency for repository-derived carbon along the simulation time at the discharge area (monitoring points: X = 80–100 m, Y = 3 m).*

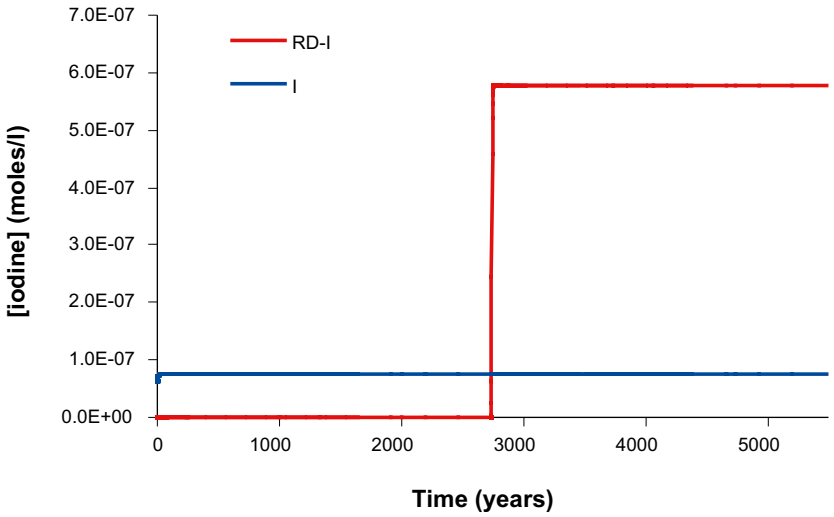

Figure 6-10. *Conservative breakthrough curves of natural iodine (I) and repository-derived iodine (RD-I) at the discharge area (integration of the monitoring points X = 80 to 100 m, Y = 3 m).*

6.2.3 Chlorine

Chlorine is a major element in the Forsmark groundwaters, and the concentration of dissolved chlorine prior to repository release is higher in the deep groundwater (0.1 mol/L) than in the till porewater (1.9×10^{-3} mol/L). The initial concentration of RDCl in deep groundwater due to repository release is 5.1×10^{-7} mol/L, which is much lower than the concentration of natural chlorine.

In the numerical modelling, chlorine, like iodine, has been considered to behave conservatively. Therefore, dilution will be the only process that reduces the concentration of RDCl from the source of radionuclide release to the discharge area. After repository relase, the concentration of RDCl in the observation points is more than five orders of magnitude lower than that of natural chlorine (Figure 6-11), and almost one and a half orders of magnitude lower than the RDCl concentration in deep groundwater after repository release.

6.2.4 Thorium

The concentration of thorium in solution prior to repository release is very similar in the deep groundwater (1.19×10^{-9} mol/L) and the till porewater (6.09×10^{-10} mol/L). In the reactive transport simulation, the amount of natural thorium in solution at the discharge area is constant through time (Figure 6-12) and almost equivalent to the concentration in the till porewater entering the system.

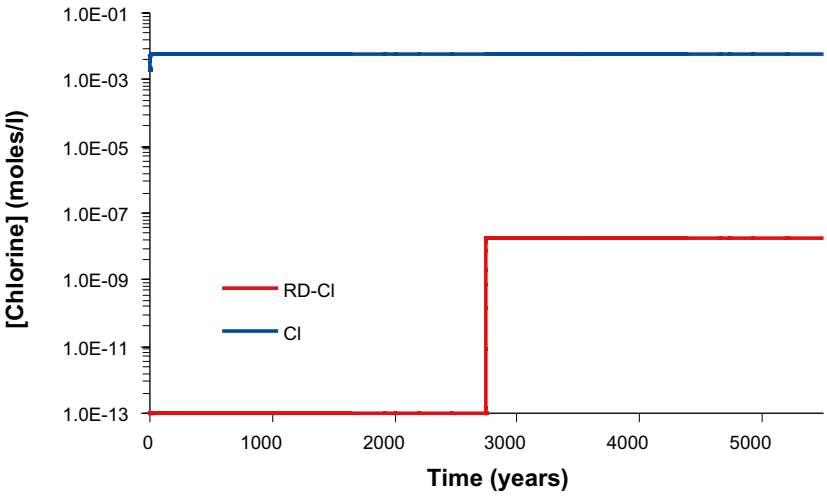

Figure 6-11. *Conservative breakthrough curves of natural chlorine (Cl) and repository-derived chlorine (RD-Cl) at the discharge area (integration of the monitoring points X = 80 to 100 m, Y = 3 m).*

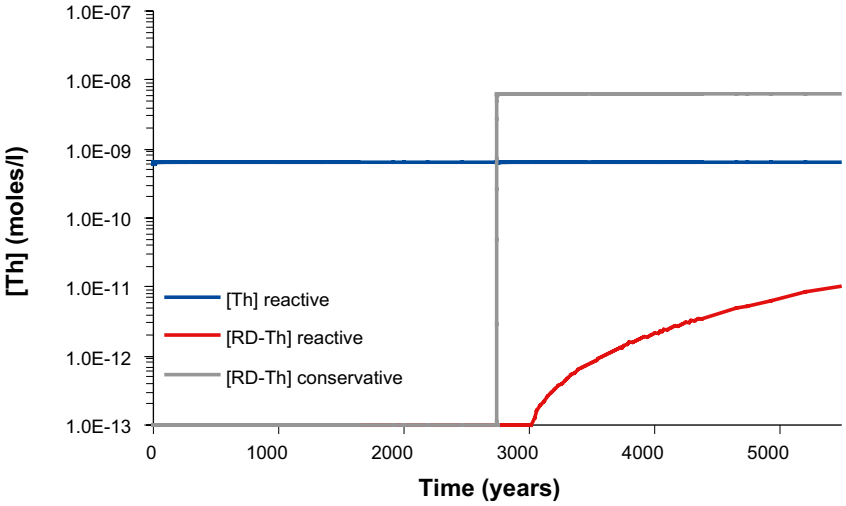

Figure 6-12. *Predicted evolution of natural thorium and of repository-derived thorium at the discharge area (integration of the monitoring points X = 80 to 100 m, Y = 3 m). Also the corresponding conservative breakthrough curve of RDTh is represented.*

According to the simulation results, the retention of natural thorium takes place by sorption onto illite (Figure 6-13), mainly as $\equiv S^{s}OTh(OH)_4^-$. In Figure 6-13 it can be noticed that the difference in concentration of natural thorium entering with deep groundwater compared to till porewater is retained by sorption onto illite.

The initial concentration of RDTh in deep groundwater due to repository release is 1.75×10^{-7} mol/L, which is approximately two orders of magnitude higher than the concentration of natural thorium. The concentration of RDTh increases gradually with time at the discharge area, and 2,700 years after repository release a steady state has not been reached yet (Figure 6-12). Saturation of amorphous thorianite is not reached in the whole simulated domain; however, most of the repository derived thorium entering into the system through the fracture is retained via surface complexation onto illite (Figure 6-13).

The retention capacity of the till system at Forsmark can be evaluated by comparing the results yielded by the reactive and conservative transport models after repository release. The quantification of the retention capacity of the till system for thorium reveals that at the end of the simulation period, RDTh concentration in the reactive transport simulation is more than two orders of magnitude lower than in the conservative transport simulation (Figure 6-12).

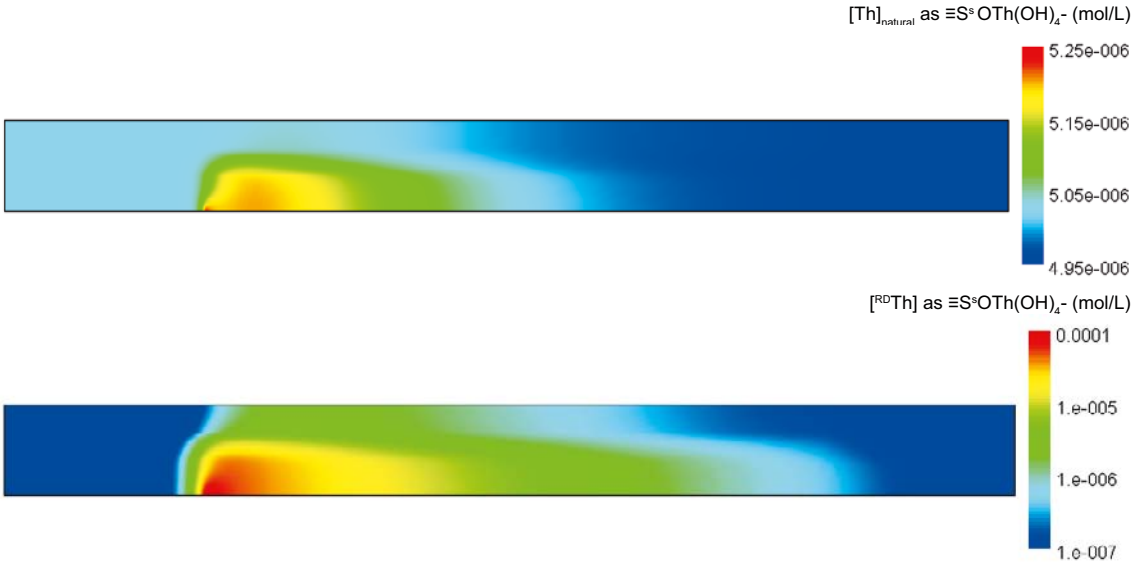

Figure 6-13. *Natural and repository derived (RD) thorium sorbed on illite as $\equiv S^sOTh(OH)_4^-$ (the most abundant complex of those considered in the model) at the end of the simulation period (2,700 years after repository release). Note the difference in scales.*

Quantitative assessment of thorium retention efficiency

The retention efficiency of repository-derived thorium is predicted to reach a maximum of nearly 100% immediately after repository release, which is maintained until the end of the simulation period (Figure 6-14).

Sensitivity analysis of thorium

The sensitivity analysis of thorium consisted in the simulation with less sorption sites on illite (from 225 to 20 meq/L). The concentration of natural thorium is almost the same in both cases (Figure 6-15). However, the concentration of RDTh in solution increases with time and at the end of the simulation is much higher (2 orders of magnitude) in the case with less complexation sites than in the reference case (Figure 6-15).

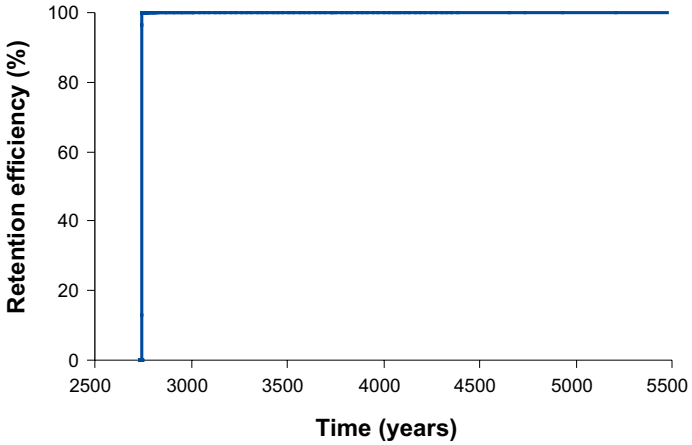

Figure 6-14. *Retention efficiency for repository-derived thorium along the simulation time at the discharge area (monitoring points: X = 80–100 m, Y = 3 m).*

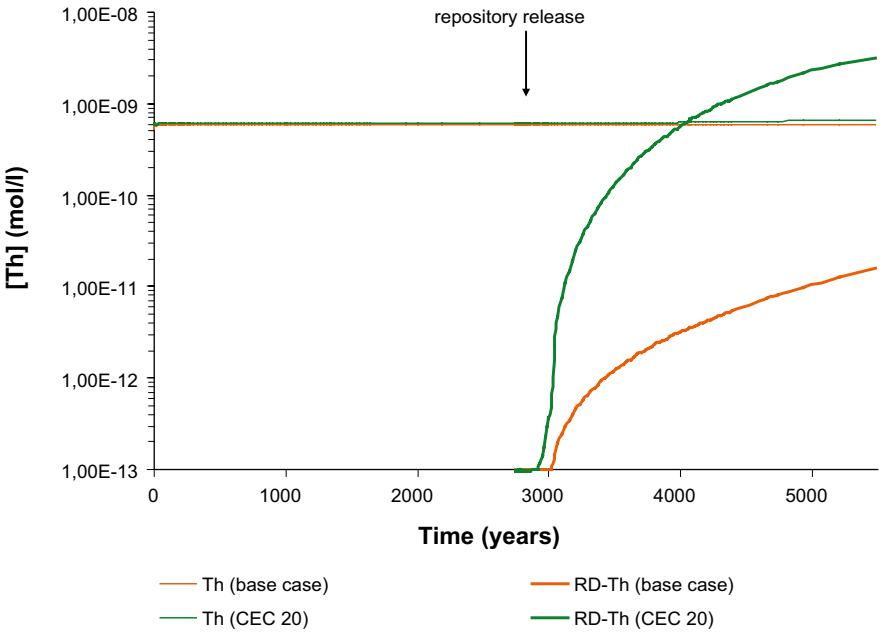

Figure 6-15. *Predicted evolution of natural thorium and repository-derived thorium concentration along the simulation time at the discharge area (monitoring point: X = 80 m, Y = 1 m). The results for the base case are represented, together with the simulation with less sorption sites.*

6.2.5 Nickel

The concentration of dissolved nickel in the deep groundwater is lower than in the till porewater (7.2×10^{-9} and 4.4×10^{-8} mol/L, respectively). After 2,700 years of simulation, the concentration of nickel at the discharge point is 5×10^{-8} mol/L (Figure 6-16), which is quite similar, but higher than the initial concentration of nickel in the till porewater. This small increase is explained by a release of sorbed nickel into solution.

The initial concentration of RDNi in deep groundwater due to repository release is 4.96×10^{-7} mol/L, which is approximately 2 orders of magnitude higher than the natural nickel concentration in deep groundwater and one order of magnitude higher than that in till groundwater.

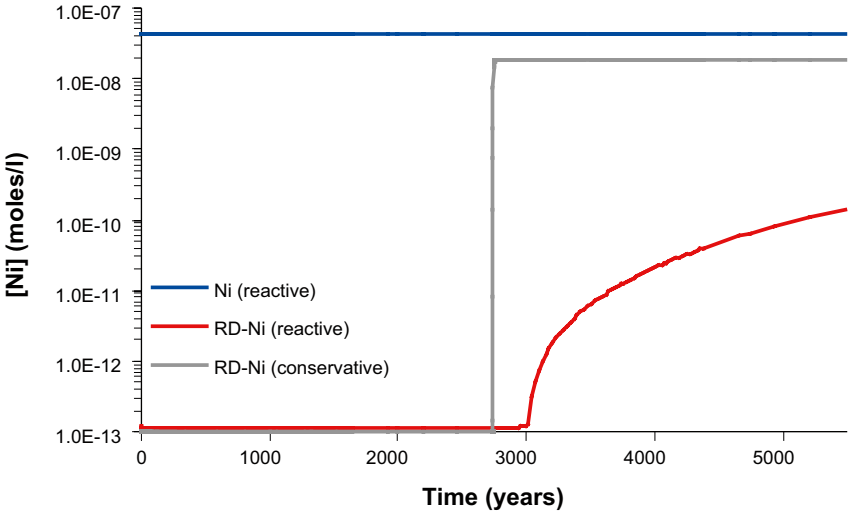

Figure 6-16. *Predicted evolution of natural nickel and repository-derived nickel at the discharge area (integration of the monitoring points X = 80 to 100 m, Y = 3 m). Also the corresponding conservative breakthrough curve of RDNi is represented.*

The quantification of the retention capacity of the till system for nickel reveals that at the end of the reactive transport simulation, RDNi concentration in the discharge area is two orders of magnitude lower than in the conservative transport simulation (Figure 6-16). This decrease is caused by the high affinity of nickel for the surface complexation sites on illite, and to a lesser extent by the adsorption onto ferrihydrite (Figure 6-17).

Quantitative assessment of nickel retention efficiency

Figure 6-18 shows the time evolution of the computed retention efficiency of repository-derived nickel. When repository release is simulated, repository-derived nickel is predicted to retain in the till system. Immediately after repository release the system reaches a retention efficiency for RDNi of 100%, and at the end of the simulation it has only dropped to 99% (Figure 6-18).

Figure 6-17. *Concentration of $^{RD}Ni^{2+}$ retained in illite and ferrihydrite at the end of the simulation period (2,700 years after repository release).*

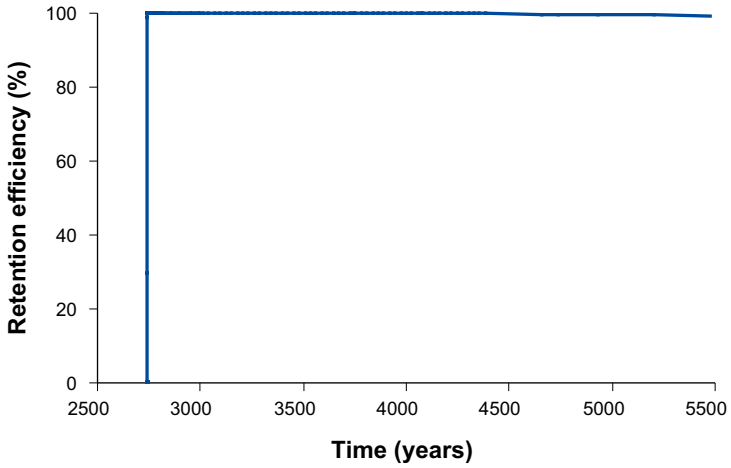

Figure 6-18. *Computed retention efficiency for repository-derived nickel along the simulation time (monitoring points: X = 80–100 m, Y = 3 m).*

Sensitivity analysis of nickel

The sensitivity analysis of nickel consisted in a simulation with less sorption sites (from 225 to 20 meq/L) on illite. The concentration of natural nickel is almost the same in both cases, while the concentration of RDNi in solution increases with time and at the end of the simulation it is one order of magnitude higher in the case with less complexation sites than in the reference case (Figure 6-19).

6.2.6 Niobium

Niobium is initially present in solution in the till porewater (1.14×10^{-9} mol/L). For the deep groundwater, no Nb concentration was available; the concentration was assumed to be negligible. The initial concentration of RDNb in the deep groundwater due to repository release is 5.25×10^{-8} mol/L, which is more than one order of magnitude higher than in the till porewater.

At the discharge area of the till deposit, the concentration of RDNb is quite similar to that of natural niobium (Figure 6-20). The numerical simulations predict that niobium is not retained in the till system, since saturation with Nb_2O_5 is not reached in the domain during the simulation period. The decrease of RDNb concentration from the deep groundwater inflow point to the discharge area of the till deposit is exclusively due to dilution.

6.2.7 Selenium

Se is considered not to be present initially in the till groundwater or the deep groundwater. The initial concentration of Se in the deep groundwater due to repository release is 3.77×10^{-11} mol/L. At the discharge area of the till deposit, the Se concentration is below the accuracy of the calculation tool ($<10^{-15}$ mol/L). The conservative curve is represented in Figure 6-21. The numerical simulations predict that selenium is retained in the till system by precipitation of the native selenium (Figure 6-22).

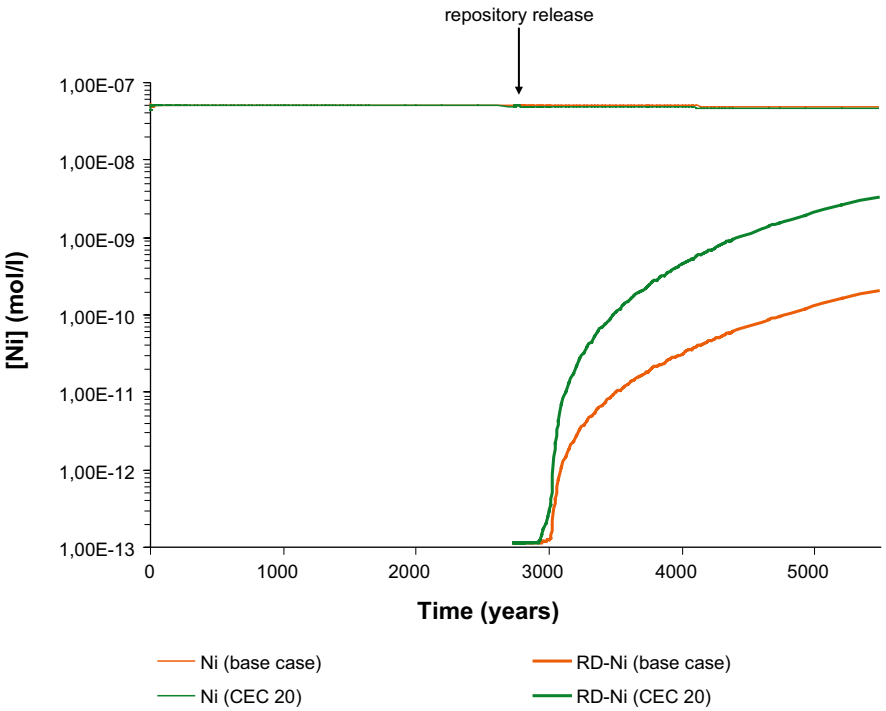

Figure 6-19. *Predicted evolution of natural and repository-derived nickel concentration along the simulation time at the discharge area (monitoring point: X = 10 m, Y = 1 m). The results for the base case are represented, together with the simulation with less sorption sites.*

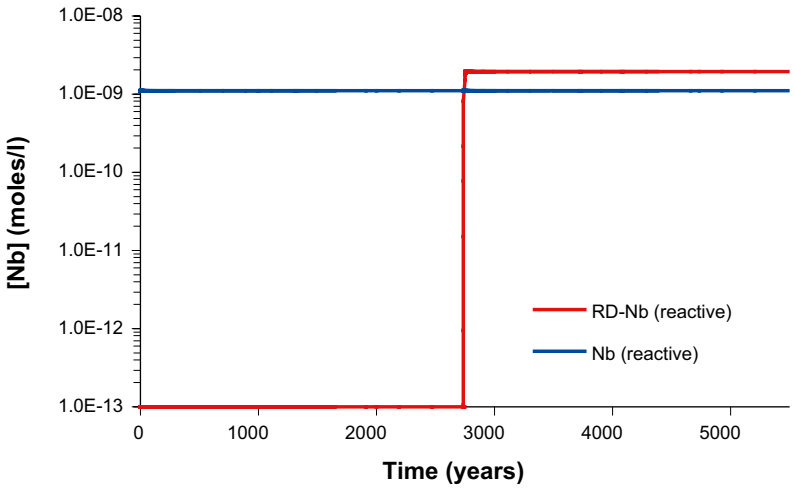

Figure 6-20. *Predicted evolution of natural niobium and repository-derived niobium at the discharge area (integration of the monitoring points X = 80 to 100 m, Y = 3 m). Since no retention is predicted, the modelled curve is the conservative breakthrough curve of RD-Nb.*

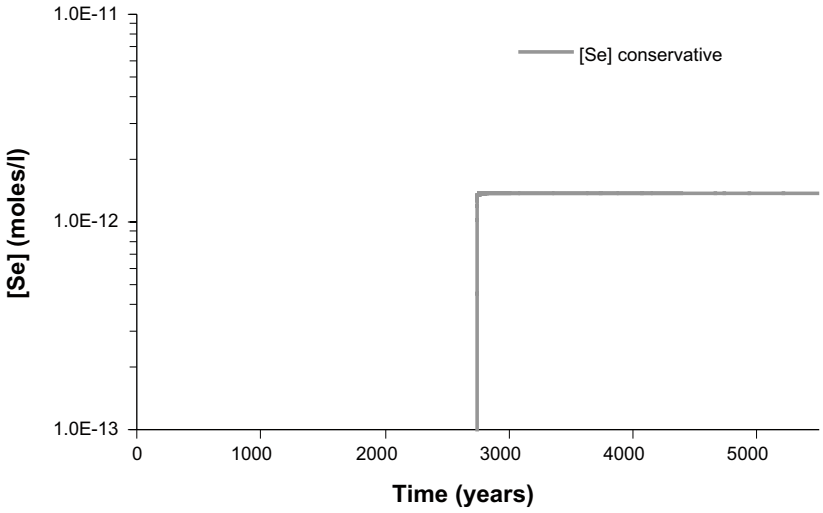

Figure 6-21. *Conservative breakthrough curve of selenium at the discharge area after repository release (integration of the monitoring points X = 80 to 100 m; Y = 3 m).*

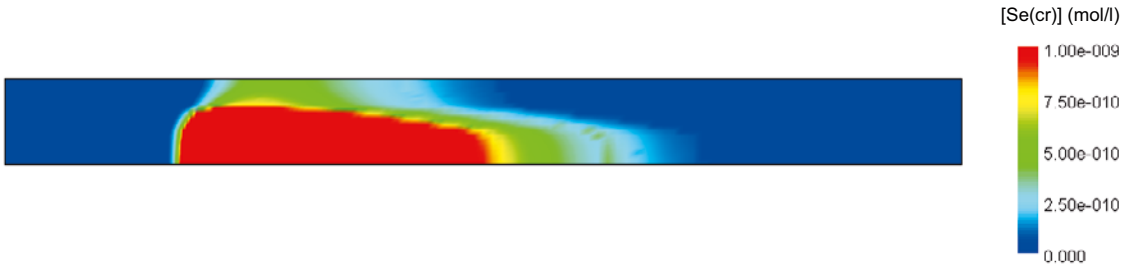

Figure 6-22. *Concentration of native selenium [Se(cr)] in the simulated till domain at the end of the simulation period (2,700 years after repository release).*

Quantitative assessment of selenium retention efficiency

The reactive transport simulation predicts that selenium from repository release does not reach the discharge area of the modelled till domain, and the calculation of the selenium retention efficiency gives a value of 100% of retention.

6.2.8 Technetium

The initial concentration of Tc in the deep groundwater due to repository release is 5.27×10^{-9} mol/L. The numerical simulations predict that technetium is not retained in the till system, since saturation with $TcO_2{\cdot}1.6H_2O$ is not reached along the simulation time. Again, as for RDNb, the decrease of Tc concentration from the deep groundwater inflow point to the discharge area of the till deposit is exclusively due to dilution (Figure 6-23).

6.2.9 Strontium

Before the release of radionuclides from the repository, the concentration of strontium in solution in the deep groundwater is one order of magnitude higher than in the till porewater. Deep groundwater affected by repository release has a RDSr concentration of 1.5×10^{-3} mol/L, which is approximately 1.5 orders of magnitude higher than the natural Sr concentration in the deep groundwater, and 3 orders of magnitude higher than the Sr concentration in the till porewater. At the end of the reactive transport simulation, ~94% of the strontium flowing out of the till deposit is derived from repository release (Figure 6-24).

The numerical modelling predicts that the till system is not efficient in retaining RDSr in the solid phase, since during most of the simulation period, the RDSr concentration at the discharge area behaves conservatively (Figure 6-24). Two retention mechanisms were considered for strontium in the reactive transport simulation; cation exchange in illite and precipitation as a solid solution [$(Ca, Sr)CO_3$]. Close to the deep groundwater discharge area, RDSr is preferentially retained via precipitation of the $(Ca,Sr)CO_3$ solid solution, while in most of the simulated till domain RDSr is more strongly retained via cation exchange on illite (Figure 6-25).

Quantitative assessment of strontium retention efficiency

Figure 6-26 shows the time evolution of computed retention efficiency of repository-derived strontium. When repository release is simulated, repository-derived strontium is predicted to be retained in the till deposit immediately after repository release (retention efficiency of 100%). However, the retention efficiency for RDSr soon drops to 0%.

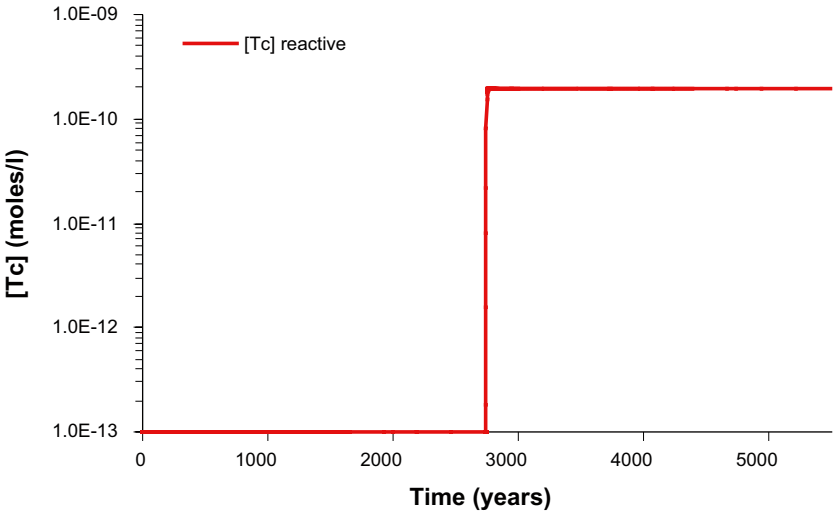

Figure 6-23. *Predicted evolution of technetium concentration at the discharge area (integration of the monitoring points X = 80 to 100 m, Y = 3 m). Since no retention is predicted, the modelled curve is the conservative breakthrough curve of Tc.*

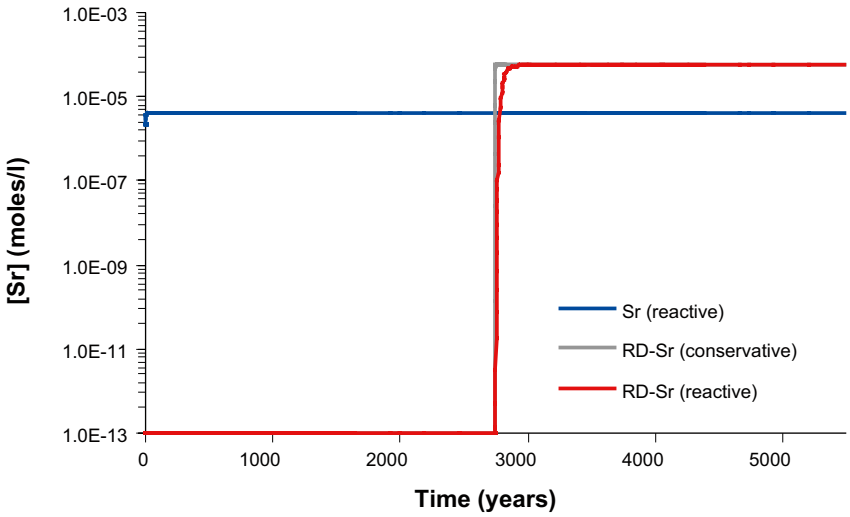

Figure 6-24. *Predicted evolution of natural strontium and repository-derived strontium at the discharge area (integration of the monitoring points X = 80 to 100 m; Y = 3 m). Also the conservative breakthrough curve of RD-Sr is represented.*

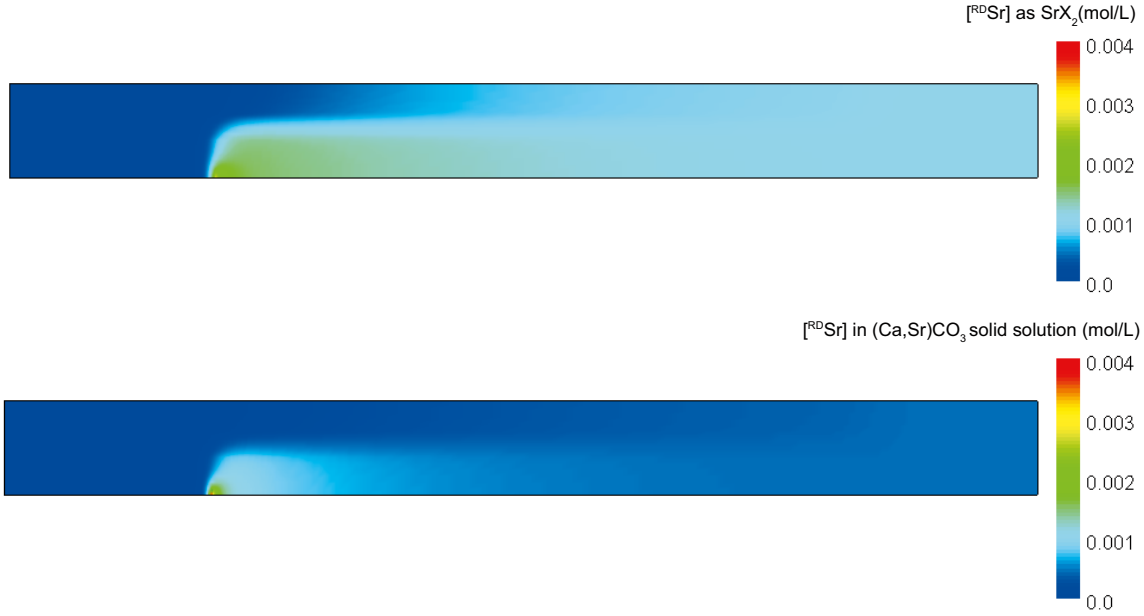

Figure 6-25. *Concentration of ^{RD}Sr retained in illite and in the $(Ca,Sr)CO_3$ solid solution at the end of the simulation period (2,700 years after repository release). ^{RD}Sr is preferentially retained in illite throughout a large part of the modelled domain.*

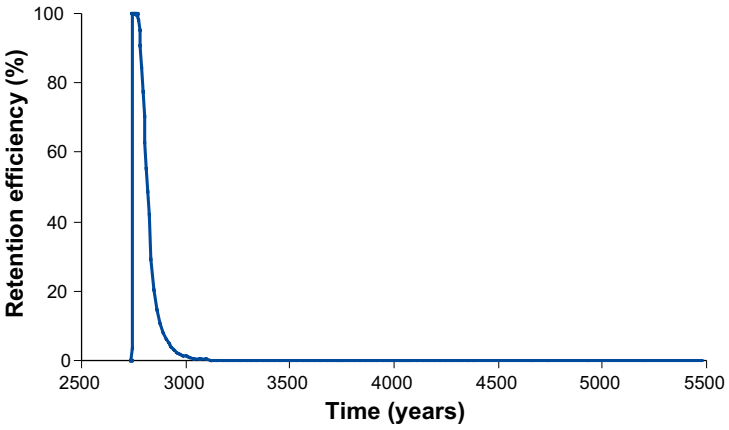

Figure 6-26. *Computed retention efficiency for repository-derived strontium along the simulation time (monitoring points: X = 80–100 m, Y = 3 m).*

Sensitivity analysis of strontium

The sensitivity analysis of strontium consisted in the simulation of three alternative cases, besides the reference case. One case is without considering the precipitation of siderite, the second is without allowing the precipitation of the $(Ca,Sr)CO_3$ solid solution, and the third is considering less cation exchange sites (one order of magnitude less than the base case).

Figure 6-27 shows the three simulations together with the reference case. For natural strontium, the concentration in solution is almost the same in the four simulations; ^{RD}Sr displays a behaviour similar to that of natural strontium. The concentration of ^{RD}Sr at the steady state is the same in the four simulations, the only difference is the arrival time of ^{RD}Sr at the observation point, which is faster in the case with less cation exchange sites than in the other three simulations, in consistence with the fact that ^{RD}Sr is mainly retained in illite.

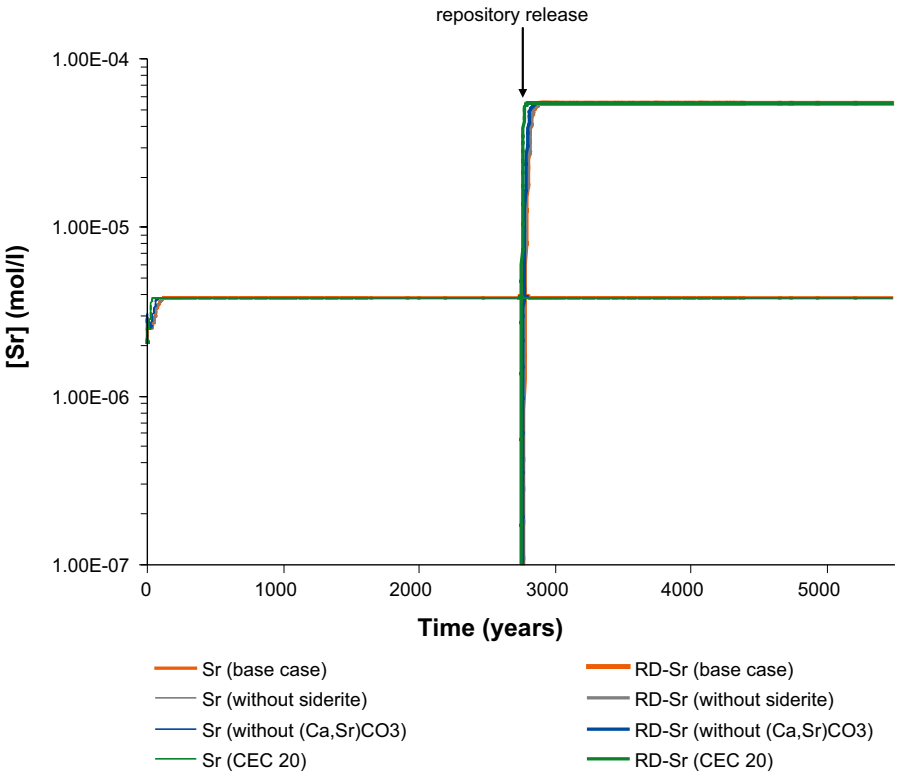

Figure 6-27. *Evolution of natural and repository-derived strontium concentrations along the simulation time at the discharge area (monitoring point: X = 80m, Y = 3 m). The reference case is represented, together with the three other cases considered in the sensitivity analysis.*

6.2.10 Uranium

Prior to repository release, the concentration of aqueous uranium is of the same order in the deep groundwater and the till porewater. The concentration of natural uranium in groundwater at the monitoring area is maintained constant during the whole simulation time period (Figure 6-28). Uranium is partly retained by illite and ferrihydrite during the whole simulation period, while the saturation of uranium phases is not reached in the modelled domain. Apatite, which could be a sink for uranium, does not precipitate in the simulated till domain.

The concentration of ^{RD}U in the deep groundwater affected by repository release is 5.66×10^{-9} mol/L. It is important to recall that this value was set as half the concentration of total uranium in the deep groundwater saturated with $UO_2{\cdot}2H_2O$. This concentration is lower than the concentration of natural uranium in the till porewater.

After 2,700 years, only 0.9% of uranium flowing out of the till system is derived from repository release (Figure 6-28). The only retention mechanism for repository-derived uranium is the sorption onto illite and ferrihydrite. Planar type cation exchange sites do not play a major role in uranium retention. In contrast, uranium is more strongly retained in surface complexation sites of illite, but mainly as uranium-carbonate complexes in the strong sites of the ferrihydrite surface (Figure 6-29).

Quantitative assessment of uranium retention efficiency

Figure 6-30 shows the time evolution of computed retention efficiency of repository-derived uranium in the till system. A retention efficiency of 100% is predicted after repository release. However, the retention efficiency starts to drop aproximately 300 years after the beginning of the release, and at the end of the simulation it is below 10%. The reduction of the efficiency for repository-derived uranium retention is due to the competition with the large amount of natural uranium entering into the system with till porewater. If less uranium is present in till porewater entering the system, then the retention efficiency for repository-derived uranium could be maintained at higher values for a longer time period.

Sensitivity analysis of uranium

The sensitivity analysis of uranium consisted in a simulation with less sorption sites on illite. In Figure 6-31 it is observed that the change in available sorption sites does not affect the retention of natural uranium or repository-derived uranium.

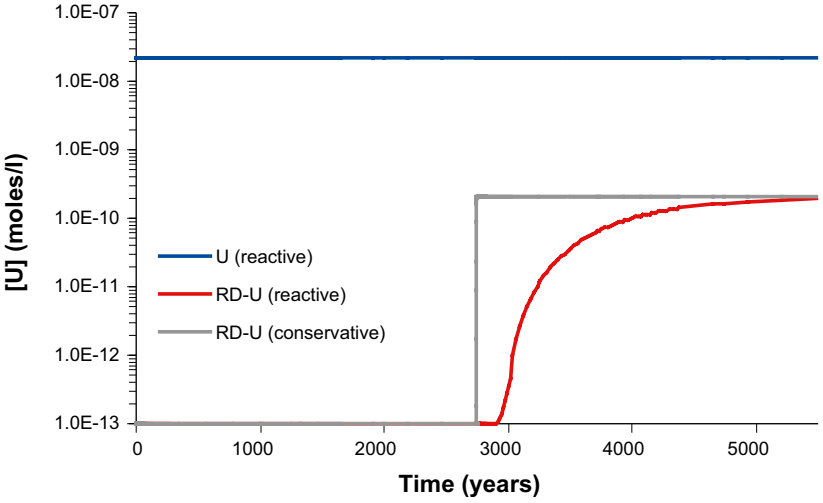

Figure 6-28. *Predicted evolution of natural uranium and repository-derived uranium at the discharge area (integration of the monitoring points X = 80 to 100 m, Y = 3 m). Also the conservative breakthrough curve of RD-U is represented.*

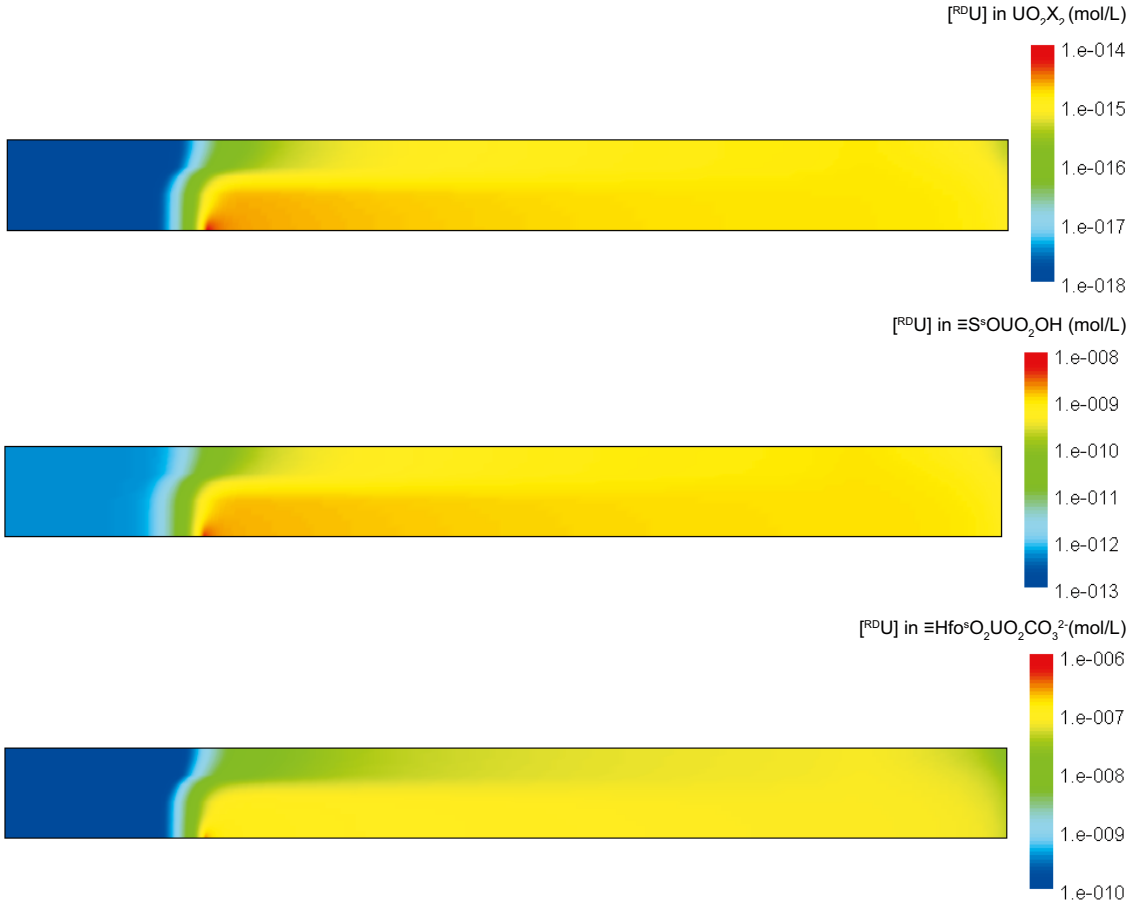

Figure 6-29. *Concentration of selected ^{RD}U species retained in illite and ferrihydrite, at the end of the simulation period (2,700 years after repository release).*

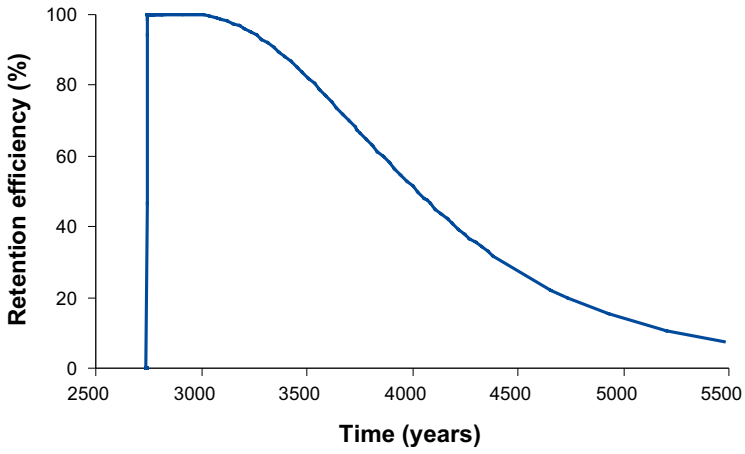

Figure 6-30. *Computed retention efficiency for repository-derived uranium during the simulation period (monitoring points X = 80–100 m, Y = 3 m).*

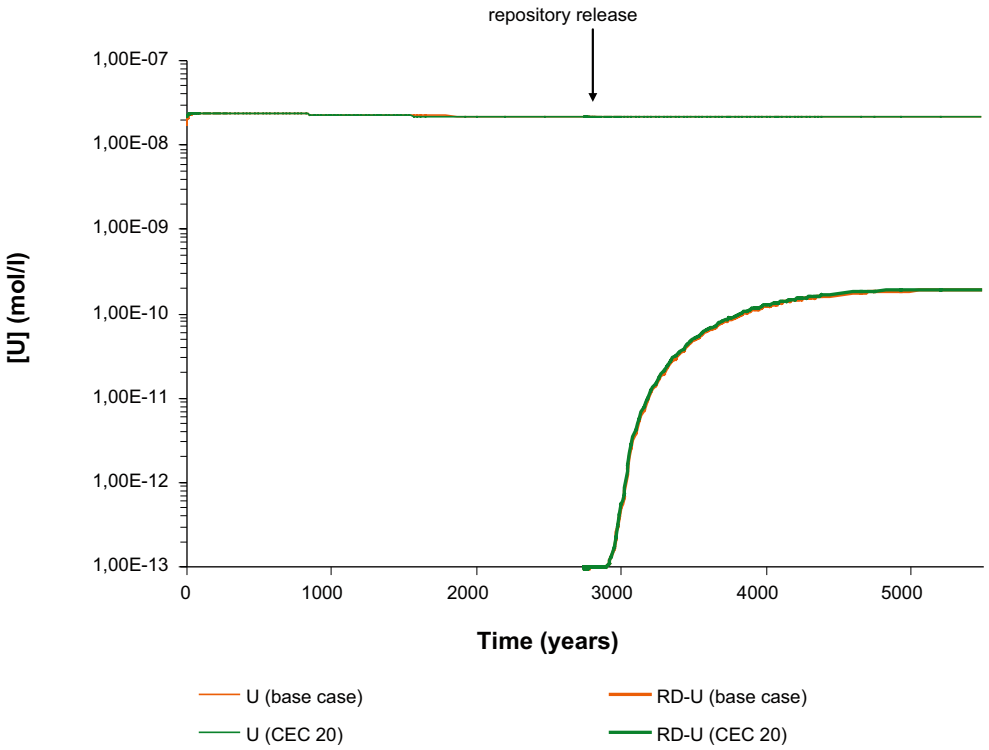

Figure 6-31. *Predicted evolution of natural and repository-derived uranium concentrations along the simulation time at the discharge area (monitoring point: X = 10 m, Y = 1 m). The results for the base case are represented, together with the simulation with less sorption sites.*

6.2.11 Caesium

Before the repository release, the aqueous concentration of caesium in the deep groundwater is approximately two orders of magnitude higher than in the till porewater. The numerical model predicts that the concentration of natural caesium in the outflowing water is constant through time (Figure 6-32).

The concentration of RDCs in the deep groundwater after repository release is 3.48×10^{-7} mol/L, which is approximately two orders of magnitude higher than the natural caesium concentration in deep groundwater, and four orders of magnitude higher than in the till porewater. Approximately 2,700 years after repository release, only 1% of the caesium flowing out of the till deposit is derived from the repository (Figure 6-32).

In the reactive transport simulation, the concentration of RDCs shows a remarkable decrease from the deep groundwater inflow point to the discharge area. This decrease takes place due to the retention of caesium via cation exchange on illite; especially Cs has high affinity for the FES (Figure 6-33).

The quantification of the retention capacity of the till system for caesium reveals that at the end of the simulation period, the concentration of RDCs in the reactive transport simulation is much lower (4 orders of magnitude) than in the conservative transport simulation (Figure 6-32).

Quantitative assessment of caesium retention efficiency

The retention efficiency for repository-derived caesium quickly reaches a maximum value of 100% (Figure 6-34), which is maintained until the end of the simulation. This demonstrates the high affinity of caesium for sorption onto illite.

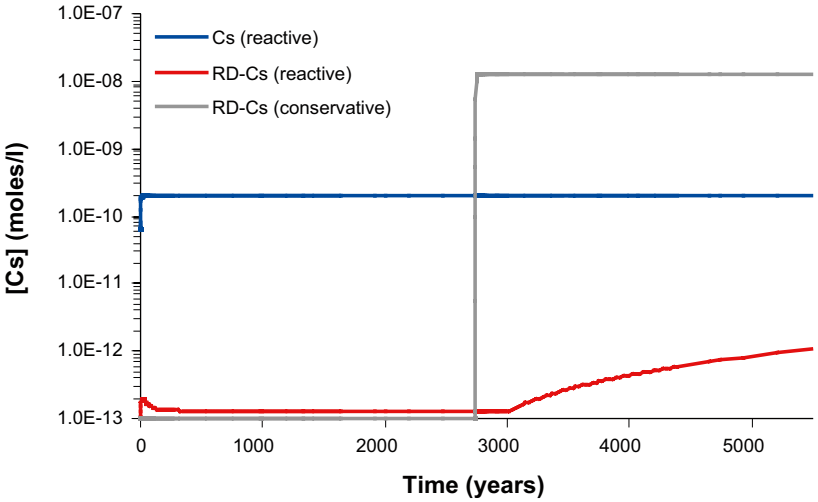

Figure 6-32. *Predicted evolution of natural caesium and repository-derived caesium at the discharge area (integration of the monitoring points X = 80 to 100 m, Y = 3 m), together with the conservative breakthrough curve of RD-Cs.*

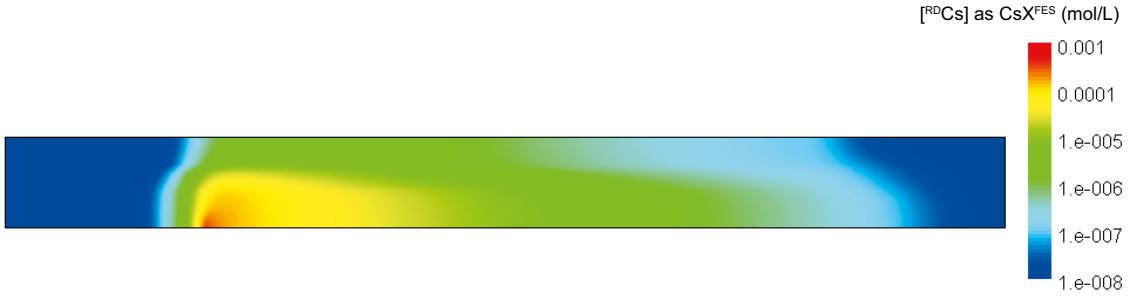

Figure 6-33. *Concentration of ^{RD}Cs retained in FES of illite at the end of the simulation period (2,700 years after repository release). Since caesium has a relatively high affinity for the FES, ^{RD}Cs is readily retained in the vicinity of the deep groundwater inflow point.*

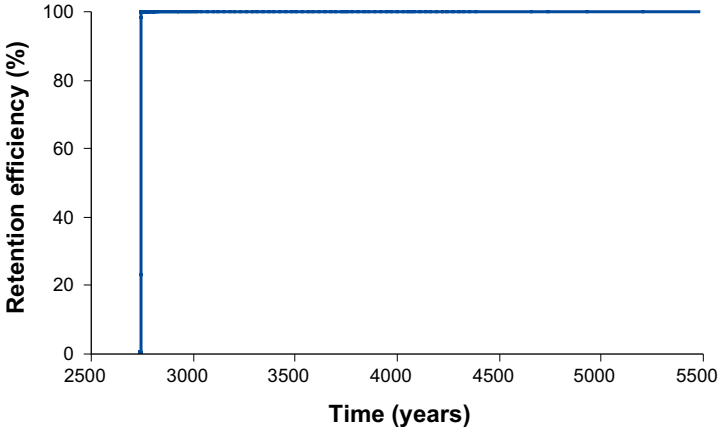

Figure 6-34. *Computed retention efficiency for repository-derived caesium along the simulation time at the discharge area (monitoring points X = 80–100 m, Y = 3 m).*

Sensitivity analysis of caesium

The sensitivity analysis of caesium consisted in a simulation with less cation exchange sites. For the case of natural caesium, the simuations predict a similar behaviour in the reference case and the case with fewer sites during most of the simulation time, although at the end of the simulation, an increase of caesium in solution is registered in the simulation with less sorption sites (Figure 6-35).

For the case of RDCs, the simulations predict that the concentration in solution increases with time after the repository release, and it is much higher in the simulation with less sorption sites. At the end of the simulation (5,400 years) the dissolved concentration of RDCs is more than two orders of magnitude higher in the simulation with less sorption sites.

6.2.12 Radium

The initial Ra concentration due to repository release in the deep groundwater is 9.15×10^{-11} mol/L. At the discharge area of the till deposit, the radium concentration after 2,700 y of repository release is 3.4×10^{-12} mol/L, in both the reactive and the conservative transport simulations (Figure 6-36). Therefore, the retention capacity of the till system is not significant for Ra. This radionuclide behaves almost conservatively, because it is only partially retained in the clay system by cation exchange processes on illite, and by incorporation in radiobarite in a small area surrounding the deep groundwater inflow point (Figure 6-37).

Quantitative assessment of radium retention efficiency

At the beginning of repository release, radium is strongly retained in the clay sediments. However, after a relatively short time period the retention efficiency has decreased to 0.6% (Figure 6-38).

Sensitivity analysis of radium

The sensitivity analysis of radium consisted of a simulation without considering the precipitation of radiobarite. The simulations predict that the breakthrough curves in the two cases are almost identical. There is only a slight difference in the concentration of dissolved Ra once the steady state is reached (Figure 6-39).

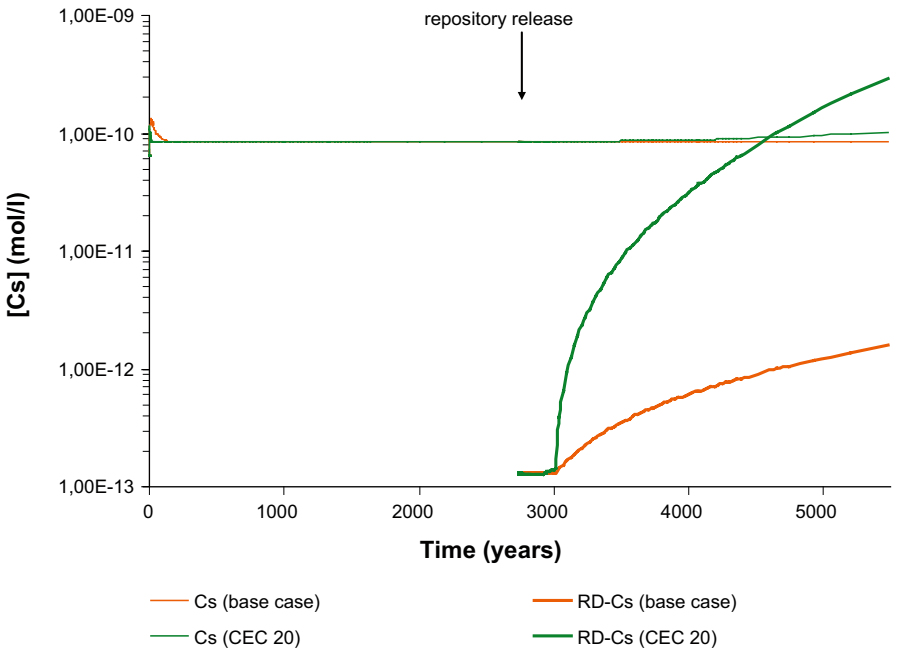

Figure 6-35. *Predicted evolution of natural and repository-derived caesium concentration along the simulation time at the discharge area (monitoring point: X = 10 m, Y = 1 m). The results for the base case are represented, together with the simulation with less sorption sites.*

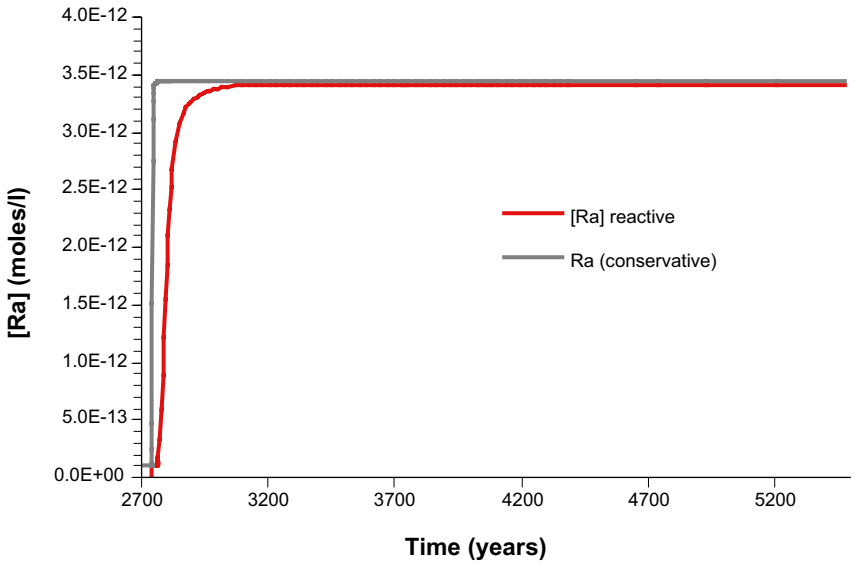

Figure 6-36. *Predicted evolution at the discharge area of repository-derived radium after repository release (integration of the monitoring points X = 80 to 100 m, Y = 3 m), together with the conservative breakthrough curve.*

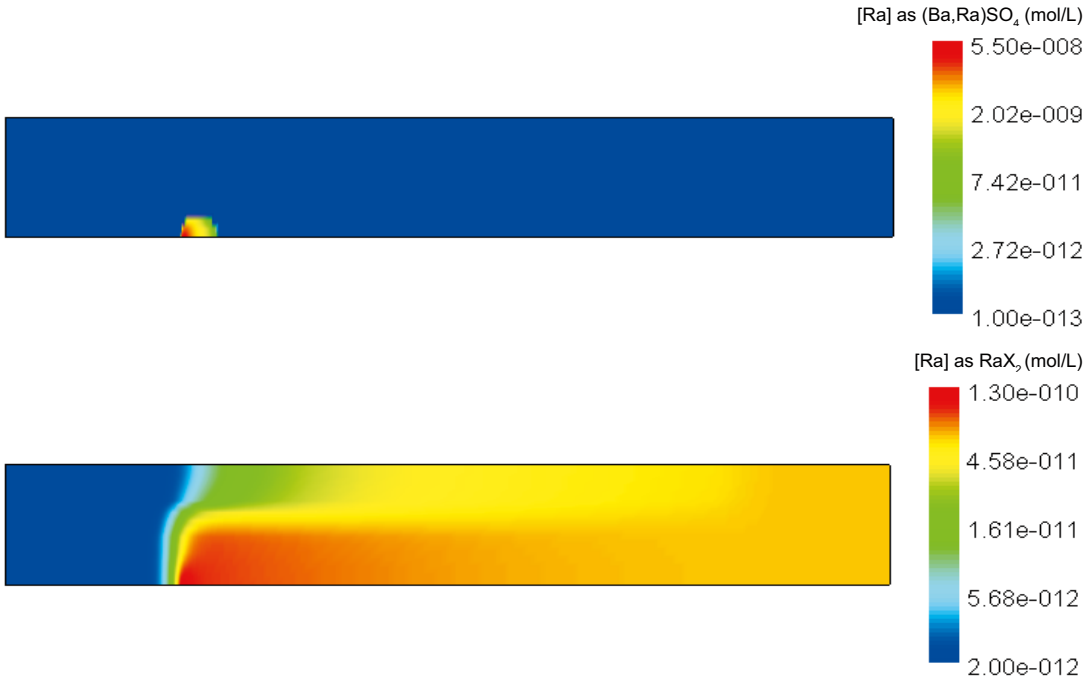

Figure 6-37. *Concentration of Ra precipitated as radiobarite and retained in planar sites of illite, at the end of the simulation period (2,700 years after repository release).*

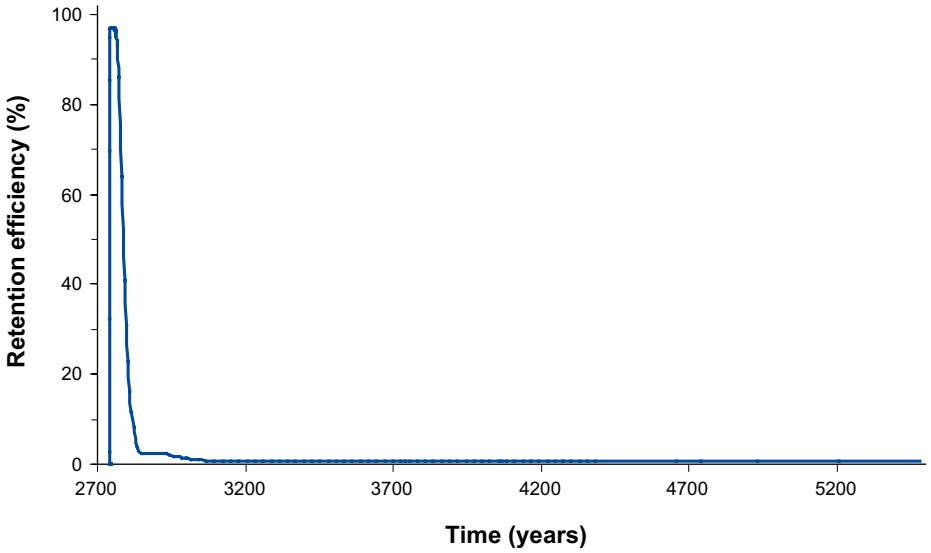

Figure 6-38. *Computed retention efficiency for repository-derived radium along the simulation time at the discharge area (monitoring points: X = 80–100 m, Y = 3 m).*

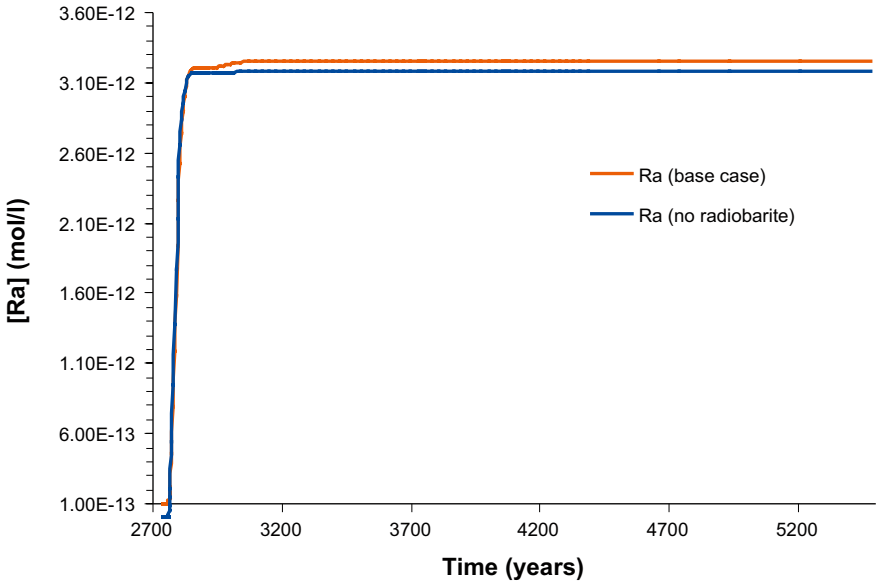

Figure 6-39. *Predicted evolution of radium concentration along the simulation time at the discharge area (monitoring point: X = 80 m, Y = 3 m).*

6.3 Retardation factor and effective distribution coefficient of repository-derived radionuclides

If the computed breakthrough curve of a reactive solute is complete (i.e. the maximum stabilised concentration has been reached), then the retardation factor (R) of a given reactive solute can be calculated from the following equation:

$$R = \frac{T_{1/2}^{R}}{T_{1/2}^{C}} \qquad \text{Equation 6-3}$$

where $T^{R}_{1/2}$ is the advective travel time of the reactive solute in the reactive transport simulation, and $T^{C}_{1/2}$ is the advective travel time of the same solute in the conservative transport simulation. Complete breakthrough curves have been computed for the radionuclides that behave conservatively, namely Nb and Tc; R is equal to one for these radionuclides. Complete breakthrough curves were also obtained for strontium, uranium, carbon and radium in the reactive transport simulation of 2,700 years (Figure 6-40). The retardation factor has been calculated at the monitoring point X = 80 m and Y = 3 m, where the fastest arrival of the contaminant is predicted. The calculated retardation factors are 24 for RDSr, 402 for RDU, 196 for RDC and 20 for Ra.

Equation 6-3 cannot be applied to estimate R for the other modelled radionuclides in the till system (RDTh, RDNi, RDCs and Se), since breakthrough curves are not complete for the reactive transport modelling. In order to obtain complete breakthrough curves for the simulated elements, a simulation to 30,000 years has been launched. It should be noted that this simulation does not take the geological, chemical and hydrological changes that will occur in a 30,000-year time perspective into account. The surface conditions at Forsmark after 30,000 years will be different from the present-day conditions simulated (for instance, permafrost conditions may have developed, groundwater may have different chemistry, and hydrogeological regimes may be different).

Thus, the only purpose of this 30,000-year simulation is to get R values that represent the transport model developed for the present geological and geochemical conditions. The results show that RDTh, RDNi, RDCs and Se have not reached a steady state even after 30,000 years. However, at the end of the simulation RDTh and RDNi have concentrations higher than those of the conservative simulation at $T^{C}_{1/2}$ and R can be computed (Figure 6-40). R is 11,819 for RDTh and 6,035 for RDNi.

Once the retardation factor is calculated, the effective distribution coefficient (Kd_e) can be obtained with the following equation that relates R with Kd_e:

$$Kd_e = (R-1)\frac{\varphi_e}{\rho_b} \qquad \text{Equation 6-4}$$

where φ_e is the effective porosity and ρ_b is the dry bulk density of the sediment (M L^{-3}). To calculate Kd_e one must give a single value of effective porosity, which is not the case for the modelled till system. A value of 0.0789 for the effective porosity was used here to calculate Kd_e. This value was obtained by /Sena 2009/ from a calibration of a conservative transport model. The dry bulk density is 1.95 kg/L. Using these values and the calculated R the following Kd_e are obtained: 7.89 L/kg for ^{14}C, 244.1 L/kg for ^{59}Ni, 0.93 L/kg for ^{90}Sr, 478.2 L/kg for ^{230}Th, 16.2 L/kg for ^{235}U, and 0.77 L/kg for ^{226}Ra. The obtained Kd_e are one to three orders of magnitude lower than those reported for till soils in Forsmark (see Table 3-3). For those radionuclides with a R of 1 (i.e. that behave conservatively) the Kd_e is equal to zero.

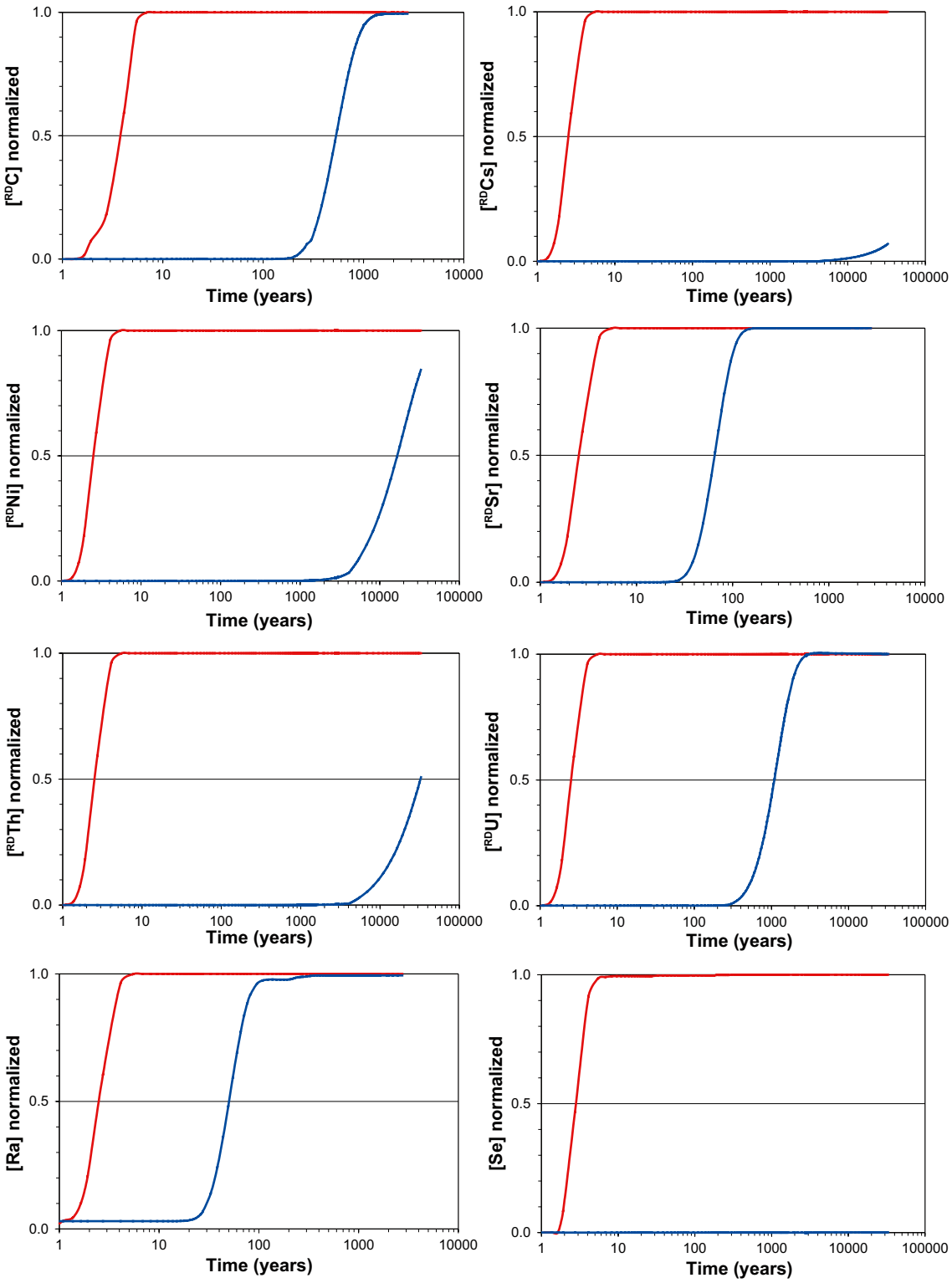

Figure 6-40. *Concentrations of radionuclides at the observation point (X = 80 m, Y = 3 m) normalised to the maximum concentration of the conservative model at steady state; red curves show conservative transport, blue curves reactive transport.*

7 Clay system numerical modelling results

7.1 Conservative transport

The groundwater flow directions and hydraulic gradients computed with the numerical model will constitute the physical driving force for the migration of radionuclides within the clay layer. Figure 7-1 shows the flow field computed with the boundary conditions prescribed for the clay system (for more details see /Grandia et al. 2007, sections 5.5 and 6.2/). In this figure it is possible to see that the flow directions are mainly vertical and upward. These flow conditions were applied to the reactive transport simulation for reference case #2.

The conservative transport for reference case #2 was studied using a tracer "A". The initial concentration of the tracer in the clay porewater was set to zero, whereas in the deep groundwater was 0.1 mol/L. The model predicts that a conservative transport pseudo-steady state is reached approximately after 500 years. It is worth noting that the time needed to reach the steady state is much longer than in the till reference case (5 to 20 years; see Section 6.1).

This reflects the contrasting hydrogeological properties of the media in the two reference cases. The first model simulates a relatively high-permeable medium (the till aquifer), with average porewater velocities in the order of 10^{-2} m·d^{-1}, while the second model simulates a low permeability medium (clay) with average porewater velocities of about 10^{-5} m·d^{-1}. These hydrogeological conditions imply that diffusion plays a more relevant role in the transport of solutes in the clay system in comparison with the till system, where advection and dispersion are dominant.

In Figure 7-3 the migration of the conservative tracer in the clay domain is tracked at different simulation time steps. In the first years of deep groundwater input the distribution of the tracer is constrained to the surroundings of the inflow point (bottom right). Later on, the tracer slowly moves through the domain. The dilution of the deep groundwater in the clay domain has been assessed with the conservative tracer. A dilution factor (see Equation 6-1) of 41% has been calculated for the discharge area of the clay system, using the value obtained at the node X = 10 m and Y = 1 m.

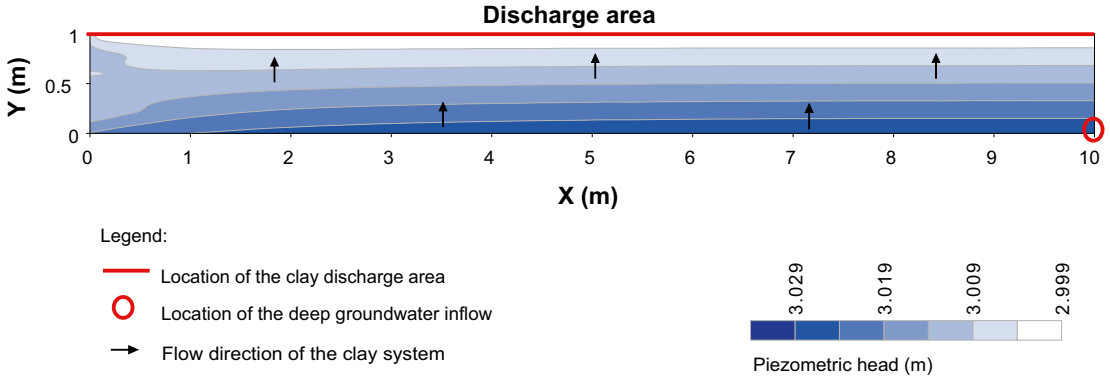

Figure 7-1. Groundwater flow directions and hydraulic gradients obtained from the numerical transport simulation after setting the prescribed boundary conditions of the clay system.

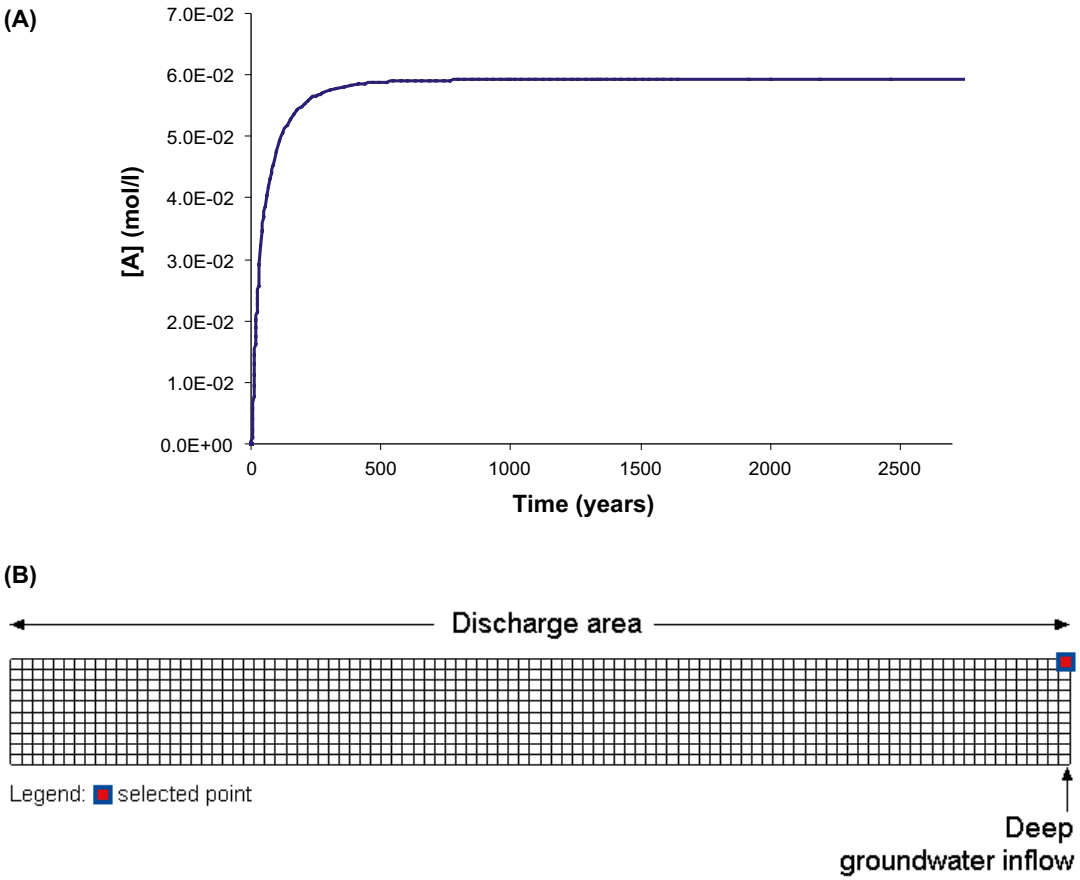

Figure 7-2. *(A) Breakthrough curve of concentration of the conservative tracer "A" in an observation point located at the discharge area. The time needed to reach the stationary state of solute transport (advective travel time) is approximately 500 years. (B) Location of the monitoring point (X = 10 m, Y = 1 m).*

Figure 7-3. *Migration of the conservative tracer in the clay domain at 100, 5,000, 24,000 and 250,000 days of simulation of deep groundwater input. Scale bar is concentration in mol/L.*

7.2 Reactive transport

The reactive behaviour of the elements Sr, U, Cs, C, Nb, Th, Ra and Ni has been simulated for a period of 2,700 years, before the release of radionuclides from repository. After this first simulation period, the release of radionuclides has been included in the simulation and the leakage from the repository has been simulated for another 2,700 years. Also Cl and I have been included in the simulations, but they are considered to behave conservatively. The results obtained for each radionuclide of interest will be reported in the following subsections, including a quantitative assessment of the retention efficiency and a sensitivity analysis where applicable.

During the initial 2,700 years of simulation, the pH and pe show similar but opposite changes with time at the monitoring point (X = 10 m, Y = 1 m). In the first 500 years, fast changes in these parameters are predicted due to re-equilibration of clay porewater with the minerals present in the system. After repository release no changes in pH or pe are observed at this point (Figure 7-4).

7.2.1 Carbon

Before the release of radionuclides from the repository, the amount of C(IV) in the deep groundwater is twice the amount of C(IV) in the clay porewater (see Table 5-7 and Table 5-11). At the observation point, the amount of C(IV) in solution increases with time, with a faster increase at the beginning, until reaching a steady state (Figure 7-5) reflecting the equilibration with calcite.

Deep groundwater affected by repository release has a ^{RD}C concentration of 2.89×10^{-7} mol/L, which is approximately four orders of magnitude lower than the concentration of natural C(IV) in deep groundwater and the clay porewater. At the end of the reactive transport simulation (~5,400 years), only ~0.0007% of the carbon flowing out of the clay deposit is derived from repository release (Figure 7-5).

Only one retention mechanism was considered for carbon in the reactive transport simulation; precipitation as a solid solution [$Ca(^{RD}C,C)O_3$]. The simulation predicts that part of the repository-derived carbon is retained via precipitation of the solid solution in the area surrounding the radionuclide-bearing deep groundwater infiltration point (Figure 7-6). The quantification of the retention capacity of the clay system for carbon reveals that at the end of the simulation period, ^{RD}C concentration in the reactive transport simulation is one order of magnitude lower than in the conservative transport simulation (Figure 7-5).

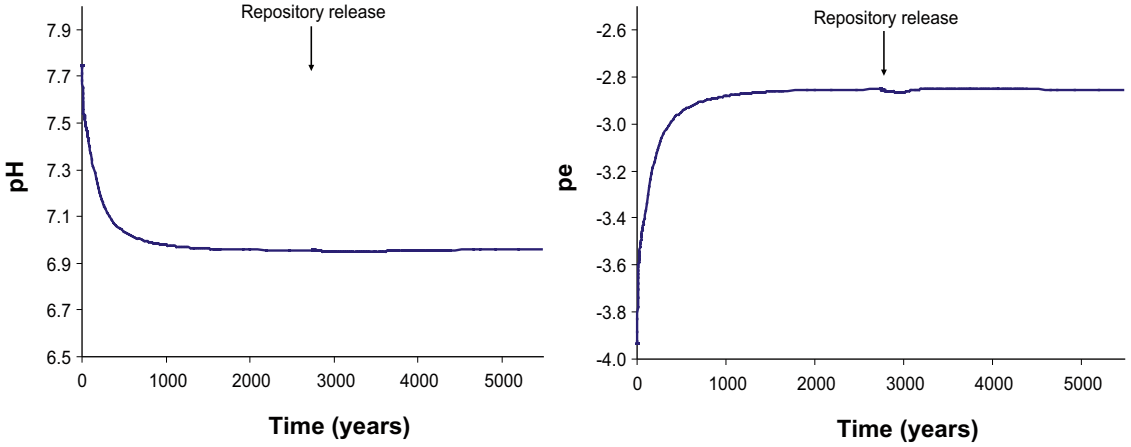

Figure 7-4. *Evolution of pH and pe during 5,400 years of reactive transport simulation (monitoring point located at X = 10 m, Y = 1 m). A rapid change of both pH and pe values in the first 250 years of simulation is predicted, followed by a gradual change towards a geochemical steady state.*

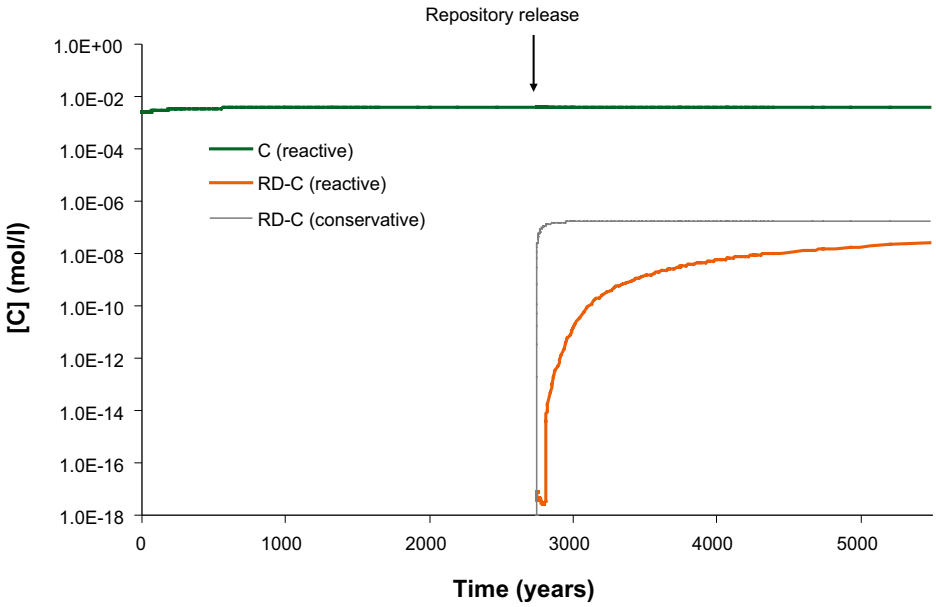

Figure 7-5. *Predicted evolution of natural C(IV) and repository-derived C(IV) at the discharge area (monitoring point: X = 10 m, Y = 1 m; modelling temperature = 15ºC). Also the conservative breakthrough curve of ^{RD}C is presented.*

Figure 7-6. *Concentration of ^{RD}C retained in the $Ca(^{14}C,C)O_3$ solid solution at the end of the simulation period (2,700 years after repository release).*

Quantitative assessment of carbon retention efficiency

Figure 7-7 shows the time evolution of computed retention efficiency of repository-derived carbon. When repository release is simulated, repository-derived carbon is predicted to be retained in the clay deposit. Immediately after repository release, the system reaches a retention efficiency for ^{RD}C of 100%. After this period, the retention efficiency for repository-derived carbon drops to 85%.

Sensitivity analysis of carbon

The sensitivity analysis for carbon consisted in the simulation of the reactive transport at 25ºC and 5ºC, to see if the concentration of dissolved carbon was significantly different from the base case (15ºC) due to isotopic fractionation. The simulations predict that the retention of ^{14}C does not vary significantly at 25ºC, 15ºC and 5ºC (Figure 7-8). The concentration of dissolved ^{14}C in the three simulations is of the same order, with a maximum of 2.56×10^{-8} mol/L at the end of the 25ºC simulation. Still, it can be observed how the retention of ^{14}C is stronger at higher temperatures (Figure 7-8).

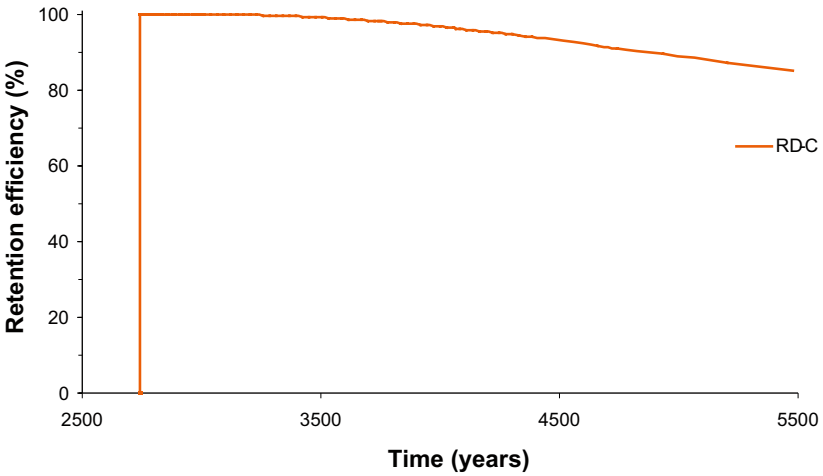

Figure 7-7. *Computed retention efficiency for repository-derived carbon along the simulation time (monitoring point: X = 10 m, Y = 1 m).*

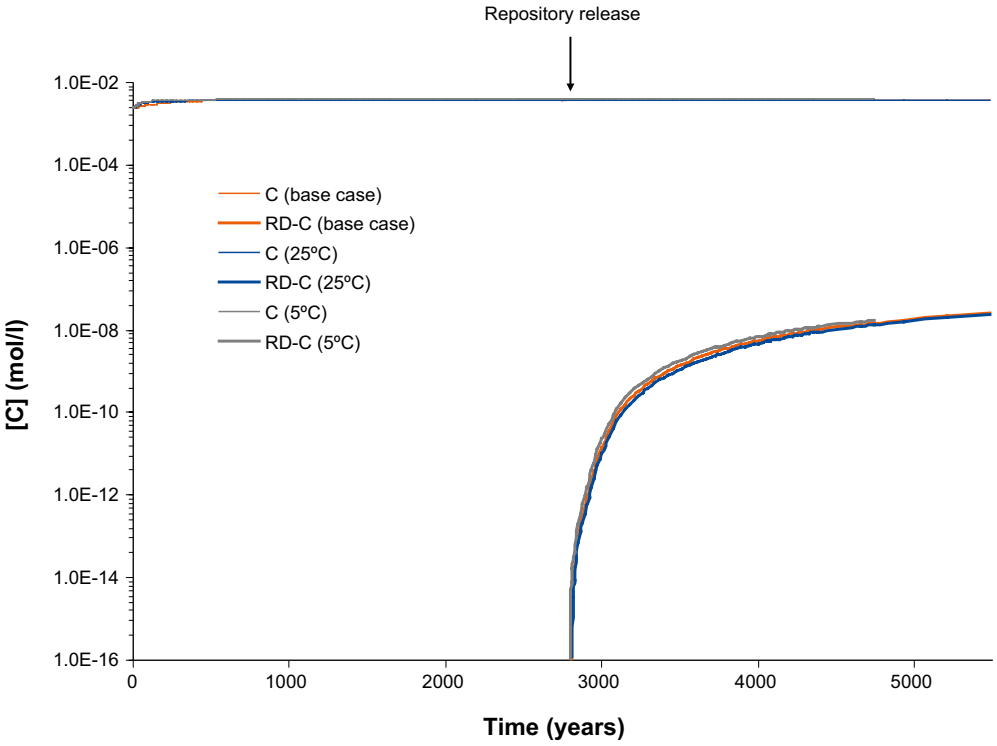

Figure 7-8. *Predicted evolution of natural carbon and repository-derived carbon concentration along the simulation time at the discharge area (monitoring point: X = 10 m, Y = 1 m). The results for the base case (15ºC) are represented, together with the simulations for 5ºC and 25ºC.*

7.2.2 Iodine

The concentration of iodine in solution prior to repository release is lower in the deep groundwater (3.4×10^{-7} mol/L) than the clay porewater (5.3×10^{-5} mol/L). The initial concentration of RDI in deep groundwater due to repository release is 1.6×10^{-5} mol/L, which is approximately 2 orders of magnitude higher than the concentration of natural iodine in the deep groundwater, but lower than the concentration of natural iodine in the clay porewater.

In the numerical modelling, iodine has been considered to behave conservatively; therefore, dilution is the only process that will diminish the concentration of RDI from the point of radionuclide release to the observation point. In Figure 7-9 it is observed how, after repository relase, the concentration of RDI is lower than that of natural iodine. During the simulation of repository release, approximately one third (30.2%) of iodine flowing out of the till deposit corresponds to RDI.

7.2.3 Chlorine

Chlorine is a major element in the Forsmark groundwaters, and the concentration of dissolved natural chlorine is higher in the deep groundwater (0.1 mol/L) than in the clay porewater (1.5×10^{-4} mol/L). The initial concentration of RDCl in deep groundwater due to repository release is 5.1×10^{-7} mol/L, which is much lower than the concentration of natural chlorine.

Chlorine, like iodine, has been considered to behave conservatively in the numerical modelling. Therefore, dilution will be the only process that will diminish the concentration of RDCl from the point of radionuclide release to the observation point. After repository relase, the concentration of RDCl in the observation point is more than five orders of magnitude lower than that of natural chlorine (Figure 7-10).

7.2.4 Thorium

The concentration of thorium in solution prior to repository release is approximately one order of magnitude higher in the deep groundwater than in the clay porewater. At the observation point, the concentration of thorium shows a sharp decrease at the very beginning, followed by a relatively fast increase until approximately 1,000 years of simulation, and then by a slower increase until the end of simulation (Figure 7-11). The retention of natural thorium, according to the simulation results, takes place by sorption onto illite, since no Th solid phases are predicted to precipitate in the modelled domain.

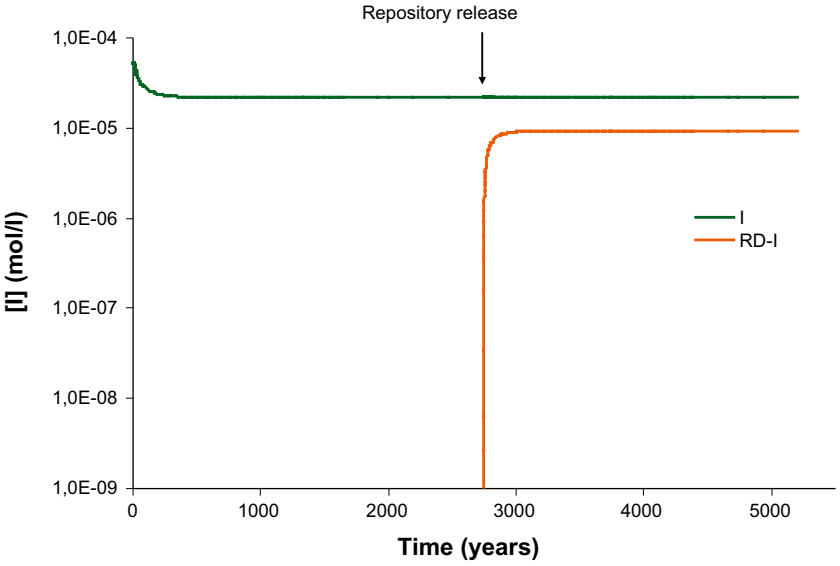

Figure 7-9. *Conservative breakthrough curves of natural iodine (I) and repository-derived iodine (RD-I) at the discharge area (monitoring point: X = 10 m; Y = 1 m).*

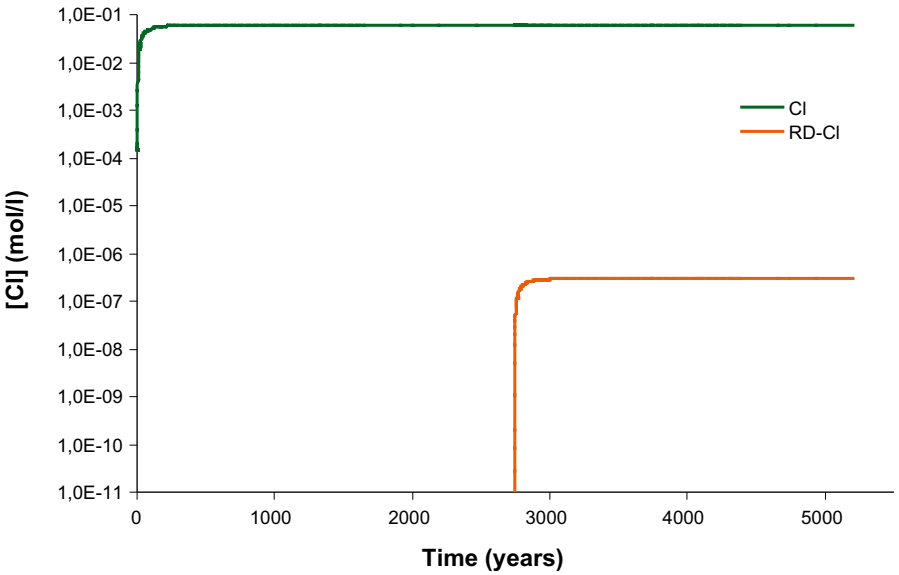

Figure 7-10. *Conservative breakthrough curves of natural chlorine (Cl) and repository-derived chlorine (RD-Cl) at the discharge area (monitoring point: X = 10 m, Y = 1 m).*

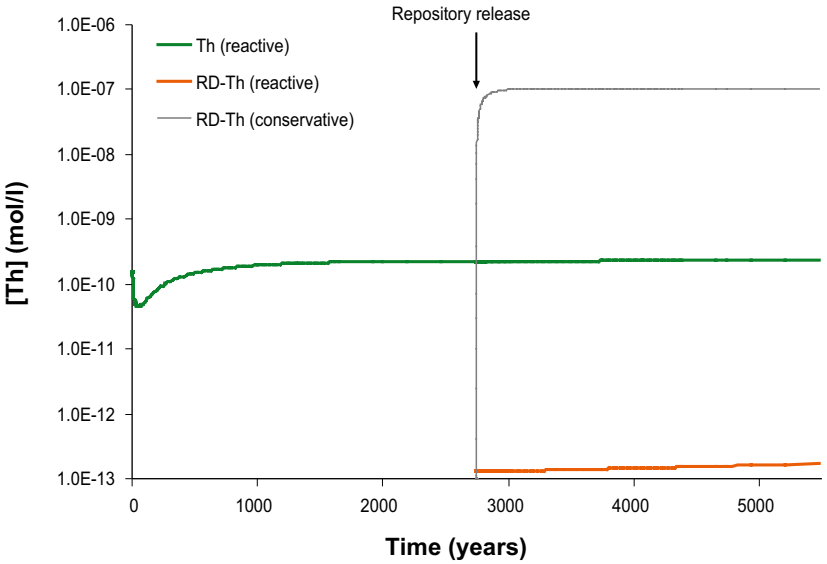

Figure 7-11. *Predicted evolution of natural thorium and of repository-derived thorium at the discharge area (monitoring point: X = 10 m, Y = 1 m). Also the conservative breakthrough curve of RDTh is presented.*

The initial concentration of RDTh in deep groundwater due to repository release is 1.75×10^{-7} mol/L, which is approximately 2 orders of magnitude higher than the concentration of natural thorium in deep groundwater and 3 orders of magnitude higher than in the clay porewater. 2,700 years after repository release, only 0.07% of thorium flowing out of the clay deposit is derived from the repository (Figure 7-11). Saturation of amorphous thorianite is not reached in the simulated domain; however, thorium is retained via surface complexation onto illite (Figure 7-12).

The quantification of the retention capacity of the clay system for thorium reveals that at the end of the simulation period, RDTh concentration in the reactive transport simulation is much lower (6 orders of magnitude) than in the conservative transport simulation (Figure 7-11).

Figure 7-12. *Concentration of two RDTh complexes retained in illite at the end of the simulation period (2,700 years after repository release).*

Quantitative assessment of thorium retention efficiency

Immediately after repository release, the retention efficiency of repository-derived thorium reaches 100%, which is maintained until the end of the simulation (Figure 7-13).

Sensitivity analysis of thorium

Figure 7-14 shows the evolution of the thorium concentration at the discharge area of the clay deposit, for the reference case and three alternative cases developed for sensitivity analysis. In three of the cases (the reference case, the simulation without humics and the simulation with less complexation sites on illite) the concentration of natural thorium is almost the same. In the case with a higher concentration of humics in the clay porewater, there is an increase in the concentration of natural thorium of approximately three times, compared to the reference case.

RDTh displays a similar trend in the reference case and the simulation without humics, while in the simulation with higher amount of humic acid the concentration of RDTh in solution is approximately three times higher. The trend of the RDTh simulation with less sorption sites on illite differs from that of natural thorium, in this case, the RDTh in solution increases with time, and at the end of the simulation, the concentration of RDTh is one order of magnitude higher than in the reference case.

7.2.5 Nickel

The concentration of dissolved nickel in the deep groundwater is similar to that in the clay porewater (7.2×10^{-9} and 4.9×10^{-9}, respectively). However, at the discharge point the concentration of nickel in solution is one order of magnitude higher after 2,700 years of simulation (Figure 7-15). During the first c 750 years of simulation, the concentration of dissolved nickel increases one order of magnitude, and then it slowly reaches a stationary state. This increase in dissolved nickel is explained by desorption of this element from illite.

The initial concentration of RDNi in deep groundwater due to repository release is 4.96×10^{-7} mol/L, which is approximately 2 orders of magnitude higher than the natural deep groundwater and the clay porewater nickel concentrations. 2,700 years after repository release, only 0.005% of nickel flowing out of the clay deposit is derived from the repository (Figure 7-15).

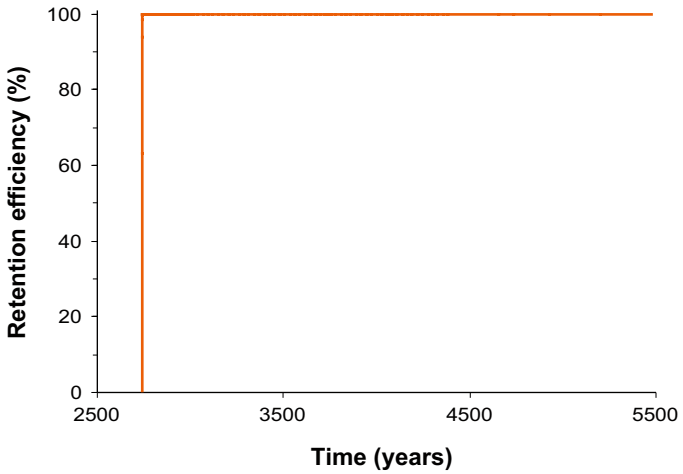

Figure 7-13. *Computed retention efficiency for repository-derived thorium along the simulation time (monitoring point: X = 10 m, Y = 1 m).*

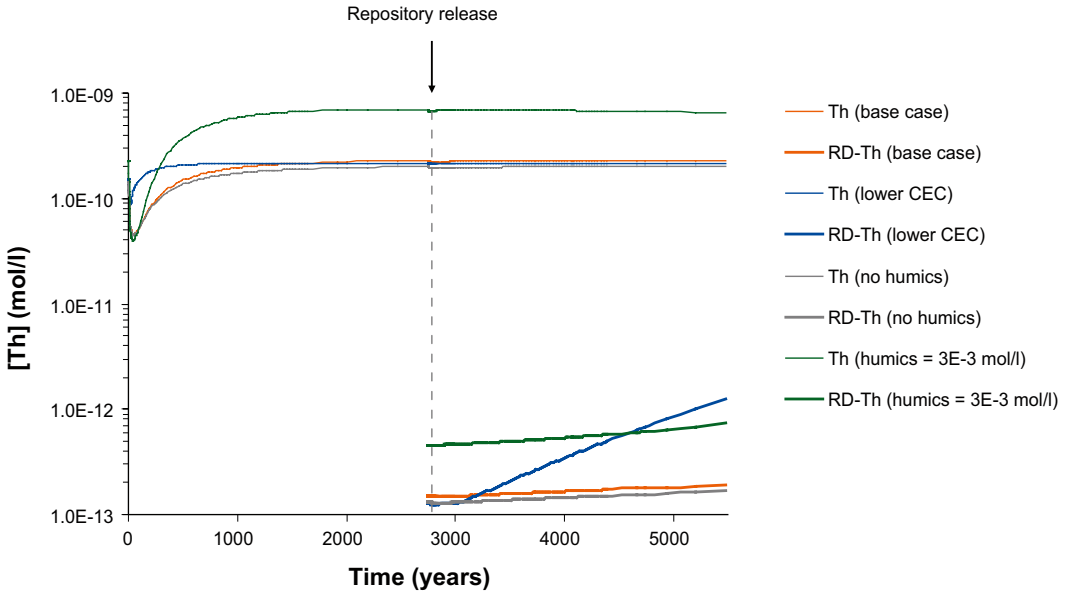

Figure 7-14. *Predicted evolution of natural thorium and repository-derived thorium concentration along the simulation time at the discharge area (monitoring point: X = 10 m, Y = 1 m). The results for the base case are represented, together with three other simulations performed for the sensitivity analysis.*

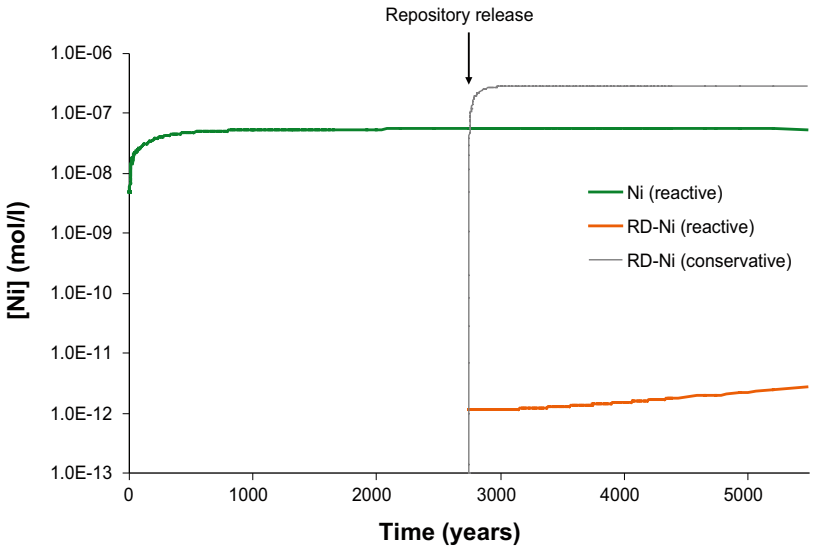

Figure 7-15. *Predicted evolution of natural nickel and repository-derived nickel after repository release, at the discharge area (monitoring point: X = 10 m, Y = 1 m). Also the conservative breakthrough curve of RD-Ni is represented.*

The quantification of the retention capacity of the clay system for nickel reveals that at the end of the simulation period, RDNi concentration in the reactive transport simulation is much lower (5 orders of magnitude) than in the conservative transport simulation (Figure 7-15). The remarkable decrease in the concentration of RDNi from the deep groundwater inflow point to the discharge area is due to the high affinity of nickel for the surface complexation sites on illite (Figure 7-16).

Quantitative assessment of nickel retention efficiency

Figure 7-17 shows the time evolution of the computed retention efficiency of repository-derived nickel. When repository release is simulated, repository-derived nickel is predicted to be retained in the clay deposit via sorption onto illite surfaces. Immediately after repository release, the system reaches a retention efficiency for RDNi of 100%, which is maintained until the end of the simulation period (Figure 7-17).

Sensitivity analysis of nickel

The sensitivity analysis of nickel involved the simulation of a case with less sorption sites on illite. Figure 7-18 shows the evolution of the nickel concentration in the discharge area of the clay deposit for the reference case and the alternative case. As expected, the concentration of natural nickel in solution is higher in the reference case, which is explained by the release into solution of natural nickel sorbed onto illite. Since the reference case has more sorption sites, more nickel will be released into solution compared to the other case simulated.

Figure 7-16. *Concentration of RDNi retained in illite at the end of the simulation period (2,700 years after repository release).*

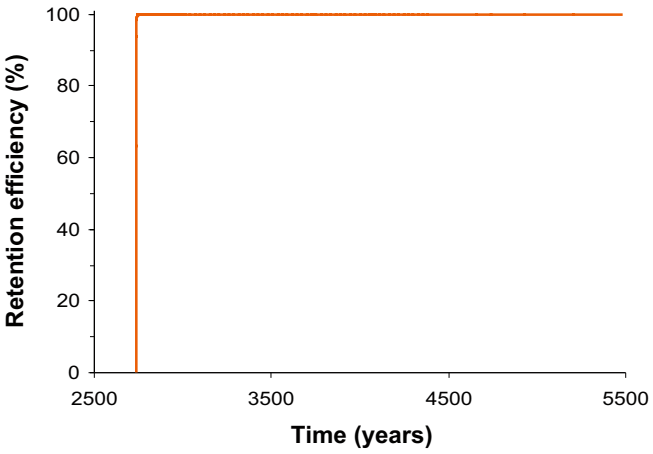

Figure 7-17. *Computed retention efficiency for repository-derived nickel along the simulation time (monitoring point: X = 10 m, Y = 1 m).*

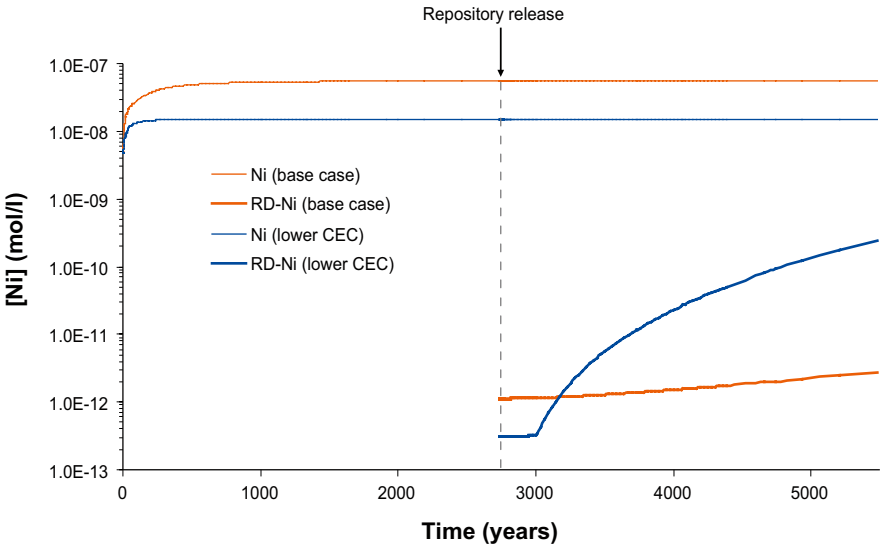

Figure 7-18. *Predicted evolution of natural and repository-derived nickel concentration along the simulation time at the discharge area (monitoring point: X = 10 m, Y = 1 m). The results for the base case are represented, together with the simulation with less sorption sites on illite.*

Opposite to natural nickel, the concentration of RDNi in solution is two orders of magnitude higher at the end of the simulation with less sorption sites compared to the reference case. This is because the higher amount of sites in the reference case favours a higher retention of RDNi in the illite surface.

7.2.6 Niobium

Niobium is present in solution in the clay porewater, while for the deep groundwater no reported concentrations of Nb were available. In the modelling. the deep groundwater concentration was assumed to be negligible. Therefore, the Nb concentration at the monitoring point decreases during the first 500 years of simulation, and then reaches a steady state.

The initial concentration of RDNb in the deep groundwater due to repository release is 5.25×10^{-8} mol/L, which is approximately 3 orders of magnitude higher than the clay porewater concentration. At the discharge area of the clay deposit, the RDNb concentration is 3.11×10^{-8} mol/L (Figure 7-19). The numerical simulations predict that niobium is not retained in the clay system, since saturation with Nb_2O_5 is not reached along the simulation time in the domain. The decrease of RDNb concentration from the deep groundwater inflow point to the discharge area of the clay deposit is exclusively due to diffusion into the clay system, which leads to dilution of the niobium concentration.

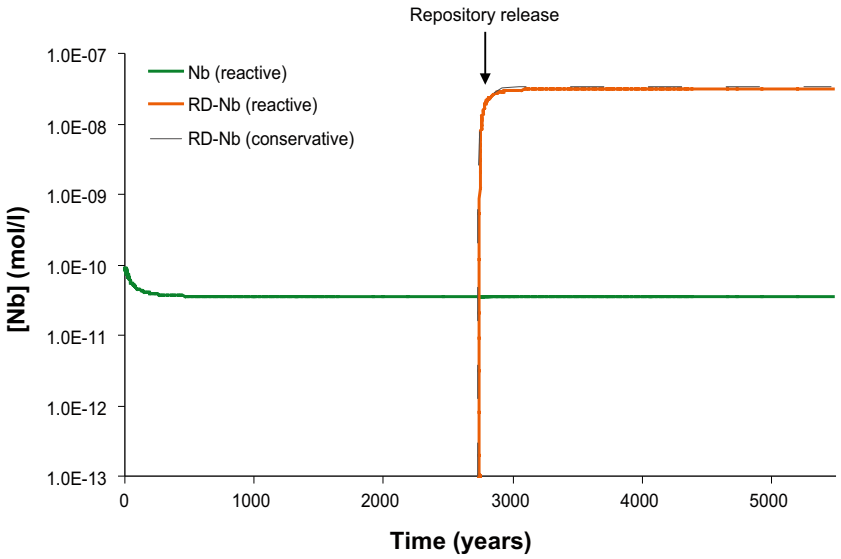

Figure 7-19. *Predicted evolution of natural niobium and repository-derived niobium after repository release at the discharge area (monitoring point X = 10 m; Y = 1 m). Also the conservative breakthrough curve of RD-Nb is presented.*

7.2.7 Selenium

Initially, selenium is not present in the clay porewater or the deep groundwater. The concentration of Se in the deep groundwater due to repository release is 3.77×10^{-11} mol/L. At the discharge area of the clay deposit, the Se concentration is 2.23×10^{-11} mol/L (Figure 7-20). The numerical simulations predict that selenium is not retained in the clay system, since saturation with Se(cr) or $FeSe_2$ is not reached during the simulation period. Similar to RDNb, the decrease of the Se concentration from the deep groundwater inflow point to the discharge area of the clay deposit is exclusively due to diffusion into the clay system, which leads to dilution of Se concentration.

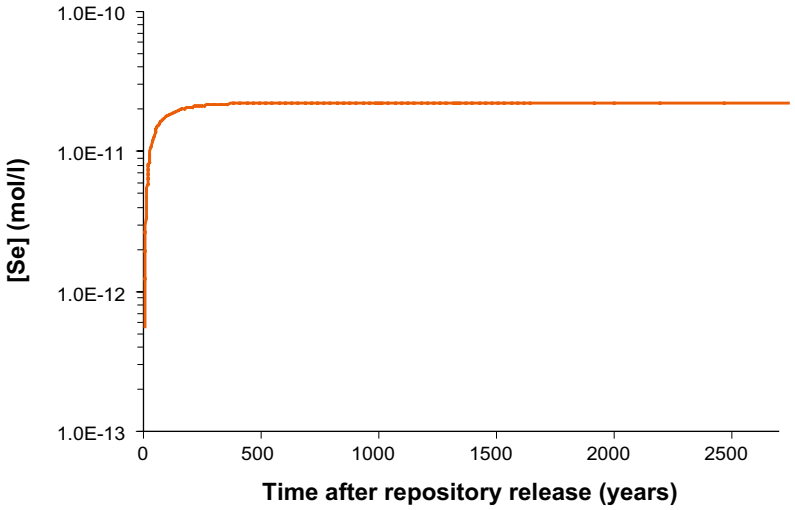

Figure 7-20. *Predicted evolution of selenium at the discharge area (monitoring point: X = 10 m; Y = 1 m). Since no retention is predicted, the modelled curve is also the conservative breakthrough curve of Se.*

7.2.8 Technetium

The initial concentration of Tc in the deep groundwater due to repository release is 5.27×10^{-9} mol/L. At the discharge area of the clay deposit, the Tc concentration is 3.12×10^{-9} mol/L (Figure 7-21). The numerical simulations predict that technetium is not retained in the clay system, since saturation with $TcO_2\cdot1.6H_2O$ is not reached along the simulation time. Again, as for RDNb and Se, the decrease of Tc concentration from the deep groundwater inflow point to the discharge area of the clay deposit is exclusively due to diffusion into the clay system, which leads to dilution of Tc.

7.2.9 Strontium

Before the release of radionuclides from the repository, the concentration of strontium in solution in the deep groundwater is two orders of magnitude higher than in the clay porewater (see Table 5-7 and Table 5-11). The aqueous strontium concentration at the monitoring point gradually increases through time, with a faster increase at the beginning, and a slower increase at the end of the simulation, reflecting the retention of strontium in the solid phase (Figure 7-22).

Deep groundwater affected by repository release has a RDSr concentration of 1.5×10^{-3} mol/L, which is approximately 1.5 orders of magnitude higher than the natural Sr concentration in deep groundwater, and 3 orders of magnitude higher than the Sr concentration in clay porewater. At the end of the reactive transport simulation, ~96% of the strontium flowing out of the clay deposit is derived from repository release (Figure 7-22).

The retention capacity of the clay system at Forsmark can be evaluated by comparing the results yielded by the reactive and conservative transport models after repository release. In the reactive transport simulation, the maximum RDSr concentration at the discharge area at the end of the simulation period (~5,400 years) is ~25% lower than the maximum RDSr content reached in the conservative transport model (Figure 7-22). This means that the clay system is moderately efficient in retaining RDSr in the solid phase.

Two retention mechanisms were considered for strontium in the reactive transport simulation: cation exchange on illite and precipitation as a solid solution [$(Ca, Sr)CO_3$]. Only part of the repository-derived strontium is retained preferentially via precipitation of $(Ca,Sr)CO_3$ relative to cation exchange on illite (Figure 7-23). The continuous increase of the strontium aqueous concentration at the discharge area (Figure 7-22) reflects the decreasing capacity of illite and $(Ca,Sr)CO_3$ to incorporate more strontium with time.

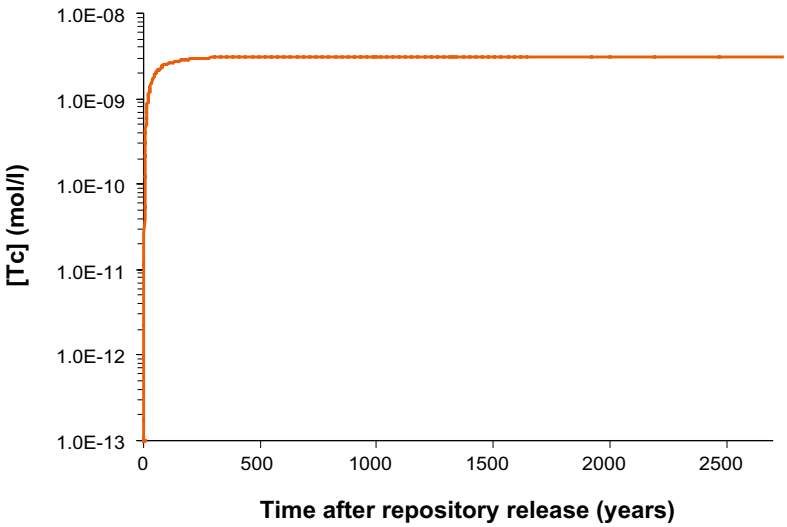

Figure 7-21. *Predicted evolution of technetium at the discharge area (monitoring point: X = 10 m; Y = 1 m). Since no retention is predicted, the modelled curve is a conservative breakthrough curve of Tc.*

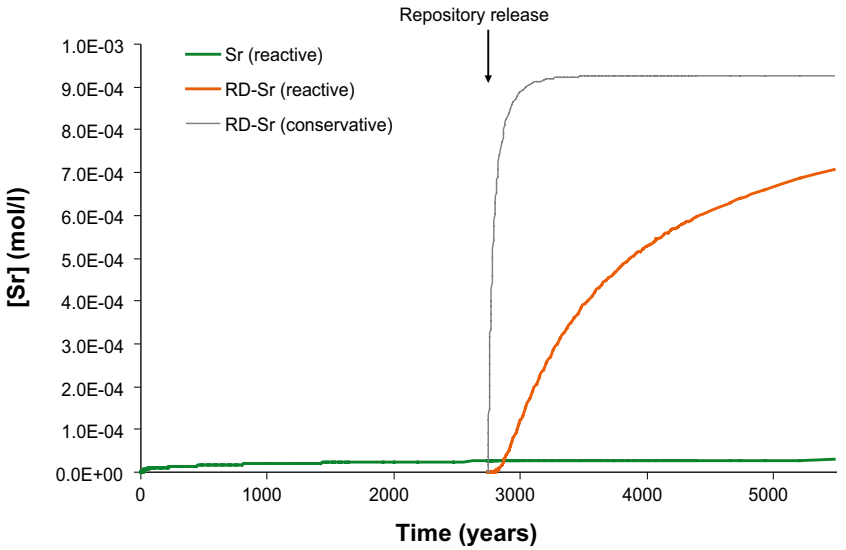

Figure 7-22. *Predicted evolution of natural strontium and repository-derived strontium at the discharge area (monitoring point: X = 10 m; Y = 1 m). Also the conservative breakthrough curve of ^{RD}Sr is presented.*

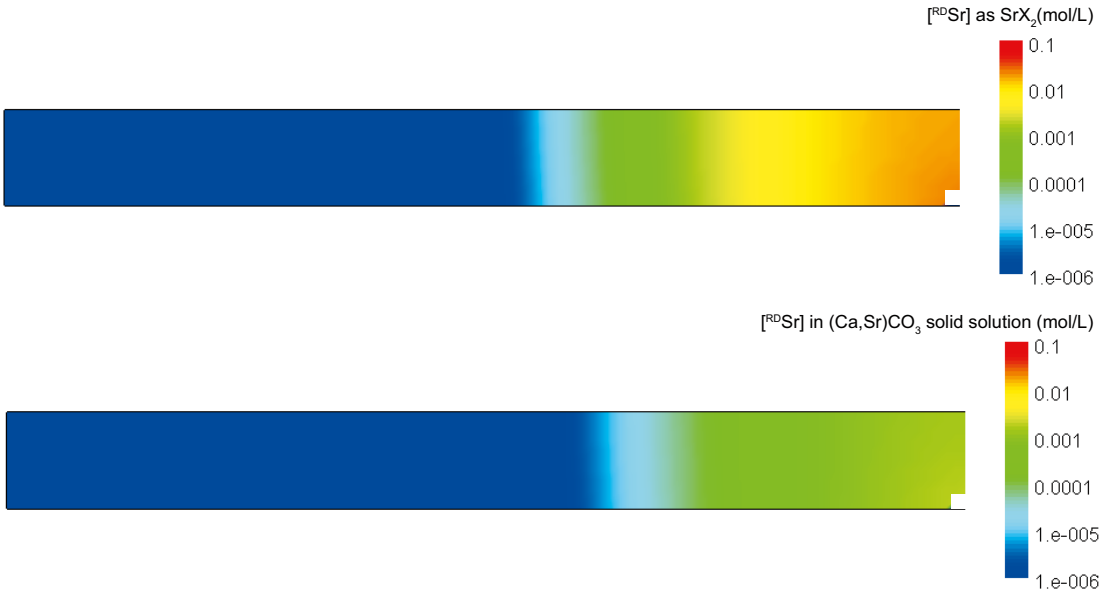

Figure 7-23. *Concentration of ^{RD}Sr retained in illite and the $(Ca,Sr)CO_3$ solid solution at the end of the simulation period (2,700 years after repository release). ^{RD}Sr is preferentially retained in illite throughout a large part of the modelled domain.*

Quantitative assessment of strontium retention efficiency

Figure 7-24 shows the time evolution of the computed retention efficiency of repository-derived strontium. At the beginning of repository release, the system reaches a retention efficiency for ^{RD}Sr of 100%, but it immediately starts to drop until reaching a value of 24% at the end of the simulation.

Sensitivity analysis of strontium

Figure 7-25 shows the evolution of the strontium concentration at the discharge area of the clay deposit, for the reference case and two alternative cases developed for sensitivity analysis (a lower CEC and not allowing the solid solution formation). The repository-derived strontium concentration is influenced by the lower CEC case. In this case, the ^{RD}Sr concentration is a little bit higher than in the reference case, reflecting that the lower density of cation exchange sites prevents a greater immobilisation of strontium in the illite interlayer (Figure 7-25).

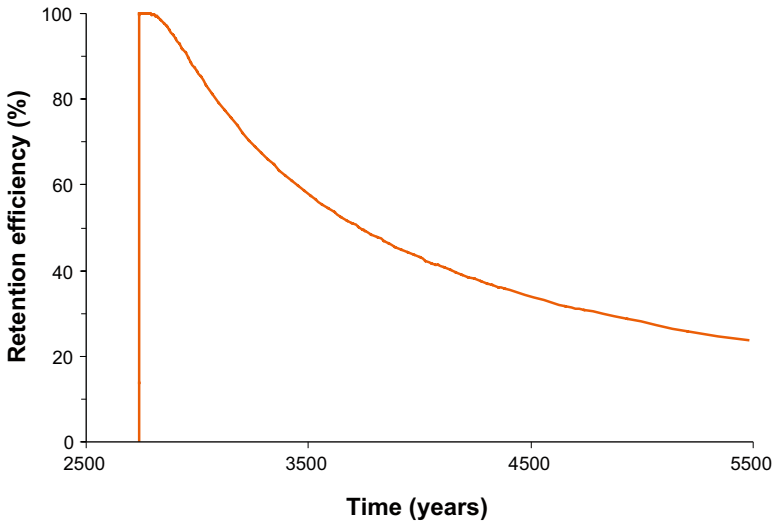

Figure 7-24. *Computed retention efficiency for repository-derived strontium along the simulation time (monitoring point: X = 10 m, Y = 1 m).*

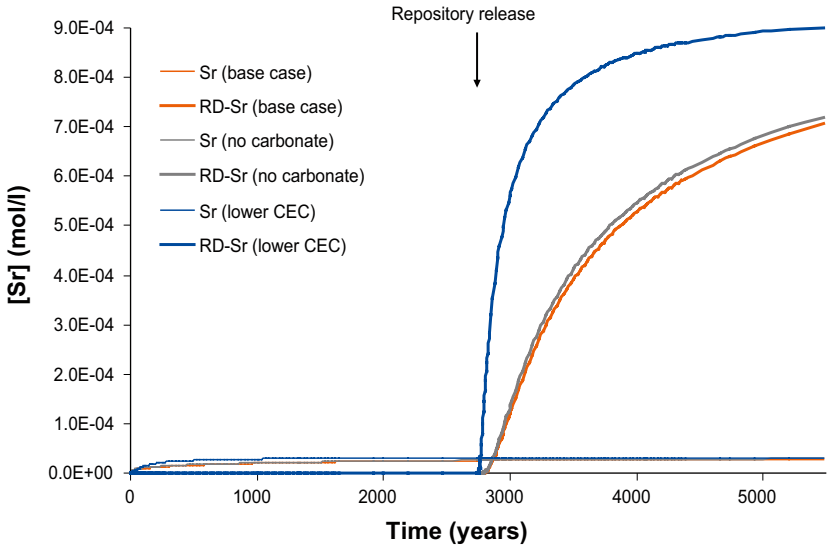

Figure 7-25. *Predicted evolution of natural and repository-derived strontium concentration along the simulation time at the discharge area (monitoring point: X = 10 m, Y = 1 m).*

7.2.10 Uranium

Prior to repository release, the concentration of aqueous uranium in the deep groundwater is approximately one order of magnitude higher than in the clay porewater (Table 5-7 and Table 5-11). The concentration of ^{RD}U in the deep groundwater affected by repository release is 5.66×10^{-9} mol/L. It is important to recall that this value was set as half the concentration of total uranium in the deep groundwater saturated with $UO_2{\cdot}2H_2O$. This concentration is approximately 6 times higher than the natural clay porewater uranium concentration.

After 2,700 years of repository release, 29% of the uranium being transported out of the clay deposit is derived from the repository (Figure 7-26). After repository relase, the reactive transport simulation predicts that uranium is partly retained by illite and partly by the precipitation of amorphous uraninite during the whole simulation period. Planar type cation exchange sites do not play a major role in uranium retention; in contrast, illite strong surface sorption sites do (Figure 7-27). The precipitation of amorphous uraninite only takes place near the deep groundwater inflow point (Figure 7-27). Apatite, which could be a sink for uranium, does not precipitate in the simulated clay domain.

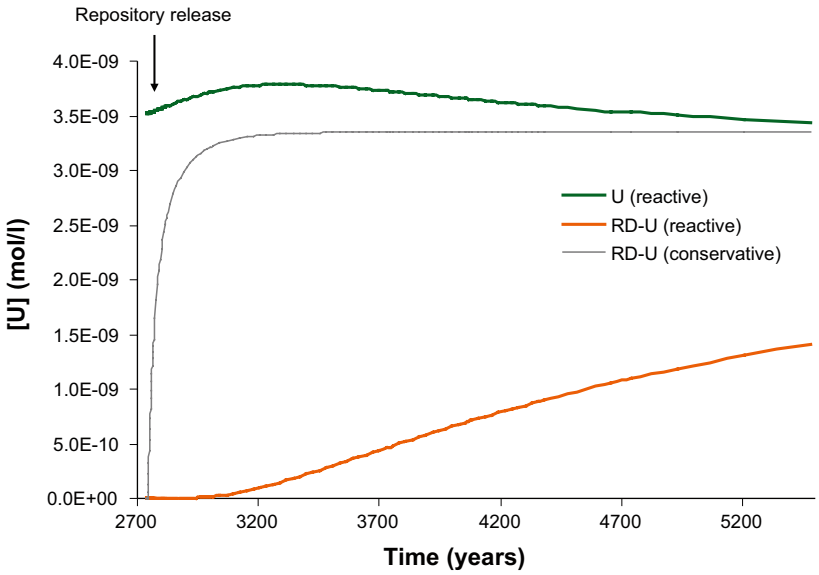

Figure 7-26. *Predicted evolution of natural uranium and repository-derived uranium (after repository release) at the discharge area (monitoring point: X = 10 m; Y = 1 m). Also the conservative breakthrough curve of ^{RD}U is presented.*

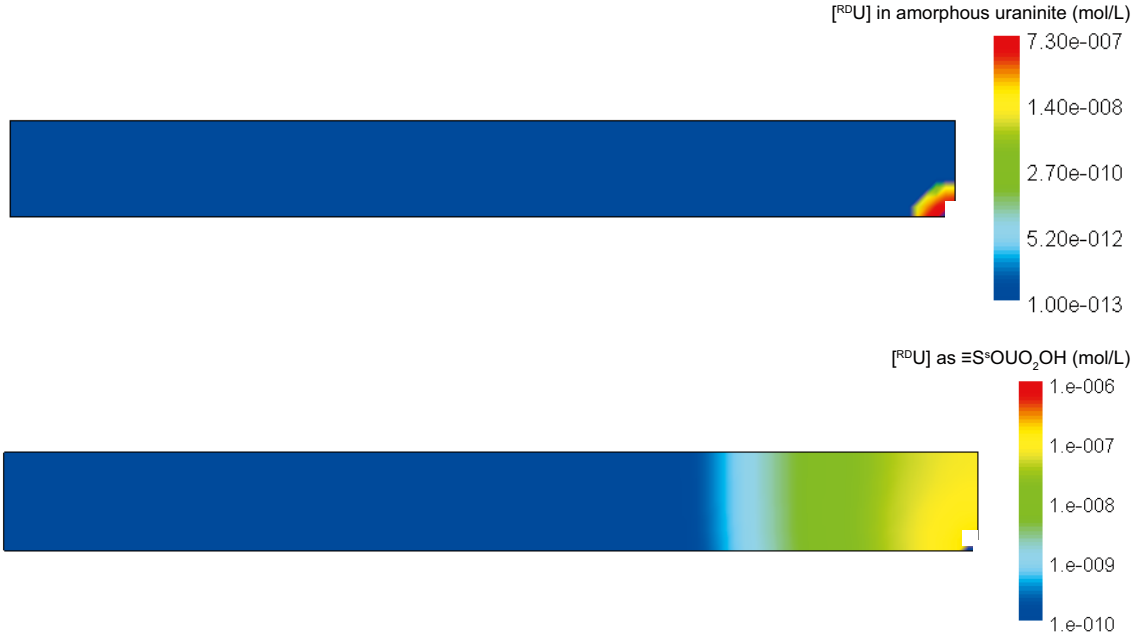

Figure 7-27. *Concentration and distribution of ^{RD}U retained in illite and in amorphous uraninite at the end of the simulation period (2,700 years after repository release). The sorption of uranium onto illite mainly occurs in the form of strong surface complexes.*

Quantitative assessment of uranium retention efficiency

Figure 7-28 shows the time evolution of the computed retention efficiency of repository-derived uranium. Immediately after repository release, the system reaches a retention efficiency for ^{RD}U of 100%. After this period, the retention efficiency for repository-derived uranium drops to 58%.

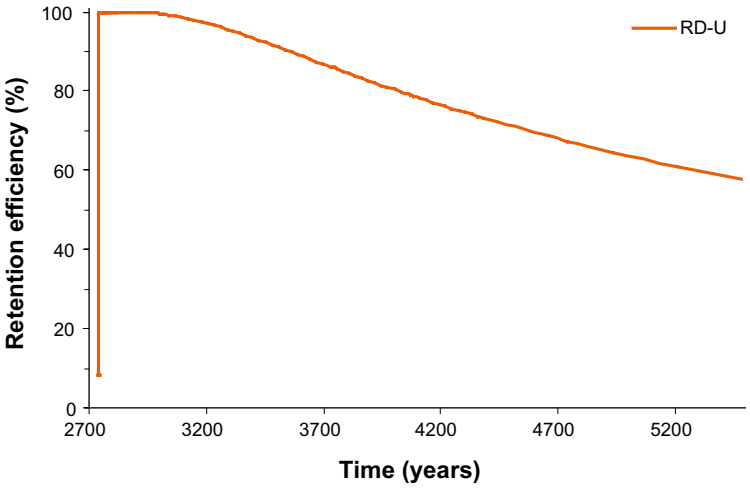

Figure 7-28. *Computed retention efficiency for repository-derived uranium along the simulation time (monitoring point: X = 10 m, Y = 1 m).*

Sensitivity analysis of uranium

Figure 7-29 shows the evolution of the uranium concentration at the discharge area of the clay deposit, for the reference case and two alternative cases developed for sensitivity analysis. The three simulations show very similar results, only a very little difference in concentration is observed: the simulation with higher concentration of humic acids (HA) and the simulation without uraninite have more uranium in solution than the base case simulation. In the simulation with a higher concentration of HA, this can be explained by a larger amount of U complexated with HA, and therefore less uranium available to sorb onto illite. The most significant difference is observed in the simulation with less sorption sites on illite. For the case of the simulation without uraninite, the lack of precipitation of this mineral phase produces a slight increase in dissolved U. At the end of the simulation period (5,400 years) the amount of ^{RD}U in solution in the base case is approximately half the amount of natural uranium.

7.2.11 Caesium

Before the release from the repository, the aqueous concentration of caesium in the deep groundwater is approximately two orders of magnitude higher than in the clay porewater. The simulation predicts an increase in caesium concentration in the outflowing water during the first 250 years. After this period, a progressive decrease is observed, mainly due to cation exchange in the illite interlayer (Figure 7-30).

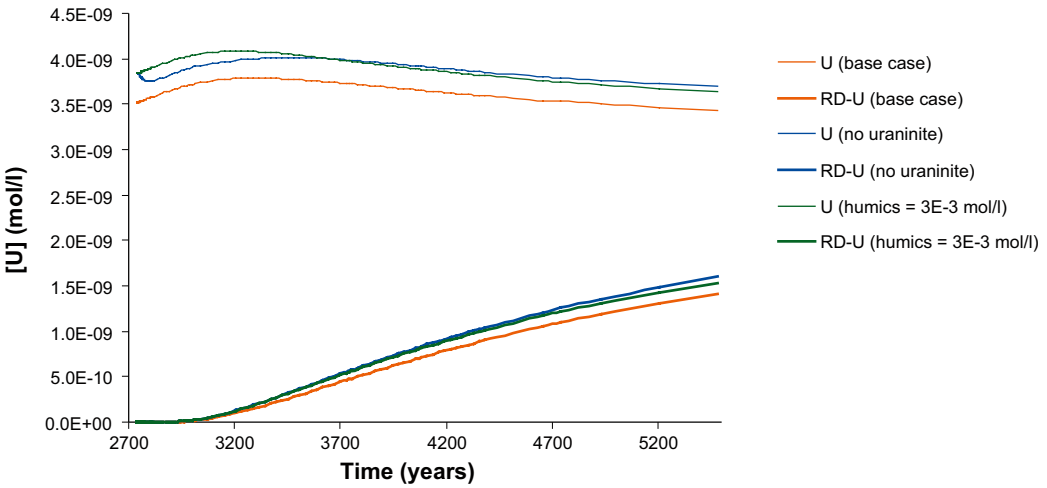

Figure 7-29. *Predicted evolution of natural and repository-derived uranium concentrations at the discharge area (monitoring point: X = 10 m, Y = 1 m) during 2,700 years of simulated repository release.*

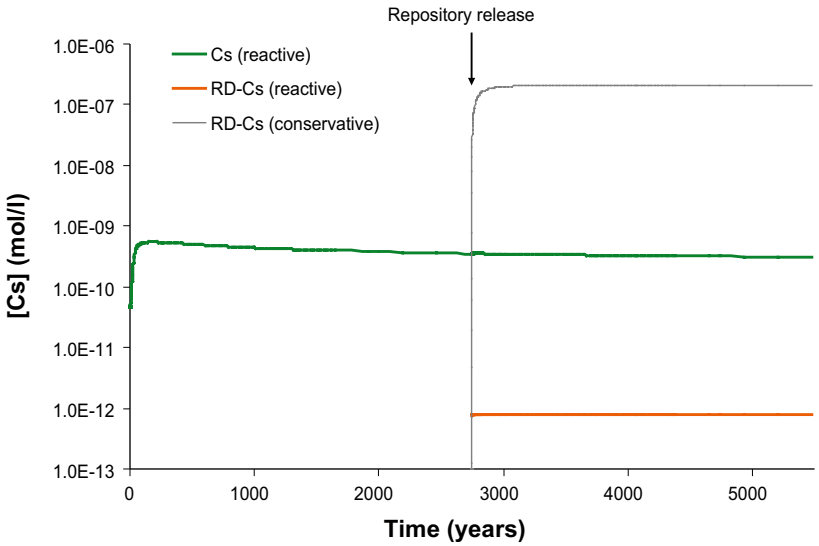

Figure 7-30. *Predicted evolution of natural caesium and repository-derived caesium at the discharge area (monitoring point: X = 10 m; Y = 1 m) in the reactive transport simulation, together with the conservative breakthrough curve of ^{RD}Cs.*

The concentration of ^{RD}Cs in the deep groundwater after repository release is 3.48×10^{-7} mol/L, which is approximately 2 orders of magnitude higher than the natural caesium concentration in deep groundwater, and 4 orders of magnitude higher than in the clay porewater. Approximately 2,700 years after repository release, only 0.3% of caesium flowing out of the clay deposit is derived from the repository (Figure 7-30).

The quantification of the retention capacity of the clay system for caesium reveals that at the end of the simulation period, the ^{RD}Cs concentration in the reactive transport simulation is much lower (5 orders of magnitude) than in the conservative transport simulation (Figure 7-30). The remarkable decrease of caesium concentration from the deep groundwater inflow point to the clay discharge area is due to the high affinity of Cs to the FES of illite, which readily retain caesium via cation exchange (Figure 7-31). Cs is also retained in illite "Type II" cation exchange sites.

Quantitative assessment of caesium retention efficiency

The retention efficiency for repository-derived caesium quickly reaches a maximum value of 100% (Figure 7-32), which is maintained until the end of the simulation.

Sensitivity analysis of caesium

A lower CEC in the illite interlayer affects the caesium sorption (Figure 7-33). The simulation of the reference case predicts a higher natural caesium concentration than the lower CEC case. This apparently contradictory result is explained by the fact that at the beginning of the simulation period the inflow of deep groundwater triggers the release of caesium that was previously retained in the planar sites of the illite interlayer. Since in the lower CEC case there is a lower cation exchange site density in the modelled domain, the amount of natural caesium released into solution by the planar sites of illite (per unit volume of water) is lower than in the reference case.

In the case of ^{RD}Cs, the lower CEC case leads to a higher concentration in solution at the end of the simulation. This reflects the decrease of the retention capacity of the clay system, due to the lower cation exchange site density compared to the reference case.

Figure 7-31. *Concentration of ^{RD}Cs retained in FES of illite at the end of the simulation period (2,700 years after repository release). Since caesium has a relatively high affinity for the FES, ^{RD}Cs is readily retained in the vicinity of the deep groundwater inflow point.*

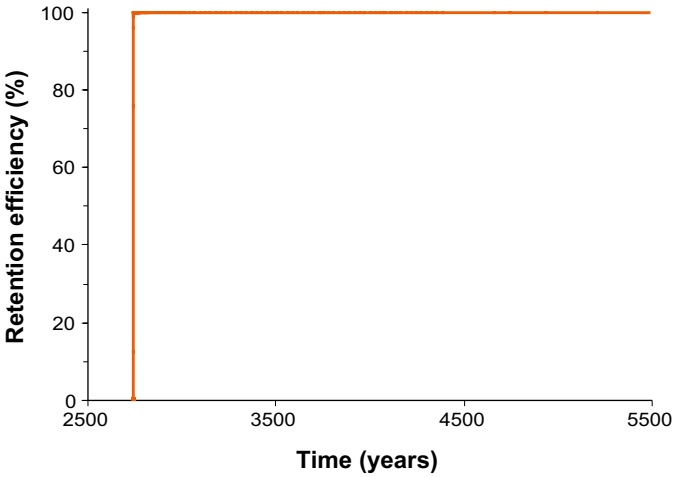

Figure 7-32. *Computed retention efficiency for repository-derived caesium along the simulation time (monitoring point: X = 10 m, Y = 1 m).*

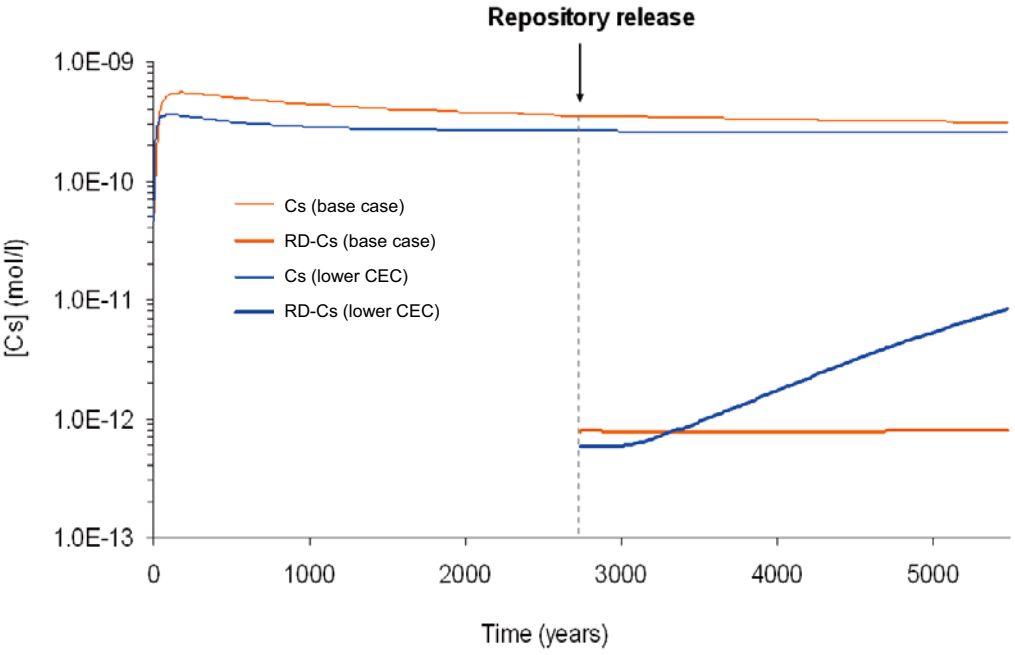

Figure 7-33. *Predicted evolution of natural Cs and repository-derived Cs concentration along the simulation time at the discharge area (monitoring point: X = 10 m, Y = 1 m).*

7.2.12 Radium

The initial concentration of radium in the deep groundwater due to repository release is 9.15×10^{-11} mol/L. At the discharge area of the clay deposit, the content of Ra is 4.3×10^{-11} mol/L after 2,700 years of reactive transport simulation, while for the conservative transport it is 5.4×10^{-11} mol/L (Figure 7-34). Radium is retained in the clay sediments at the beginning of the simulation, but the retention capacity decreses with time and at the end of the simulation (2,700 y after repository release) the concentration of Ra is of the same order in the reactive and conservative simulations. Saturation with radiobarite is not reached along the simulation time. Therefore, Ra is only partially retained in the clay system by cation exchange processes on illite (Figure 7-35).

Quantitative assessment of radium retention efficiency

Radium is strongly retained in the clay sediments at the beginning of repository release (100% of retention efficiency; Figure 7-36). However, the retention efficiency decreases with time, down to 21% at 2,700 years after the beginning of the repository release.

Sensitivity analysis of radium

A lower CEC in the illite interlayer affects the sorption of radium (Figure 7-37). The low-CEC simulation predicts that radium is almost conservative. At the end of the simulation no radium is retained.

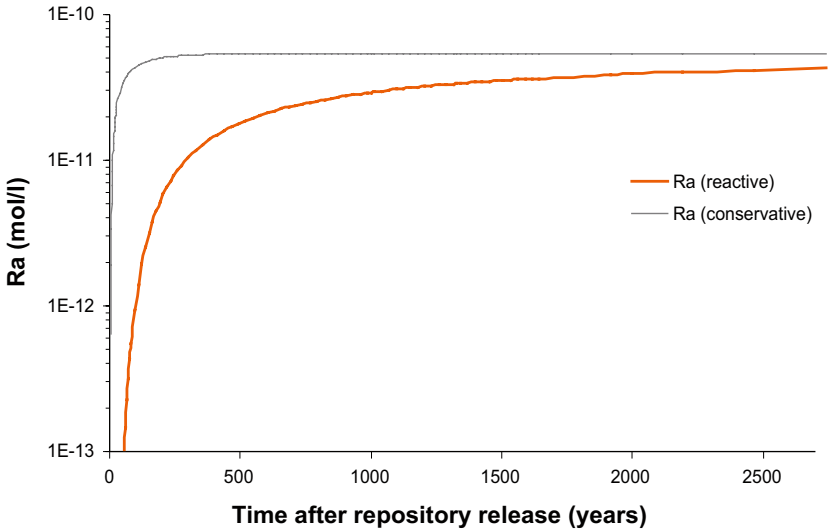

Figure 7-34. *Predicted evolution of repository-derived radium at the discharge area (monitoring point: X = 10 m, Y = 1 m) after repository release, together with the conservative breakthrough curve.*

Figure 7-35. *Concentration of Ra retained in planar sites of illite at the end of the simulation period (2,700 years after repository release).*

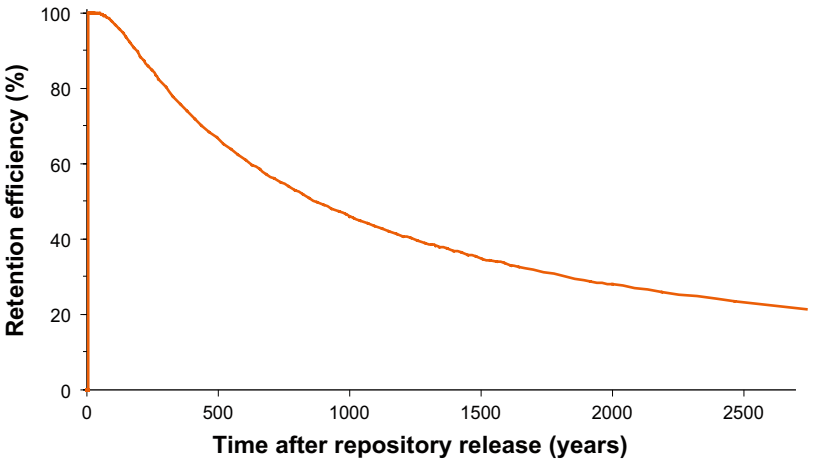

Figure 7-36. *Computed retention efficiency for repository-derived radium along the simulation time (monitoring point: X = 10 m, Y = 1 m).*

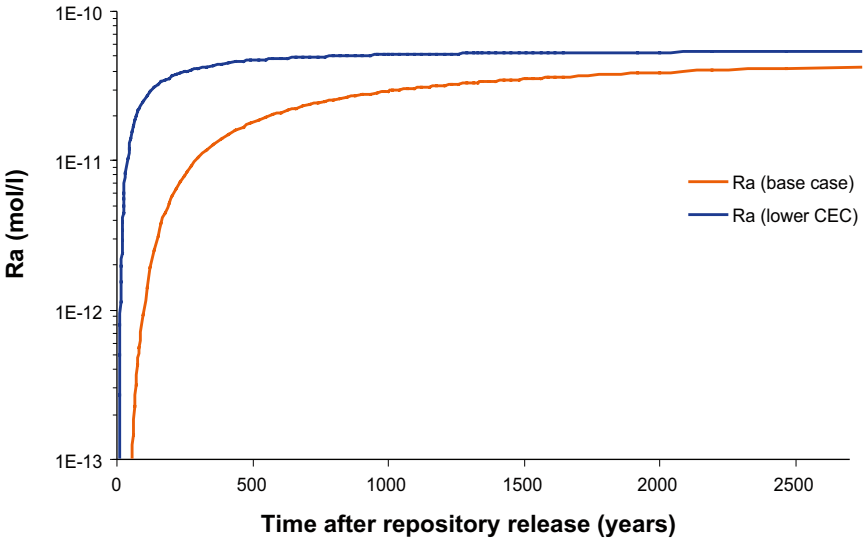

Figure 7-37. *Predicted evolution of radium concentration along the simulation time, at the discharge area (monitoring point: X = 10 m, Y = 1 m).*

7.3 Retardation factor and effective distribution coefficient of repository-derived radionuclides

As explained in Section 6.3, if the computed breakthrough curve of a reactive solute is complete (i.e. the maximum stabilised concentration has been reached), then the retardation factor (R) of a given reactive solute can be calculated with Equation 6-3.

Complete breakthrough curves have been computed only for those radionuclides that behave conservatively, namely Nb, Se and Tc, which have a retardation factor equal to one. Breakthrough curves are not complete for the reactive transport modelling of the other radionuclides; however, at the end of the simulation, RDSr and Ra have concentrations higher than those of the conservative simulation at $T^{C}_{1/2}$ and R can be computed (Figure 7-38). The results are that R for RDSr is 30 and for Ra it is 27.

In order to obtain complete breakthrough curves for the other simulated elements (RDC, RDCs, RDNi and RDTh), a simulation to 30,000 years has been launched. As explained before, this simulation does not take the geological, hydrogeological and geochemical changes that are predicted to take place in this time frame into account, and the only purpose of the simulation is to get R values. The results show that RDTh, RDNi, RDCs and RDC have not reached a steady state (Figure 7-38). At the end of

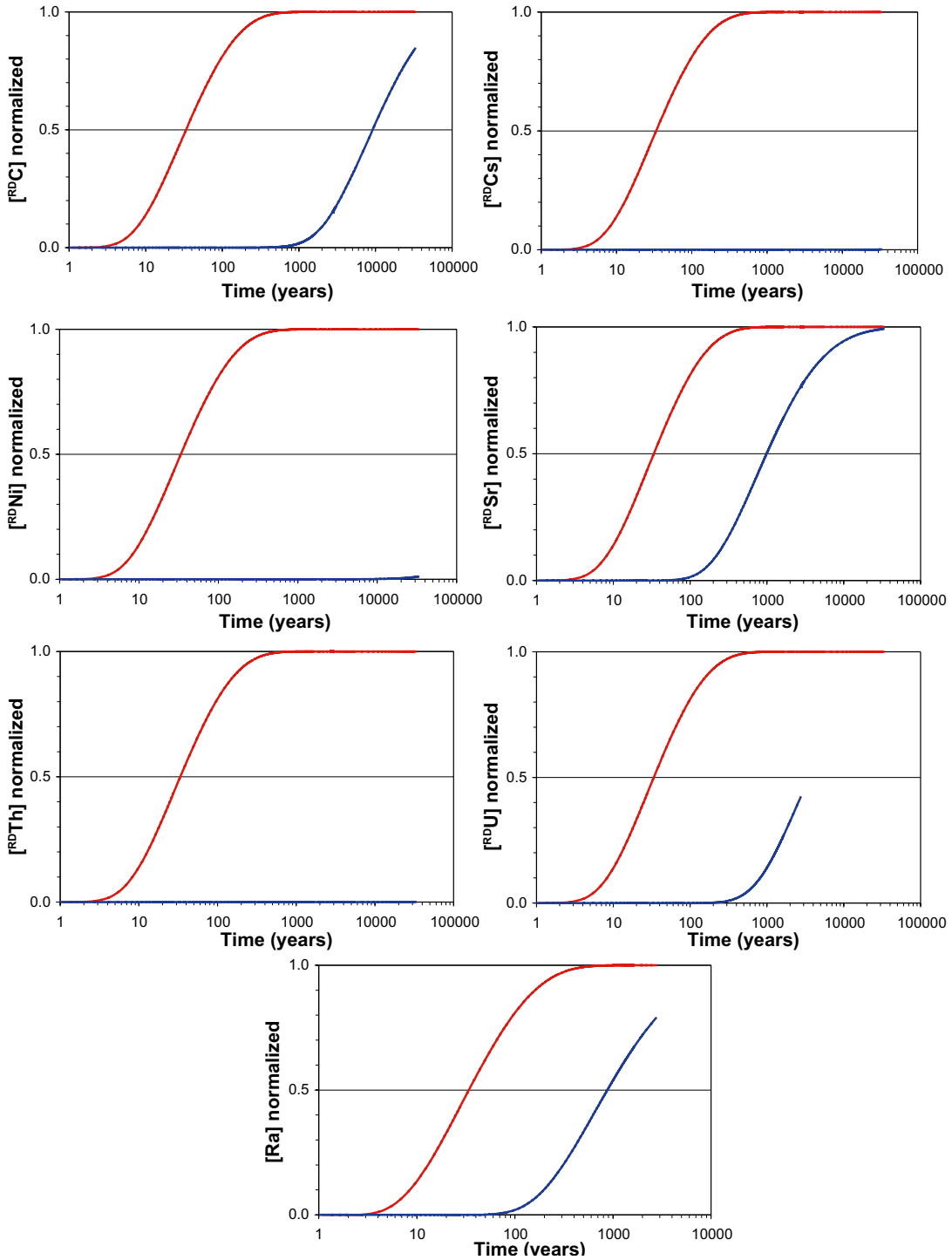

Figure 7-38. *Concentrations of radionuclide at the observation point (X = 10 m, Y = 1 m) normalised to the maximum concentration of the consevative model at steady state; red curves show conservative transport, blue curves reactive transport.*

the simulation only ^{RD}C has reached concentrations higher than that of the conservative simulation at $T^{C}_{1/2}$ and R can be calculated, giving a value of 291. For ^{RD}U, the simulation could not reach the $T^{C}_{1/2}$, due to numerical problems, and only a lower limit of the R value (>158) could be determined.

Using Equation 6-4, the Kd_e can be calculated in those cases were R is available. The calculated Kd_e values are: 29 L/kg for ^{14}C, 2.9 L/Kg for ^{90}Sr, >15.7 L/kg for ^{235}U, and 2.6 L/kg for ^{226}Ra. The obtained Kd_e for Sr and U are two and three orders of magnitude, respectively, lower than those reported for lake sediments in Forsmark (see Table 3-5). For those radionuclides with an R of 1 (i.e. that behave conservatively) the Kd_e is equal to zero.

8 Summary and discussion

8.1 Summary and interpretation of main results

The repository-derived radionuclides that behave conservatively (e.g. ^{129}I and ^{36}Cl) are expected to discharge very quickly to the surface water, both in the till (Figure 8-1) and the clay system (Figure 8-2). It should be noticed that the concentration steady state for conservative radionuclides is reached approximately 500 years later in the clay system than in the till, due to the contrasting hydrogeological properties of the media. The hydraulic conductivity is two to three orders of magnitude higher in the till than in the clay system. As a result, advection and dispersion are the dominant transport processes in the till system, while in the clay system (low permeability medium) diffusion plays a more significant role.

The results of the calculations show that, as expected, the deep groundwater is initially not in equilibrium with the systems under consideration. Therefore, once deep groundwater enters the QD system it reacts to attain equilibrium, so that the most significant changes occur near the entering point for deep groundwater. Far from this point the changes are less pronounced as the degree of disequilibrium is lower.

The quantitative modelling exercise showed that, besides repository-derived Cl and I, also ^{94}Nb and ^{99}Tc behave conservatively in the till and clay systems, and the same can be observed for ^{79}Se in the clay. It is worth noting that only the precipitation of pure phases was considered as a process potentially able to retain Nb, Se and Tc. In the Forsmark (assumed) conditions Nb and Tc solids are far from saturation, and the same happens with Se in the clay sediments, despite the fact that high concentrations of these elements were considered to migrate from the repository.

All the calculations have been done by considering the concentrations of radionuclides as they can occur in the near-field of a repository in case of a release. It is reasonable to think that along the path from near-field to near-surface sediments some reactions can occur, leading to lower concentrations of radionuclides. Therefore, it would be of interest to study the effect of lower radionuclide concentrations on the retention capacity of the Quaternary deposits in future developments.

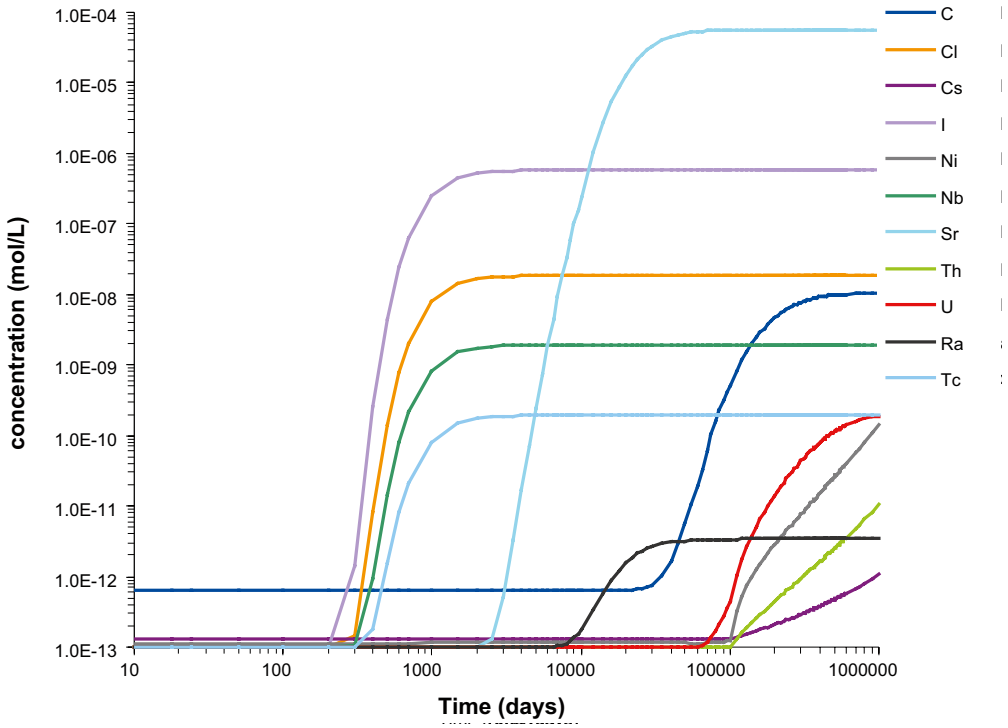

Figure 8-1. *Integrated breakthrough curves of repository-derived radionuclide concentrations at the discharge area of the till domain (see Figure 5-1 for location).*

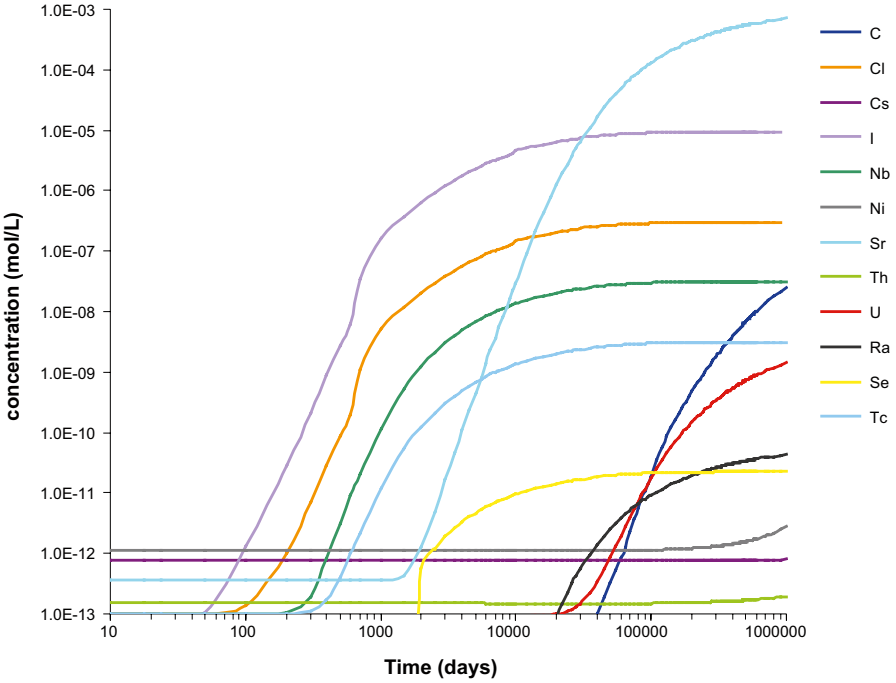

Figure 8-2. *Simulated breakthrough curves of repository-derived radionuclide concentrations at the observation point of the discharge in the clay domain (see location in Figure 5-2).*

According to the reported Kd values for Forsmark sediments, Nb has a high affinity for the solid phase /Engdahl et al. 2008, Sheppard et al. 2009/. However, the model predicts no retention of Nb (natural + repository derived) because the saturation of Nb_2O_5 is not reached at any point and at any time. In the natural system, Nb could be partially retained by sorption onto sediment particles, which could explain the high Kd values reported for Nb, based on the in situ measurements.

Tc is also behaving conservatively in the numerical modelling. For the case of the till system, this is consistent with the fact that under oxidising conditions the main Tc(VII) aqueous complex is TcO_4^-, i.e. an anion. For the case of the clay system, the more reducing environment favours the stability of Tc(IV) species, although in the modelled domains the concentration of Tc in solution was not high enough for the precipitation of TcO_2. Reported Kd for Tc reveal that this element is poorly retained in soils /Sheppard et al. 1990/.

In the case of Se, the simulation of the clay system shows that no solid phases will precipitate in the whole domain. The precipitation of pure phases is not the only mechanism that can potentially retain Se, but it was the only one considered in the simulations. In the real case, the concentration of dissolved selenium in the clay system could decrease, for example, by its sorption onto organic matter or by its incorporation to newly formed sulphides. These processes were not implemented in the numerical models due to the lack of reliable parameters for their quantification, but the reported range of Kd for Se in Forsmark lake sediments (9,500 to 100,000 L/kg /Engdahl et al. 2008/) confirms that this element is effectively retained in these environments.

In the till domain, the Eh-pH conditions and the concentration of dissolved Se (in the order of 1×10^{-15} to 1.6×10^{-15} mol/L) favours the precipitation of native selenium. The release of this radionuclide to the discharge area of the till domain is completely prevented, and the retention efficiency of the till domain for this radionuclide is 100%. However, it is emphasised that the stability field of native selenium under the conditions of interest is very narrow, and a slight change in Eh and/or pH will prevent its precipitation (Figure 8-3).

The next radioelements to discharge in both domains are ^{90}Sr and ^{226}Ra. After them, ^{14}C and U will follow, while ^{135}Cs, ^{230}Th and ^{59}Ni are the radionuclides showing the strongest effects of retardation (Figure 8-1 and Figure 8-2). Conversely to Nb and Se, all the significant processes that could apparently retain Sr in the till and clay domains were included in the simulations. The numerical modelling indicates that the till system is not efficient in retaining ^{90}Sr, which is only partially retained by cation exchange onto illite and, close to the deep groundwater discharge point, in the $(Ca,Sr)CO_3$ solid solution.

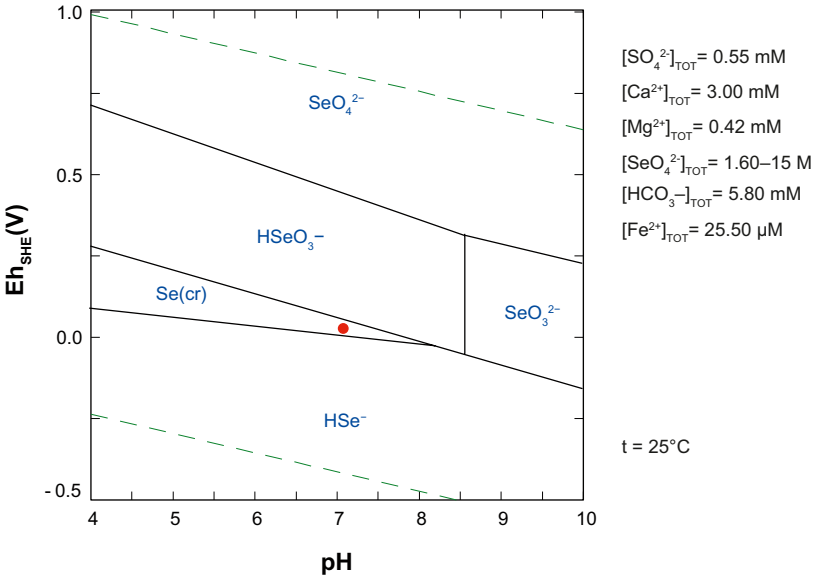

Figure 8-3. *Eh-pH diagram of Se species for a groundwater from the till domain, close to the deep groundwater inflow point. The red point indicates the (very narrow) pH-Eh range in the simulated till domain after repository release.*

The clay system also shows a decreasing capacity to retain ^{90}Sr with time. In fact, at the end of the simulation period (~3,000 years), the maximum ^{90}Sr concentration at the discharge area is only 25% lower than in the conservative transport simulation. The sensitivity analysis shows that the arrival of ^{90}Sr at the discharge area is controlled by the amount of cation exchange sites, indicating that the slight retention of ^{90}Sr is mainly due to sorption onto illite.

Ra is partially retained by cation exchange in both till and clay sediments, but it is also scavenged from solution by the precipitation of (Ba,Ra)SO_4 under the conditions prevailing in the till. The retention efficiency of till for Ra drops very fast to almost zero, while such a decrease is more gradual in the clay domain, down to 20% after almost 3,000 years of simulation. This indicates that the maximum retention capacity of illite is reached and no more Ra can be accommodated in the case of the till. It is worth noting that slight changes in groundwater composition could preclude the precipitation of radiobarite and radium uptake in the till. The sensitivity analysis indicates that if less sorption sites are available on illite (a ten-fold decrease), the arrival of Ra at the discharge areas takes place earlier.

For repository-derived radiocarbon, the main retention mechanism considered in the Forsmark near-surface system is carbonate precipitation. The models predict that ^{14}C could be efficiently retained in the clay system. After 2,700 years of repository release, the ^{14}C concentration at the discharge area of the clay system is one order of magnitude lower in the reactive transport simulation than in the conservative simulation. On the contrary, in the till system the retention efficiency of ^{14}C drops very fast, and radiocarbon behaves conservatively during most of the simulation time. The sensitivity analysis, which considered temperatures of 5, 15 and 25ºC, did not show significant differences in the retention of radiocarbon due to isotopic fractionation processes.

Repository-derived uranium is another of the simulated elements that is only partially retained in the till and clay systems. For the till system, the numerical modelling shows that the retention efficiency will be at its maximum at the beginning of the repository release, and then will decrease significantly with time. At the end of the simulation (2,700 years) uranium will behave almost conservatively (Table 8-1). In the till domain, sensitivity analyses show that a lesser amount of sorption sites does not affect the concentration of uranium in solution, since it is mostly retained by iron hydroxide. In the clay domain, U will be retained due to the precipitation of amorphous uraninite and the sorption onto illite. The sensitivity analysis of the clay domain shows that an increase of one order of magnitude in the concentration of dissolved humic acids does not significantly change the concentration of dissolved uranium.

Table 8-1. Retention efficiency (E, defined in Equation 6-2) after 2,700 years of simulated repository release, retardation factor (R, Equation 6-3), arrival time of 1% and effective Kd (Kd_e, Equation 6-4, in L/kg) at the discharge area of the simulated domains.

Element	E (2700 y) Till	E (2700 y) Clay	arrival 1% Till	arrival 1% Clay	R Till	R Clay	Kd_e Till	Kd_e Clay
^{14}C	0.83%	85%	205 y	810 y	196	291	7.89	29
^{36}Cl	0%	0%	1.4 y	4 y	1	1	0	0
^{135}Cs	100%	100%	9500 y	>> 33000 y	-	-	-	-
^{129}I	0%	0%	1.4 y	4 y	1	1	0	0
^{94}Nb	0%	0%	1.4 y	4 y	1	1	0	0
^{59}Ni	99.2%	100%	2500 y	32000 y	6035	-	244.1	-
^{90}Sr	0.02%	23.6%	29 y	94 y	24	30	0.93	2.9
^{230}Th	99.8%	100%	4300 y	>> 33000 y	11819	-	478.2	-
^{235}U	7.62%	57.1%	340 y	329 y	402	>158	16.2	>15.7
^{226}Ra	2.98%	21.2%	23 y	82 y	20	27	0.77	2.6
^{79}Se	100%	0%	>> 33000 y	4 y	-	1	-	0
^{99}Tc	0%	0%	1.4 y	4 y	1	1	0	0

The most strongly retarded radionuclides in the modelled domains are ^{135}Cs, ^{59}Ni and ^{230}Th. The computed retention efficiencies for these radionuclides at the end of the simulations of the till and clay domains are 100% (Table 8-1). In the clay system these elements are very efficiently retained by illite due to the high affinity of these elements for the illite surfaces. In the till domain, Ni is also retained by ferrihidrite, although in much lesser amount than by illite. The sensitivity analysis of the clay system shows that a decrease of one order of magnitude in the amount of illite sorption sites produces an increase of one order of magnitude of ^{230}Th and ^{135}Cs in solution and of two orders for ^{59}Ni. In the till system, the increase in concentrations due to the same change in sorption sites is of two orders of magnitude for ^{230}Th and ^{135}Cs and of one order of magnitude for ^{59}Ni. As expected, the decrease in sorption sites produces also a decrease in the corresponding retardation factors of these radionuclides (Table 8-2).

The arrival times of 1% of repository-derived radionuclide at the discharge areas of the till and clay systems are in agreement with the calculated retention efficiency (Table 8-1). The fastest arrival corresponds to the radionuclides that behave conservatively, while for other radionuclides the arrival time is over 33,000 y.

The retardation factor (R) is another parameter that indicates to what extent the different radionuclides are retained in the sediments. Calculated R from breakthrough curves are reported in Table 8-1 and Table 8-2. R is 1 for the conservative radionuclides and it reaches values up to 11,800 for ^{230}Th in the clay system. In some cases the delay was so long that R could not be computed. This was the case for ^{135}Cs, ^{59}Ni and ^{230}Th in the clay domain and for ^{135}Cs and ^{79}Se in the till domain.

The sensitivity analysis revealed that R values are correlated with the amount of sorption sites for those radionuclides that are mainly retained on illite (Table 8-2). When the amount of sorption sites is reduced by one order of magnitude, R decreases up to one order of magnitude for ^{230}Th and ^{226}Ra (Table 8-2). In the case of ^{235}U and ^{90}Sr in the till, the reduction of R is not so significant because other processes are also involved in their retention (sorption onto ferrihydrite and precipitation of carbonate solid solution, respectively).

Table 8-2. Retardation factor (R) and effective Kd (Kd_e, in L/kg) for the sensitivity analysis with less illite sorption sites (lss) and the base case (bc). The lss simulation was run up to 2,700 y and the bc simulation up to 33,000 y. R and Kd_e could not be computed for Ni and Cs in the lss simulation.

Element	$R_{(bc)}$ Till	$R_{(lss)}$ Till	$R_{(bc)}$ Clay	$R_{(lss)}$ Clay	$Kd_{e\ (bc)}$ Till	$Kd_{e\ (lss)}$ Till	$Kd_{e\ (bc)}$ Clay	$Kd_{e\ (lss)}$ Clay
^{90}Sr	24	9	30	5.4	0.93	0.32	2.9	0.44
^{230}Th	11819	1000	-	-	478.2	40.4	-	-
^{235}U	402	390	>158	n.c	16.2	15.7	>15.7	n.c.
^{226}Ra	20	n.s.	27	3.33	0.77	n.c.	2.6	0.23

8.2 Computed Kd versus Kd derived from in situ observations

Effective Kd (Kd_e) can be calculated based on computed retardations. To calculate Kd_e one must give a single value of effective porosity, which is not the case for the modelled till system. A value of 0.0789 for the effective porosity in the till was used to calculate Kd_e. This value was obtained by /Sena 2009/ from a calibration of a conservative transport model. The porosity in the clay system was 0.2. The dry bulk density was 1.95 kg/L in the till and 2.0 kg/L in the clay system. The calculated Kd_e at the monitoring points are reported in Table 8-1 and Table 8-2.

Furthermore, a Kd mapping of the whole simulated till and clay domains was carried out by plotting the ratio of calculated concentrations in the solid and aqueous phases (Figure 8-4 and Figure 8-5 respectively). It is important to note that the computed Kd of each natural isotope is equal to that of the corresponding repository-derived radionuclide /Sena 2009/, with the exception of natural carbon and repository-derived carbon, for which a slight but not significant difference in Kd is observed due to isotopic fractionation processes.

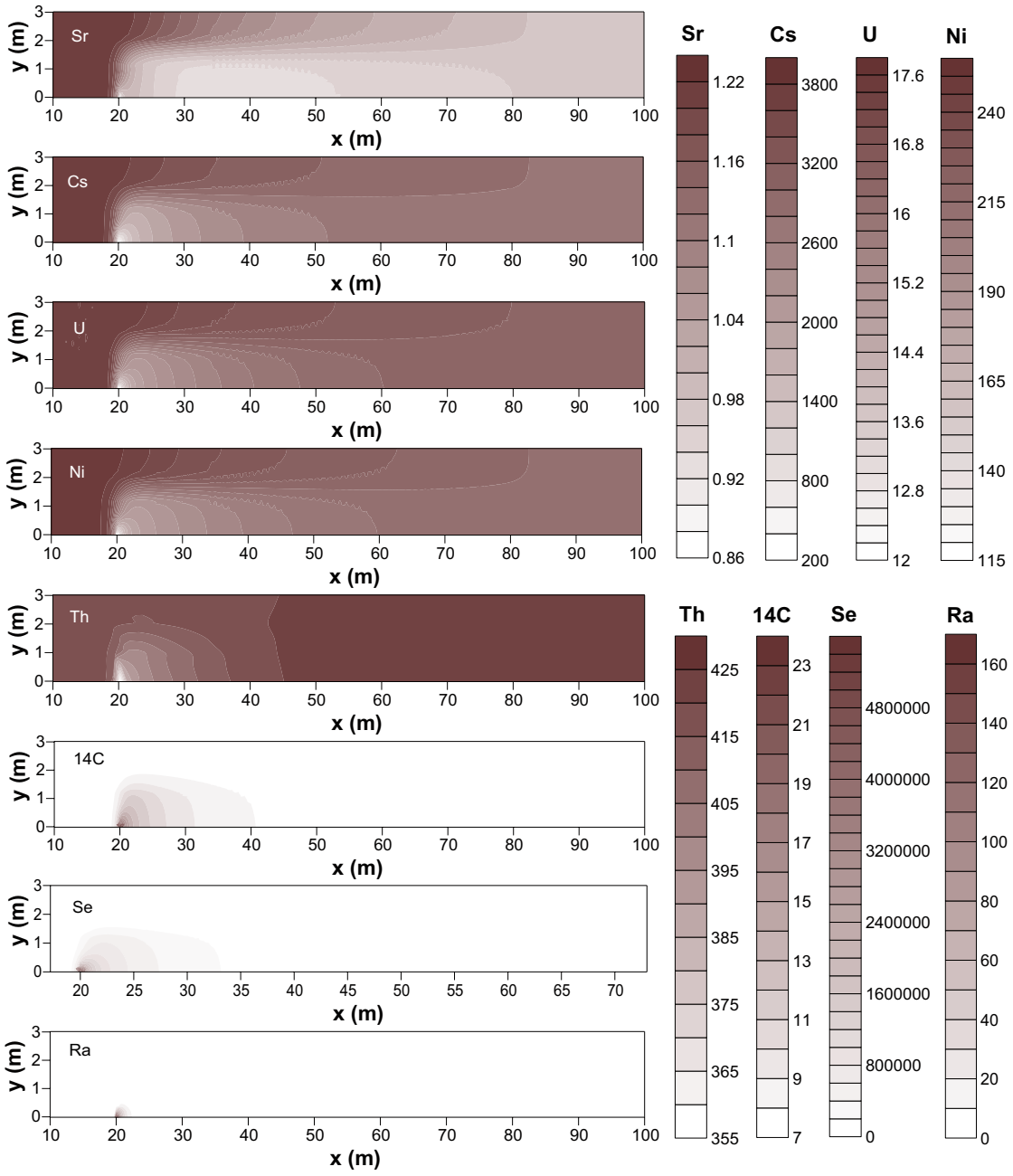

Figure 8-4. *Distribution maps of Kd (L/kg) for selected elements in the till domain after 2,700 years of radionuclide release (deep groundwater inflow point: X = 20 m, Y = 0 m).*

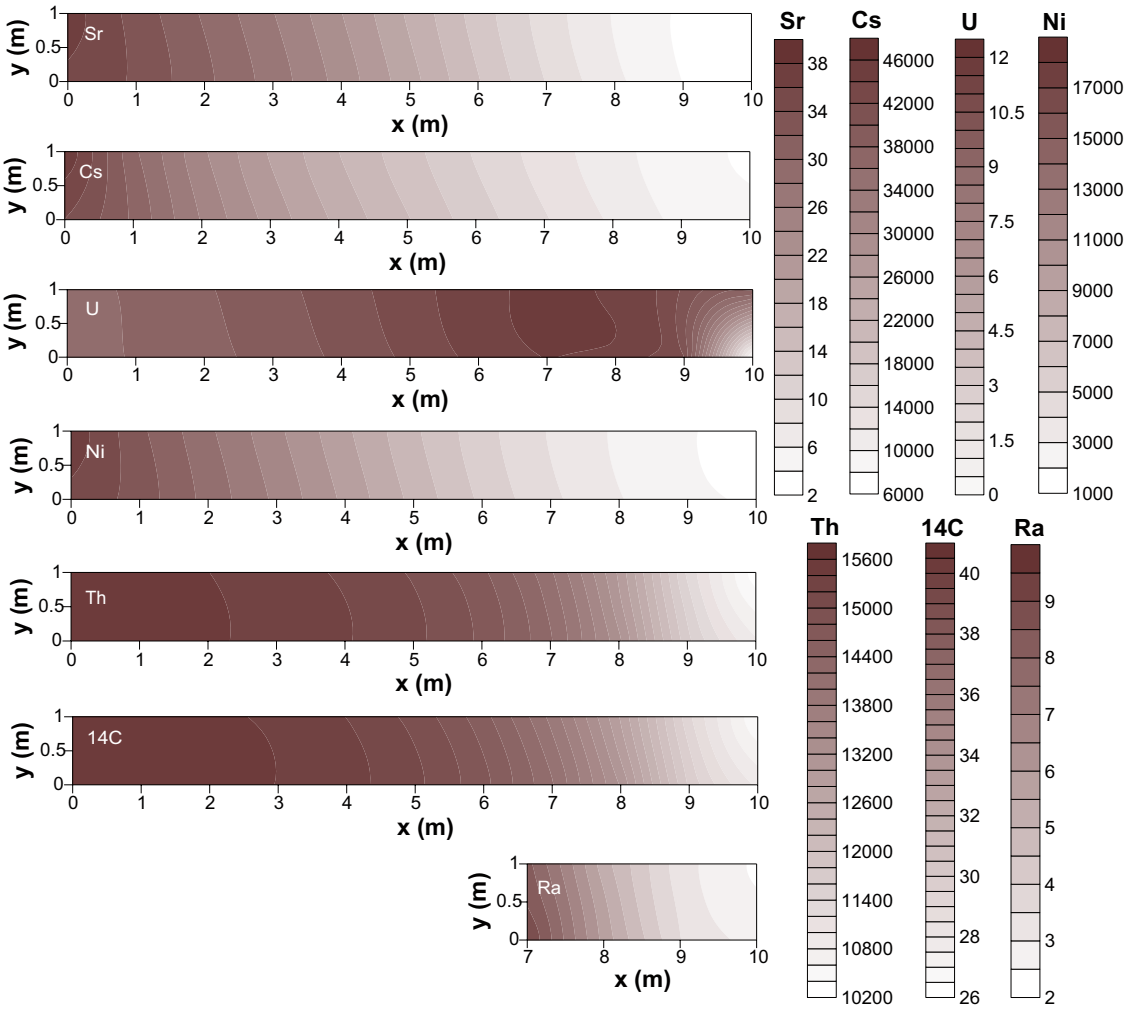

Figure 8-5. *Distribution maps of Kd (L/kg) for selected elements in the clay domain after 2,700 years of radionuclide release (deep groundwater inflow point: X = 10 m, Y = 0 m).*

As already pointed out by /Sena 2009/, once the geochemical quasi-steady state has been approached, the Kd of the selected radionuclides is relatively stable in time, but it is not homogeneous in space. In the till domain, the radionuclides that are mostly retained by sorption onto clay and Fe hydroxide (namely ^{90}Sr, ^{135}Cs, ^{235}U, ^{59}Ni, ^{230}Th) show a decrease in the Kd in the area affected by the deep groundwater (Figure 8-4).

For ^{79}Se, ^{14}C and ^{226}Ra, the maximum Kd values are reached in the vicinity of the deep groundwater inflow point, where native Se, $(Ca,Sr)CO_3$ and radiobarite precipitate (Figure 8-4). In the clay system a decrease in Kd is also computed in the area affected by the deep groundwater, for all those elements that are retained either by sorption onto illite and/or incorporation to solid phases (Sr, Cs, U, Ni, Th, C and Ra) (Figure 8-5).

As expected, the computed Kd values are not equal in the till and clay domains. In general they are up to one order of magnitude higher in the clay domain for Sr and Cs and up to two orders of magnitude higher for Ni and Th (Table 8-3). The stronger retention of these elements in the clay domain is explained by the larger amount of illite, which implies a larger amount of available sorption sites. C shows a higher Kd value in the clay domain, but in the same order of magnitude as in the till (Table 8-3). In contrast, Kd values of Ra are up to two orders of magnitude higher in the till domain than in the clay (Table 8-3), due to the precipitation of radiobarite. U shows Kd values in the same order of magnitude in both systems, but slightly higher in the till.

According to the computed Kd, the most retained radionuclides in the till system are Se and Cs, followed by Th and Ni, and then by U, Sr, C and Ra with much lower Kd. The computed Kd values of Ni, Cs, and U are one order of magnitude lower than desorption Kd values reported for till soils in

Table 8-3. Range of Kd (L/kg) in the simulated till and clay domains after 2,700 y of repository release (base case simulations), and reported Kd in Forsmark sediments and soils.

Element	Calculated Kd range		Measured Kd range	
	Till	Clay	Till soils[a]	Lake seds.[b]
C	7 - 24	26 - 42		
Cl	0	0	4.4 - 37	7 - 93
Cs	200 - 4000	6000 - $4.8 \cdot 10^4$	$2.8 \cdot 10^4$; $1.2 \cdot 10^5$	6857 - $1.1 \cdot 10^5$
I	0	0	>90 - >210	302 - 2471
Nb	0	0	$3.6 \cdot 10^4$	$8.1 \cdot 10^4$ - $2.7 \cdot 10^5$
Ni	115 - 255	1000 - $1.9 \cdot 10^4$	3000; 3800	9375 - $3.1 \cdot 10^4$
Sr	0.86 - 1.24	2 - 40		214 - 389
Th	355 - 430	$1.0 \cdot 10^4$ - $1.6 \cdot 10^4$	$3.1 \cdot 10^4$ - $2.5 \cdot 10^5$	$1.3 \cdot 10^5$ - $2.9 \cdot 10^5$
U	12 - 17.8	>15.7	610 - 3300	1435 - 5200
Ra	0 - 170	2 - 10		
Se	0 - $5.6 \cdot 10^6$	0	10 - 14	9545 - $1.0 \cdot 10^5$
Tc	0	0		

a) data from /Sheppard et al. 2009/.
b) data from /Engdahl et al. 2008/.

Forsmark, and two to three orders of magnitude lower for Th (Table 8-3). Desorption Kd values in /Sheppard et al. 2009/ were obtained after partial extraction with aqua regia; therefore, the elements present in non-reactive silicates were not considered in the Kd calculation.

Soil Kd values should not be directly compared with those of the till sediment, since the environmental conditions and parameters that could influence Kd are different in the two materials. In addition, organic material in the soil could also be a sink for some of the considered radionuclides, such as Ni, U and Th, although this process was not simulated in the model.

Selenium is an interesting exception because the model computes that it is strongly retained in the till system, while the reported Kd values reveal that Se is poorly retained in Forsmark till soils (Table 8-3). As already mentioned, the predicted Eh-pH conditions are favourable to native Se precipitation in the simulated till domain, but this process is so sensitive to small changes in the groundwater Eh/pH that it should be only qualitatively considered (see Figure 8-3).

In the case of the clay system, computed Kd show that Cs, Ni and Th will be strongly retained, while Sr, U, C and Ra will be less retained (Table 8-3). Kd of Ni and Cs are in the range of those reported by /Engdahl et al. 2008/ for Forsmark lake sediments, while computed Kd values of Th and Sr are one order of magnitude lower and those of U two orders of magnitude lower (Table 8-3). The lower computed Kd values of Th, U and Sr can be explained by the fact that /Engdahl et al. 2008/ used an extraction method that produces the total dissolution of these sediments. Therefore their reported Kd are not only describing the exchangeable fraction of the solid phase, but also the fraction present in silicates assumed non-reactive in the simulated time frame. The fact that sorption onto organic material is not considered, could also explain the lower computed Kd of Th and U.

Effective Kd for Ra are below 3 L/kg in the simulated till and clay domains. No Kd data for Ra is available for Forsmark. However, /Sheppard et al. 2009/ predicted Kd values for Ra in Forsmark samples by applying a stepwise regression of data from the literature. Predicted Kds in Forsmark samples range between 0.033 and 910 L/kg with the regression of the /Sheppard et al. 2006/ data set, and between 16 and $1.2 \cdot 10^7$ L/kg with the regression of the /Thibault et al. 1990/ data. /Sheppard et al. 2009/ also combined data from /Sheppard et al. 2006, Thibault et al. 1990, Vandenhove and van Hees 2007/, resulting in a new regression, which only applies for soils with up to 20% of organic carbon. With the new regression, the predicted Kd of two Forsmark clayey tills are 130 and 73 L/kg. The effective Kd obtained in the simulations are therefore closer to the lower values predicted for Ra in the Forsmark soils.

Despite the fact that computed Kd and experimentally determined Kd differ in most cases, the general trend observed for the Forsmark till soils and lake sediments is relatively consistent. Computed and experimental values agreed in that the most strongly retained elements are Th, Cs and Ni, followed by U and Sr. Se is an exception because no retention is computed for the clay and a strong retention is computed for the till, while experimental Kd show just the opposite behaviour. Nb is another exception, because it is strongly retained according to "measured" Kd but only weakly retained according to the modelling results.

An interesting point to be discussed is that Kd values estimated from in situ measurements usually are taken as constant values for a given site and sediment type, whereas modelling results clearly show that Kd values are heterogenous in space. However, the effective Kd values are determined directly from the breakthrough curves in the discharge areas of the models, so they represent "upscaled" Kd value for the whole domain. In this sense, effective Kd computed by reactive transport simulations will constitute an appropriate way to simulate mass transfer in the simplified box models often used for performance assessment and dose calculations. However, no attempt has been made within the present work to find theoretical relations between the heterogeneous spatial distribution of Kd values and the effective Kd determined by breakthrough curves that could be used for this purpose.

8.3 Comparison with previous models

Finally, we can make a comparison between the results obtained in the present work and those obtained by /Sena et al. 2008/, who simulated the retention of U, Sr, Cs and Ra in the same till and clay domains as implemented in the present simulations. The differences in the results of the two groups of simulations, if any, should be related to the following facts: (a) the deep groundwater used is not the same in the two cases; (b) for uranium and radium, the retention by sorption onto illite was implemented for the first time in the present work; (c) for Sr, Mg and Ca, the selectivity coefficients for illite planar sites used in the present study differ from those used by /Sena et al. 2008/; and (d) the incorporation of Ni could lead to competition with U for HFO sorption sites.

Regarding the first point, as explained in Section 5.8.1, the main differences between the groundwaters are found in the Fe and natural U concentrations; the former show a a ten-fold decrease, and the latter is 24 times higher in the new deep groundwater. Other differences are related to the concentrations of Ba and C (inorganic), which show a two-fold increase, and those of ammonium and K, which show a two-fold decrease in the deep groundwater selected in the present study.

The retention of U and Ra by illite was not implemented in the simulations by /Sena et al. 2008/. For the case of Ra, the influence of the retention by illite is not significant, since the Ra concentrations at the discharge areas of both the till and clay domains are almost the same in the two groups of simulations. For the clay system a difference is observed in the retention efficiency; in the simulation of /Sena et al. 2008/ Ra behaves conservatively, while in the present modeling Ra is somewhat retarded (R=27) due to the sorption by illite.

In the numerical simulations of /Sena et al. 2008/, Ra is retained in the till system by the precipitation of radiobarite (the retention efficiency drops from 100 to 30 after 2,700 y of repository release), while in the present simulation Ra behaves almost conservatively during most of the simulation time (Figure 6-36). Therefore, the precipitation of radiobarite is not exerting the same retention of Ra in both simulations. The difference could be found in the different Ra/Ba ratios in the considered deep groundwaters, which would lead to precipitation of radiobarite with different Ra/Ba ratios.

For RDU in the till system, retention by HFO is predicted in both simulations (i.e. previous and present), and also by illite in the present simulation. The retention efficiency drops faster and to lower values in the present simulation, despite the fact that two retention processes are considered. This can be explained by the competition of RDU with Ni (and RDNi) for sorption sites on HFO. This is the main retention mechanism for RDU in the till, since it has a much higher affinity for the HFO surfaces. (Remember that Ni was not considered in the simulations by /Sena et al. 2008/, and hence did not affect U sorption).

In the case of the clay system, retention by precipitation of uraninite is predicted in both simulations, and also retention by illite in the present simulation. The retention efficiency of RDU in the clay is higher in the present simulation, due to the sorption onto illite. Nevertheless, after 2,700 y of repository release, the concentration of RDU at the discharge area is almost the same for the two groups of simulations (for each domain).

For RDCs, previous and present simulations predict very similar results. In the case of RDSr, its behaviour in the clay domain is very similar in all simulations. In the till system, the only difference is that in the simulation of /Sena et al. 2008/ there is a longer delay in the arrival of RDSr at the discharge area. Therefore, the change in the selectivity coefficient of Sr for illite planar sites does not significantly affect the results.

9 Conclusions

Conceptual description and numerical simulations of radionuclide reactive transport in Forsmark till and clay sediments show that cation exchange and surface complexation on illite are active processes for the retention of several radionuclides (U, Th, Ni, Cs, Sr, Ra). Surface complexation on iron hydroxide is an active process in the till system, able to effectively retain U and Ni. Another retention process of importance is the incorporation of the radionuclides into mineral phases, either by the precipitation of pure phases or of solid solutions. Quantitative modelling has been useful to illustrate the incorporation of C and Sr in the carbonate solid solution in both domains (till and clay), as well as the precipitation of uraninite in the clay sediments and the precipitation of native selenium and radiobarite in the till.

Other mineral phases that could, a priori, retain U, Se, Nb and Tc do not precipitate in the simulations, either due to the pH-Eh conditions and/or because the dissolved concentration of the element is not high enough under the simulation conditions. It is important to keep in mind that changes in these parameters and boundary conditions could modify the predicted behaviour of these elements.

The radionuclides that are most significantly retarded are Th, Ni and Cs, mainly through sorption onto illite. Therefore, if the amount of illite (or available sorption sites) decreases, the retardation of these elements will also decrease accordingly, as illustrated by the sensitivity analyses performed. The high degree of retardation predicted for these elements is in good agreement with reported Kd values for Forsmark till and lake sediments. According to the models, Cs, Th and Ni are highly retained, while C, U, Sr and Ra are more mobile. The simulations also show that Nb and Tc behave conservatively in both domains, as expected due to their anionic character under these conditions, and Se only in the clay domain.

The reported Kd of the Forsmark soils and sediments, although not directly comparable to the calculated effective Kds, show a similar general trend (i.e. the most strongly retained elements are Th, Cs and Ni, followed by U and Sr). Se and Nb are the two exceptions where the computed behaviour does not agree with reported Kd values. It also needs to be recalled that not all the possible retention processes considered in the conceptual model were included in the simulation, due to either the lack of reliable knowledge and/or the scarcity of thermodynamic data.

Besides the retention mechanisms, other processes that reduce radionuclide concentrations are dilution of the radionuclide-bearing deep groundwater, which applies to all elements, and decay, as we are dealing with radionuclides. The radionuclides that will be more significantly reduced by decay are ^{226}Ra and ^{90}Sr, although ^{226}Ra is a permanent product of the decay of ^{238}U. In this sense, if one considers the possibility that carbonate will be dissolved in a future evolution of the simulated domains, the release into water of the previously retained Sr will not be of significance, while for the case of ^{14}C, due to its longer half-life, it could still be present in the system and contribute to increased radioactive doses.

References

SKB's (Svensk Kärnbränslehantering AB) publications can be found at www.skb.se/publications.

Abdelouas A, Grambow B, Fattahi M, Andrès Y, Leclerc-Cessac E, 2005. Microbial reduction of ^{99}Tc in organic matter-rich soils. Science of the Total Environment, 336, pp 255–268.

Andersson E, Tudorancea M-M, Tudorancea C, Brunberg A-K, Blomqvist P, 2003. Water chemistry, biomass and production of biota in lake Eckarfjärden during 2002. SKB R-03-27, Svensk Kärnbränslehantering AB.

Ashworth D J, Shaw G, 2006a. Effects of moisture content and redox potential on in situ K_d values for radioiodine in soil. Science of the Total Environment, 359, pp 244–254.

Ashworth D J, Shaw G, 2006b. A comparison of the soil migration and plant uptake of radioactive chlorine and iodine from contaminated groundwater. Journal of Environmental Radioactivity, 89, pp 61–80.

Ashworth D J, Shaw G, Butler A P, Ciciani L, 2003. Soil transport and plant uptake of radio-iodine from near-surface groundwater. Journal of Environmental Radioactivity, 70, pp 99–114.

Avery S V, 1996. Fate of caesium in the environment: distribution between the abiotic and biotic components of aquatic and terrestrial ecosystems. Journal of Environmental Radiactivity, 30, pp 139–171.

Baeyens B, Bradbury M H, 2004. Cation exchange capacity measurements on illite using the sodium and cesium isotope dilution technique: effects of the index cation, electrolyte concentration and competition: modeling. Clays and Clay Minerals, 52, pp 421–431.

Bard A J, Parsons R, Jordan J (eds), 1985. Standard potentials in aqueous solution. Oxford, U.K.: International Union of Pure and Applied Chemistry.

Bastviken D, Thomsen F, Svensson T, Karlsson S, Sandén P, Shaw G, Matucha M, Oberg G, 2007. Chloride retention in forest soil by microbial uptake and by natural chlorination of organic matter. Geochimica et Cosmochimica Acta, 71, pp 3182–3192.

Belzile N, Chen Y-W, Xu R, 2000. Early diagenetic behaviour of selenium in freshwater sediments. Applied Geochemistry, 15, pp 1439–1454.

Bertine K K, 1972. The deposition of molybdenum in anoxic waters. Marine Chemistry, 1, pp 43–53.

Bibak A, Borggaard O K, 1994. Molybdenum adsorption by aluminum and iron oxides and humic acid. Soil Science, 158, pp 323–328.

Bigeleisen J, 1952. The effects of isotopic substitution on the rates of chemical reactions. Journal of Physical Chemistry, 56, pp 823–828.

Bigeleisen J, Mayer M G, 1947. Calculation of equilibrium constants for isotopic exchange reactions. Journal of Chemical Physics, 15, pp 261–267.

Bird G A, Shwartz W, 1996. Distribution coefficients, K_ds, for iodide in Canadian Shield Lake Sediments under oxic and anoxic conditions. Journal of Environmental Radiactivity, 35, pp 261–279.

Blount C W, 1977. Barite solubilities and thermodynamic quantities up to 300ºC and 1,400 bars. American Mineralogist, 62, pp 942–957.

Bosson E, Gustafsson L-G, Sassner M, 2008. Numerical modelling of surface hydrology and near-surface hydrogeology at Forsmark. Site descriptive modelling, SDM-Site Forsmark. SKB R-08-09, Svensk Kärnbränslehantering AB.

Bradbury M H, Baeyens B, 2000. A generalised sorption model for the concentration dependent uptake of caesium by argillaceous rocks. Journal of Contaminant Hydrology, 42, pp 141–163.

Bradbury M H, Baeyens B, 2009a. Sorption modelling on illite Part I: Titration measurements and the sorption of Ni, Co, Eu and Sn. Geochimica et Cosmochimica Acta, 73, pp 990–1003.

Bradbury M H, Baeyens B, 2009b. Sorption modelling on illite. Part II: Actinide sorption and linear free energy relationships. Geochimica et Cosmochimica Acta, 73, pp 1004–1013.

Breynaert E, Bruggeman C, Maes A, 2008. XANES-EXAFS analysis of Se solid phases reaction products formed upon contacting Se(IV) with FeS_2 and FeS. Environmental Science &Technology, 42, pp 3595–3601.

Brouwer E, Baeyens B, Maes A, Cremers A, 1983. Cesium and rubidium ion equilibria in illite clay. Journal of Physical Chemistry, 87, pp 1213–1219.

Bruggeman C, 2008. Redox processes in geological formations: lessons learned for understanding and predicting the transport behaviour of redox-sensitive radionuclides. In: 4th Annual Workshop Proceedings of the Integrated Project "Fundamental Processes of Radionuclide Migration" (6th EC FP IP FUNMIG). Karlsruhe, Germany, 24–27 November 2008. Karlsruhe: Forschungszentrum Karlsruhe.

Bruggeman C, Maes A, Vancluysen J, Vandemussele P, 2005. Selenite reduction in Boom clay: effect of FeS_2, clay minerals and dissolved organic matter. Environmental Pollution, 137, pp 209–221.

Bruno J, Stumm W, Wersin P, Brandberg F, 1992. On the influence of carbonate in mineral dissolution: Part 1. The thermodynamics and kinetics of hematite dissolution in bicarbonate solutions at T=25ºC. Geochimica et Cosmochimica Acta, 56, pp 1139–1148.

Bruno J, Duro L, de Pablo J, Casas I, Ayora C, Delgado J, Gimeno M J, Peña J, Linklater C, Pérez del Villar L, Gómez P, 1998. Estimation of the concentrations of trace metals in natural systems. The application of codissolution and coprecipitation approaches to El Berrocal (Spain) and Poços de Caldas (Brazil). Chemical Geology, 151, pp 277–291.

Bruno J, Duro L, Grivé M, 2002. The applicability and limitation of thermodynamic geochemical models to simulate trace element behaviour in natural waters. Lessons learned from natural analogue studies. Chemical Geology, 190, pp 371–393.

Burke I, Boothman C, Lloyd J R, Mortimer R J G, Livens F R, Morris C, 2005. Effects of progressive anoxia on the solubility of technetium in sediments. Environmental Science & Technology, 39, pp 4109–4116.

Calvert S E, Pedersen T F, 1993. Geochemistry of recent oxic and anoxic marine sediments: implications for the geological record. Marine Geology, 113, pp 67–88.

Casas I, Bruno J, Cera E, Finch R J, Ewing R C, 1994. Kinetic and thermodynamic studies of uranium minerals. Assessment of the long-term evolution of spent nuclear fuel. SKB TR 94-16, Svensk Kärnbränslehantering AB.

Chabroullet C, Coppin F, Martin-Garin A, Floriani M, Tinseau E, Gaudet J-P, 2006. Se-soil organic matter interactions: direct or indirect association? Geochimica et Cosmochimica Acta, 70, p A93.

Charles D, Prime D, 1983. Desorption behaviour of artificial radionuclides sorbed on to estuarine silt: (I) caesium-137 and ruthenium-106, (II) zirconium-95 and niobium-95. Environmental Pollution Series B, Chemical and Physical, 5, pp 273–295.

Charlet L, Scheinost A C, Tournassat C, Greneche J M, Géhin A, Fernández-Martínez A, Coudert S, Tisserand D, Brendle J, 2007. Electron transfer at the mineral/water interface: Selenium reduction by ferrous iron sorbed on clay. Geochimica et Cosmochimica Acta, 71, pp 5731–5749.

Chen C, Wang X, 2007. Sorption of Th (IV) to silica as a function of pH, humic/fulvic acid, ionic strength, electrolyte type. Applied Radiation and Isotopes, 65, pp 155–163.

Chen C-C, Hayes K F, 1999. X-ray absorption spectroscopy investigation of aqueous Co(II) and Sr(II) sorption at clay–water interfaces. Geochimica et Cosmochimica Acta, 63, pp 3205–3215.

Choppin G R, Shanbhag P M, 1981. Binding of calcium with humic acid. Journal of Inorganic and Nuclear Chemistry, 43, pp 921–922.

Comans R N J, Middelburg J J, Zonderhuis J, Woittiez J R W, de Lange G J, Das H A, van der Weijden C H, 1989. Mobilization of radiocesium in pore waters of lake sediments. Nature, 339, pp 367–369.

Councell T B, Landa E R, Lovley D R, 1997. Microbial reduction of iodate. Water, Air, & Soil Pollution, 100, pp 99–106.

Cross J E, Ewart F T, 1991. Hatches – a thermodynamic database and management system. Radiochimica Acta, 52/53, pp 421–422.

Cruywagen J J, Heyns J B B, Rohwer E F C H, 1976. Spectrophotometric investigation of the protonation of monomeric molybdic acid in sodium perchlorate medium. Journal of Inorganic and Nuclear Chemistry, 38, pp 2033–2036.

Cui D, Eriksen T E, 1996a. Reduction of pertechnetate by ferrous iron in solution: influence of sorbed and precipitated Fe(II). Environmental Science & Technology, 30, pp 2259–2262.

Cui D, Eriksen T E, 1996b. Reduction of pertechnetate in solution by heterogeneous electron transfer from Fe(II)-containing geological material. Environmental Science & Technology, 30, pp 2263–2269.

Curie P, Curie Mme P, Bémont G, 1898. On a new, strongly radioactive substance, contained in pitchblende. Comptes Rendus, 127, pp 1215–1217.

Dellwig O, Beck M, Lemke A, Lunau M, Kolditz K, Schnetger B, Brumsack H-J, 2007. Non-conservative behaviour of molybdenum in coastal waters: coupling geochemical, biological, and sedimentological processes. Geochimica et Cosmochimica Acta, 71, pp 2745–2761.

Doerner H, Hoskins W M, 1925. Co-precipitation of barium and radium sulphates. Journal of the American Chemical Society, 47, pp 662–675.

Doig L E, Liber K, 2007. Nickel speciation in the presence of different sources and fractions of dissolved organic matter. Ecotoxicology and Environmental Safety, 66, pp 169–177.

Duc M, Lefèvre G, Fédoroff M, Jeanjean J, Rouchaud J C, Monteil-Rivera F, Dumonceau J, Milonjic S, 2003. Sorption of selenium anionic species on apatites and iron oxides from aqueous solutions. Journal of Environmental Radioactivity, 70, pp 61–72.

Duc M, Lefèvre G, Fédoroff M, 2006. Sorption of selenite ions on hematite. Journal of Colloid and Interface Science, 298, pp 556–563.

Duff M C, Urbanik Coughlin J, Hunter D B, 2002. Uranium co-precipitation with iron oxide minerals. Geochimica et Cosmochimica Acta, 66, pp 3533–3547.

Dumat C, Staunton S, 1999. Reduced adsorption of caesium on clay minerals caused by various humic substances. Journal of Environmental Radioactivity, 46, pp 187–200.

Duro L, Grivé M, Cera E, Domènech C, Bruno J, 2006a. Update of a thermodynamic database for radionuclides to assist solubility limits calculation for performance assessment. SKB TR-06-17, Svensk Kärnbränslehantering AB.

Duro L, Grivé M, Cera E, Gaona X, Domènech C, Bruno J, 2006b. Determination and assessment of the concentration limits to be used in SR-can. SKB TR-06-32, Svensk Kärnbränslehantering AB.

Dzombak D A, Morel F M M, 1990. Surface complexation modeling: hydrous ferric oxide. New York: Wiley.

Ekström L P, Firestone R B, 1999. WWW table of radioactive isotopes. Version 2.1, February 1999. [Online]. Available at: http://ie.lbl.gov/toi/.

Engdahl A, Rådén R, Borgiel M, Omberg L-G, 2008. Oskarshamn and Forsmark site investigation. Chemical composition of suspended material, sediment and pore water in lakes and sea bays. SKB P-08-81, Svensk Kärnbränslehantering AB.

Erickson B E, Helz G R, 2000. Molybdenum(VI) speciation in sulfidic waters: stability and lability of thiomolybdates. Geochimica et Cosmochimica Acta, 64, pp 1149–1158.

Falk W E, Read D, Thomas J B, 1996. Chemval2: thermodynamic database. EUR 16897, European Commission.

Farrell J, Bostick W D, Jarabek R J, Fiedor J N, 1999. Electrosorption and reduction of pertechnetate by anodically polarized magnetite. Environmental Science & Technology, 33, pp 1244–1249.

Finch R J, 1994. Paragenesis and crystal chemistry of the uranyl oxide hydrates. Ph. D. thesis. University of New Mexico.

Finch R J, Murakami T, 1999. Systematics and paragenesis of uranium minerals. In: Burns P, Finch R (eds). Uranium: mineralogy, geochemistry and the environment. Washington: Mineralogical Society of America. (Reviews in Mineralogy 38), pp 91–180.

Fuhrmann M, Bajt S, Schoonen M A A, 1998. Sorption of iodine on minerals investigated by X-ray absorption near edge structure (XANES) and ^{125}I tracer sorption experiments. Applied Geochemistry, 13, pp 127–141.

Fukui M, Fujikawa Y, Satta N, 1996. Factors affecting interaction of radioiodide and iodate species with soil. Journal of Environmental Radioactivity, 31, pp 199–216.

Fuller C C, Bargar J R, Davis J A, Piana M J, 2002. Mechanisms of uranium interactions with hydroxyapatite: implications for groundwater remediation. Environmental Science & Technology, 36, pp 158–165.

Gamsjäger H, Bugajski J, Gajda T, Lemire R J, Preis W, 2005. Chemical thermodynamics. Vol 6. Thermodynamics of nickel. Amsterdam: Elsevier.

Garbisu C, Ishii T, LeightonT, Buchanan B B, 1996. Bacterial reduction of selenite to elemental selenium. Chemical Geology, 132, pp 199–204.

Geraedts K, Maes A, 2008. Determination of the conditional interaction constant between colloidal technetium(IV) and Gorleben humic substances. Applied Geochemistry, 23, pp 1127–1139.

Goldberg S, Su C, Forster H S, 1998. Sorption of molybdenum on oxides, clay minerals and soils. In: Jenne E A (ed). Adsorption of metals by geomedia. San Diego: Academic Press, ch 19.

Goldhaber M B, Hemingway B S, Mohagheghi A, Reynolds R L, Northrop H R, 1987. Origin of coffinite in sedimentary rocks by a sequential adsorption-reduction mechanism. Bulletin de Minéralogie, 110, pp 131–144.

Goldschmidt B, 1938. Sur la précipitation mixte des sulfates de baryum et strontium. Comptes Rendus Hebdomadaires des Séances de l'Académie des Sciences, 206, p 1110.

Grandia F, Sena C, Arcos D, Molinero J, Duro L, Bruno J, 2007. Quantitative assessment of radionuclide retention in the near-surface system at Forsmark. Development of a reactive transport model using Forsmark 1.2 data. SKB R-07-64, Svensk Kärnbränslehantering AB.

Grandia F, Merino J, Bruno J, 2008. Assessment of the radium-barium co-precipitation and its potential influence on the solubility of Ra in the near-field. SKB TR-08-07, Svensk Kärnbränslehantering AB.

Green-Pedersen H, Pind N, 2000. Preparation, characterization, and sorption properties for Ni(II) of iron oxyhydroxide–montmorillonite. Colloids and Surfaces A: Physicochemical and Engineering Aspects, 168, pp 133–145.

Grenthe I, Fuger J, Konings R J M, Lemire R J, Muller A B, Nguyen-Trung C, Wanner H, 1992. Chemical thermodynamics. Vol 1. Chemical thermodynamics of uranium. Amsterdam: North-Holland.

Grivé M, 2005. The linkage between uranium, iron and carbon cycling. Processes at interfaces: evidences from combined solution chemical and spectroscopic studies. Ph. D. thesis. Universitat Politècnica de Catalunya.

Gu B, Chen J, 2003. Enhanced microbial reduction of Cr(VI) and U(VI) by different natural organic matter fractions. Geochimica et Cosmochimica Acta, 67, pp 3575–3582.

Guillaumont R, Fanghänel J, Neck V, Fuger J, Palmer D A, Grenthe I, Rand M H, 2003. Chemical thermodynamics. Vol 5. Update on the chemical thermodynamics of uranium, neptunium, plutonium, americium and technetium. Amsterdam: Elsevier.

He M, Jiang S, Jiang S, Diao L, Wu S, Li C, 2002. Measurement of the half-life of ^{79}Se with PX-AMS. Nuclear instruments and methods in Physics Research, Section B: Beam Interactions with Materials and Atoms, 194, pp 393–398.

Hedenström A, 2004. Forsmark site investigation. Investigation of marine and lacustrine sediment in lakes. Stratigraphical and analytical data. SKB P-04-86, Svensk Kärnbränslehantering AB.

Hedenström A, Sohlenius G, 2008. Description of the regolith at Forsmark. Site descriptive modelling, SDM-Site Forsmark. SKB R-08-04, Svensk Kärnbränslehantering AB.

Helz G R, Miller C V, Charnock J M, Mosselmans J F W, Pattrick R A D, Garner C D, Vaughan D J, 1996. Mechanism of molybdenum removal from the sea and its concentration in black shales: EXAFS evidence. Geochimica et Cosmochimica Acta, 60, pp 3631–3642.

Henrot J, 1989. Bioaccumulation and chemical modification of Tc by soil bacteria. Health Physics, 57, pp 239–245.

Hird A B, Rimmer D L, Livens F R, 1995. Total caesium-fixing potentials of acid organic soils. Journal of Environmental Radioactivity, 26, pp 103–118.

Hou X L, Fogh C L, Kucera J, Andersson K G, Dahlgaar H, Nielsen S P, 2003. Iodine-129 and Caesium-137 in Chernobyl contaminated soil and their chemical fractionation. The Science of the Total Environment, 308, pp 97–109.

Howard J H, 1977. Geochemistry of selenium: formation of ferroselite and selenium behaviour in the vicinity of oxidising sulphide and uranium deposits. Geochimica et Cosmochimica Acta, 41, pp 1665–1678.

Hsi C-K D, Langmuir D, 1985. Adsorption of uranyl onto ferric oxyhydroxides: applications of the surface complexation site-binding model. Geochimica et Cosmochimica Acta, 49, pp 1931–1941.

Hu Q, Zhao P, Moran J E, Seaman J C, 2005. Sorption and transport of iodine species in sediments from the Savannah River and Hanford Sites. Journal of Contaminant Hydrology, 78, pp 185– 205.

Hummel W, Berner U, Curti E, Pearson F J, Thoenen T, 2002. Nagra/PSI chemical thermodynamic data base 01/01. Boca Raton: Universal Publishers.

Johansson P-O, 2008. Description of surface hydrology and near-surface hydrogeology at Forsmark. Site descriptive modelling, SDM-Site Forsmark. SKB R-08-08, Svensk Kärnbränslehantering AB.

Johansson P-O, Öhman J, 2008. Presentation of meteorological, hydrological and hydrogeological monitoring data from Forsmark. Site descriptive modelling, SDM-Site Forsmark. SKB R-08-10, Svensk Kärnbränslehantering AB.

Johansson P-O, Werner K, Bosson E, Berglund S, Juston J, 2005. Description of climate, surface hydrology, and near-surface hydrogeology. Preliminary site description. Forsmark area – version 1.2. SKB R-05-06, Svensk Kärnbränslehantering AB.

Johnson J W, Oelkers E H, Helgeson H C, 1992. SUPCRT92: a software package for calculating the standard molal thermodynamic properties of minerals, gases, aqueous species, and reactions from 1 to 5,000 bar and 0 to 1,000ºC. Computers & Geosciences, 18, pp 899–947.

Johnson J, Anderson G, Parkhurst D, 2000. Database from "thermo.com.V8.R6.230" prepared by at Lawrence Livermore National Laboratory (revision 1.11). LLNL report.

Kaback D S, Runnells D D, 1980. Geochemistry of molybdenum in some stream sediments and waters. Geochimica et Cosmochimica Acta, 44, pp 453–456.

Kaplan D I, 2003. Influence of surface charge of an Fe-oxide and an organic matter dominated soil on iodide and pertechnetate sorption. Radiochimica Acta, 91, pp 173–178.

Kaplan D I, Serne R J, Parker K E, Kutnyakov I V, 2000. Iodide sorption to subsurface sediments and illitic minerals. Environmental Science & Technology, 34, pp 399–405.

Killey R W D, Rao R R, Eyvindson S, 1998. Radiocarbon speciation and distribution in an aquifer plume and groundwater discharge area, Chalk River, Ontario. Applied Geochemistry, 13, pp 3–16.

Kipp K L, 1997. Guide to the revised heat and solute transport simulator HST3D – Version 2. Denver, Co: U.S. Geological Survey. (Water-resources investigations report 97–4157).

Knett J, 1904. Indirekter Nachweis von Radium in den Karlsbader Thermen. Sitzungsberichte der Akademie der Wissenschaften in Wien, 113, Abt. II a, pp 753–762.

Kodama S, Takahashi Y, Okumura K, Uruga T, 2006. Speciation of iodine in solid environmental samples by iodine K-edge XANES: application to soils and ferromanganese oxides. Science of the Total Environment, 363, pp 275–284.

Krestou A, Xenidis A, Panias D, 2004. Mechanism of aqueous uranium(VI) uptake by hydroxyapatite. Minerals Engineering, 17, pp 373–381.

Köhler S J, Dufaud F, Oelkers E H, 2003. An experimental study of illite dissolution kinetics as a function of pH from 1.4 to 12.4 and temperature from 5 to 50ºC. Geochimica et Cosmochimica Acta, 67, pp 3583–3594.

Laaksoharju M, Smellie J, Tullborg E-L, Gimeno M, Hallbeck L, Molinero J, Waber N, 2008. Bedrock hydrogeochemistry Forsmark. Site descriptive modelling, SDM-Site Forsmark. SKB R-08-47, Svensk Kärnbränslehantering AB.

Lakshtanov L Z, Stipp S L S, 2007. Experimental study of nickel(II) interaction with calcite: adsorption and coprecipitation. Geochimica et Cosmochimica Acta, 71, pp 3686–3697.

Lamble G M, Lee J F, Staudt W J, Reeder R J, 1995. Structural studies of selenate incorporation into calcite crystals. Physica B: Condensed Matter, 208-209, pp 589–590.

Langmuir D, 1997. Aqueous environmental geochemistry. Upper Saddle River, N.J.: Prentice-Hall.

Langmuir D, Herman J S, 1980. The mobility of thorium in natural waters at low temperatures. Geochimica et Cosmochimica Acta, 44, pp 1753–1766.

Lee R T, Shaw G, Wadey P, Wang X, 2001. Specific association of ^{36}Cl with low molecular weight humic substances in soils. Chemosphere, 43, pp 1063–1070.

Lenhart J J, Cabaniss S E, MacCarthy P, Honeyman B D, 2000. Uranium (VI) complexation with citric, humic and fulvic acids. Radiochimica Acta, 88, pp 345–353.

Li W C, Victor D M, Chakrabarti C L, 1980. Effect of pH and uranium concentration on interaction of uranium(VI) and uranium (IV) with organic ligands in aqueous solutions. Analytical Chemistry, 52, pp 520–523.

Lindborg T (ed), 2005. Description of surface systems. Preliminary site description Forsmark area – version 1.2. SKB R-05-03, Svensk Kärnbränslehantering AB.

Lindborg T (ed), 2008. Surface system Forsmark. Site descriptive modelling, SDM-Site Forsmark. SKB R-08-11, Svensk Kärnbränslehantering AB.

Lloyd J R, Ridley J, Khizniak T, Lyalikova N N, Macaskie L E, 1999. Reduction of technetium by Desulfovibrio desulfuricans: biocatalyst characterization and use in a flowthrough bioreactor. Applied and Environmental Microbiology, 65, pp 2691–2696.

Lloyd J R, Sole V A, van Praagh C V G, Lovley D R, 2000. Direct and Fe(II)-mediated reduction of technetium by Fe(III)-reducing bacteria. Applied and Environmental Microbiology, 66, pp 3743–3749.

Lloyd J R, Mabbet A N, Williams D R, Macaskie L E, 2001. Metal reduction by sulphate-reducing bacteria: physiological diversity and metal specificity. Hydrometallurgy, 59, pp 327–337.

Loft S, Tipping E W, Sanchez A L, Dodd B A, 2002. Modelling the role of humic acid in radiocaesium distribution in a British upland peat soil. Journal of Environmental Radioactivity, 61, pp 133–147.

Lorens R B, 1981. Sr, Cd, Mn and Co distribution coefficients in calcite as a function of calcite precipitation rate. Geochimica et Cosmochimica Acta, 45, pp 553–561.

Losi M E, Frankenberger Jr W T, 1998. Reduction of selenium oxyanions by Enterobacter cloacae strain SLDa-1. In: Frankenberger Jr W T, Engberg R A (eds). Environmental chemistry of selenium. New York: Marcel Dekker, pp 515–544.

Lu N P, Mason C F V, 2001. Sorption-desorption behavior of strontium-85 onto montmorillonite and silica colloids. Applied Geochemistry 16, pp 1653–1662.

MacNeal J M, Balistrieri L S, 1989. Geochemistry and occurrence of selenium: an overview. In: Selenium in agriculture and the environment: proceedings of a symposium of the American Society of Agronomy and Soil Science Society of America in New Orleans, 2 December 1986. Madison, Wis.: American Society of Agronomy. (Soil Science Society of America special publication 23), pp 1–13.

Martens D A, Suarez D L, 1999. Transformation of volatile methylated selenium in soil. Soil Biology and Biochemistry, 31, pp 1355–1361.

Masscheleyn P H, Delaune R D, Patrick W H, 1991. Biogeochemical behaviour of selenium in anoxic soils and sediments: an equilibrium thermodynamics approach. Journal of Environmental Science and Health, part A, 26, pp 555–573.

Murakami T, Ohnuki T, Isobe H, Sato T, 1997. Mobility of uranium during weathering. American Mineralogist, 82, pp 888–889.

Muramatsu Y, Uchida S, Sriyotha P, Sriyotha K, 1990. Some considerations on the sorption and desorption phenomena of iodide and iodate on soil. Water, Air, and Soil Pollution, 49, pp 125–138.

Nash K L, Choppin G R, 1980. Interaction of humic and fulvic acids with Th(IV). Journal of Inorganic and Nuclear Chemistry, 42, pp 1045–1050.

Naumov G B, Ryzhenko B N, Khodakovsky I L, 1974. Handbook of thermodynamic data. Translated from Russian. Menlo Park, Cal.: U.S. Geological Survey.

Oberg G, 1998. Chloride and organic chlorine in soil. Acta Hydrochimica et Hydrobiologica, 26, pp 137–144.

Ogard A E, Thompson J L, Rundberg R S, Wolfsberg K, Kubik P W, Elmore D, Bentley H W, 1988. Migration of chlorine-36 and tritium from an underground nuclear test. Radiochimica Acta, 44-45, pp 213–217.

Ohnuki T, Yoshida T, Ozaki T, Samadfam M, Kozai N, Yubuta K, Mitsugashira T, Kasama T, Francis A J, 2005. Interactions of uranium with bacteria and kaolinite clay. Chemical Geology, 220, pp 237–243.

Olin A, Noläng B, Osadchii E G, Öhman L O, Rosén E, 2005. Chemical thermodynamics. Vol 7. Chemical thermodynamics of selenium. Amsterdam: Elsevier.

Oremland R S, Hollibaugh J T, Maest A S, Pressor T S, Miller L G, Culbertson C W, 1989. Selenate reduction to elemental selenium by anaerobic bacteria in sediments and culture: biogeochemical significance of a novel, sulfate-independent respiration. Applied and Environmental Microbiology, 55, pp 2333–2343.

Outridge P M, Stern G A, Hamilton P B, Percival J B, McNeely R, Lockhart W L, 2005. Trace metal profiles in the varved sediment of an Arctic lake. Geochimica et Cosmochimica Acta, 69, pp 4881–4894.

Pabalan R T, Turner D R, Bertetti F P, Prikryl J D, 1998. Uranium(VI) sorption onto selected mineral surfaces: key geochemical parameters. In: Jenne E A (ed). Adsorption of metals by geomedia: variables, mechanisms, and model applications. San Diego: Academic Press, pp 99–130.

Parkhurst D L, Appelo C A J, 1999. User's guide to PHREEQC (version 2): a computer program for speciation, batch-reaction, one-dimensional transport and inverse geochemical calculations. Denver, Co: U.S. Geological Survey. (Water- resources investigations report 99-4259).

Parkhurst D L, Kipp K L, Engesgaard P, Charlton S R, 2004. PHAST – A program for simulating ground-water flow, solute transport, and multicomponent geochemical reactions. Techniques and Methods 6–A8. Denver, Co: U.S. Geological Survey.

Payne T E, Davis J A, Waite T D, 1996. Uranium adsorption on ferrihydrite – effects of phosphate and humic acid. Radiochimica Acta, 74, pp 239–243.

Peak D, 2006. Adsorption mechanisms of selenium oxyanions at the aluminum oxide/water interface. Journal of Colloid and Interface Science, 303, pp 337–345.

Peiffert C, Nguyen-Trung C, Landais P, 1997. Etude experimentale de la solubilité des oxydes de Nb(V) crystallisé et amorphe dans des solutions aqueuses. Rapport C RP 0CRE 97-003, Agence nationale pour la gestion des déchets radioactifs (ANDRA).

Pepper S E, Bunker D J, Bryan N D, Livens F R, Charnock J M, Pattrick R A D, Collison D, 2003. Treatment of radioactive wastes: An X-ray absorption spectroscopy study of the reaction of technetium with green rust. Journal of Colloid and Interface Science, 268, pp 408–412.

Percival J B, Hunt P, Wygergangs M, 2001. Mineralogical investigations of Canadian till and lake- and stream-sediment reference materials: Part 1. Standardized X-ray diffraction and scanning electron microscope methods. Geological Survey of Canada, Current Research, 2001-E9.

Pérez del Villar L, Bruno J, Campos R, Gómez P, Cózar J S, Garralón A, Buil B, Arcos D, Carretero G, Ruiz Sánchez-Porro J, Hernán P, 2002. The uranium ore from Mina Fe (Salamanca, Spain) as a natural analogue of processes in a spent fuel repository. Chemical Geology, 190, pp 395–415.

Poinssot C, Baeyens B, Bradbury M H, 1999. Experimental and modelling studies of caesium sorption on illite. Geochimica et Cosmochimica Acta, 63, pp 3217–3227.

Puigdomènech I, 2009. MEDUSA: Make equilibrium diagrams using sophisticated algorithms. Software based on: Puigdomenech I, 1983. INPUT, SED and PREDOM: computer programs drawing equilibrium diagrams. Technical report TRITA-OOK-3010, Royal Institute of Technology (KTH), Stockholm.

Radlinger G, Heuman K G, 2000. Transformation of iodide in natural and wastewater systems by fixation on humic substances. Environmental Science & Technology, 34, pp 3932–3936.

Rand M, Fuger J, Grenthe I, Neck V, Rai D, 2009. Chemical thermodynamics. Vol 11. Chemical thermodynamics of thorium. Paris: Nuclear Energy Agency, Organisation for Co-operation and Development.

Rard J A, Rand M H, Anderegg G, Wanner H, 1999. Chemical thermodynamics. Vol 3. Chemical thermodynamics of technetium. Amsterdam: Elsevier.

Reiller P, 2005. Pronosticating the humic complexation for redox sensitive actinides through analogy, using the charge neutralisation model. Radiochimica Acta, 93, pp 43–55.

Reiller P, Moulin V, Casanova F, Dautel C, 2002. Retention behaviour of humic substances onto mineral surfaces and consequences upon thorium (IV) mobility: case of iron oxides. Applied Geochemistry, 17, pp 1551–1562.

Reiller P, Moulin V, Casanova F, Dautel C, 2003. On the study of Th(IV)-humic acid interactions by competition sorption studies with silica and determination of global interaction constants. Radiochimica Acta, 91, pp 513–524.

Reiller P, Casanova F, Moulin V, 2005. Influence of addition order and contact time on thorium(iv) retention by hematite in the presence of humic acids. Enviromental Science and Technology, 39, pp 1641–1648.

Robie R A, Hemingway B S, 1995. Thermodynamic properties of minerals and related substances at 298.15 K and 1 bar (10^5 Pascals) pressure and at higher temperatures. U.S. Geological Survey Bulletin, 2131.

Robie R A, Hemingway B S, Fisher J R, 1979. Thermodynamic properties of minerals and related substances at 298.15 K and 1 bar (10^5 Pascals) pressure and at higher temperatures. U.S. Geological Survey Bulletin, 1452.

Robit-Pointeau V, Poinssot C, Vitorge P, Grambow B, Cui D, Spahiu K, Catalette H, 2006. Assessment of the relevance of coffinite formation within the near-field environment of spent nuclear fuel geological disposals. Materials Research Society Symposium Proceedings, 932, pp 489–496.

Roden E E, Leonardo M R, Ferris F G, 2002. Immobilization of strontium during iron biomineralization coupled to dissimilatory hydrous ferric oxide reduction. Geochimica et Cosmochimica Acta, 66, pp 2823–2839.

Rovira M, Giménez J, Martínez M, Martínez-Lladó X, de Pablo J, Martí V, Duro L, 2008. Sorption of selenium(IV) and selenium(VI) onto natural iron oxides: Goethite and hematite. Journal of Hazardous Materials, 150, pp 279–284.

Sandino A, Bruno J, 1992. The solubility of $(UO_2)_3(PO_4)_2{\cdot}4H_2O(s)$ and the formation of U(VI) phosphate complexes: their influence in uranium speciation in natural waters. Geochimica et Cosmochimica Acta, 56, pp 4135–4145.

Santschi P H, Schwehr K A, 2004. $^{129}I/^{127}I$ as a new environmental tracer or geochronometer for biogeochemical or hydrodynamic processes in the hydrosphere and geosphere: the central role of organo-iodine. Science of the Total Environment, 321, pp 257–271.

Sawhney B L, 1972. Selective sorption and fixation of cations by clay minerals: a review. Clays and Clay Minerals, 20, pp 93–100.

Scheidegger A M, Lamble G M, Sparks D L, 1997. Spectroscopic evidence for the formation of mixed-cation hydroxide phases upon metal sorption on clays and aluminium oxides. Journal of Colloid and Interface Science, 186, pp 118–128.

Scheinost A C, Kirsch R, Banerjee D, Fernandez-Martinez A, Zaenker H, Funke H, Charlet L, 2008. X-ray absorption and photoelectron spectroscopy investigation of selenite reduction by Fe^{II}-bearing minerals. Journal of Contaminant Hydrology, 102, pp 228–245.

Schmidtz K, Aumann D C, 1995. A study on the association of two iodine isotopes, of natural ^{127}I and of the fission product ^{129}I, with soil components using a sequential extraction procedure. Journal of Radioanalytical and Nuclear Chemistry, 198, pp 229–236.

Seaman J C, Meehan T, Bertsch P M, 2001. Immobilization of Cesium-137 and uranium in contaminated sediments using soil amendments. Journal of Environmental Quality, 30, pp 1206–1213.

Sena C, 2009. Numerical modelling of radionuclide migration in near-surface systems. Ph. D. thesis. Department of Geosciences, University of Aveiro, Portugal.

Sena C, Grandia F, Arcos D, Molinero J, Duro L, 2008. Complementary modelling of radionuclide retention in the near-surface system at Forsmark. Development of a reactive transport model using Forsmark 1.2 data. SKB R-08-107, Svensk Kärnbränslehantering AB.

Shahwan T, Erten H N, 2004. Temperature effects in barium sorption on natural kaolinite and chlorite-illite clays. Journal of Radioanalytical and Nuclear Chemistry, 260, pp 43–48.

Shanbhag P M, Choppin G R, 1981. Binding of uranyl by humic acid. Journal of Inorganic and Nuclear Chemistry, 43, pp 3369–3372.

Shaw G, Bell J N B, 1991. Competitive effects of potassium and ammonium on caesium uptake kinetics in wheat. Journal of Environmental Radioactivity, 13, pp 283–296.

Shenber M A, Eriksson A, 1993. Sorption behaviour of caesium in various soils. Journal of Environmental Radioactivity, 19, pp 41–51.

Sheppard S C, 2003. Interpolation of solid/liquid partition coefficients, K_d, for iodine in soils. Journal of Environmental Radioactivity, 70, pp 21–27.

Sheppard S C, Sheppard M I, Evenden W G, 1990. A novel nethod used to examine variation in Tc sorption among 34 soils, aerated and anoxic. Journal of Environmental Radioactivity, 11, pp 215–233.

Sheppard S, Long J, Sanipelli B, Sohlenius G, 2009. Solid/liquid partition coefficients (Kd) for selected soils and sediments at Forsmark and Laxemar-Simpevarp. SKB R-09-27, Svensk Kärnbränslehantering AB.

Siddique T, Zhang Y, Okeke B C, Frankenberger W T, 2006. Characterization of sediment bacteria involved in selenium reduction. Bioresource Technology, 97, pp 1041–1049.

SKB, 2006. Long-term safety for KBS-3 repositories at Forsmark and Laxemar – a first evaluation. Main Report of the SR-Can project. SKB TR-06-09, Svensk Kärnbränslehantering AB.

Sohlenius G, Rudmark L, 2003. Forsmark site investigation. Mapping of unconsolidated Quaternary deposits. Stratigraphical and analytical data. SKB P-03-14, Svensk Kärnbränslehantering AB.

Sohlenius G, Bergman T, Snäll S, Lundin L, Lode E, Stendahl J, Riise A, Nilsson J, Johansson T, Göransson M, 2006. Oskarshamn site investigation. Soils, Quaternary deposits and bedrock in topographic lineaments situated in the Laxemar subarea. SKB P-06-121, Svensk Kärnbränslehantering AB.

Staunton S, Dumat C, Zsolnay A, 2002. Possible role of organic matter in radiocaesium adsorption in soils. Journal of Environmental Radioactivity, 58, pp 163–173.

Stumm W, Morgan J J, 1996. Aquatic chemistry: chemical equilibria and rates in natural waters. 3rd ed. New York: Wiley.

Szilagyi M, 1967. Sorption of molybdenum by humus preparations. Geochemistry lnternational, 4, pp 1165–1167.

Tagami K, Uchida S, 1999. Chemical transformation of technetium in soil during the change of soil water conditions. Chemosphere, 38, pp 963–971.

Templeton A S, Trainor T P, Spormann A M, Brown G E, 2003. Selenium speciation and partitioning within Burkholderia cepacia biofilms formed on α-Al_2O_3 surfaces. Geochimica et Cosmochimica Acta, 67, pp 3547–3557.

Tesoriero A J, Pankow J F, 1996. Solid solution partitioning of Sr^{2+}, Ba^{2+}, and Ca^{2+} to calcite. Geochimica et Cosmochimica Acta, 60, pp 1053–1064.

Thibault D H, Sheppard M I, Smith P A, 1990. A critical compilation and review of default soil solid/liquid partition coefficients, Kd, for use in environmental assessments. AECL – 10125, Atomic Energy of Canada Limited.

Thorstenson D C, Parkhurst D L, 2002. Calculation of individual isotope equilibrium constants for implementation in geochemical models. Denver, Co: U.S. Geological Survey. (Water-resources investigations report 02-4172).

Ticknor K V, 1994. Sorption of nickel on geological materials. Radiochimica Acta, 66–67, pp 341–348.

Tribovillard N, Riboulleau A, Lyons T, Baudin F, 2004. Enhanced trapping of molybdenum by sulfurized marine organic matter of marine origin in Mesozoic limestones and shales. Chemical Geology, 213, pp 385– 401.

Trivedi P, Axe L, 1999. A comparison of strontium sorption to hydrous aluminum, iron, and manganese oxides. Journal of Colloid and Interface Science, 218, pp 554–563.

Tröjbom M, Söderbäck B, 2006. Chemical characteristics of surface systems in the Forsmark area. Visualisation and statistical evaluation of data from shallow groundwater, precipitation, and regolith. SKB R-06-19, Svensk Kärnbränslehantering AB.

Tröjbom M, Söderbäck B, Johansson P-O, 2007. Hydrochemistry in surface water and shallow groundwater. Site descriptive modelling, SDM-Site Forsmark. SKB R-07-55, Svensk Kärnbränslehantering AB.

Turner G D, Zachara J M, McKinley J P, Smith S C, 1996. Surface-charge properties and UO_2^{2+} adsorption of a subsurface smectite. Geochimica et Cosmochimica Acta, 60, pp 3399–3414.

Urey H C, 1947. The thermodynamic properties of isotopic substances. Journal of the Chemical Society, 1947, pp 562–581.

van Beinum W, Hofmann A, Meeussen J C L, Kretzschmar R, 2005. Sorption kinetics of strontium in porous hydrous ferric oxide aggregates. I. The Donnan diffusion model. Journal of Colloid and Interface Science, 283, pp 18–28.

Vandenhove H, van Hees M, 2007. Predicting radium availability and uptake from soil properties. Chemosphere, 69, pp 664–674.

van Geen A, Robertson A P, Leckie J O, 1994. Complexation of carbonate species at the goethite surface: Implications for adsorption of metal ions in natural waters. Geochimica et Cosmochimica Acta, 58, pp 2073–2086.

Vaughan D J, Craig J R, 1978. Mineral chemistry of metal sulfides. New York: Cambridge University Press.

Vorlicek T P, Helz G R, 2002. Catalysis by mineral surfaces: implications for Mo geochemistry in anoxic environments. Geochimica et Cosmochimica Acta, 66, pp 3679–3692.

Vorlicek T P, Kahn M D, Kasuza Y, Helz G R, 2004. Capture of molybdenum in pyriteforming sediments: role of ligandinduced reduction by polysulfides. Geochimica et Cosmochimica Acta, 68, pp 547– 556.

Wagman D D, Evans W H, Parker V B, Schumm R H, Halow I, Bailey S M,Churney K L, Nuttall R L, 1982. The NBS tables of chemical thermodynamic properties, selected values for inorganic and C_1 and C_2 organic substances in SI units. Journal of Physical and Chemical Reference Data, 11, suppl 2.

Wang X, Liu X, 2005. Sorption and desorption of radioselenium on calcareous soil and its solid components studied by batch and column experiments. Applied Radiation and Isotopes, 62, pp 1–9.

Waite T D, Davis J A, Payne T E, Waychunas G A, Xu N, 1994. Uranium (VI) adsorption to ferrihydrite: application of a surface complexation model. Geochimica et Cosmochimica Acta, 58, pp 5465–5478.

Wharton M J, Atkins B, Charnock J M, Livens F R, Pattrick R A D, Collison D, 2000. An X-ray absorption spectroscopy study of the coprecipitation of Tc and Re with mackinawite (FeS). Applied Geochemistry, 15, pp 347–354.

Whitehead D C, 1974. The sorption of iodide by soil components. Journal of the Science of Food and Agriculture, 25, pp 73–79.

Wieser M E, 2006. Atomic weights of the elements 2005 (IUPAC technical report). Pure and Applied Chemistry, 78, pp 2051–2066.

Wildung R E, Gorby Y A, Krupka K M, Hess N J, Li S W, Plymale A E, McKinley J P, Fredrickson J K, 2000. Effect of electron donor and solution chemistry on products of dissimilatory reduction of technetium by Shewanella putrefaciens. Applied and Environmental Microbiology, 66, pp 2451–2460.

Yim M S, Caron F, 2006. Life cycle and management of carbon-14 from nuclear power generation. Progress in Nuclear Energy, 48, pp 2–36.

Yoshida S, Muramatsu Y, Uchida S, 1998. Soil-solution distribution coefficients, Kds, of I^- and IO_3^- for 68 Japanese soils. Radiochimica Acta, 82, pp 293–297.

Zhang Y, Moore J N, 1996. Selenium fractionation and speciation in a wetland system. Environmental Science & Technology, 30, pp 2613–2619.

Zhang Y, Moore J N, 1997. Interaction of selenate with a wetland sediment. Applied Geochemistry, 12, pp 685–691.

Zhang P, Sparks D L, 1990. Kinetics of selenate and selenite adsorption/desorption at the goethite/water interface. Environmental Science and Technology, 24, pp 1848–1856.

Zhou C-M, Wu Z-D, 2006. Calculation of half-life for ^{79}Se decay. Nuclear Science and Techniques, 17, pp 21–23.

Zhou P, Yan H, Gu B, 2005. Competitive complexation of metal ions with humic substances. Chemosphere, 58, pp 1327–1337.

Åström M E, Peltola P, Virtasalo J J, Kotilainen A T, Salminen R, 2008. Niobium in boreal stream waters and brackish-water sediments. Geochemistry: Exploration, Environment, Analysis, 8, pp 139–148.